ON A GENERALIZED LAMINATE THEORY WITH APPLICATION TO BENDING, VIBRATION, AND DELAMINATION BUCKLING IN COMPOSITE LAMINATES

by

Ever J. Barbero

Dissertation submitted to the Faculty of the
Virginia Polytechnic Institute and State University
in partial fulfillment of the requirements for the degree of
Doctor of Philosophy
in
Engineering Mechanics

APPROVED:

J.N. Reddy, Chairman

R. H. Plaut

L. Librescu

R. T. Haftka

S. L. Hendricks

October, 1989

Blacksburg, Virginia

ON A GENERALIZED LAMINATE THEORY WITH APPLICATION TO BENDING, VIBRATION, AND DELAMINATION BUCKLING IN COMPOSITE LAMINATES

by

Ever J. Barbero

J. N. Reddy, Chairman

Engineering Mechanics

(ABSTRACT)

In this study, a computational model for accurate analysis of composite laminates and laminates with including delaminated interfaces is developed. An accurate prediction of stress distributions, including interlaminar stresses, is obtained by using the Generalized Laminate Plate Theory of Reddy in which layer-wise linear approximation of the displacements through the thickness is used. Analytical as well as finite-element solutions of the theory are developed for bending and vibrations of laminated composite plates for the linear theory. Geometrical nonlinearity, including buckling and postbuckling are included and used to perform stress analysis of laminated plates. A general two-dimensional theory of laminated cylindrical shells is also developed in this study. Geometrical nonlinearity and transverse compressibility are included. Delaminations between layers of composite plates are modelled by jump discontinuity conditions at the interfaces. The theory includes multiple delaminations through the thickness. Geometric nonlinearity is included to capture layer buckling. The strain energy release rate distribution along the boundary of delaminations is computed by a novel algorithm. The computational models presented herein are accurate for global behavior and particularly appropriate for the study of local effects.

ACKNOWLEDGEMENTS

Special tribute goes to my adivsor, Dr. J. N. Reddy for his professional and personal guidance and support. My sincere thanks to the members of my committee, Professors R. Plaut, L. Librescu, R. Haftka and S. Hendricks for reading of the dissertation. The support of Alcoa Technical Laboratories and the colloboration of are gratefully acknowledged. The financial support form the Cunningham Year Dissertation Fellowship during Fall 1989 is also appreciated.

I express my sincere appreciation for the help received from faculty and students, particularly from my friend . I also thank for the skillful typing of this dissertation, which is full of complex mathematical expressions.

I feel deep appreciation and love to my mother, and my father, , who showed me how to recognize values of life.

DEDICATION

This work is dedicated to my wife, . Without her love, encouragement and help, this dissertation would never be completed.

TABLE OF CONTENTS

TABLE OF CONTENTS (CONTINUED)

TABLE OF CONTENTS (CONTINUED)

LIST OF FIGURES

LIST OF FIGURES (continued)

LIST OF FIGURES (continued)

LIST OF FIGURES (continued)

LIST OF TABLES

Chapter 1

INTRODUCTION

1.1 Background

The objective of this study is to accurately analyze laminated composite plates containing localized damage and singularities. One of such damage modes of definite importance on the performance of composite structures is delamination buckling and growth in laminated plates subject to in-plane compressive loads.

While the accuracy of the analysis is of paramount importance to the correct evaluation of damage in composites, the cost of the solution affects the class of problems that can be analyzed with fixed resources. The objective is to raise the quality of the analysis beyond that provided by classical theories of plates while keeping the cost of the solutions well below the cost of a three-dimensional analysis. There are many examples where a classical plate theory solution is inadequate. An analytical tool is proposed, which is as accurate as a fully nonlinear three-dimensional analysis for the problems of interest to this study.

The proposed analysis procedure is based on the reduction of the 3-D problem to a 2-D one by using a refined plate theory. This allows reduction of the complexity and the cost of the analysis, while representing all the important aspects of the problem under consideration.

The advantages of a plate theory over a 3-D analysis are many. In the application of 3-D finite elements to bending of plates, the aspect

ratio of the elements must be kept to a reasonable value in order to avoid shear locking. If the laminated plate is modelled with 3-D elements, an excessively refined mesh in the plane of the plate needs to be used because the thicknesses of individual lamina dictate the aspect ratio of an element. On the other hand, a finite element model based on a plate theory does not have any aspect ratio limitation because the thickness dimension is eliminated at the beginning. However, the hypothesis commonly used in the conventional plate (both classical and refined) theories leads to a poor representation of stresses in cases of interest, namely small thickness ratio (thickness over damage-size) problems and problems with dissimilar material layers (damaged and undamaged).

A 2-D laminate theory that provides a compromise between the 3-D theory and conventional plate theories is the Generalized Laminated Plate Theory (GLPT) of Reddy [1], with layer-wise smooth representation of displacements through the thickness. Although this theory is computationally more expensive than the conventional laminate theories, it predicts stresses very accurately. Furthermore, it has the advantage of all plate theories in the sense that the problem is reduced to two dimensions. Therefore, the discretization by the finite element method needs to be refined only in the areas of interest and does not suffer from aspect ratio limitations associated with 3-D finite element models.

Any plate theory used in delamination buckling must be able to represent the kinematics of the delamination properly. This means that the discontinuity in the displacements must be modelled. As we shall

see later, the GLPT can be extended to model the kinematics of delamination in an efficient fashion.

We must account for geometric nonlinearity to capture the buckling phenomena. However, we would like to include only the nonlinearities that are important to the class of problems to be considered in order to keep the cost of the analysis to a minimum. The von Kármán hypothesis of retaining the squares and products of derivatives of the transverse deflection in the nonlinear strain-displacement relations will be sufficient for the purpose.

The representation of displacements and stresses in the damaged area must be accurate. For the case of delaminations, an accurate solution is necessary for the application of a fracture criterion to predict the onset of delamination growth. An efficient and reliable computation of the fracture criterion is essential to apply the model to complex situations with confidence. Among the fracture criteria, the energy criteria are the most accepted. The virtual crack extension method is applicable to delamination because the delamination is most likely to propagate in self similar form. We propose to extend and improve the virtual crack extension method as we shall see in the description of the Jacobian Derivative Method (JDM).

1.2 Objectives of the Present Research

The objective of this study is to develop theoretical and approximate models to accurately analyze laminated composite plates using a generalized laminate plate theory [1]. Linear Lagrange interpolation functions will be used in the generalized laminate plate

theory of Reddy [1] for the approximation of the inplane displacements through the thickness. Inextensibility of the transverse normals will be assumed.

Close form solutions to the theory will be developed and compared to 3-D elasticity solutions and to other conventional plate theories. Other non-classical closed form solutions, such as cylindrical bending for arbitrary boundary conditions, will be developed and will serve as a benchmark for the approximate methods to be presented.

The generalized laminated-plate theory will be extended to cylindrical shells. Some classical form solutions will be developed for the case of Lagrange-linear interpolation through the thickness, in order to assess the quality of the theory.

The finite element model of the plate theory will be developed and evaluated. Of particular conern is the ability of the theory to accurately model both the global and the local behavior of plates. A precise representation of the inplane and interlaminar shear stresses is expected at detailed regions where small aspect ratio (size over thickness) elements are used. Also, a correct evaluation of global response is expected when a few large elements are used in the model.

A procedure to recover interlaminar shear stresses from the equilibrium equations will be developed. The finite element model will be applied to laminated-composite plates and laminated-hybrid plates (e.g., ARALL).

The generalized laminated-plate theory will be further extended to model the kinematics of multiple delaminations. Essential nonlinear behavior will be included to model delamination buckling. The theory

will be applied to embedded delaminations that are entirely separated from the base laminate after buckling. Nonlinear behavior, without delaminations, will be compared to existing solutions.

Finally, an improvement of the virtual crack extension method will be developed and applied to laminated composite plates with delaminations. The strain energy release-rate distribution along the crack-front (delamination boundary) can be computed considering the virtual extension of the crack. Evaluation of the strain energy release-rate G(s) using an energy method has the advantage that standard finite elements can be used at the crack front. It is expected that a single, self-similar, virtual crack extension will be sufficient to compute the distribution of G(s) along the crack front.

The main result of this research is an extremely accurate, yet economic, analysis tool for laminated composite materials with localized damage and singularities. The GLPT is shown to be a highly versatile tool to model laminated composite plates. The extension to delaminated plates provides an analysis capability for laminated composite plates with an arbitrary number of delaminations. The analysis is shown to be as accurate as a fully nonlinear 3D-elasticity solution, yet significantly less expensive. The scope of this study is necessarily limited. Application of the GLPT to other problems is envisioned. This study will show both the fundamentals of the theory of GLPT and its extensions to shells and modelling of delaminations.

1.3 Literature Review

1.3.1 Plate Theories

The field of plate theories was and still is a strong area of research as we may conclude from the number of publications in the field. This is motivated by the strong interest of scientists and engineers to analyze one of the more common structural components, namely plates. Plates are three-dimensional continua bounded by two flat planes, separated by small distance, called thickness of the plate. The thickness is very small compared to the in-plane dimensions of the plate. This allows approximation of thickness effects and reduction of the three-dimensional equations of elasticity to two-dimensional equations in terms of thickness-averaged forces and moments.

Mainly two methods have been used to reduce the three-dimensional equations of elasticity to a two-dimensional set of equations. The assumed-displacement method, first used by Baset [2], consists of expanding the displacement field as a linear combination of unknown functions and various powers of the thickness coordinate. The assumed-stress method, first used by Boussinesq [3], consists of integrating the stresses through the thickness taking moments of different orders to produce a set of stress resultants. Although the kinematic assumption is not specifically stated in the stress method, it is still implicit in the election of which moments to consider. The classical plate theory, for example, can be derived either way. Since the displacement method clearly states the form of the displacement distribution through the thickness, and we can arrive at exactly the same equations using the

stress method, it is clear that the restrictions on the kinematics are used in both methods.

Most of the displacement theories use continuous (in the thickness coordinate) approximation of the displacements through the thickness. The simplest theory uses the hypothesis of Kirchhoff and is called classical plate theory, which does not account for the transverse shear strains. Shear deformation effects were included by Hildebrand, Reissner and Thomas [4], Hencky [5], Midlin [6], Uflyand [8], and Reissner [9]. Laminated composites motivated additional research on shear deformation theories, because the displacements, frequencies and buckling loads obtained using classical plate theory are poor even for moderate aspect ratios (i.e., side-to-thickness ratios up to 40). Classical plate theory for nonhomogeneous plates was considered by Reissner and Stavsky [10,11] and Lekhnitskii [12]. The importance of shear deformation in composite laminates was illustrated for example, by Pagano [13]. Early attempts to include shear deformation in plate theories are due to Stavsky [14], Ambartsumyan [15] and Whitney [16]. Yang, Norris and Stavsky [7] extended the Hencky-Mindlin theory, termed the first-order shear deformation theory by Reddy [17,18], to laminated plates, and later Whitney and Pagano [19] presented the Navier solutions to the first-order shear deformation theory [6]. Whitney and Pagano [19,20] concluded that consideration of shear deformation alone cannot substantially improve the inplane stress distributions of plate theories. Higher-order theories were developed in an attempt to improve the in-plane stress distributions. Among them, Whitney [21] and Nelson and Lorch [22], and Lo, Christensen, and Wu [23] used second-order

theories (i.e., displacements are expanded upto the quadratic terms in the thickness coordinate). Reddy [24] presented a third-order theory which satisfies stress-free boundary conditions on the bounding planes of the plate.

More successful in predicting the in-plane and interlaminar stresses are those theories that allow for a layer wise representation of the displacements through the thickness. Yu [25] and Durocher and Solecki [26] considered the case of a three-layer plate. Mau [27], Srinivas [28], Sun and Whitney [29], Seide [30] derived theories for layer wise linear displacements. Librescu [31,32] presented a multilayer shell theory and considered geometric nonlinearity. Pryor and Baker [34] presented a finite element model based on linear functions on each layer. Reddy [1] derived a Generalized Laminate Plate Theory in which the distribution of displacements can be chosen arbitrarily depending on the requirements of the analysis. Reissner's mixed variational principle [35] has been used to include the interlaminar stresses as primary variables. Both continuous functions and piece-wise linear functions were used by Murakami [36] and Toledano and Murakami [37]. While the mixed theories are more complex than displacement theories, they do not outperform the latter ones in accuracy of the stresses. Furthermore, integration of the 3-D equilibrium equations allows us to compute the interlaminar shear stresses from the results of displacement-based theories as it was proposed by Pryor and Baker [34] and Chaudhuri [38] for Seide's theory [30], and generalized in this work for Reddy's generalized laminate plate theory [1].

1.3.2 Delaminations and Delamination-Buckling

Delaminations between laminae are common defects in laminates, usually developed either during manufacturing or during operational life of the laminate (e.g., fatigue, impact). Delaminations may buckle and grow in panels subjected to in-plane compressive loads. Delaminated panels have reduced load-carrying capacity in both the pre- and post-buckling regime. However, under certain circumstances, the growth of delaminations can be arrested. An efficient use of laminated composite structures requires an understanding of the delamination onset and growth. An analysis methodology is necessary to model composite laminates in the presence of delaminations.

Self similar growth of the delamination along an interface between layers is suggested by the laminated nature of the panel. It was also noted by Obreimoff [39] and Inoue and Kobatake [40] that axial compressive load applied in the direction of the delamination promotes further growth in the same direction. One-dimensional and two-dimensional models for the delamination problem were proposed by Chai [41], Simitses, Sallam and Yin [42], Kachanov [43], Ashizawa [44], Sallam and Simitses [45] and Kapania and Wolfe [46]. According to these models, the delamination can grow only after the debonded portion of the laminate buckles. However, the delamination can also grow due to shear modes II and III. A new theory to be developed in this study will be able to account for these effects.

The spontaneous growth of a delamination while the applied load is constant is called "unstable growth". If the load has to be increased

to promote further delamination, the growth is said to be "stable growth". The onset of delamination growth can be followed by stable growth, or unstable indefinite growth or even unstable growth followed by arrest and subsequent stable growth.

Most existing analyses calculate the buckling load of the debonded laminate using bifurcation analysis (see Chai [41], Simitses et al. [42], Webster [47], and Shivakumar and Whitcomb [54]). Bifurcation analysis is not appropriate for debonded laminates that have bending-extension coupling, as noted by Simitses et al. [42]. Even laminates that are originally symmetric, once delaminated, experience bending-extension coupling. Most likely the delaminations are unsymmetrically located and the resulting delaminated layers become unsymmetric. Therefore, inplane compressive load produces lateral deflection and the primary equilibrium path is not trivial ($w \neq 0$). Furthermore, bifurcation analysis does not permit computation of the strain energy release rate.

Nonlinear plate theories have been used to analyze the post-buckling behavior of debonded laminates. Bottega [48], Yin [49], and Fei and Yin [50] analyzed the problem of a circular plate with concentric, circular delamination. The von Kármán type of nonlinearity has been used in most analyses. Multiple delaminations through the thickness of isotropic beams were considered by Wolfe and Kapania [51,52].

Most of the analyses performed have been restricted to relatively simple models. The material was considered isotropic in most cases and orthotropic in a few, thus precluding the possibility of analyzing the

influence of the stacking sequence and bending-extension coupling. However, an understanding of the basic principles involved has been established, thus allowing the derivation of more complex models that can further contribute to this area of study.

The Rayleigh-Ritz method has been used by Chai [41], Chai and Babcock [53], and Shivakumar and Whitcomb [54] to obtain approximate solutions to the simple models so far proposed. Orthotropic laminates were considered by Chai and Babcock [55] and circular delaminations by Webster [47].

The finite element method was used by Whitcomb [56] to analyze through-width delaminated coupons. Plane-strain elements were used to model sections of beams, or plates in cylindrical bending. The analysis of delaminations of arbitrary shape in panels requires the use of three-dimensional elements, with a considerable computational cost. A three-dimensional, fully nonlinear finite element analysis was used by Whitcomb [57], where it was noted that "...plate analysis is potentially attractive because it is inherently much less expensive than 3D analysis." Plate elements and multi-point constraints have been used by Whitcomb [58] to study delamination buckling and by Wilt, Murthy and Chamis [59] to study free-edge delaminations. This approach is inconvenient in many situations. First, the MPC require a large number of nodes to simulate actual contact between laminae. Second, a new plate element is added for each delamination. The MPC approach becomes too complex for the practical situation of multiple delaminations through the thickness. Third, all plate elements have their middle surface on the same plane, which is unrealistic for the case of

delaminated laminae that have their middle surface at different locations through the thickness of the plate. This study proposes to develop a plate theory able to represent any number of delaminations through the thickness of the plate.

1.3.3 Fracture Mechanics Analysis

After the local buckling occurs, the delamination can grow only if the fracture can be further extended. The Griffith's Fracture Criterion for the initial growth of the delamination has been used by Chai [41], and Kachanov [43]. According to the Griffith's Criterion the surface of the crack grows only if the strain energy released by the structure (while going to the new configuration) is greater than the energy required to create the new surface.

The Griffith's criterion requires the computation of the energy-release rate for a virtual extension of the delaminated area. The energy release rate of delaminations has been computed by numerical differentiation of the total strain energy by Chai [41], or using the J-integral method by Yin et al. [60]. The different fracture opening-modes and their corresponding energy-release rates were considered by Whitcomb [56]. A variation of the virtual crack closure method was used by Whitcomb and Shivakumar [58] to compute the strain energy release rate from a plate and multi-point-constraint analysis.

The finite element method is well established as a tool for determination of stress intensity factors in fracture mechanics. Isoparametric elements are among the most frequently used elements due to their ability to model the geometry of complex domains. The quarter

point element introduced by Henshell [61] and Barsoum [62] became very popular in Linear Elastic Fracture Mechanics (LEFM) because it can represent accurately the singularities involved in LEFM problems. Its use has been extended to other problems as well by Barsoum [63].

Numerous methods to compute stress intensity factors have appeared over the years. Most of them are designed for 2D problems and their extension to 3D problems is not without complications. Some methods are specially tailored for 3D analysis (for a review see Raju and Newman [64]). The direct methods obtain the stress intensity factor as part of the solution. They require special elements that incorporate the crack tip singularity, for example Tong, Pian and Lasry [65]. The indirect methods compute the stress intensity factor from displacements or stresses obtained independently. Among the more popular indirect methods we have extrapolation of displacements or stresses around the crack tip as done by Chan, Tuba and Wilson [66] and the nodal-force method of Raju and Newman [67,68]. We can also use integral methods like the J-integral method of Rice [69], the modified crack closure integral of Rybicki and Kanninen [70], and various generalizations as the one by Ramamurthy et al. [71], and the virtual crack extension method of Hellen [72] and Parks [73]. The indirect and integral methods can be used with conventional elements or with special elements that incorporate the appropriate singularity at the crack front.

Chapter 2

THE GENERALIZED LAMINATED PLATE THEORY

2.1 Introduction

Laminated composite plates have motivated the development of refined plate theories to overcome certain shortcomings of the classical theories when applied to composites. The first-order and higher-order shear deformation theories yield improved global response, such as maximum deflections and natural frequencies, due to the inclusion of shear deformation effects. Conventional theories based on a single continuous and smooth displacement field through the thickness of the plate give poor estimation of interlaminar stresses. Since important modes of failure are related to interlaminar stresses, refined plate theories that can model the local behavior of the plate more accurately have been developed. The Generalized Laminated Plate Theory will be shown to provide excellent predictions of the local response, i.e., interlaminar stresses, inplane displacements and stresses, etc. This is due to the refined representation of the laminated nature of composite plates provided by GLPT and to the cosideration of shear deformation effects.

2.2 Formulation of the Theory

Consider a laminated plate composed of N orthotropic lamina, each being oriented arbitrarily with respect to the laminate (x,y) coordinates, which are taken to be in the midplane of the laminate. The displacements (u_1,u_2,u_3) at a generic point (x,y,z) in the laminate are assumed to be of the form [1],

$$u_1(x,y,z) = u(x,y) + U(x,y,z)$$
$$u_2(x,y,z) = v(x,y) + V(x,y,z)$$
$$u_3(x,y,z) = w(x,y), \tag{2.1}$$

where (u,v,w) are the displacements of a point (x,y,0) on the reference plane of the laminate, and U and V are functions which vanish on the reference plane:

$$U(x,y,0) = V(x,y,0) = 0. \tag{2.2}$$

In order to reduce the three-dimensional theory to a two-dimensional one, it is necessary to make an assumption concerning the variation of U and V with respect to the thickness coordinate, z. To keep the flexibility of the degree of variation of the displacements through the thickness, we assume that U and V are approximated as

$$U(x,y,z) = \sum_{j=1}^{n} u^j(x,y)\phi^j(z)$$
$$V(x,y,z) = \sum_{j=1}^{n} v^j(x,y)\phi^j(z), \tag{2.3}$$

where u^j and v^j are undetermined coefficients and ϕ^j are any continuous functions that satisfy the condition

$$\phi^j(0) = 0 \text{ for all } j = 1,2,\ldots,n. \tag{2.4}$$

The approximation in Eq. (2.3) can also be viewed as the global semi-discrete finite-element approximations [74] of U and V through the thickness. In that case ϕ^j denote the global interpolation functions, and u^j and v^j are the global nodal values of U and V (and possibly their derivatives) at the nodes through the thickness of the laminate. For example, a finite element approximation based on the Lagrangian interpolation through the thickness can be obtained from Eq. (2.3) by

setting $n = pN + 1$, where

N = number of layers through thickness

p = degree of the global interpolation polynomials, $\phi^j(z)$, and

u^j, v^j = global nodal values of U and V.

For $p = 1$ (i.e., linear interpolation), we have $n = N + 1$ and

$$u^1 = U_1^{(1)},\ u^2 = U_2^{(1)} = U_1^{(2)},\ldots,u^k = U_2^{(k-1)} = U_1^{(k)}$$

$$v^1 = V_1^{(1)},\ v^2 = V_2^{(1)} = V_1^{(2)},\ldots,v^k = V_2^{(k-1)} = V_1^{(k)} \qquad (2.5)$$

where $U_i^{(k)}$, for example, denotes the value of U at the i-th node of the k-th lamina, Figure 2.1. The linear global interpolation functions are given by

$$\phi^k(z) = \begin{cases} \Psi_2^{(k-1)}(z) & , \ z_{k-1} \le z \le z_k \\ \Psi_1^{(k)}(z) & , \ z_k \le z \le z_{k+1} \end{cases} \qquad (k = 1,2,\ldots,N) \quad (2.6)$$

where $\Psi_i^{(k)}$ $(i = 1,2)$ is the local (i.e. layer) Lagrange interpolation function associated with the i-th node of the k-th layer, Figure 2.1. If the midplane does not coincide with an interface, it is used as an interface to satisfy Equation (2.2). If for example u^r, v^r correspond to the midplane interface, Equation (2.2) is satisfied by setting $u^r = v^r = 0$. Therefore n reduces to $n = N$. Since $u^r = v^r = 0$ at the midplane interface, those variables are no longer needed and they are eiminated. The remaining variables are then renumbered with $j = 1,\ldots N$ as shown in Figure 2.2 for a four layer laminate.

The equilibrium equations of the theory can be derived using the Hamilton principle:

$$0 = \int_0^t \int_\Omega \{N_x(\frac{\partial \delta u}{\partial x}) + N_y(\frac{\partial \delta v}{\partial y}) + N_{xy}(\frac{\partial \delta u}{\partial y} + \frac{\partial \delta v}{\partial x})$$

$$+ Q_x \frac{\partial \delta w}{\partial x} + Q_y \frac{\partial \delta w}{\partial y}$$

$$+ \sum_{j=1}^{n} [N_x^j \frac{\partial \delta u^j}{\partial x} + N_y^j \frac{\partial \delta v^j}{\partial y} + N_{xy}^j (\frac{\partial \delta u^j}{\partial y} + \frac{\partial \delta v^j}{\partial x})$$

$$+ Q_x^j u^j + Q_y^j v^j] - q\delta w\} dA dt - \int_0^t \int_\Omega [I_o(\dot{u}\delta\dot{u} + \dot{v}\delta\dot{v} + \dot{w}\delta\dot{w})$$

$$+ \sum_{j=1}^{n} I^j(\dot{u}^j\delta\dot{u} + \dot{u}\delta\dot{u}^j + \dot{v}^j\delta\dot{v} + \dot{v}\delta\dot{v}^j)$$

$$+ \sum_{i,j=1}^{n} I^{ij}(\dot{u}^i\delta\dot{u}^j + \dot{v}^i\delta\dot{v}^j)]dA dt. \qquad (2.7)$$

where

$$(N_x, N_y, N_{xy}) = \int_{-h/2}^{h/2} (\sigma_x, \sigma_y, \sigma_{xy}) dz$$

$$(Q_x, Q_y) = \int_{-h/2}^{h/2} (\sigma_{xz}, \sigma_{yz}) dz$$

$$(N_x^j, N_y^j, N_{xy}^j) = \int_{-h/2}^{h/2} (\sigma_x, \sigma_y, \sigma_{xy})\phi^j(z) dz$$

$$(Q_x^j, Q_y^j) = \int_{-h/2}^{h/2} (\sigma_{xz}, \sigma_{yz}) \frac{d\phi^j}{dz}(z) dz \qquad (2.8)$$

$$I_o = \int_{-h/2}^{h/2} \rho dz \; ; \; I^j = \int_{-h/2}^{h/2} \rho\phi^j dz \; ; \; I^{ij} = \int_{-h/2}^{h/2} \rho\phi^i\phi^j dz$$

$(\sigma_x, \sigma_y, \sigma_{xy}, \sigma_{xz}, \sigma_{yz})$ are the stresses, q is the distributed transverse load, and ρ is the mass density.

The Euler-Lagrange equations of the theory are given by

$$
\begin{aligned}
&N_{x,x} + N_{xy,y} = I_o\ddot{u} + \sum_{j=1}^{n} I^j\ddot{u}^j \\
&N_{xy,x} + N_{y,y} = I_o\ddot{v} + \sum_{j=1}^{n} I^j\ddot{v}^j \\
&Q_{x,x} + Q_{y,y} + q = I_o\ddot{w} \\
&N^j_{x,x} + N^j_{xy,y} - Q^j_x = I^j\ddot{u} + \sum_{j=1}^{n} I^{ij}\ddot{u}^i \\
&N^j_{xy,x} + N^j_{y,y} - Q^j_y = I^j\ddot{v} + \sum_{j=1}^{n} I^{ij}\ddot{v}^i
\end{aligned}
\tag{2.9a}
$$

for $j = 1,2,\ldots,n$. Thus there are $2n + 1$ differential equations in $(2n + 1)$ variables (u, v, w, u^j, v^j). The form of the geometric and force boundary conditions is given below:

Geometric (Essential)	Force (Natural)
u	$N_x n_x + N_{xy} n_y$
v	$N_{xy} n_x + N_y n_y$
w	$Q_x n_x + Q_y n_y$
u^j	$N^j_x n_x + N^j_{xy} n_y$
v^j	$N^j_{xy} n_x + N^j_y n_y$

(2.9b)

where (n_x, n_y) denote the direction cosines of a unit normal to the boundary of the midplane Ω. The lamina constitutive equations tranformed to structural coordinates are:

$$\begin{Bmatrix} \sigma_x \\ \sigma_y \\ \sigma_{xy} \\ \sigma_{xz} \\ \sigma_{yz} \end{Bmatrix}^{(k)} = \begin{bmatrix} \bar{Q}_{11} & \bar{Q}_{12} & \bar{Q}_{16} & 0 & 0 \\ \bar{Q}_{12} & \bar{Q}_{22} & \bar{Q}_{26} & 0 & 0 \\ \bar{Q}_{16} & \bar{Q}_{26} & \bar{Q}_{66} & 0 & 0 \\ 0 & 0 & 0 & \bar{Q}_{55} & Q_{54} \\ 0 & 0 & 0 & \bar{Q}_{54} & Q_{44} \end{bmatrix}^{(k)} \begin{Bmatrix} \varepsilon_x \\ \varepsilon_y \\ \gamma_{xy} \\ \gamma_{xz} \\ \gamma_{yz} \end{Bmatrix}^{(k)} \quad (2.10)$$

where $Q_{ij}^{(k)}$ are the reduced stiffnesses of the k-th orthotropic lamina, obtained under the plane stress assumption [75].

The constitutive equations of the laminate are given by

$$\begin{Bmatrix} N_x \\ N_y \\ N_{xy} \\ Q_x \\ Q_y \end{Bmatrix} = \begin{bmatrix} A_{11} & A_{12} & A_{16} & 0 & 0 \\ A_{12} & A_{22} & A_{26} & 0 & 0 \\ A_{16} & A_{26} & A_{66} & 0 & 0 \\ 0 & 0 & 0 & A_{55} & A_{45} \\ 0 & 0 & 0 & A_{45} & A_{44} \end{bmatrix} \begin{Bmatrix} \frac{\partial u}{\partial x} \\ \frac{\partial v}{\partial y} \\ \frac{\partial u}{\partial y} + \frac{\partial v}{\partial x} \\ \frac{\partial w}{\partial x} \\ \frac{\partial w}{\partial y} \end{Bmatrix}$$

$$+ \sum_{j=1}^{n} \begin{bmatrix} B_{11}^j & B_{12}^j & B_{16}^j & 0 & 0 \\ B_{12}^j & B_{22}^j & B_{26}^j & 0 & 0 \\ B_{16}^j & B_{26}^j & B_{66}^j & 0 & 0 \\ 0 & 0 & 0 & \bar{B}_{55}^j & \bar{B}_{45}^j \\ 0 & 0 & 0 & \bar{B}_{45}^j & \bar{B}_{44}^j \end{bmatrix} \begin{Bmatrix} \frac{\partial u^j}{\partial x} \\ \frac{\partial v^j}{\partial y} \\ \frac{\partial u^j}{\partial y} + \frac{\partial v^j}{\partial x} \\ u^j \\ v^j \end{Bmatrix}$$

$$\begin{Bmatrix} N_x^j \\ N_y^j \\ N_{xy}^j \\ Q_x^j \\ Q_y^j \end{Bmatrix} = \begin{bmatrix} B_{11}^j & B_{12}^j & B_{16}^j & 0 & 0 \\ B_{12}^j & B_{22}^j & B_{26}^j & 0 & 0 \\ B_{16}^j & B_{26}^j & B_{66}^j & 0 & 0 \\ 0 & 0 & 0 & \bar{B}_{55}^j & \bar{B}_{45}^j \\ 0 & 0 & 0 & \bar{B}_{45}^j & \bar{B}_{44}^j \end{bmatrix} \begin{Bmatrix} \frac{\partial u}{\partial x} \\ \frac{\partial v}{\partial y} \\ \frac{\partial u}{\partial y} + \frac{\partial v}{\partial x} \\ \frac{\partial w}{\partial x} \\ \frac{\partial w}{\partial y} \end{Bmatrix}$$

$$+ \sum_{k=1}^{n} \begin{bmatrix} D_{11}^{jk} & D_{12}^{jk} & D_{16}^{jk} & 0 & 0 \\ D_{12}^{jk} & D_{22}^{jk} & D_{26}^{jk} & 0 & 0 \\ D_{16}^{jk} & D_{26}^{jk} & D_{66}^{jk} & 0 & 0 \\ 0 & 0 & 0 & \bar{D}_{55}^{jk} & \bar{D}_{45}^{jk} \\ 0 & 0 & 0 & \bar{D}_{45}^{jk} & \bar{D}_{44}^{jk} \end{bmatrix} \begin{Bmatrix} \frac{\partial u^k}{\partial x} \\ \frac{\partial v^k}{\partial y} \\ \frac{\partial u^k}{\partial y} + \frac{\partial v^k}{\partial x} \\ u^k \\ v^k \end{Bmatrix} \quad (2.11a)$$

where

$$A_{pq} = \sum_{k=1}^{N} \int_{z_k}^{z_{k+1}} Q_{pq}^{(k)} dz \quad (p,q = 1,2,6;4,5)$$

$$B_{pq}^j = \sum_{k=1}^{N} \int_{z_k}^{z_{k+1}} Q_{pq}^{(k)} \phi^j dz \quad (p,q = 1,2,6)$$

$$D_{pq}^{ji} = \sum_{k=1}^{N} \int_{z_k}^{z_{k+1}} Q_{pq}^{(k)} \phi^j \phi^i dz \quad (p,q = 1,2,6)$$

$$\bar{B}_{pq}^j = \sum_{k=1}^{N} \int_{z_k}^{z_{k+1}} Q_{pq}^{(k)} \frac{d\phi^j}{dz} dz \quad (p,q = 4,5)$$

$$\bar{D}^{ji}_{pq} = \sum_{k=1}^{N} \int_{z_k}^{z_{k+1}} Q^{(k)}_{pq} \frac{d\phi^j}{dz} \frac{d\phi^i}{dz} dz \quad (p,q = 4,5) \qquad (2.11b)$$

for all i,j = 1,2,...,n.

Regardless of the functions $\phi^j(z)$ used, the coefficients A_{pq} are the same as in Classical Lamination Theory (CLT):

$$A_{pq} = \sum_{k=1}^{N} Q^k_{pq} h^k \qquad (2.12)$$

where N is the number of layers and h^k is the thickness of the k-th layer in the laminate. When $\phi^j(z)$ are linear in each layer, we have that for the j-th location through the thickness, $\phi^j(z) \neq 0$ only on the two adjacent layers k = j and k = j - 1, see Figure 2.1. Therefore

$$B^j_{pq} = Q^{j-1}_{pq} \frac{h^{j-1}}{2} + Q^j_{pq} \frac{h^j}{2} \quad ; \quad (p,q = 1,2,6) \qquad (2.13a)$$

It can be shown also that

$$\frac{d\phi^j}{dz} = \begin{cases} 1/h^{j-1} \text{ for } z_{j-1} < z < z_j \\ -1/h^j \text{ for } z_j < z < z_{j+1} \\ 0 \text{ elsewhere} \end{cases} \qquad (2.14)$$

Therefore

$$\bar{B}^j_{pq} = Q^{j-1}_{pq} - Q^j_{pq} h^{j-1} \quad ; \quad (p,q = 4,5) \qquad (2.13b)$$

The same arguments apply for the coefficients of the D-matrix. If i = j we have

$$D^{ii}_{pq} = Q^{i-1}_{pq} \frac{h^{i-1}}{3} + Q^i_{pq} \frac{h^i}{3} \quad ; \quad (p,q = 1,2,6) \qquad (2.15a)$$

and

$$\bar{D}^{ii}_{pq} = \frac{Q^{i-1}_{pq}}{h^{i-1}} - \frac{Q^{i}_{pq}}{h^{i}} \quad ; \quad (p,q = 4,5) \tag{2.15b}$$

If $i \neq j$ we must note that only the layers where ϕ^i and ϕ^j overlap contribute to the integral, then $\phi^i\phi^j \neq 0$ only if $j = i \pm 1$, see Figure 2.1.

Therefore

$$D^{ij}_{pq} = D^{ji}_{pq} = Q^{i}_{pq}\frac{h^i}{6} \quad ; \quad \begin{matrix}(j = i + 1)\\(p,q = 1,2,6)\end{matrix} \tag{2.15c}$$

and

$$\bar{D}^{ij}_{pq} = \bar{D}^{ji}_{pq} = -\frac{Q_{pq}}{h^i} \quad ; \quad \begin{matrix}(j = i + 1)\\(p,q = 4,5)\end{matrix} \tag{2.15d}$$

All the coefficients B^j_{pq}, $\bar{B}^j_{pq}$, D^{ij}_{pq}, $\bar{D}^{ij}_{pq}$ with $i,j = 1,\ldots N+1$ are computed using the entire set of interpolation functions ϕ^j including that corresponding to the midplane, as illustrated in Figure 2.1. Next, the coefficients B^r_{pq}, $\bar{B}^r_{pq}$, D^{rj}_{pq}, D^{ir}_{pq}, $\bar{D}^{rj}_{pq}$, $\bar{D}^{ir}_{pq}$ with r denoting the midplane position are eliminated. The remaining coefficients are then renumbered with $i,j = 1,\ldots N$ as illustrated in Figure 2.2.

As an example, consider a three-layer [0/90/0] laminate with all layers of the same thickness h/3 and the following material properties: $E_2 = 1.0$ msi, $E_1/E_2 = 25$, $G_{12}/E_2 = 0.5$, $G_{13} = G_{12}$, $G_{23}/E_2 = 0.2$, $\nu_{12} = \nu_{13} = 0.25$. Using these material properties, we obtain the following lamina constitutive equations, for the 0°-layer:

$$[Q_0] = \begin{bmatrix} 25.0627 & 0.25062 & 0.0 & 0.0 & 0.0 \\ 0.25062 & 1.00251 & 0.0 & 0.0 & 0.0 \\ 0.0 & 0.0 & 0.5 & 0.0 & 0.0 \\ 0.0 & 0.0 & 0.0 & 0.2 & 0.0 \\ 0.0 & 0.0 & 0.0 & 0.0 & 0.5 \end{bmatrix} \tag{2.16a}$$

and for the 90°-layer:

$$[Q_{90}] = \begin{bmatrix} 1.00251 & 0.25062 & 0.0 & 0.0 & 0.0 \\ 0.25062 & 25.0627 & 0.0 & 0.0 & 0.0 \\ 0.0 & 0.0 & 0.5 & 0.0 & 0.0 \\ 0.0 & 0.0 & 0.0 & 0.5 & 0.0 \\ 0.0 & 0.0 & 0.0 & 0.0 & 0.2 \end{bmatrix} \qquad (2.16b)$$

Since the midplane does not coincide with an interface, we model the plate as a four-layer laminate with two 0°-layers of thickness h/3 and two 90°-layers of thickness h/6. According to (2.12-2.15) we obtain before elimination

$$A = \begin{bmatrix} 17.0426 & 0.25062 & 0.0 & 0.0 & 0.0 \\ & 9.02257 & 0.0 & 0.0 & 0.0 \\ & & 0.5 & 0.0 & 0.0 \\ & & & 0.3 & 0.0 \\ & & & & 0.4 \end{bmatrix} \qquad (2.17)$$

$$B^1 = \begin{bmatrix} 4.17711 & 0.04177 & 0.0 & 0.0 & 0.0 \\ & 0.16708 & 0.0 & 0.0 & 0.0 \\ & & 0.08333 & 0.0 & 0.0 \\ & & & -0.2 & 0.0 \\ & & & & -0.5 \end{bmatrix} \qquad (2.18a)$$

$$B^2 = \begin{bmatrix} 4.26065 & 0.06266 & 0.0 & 0.0 & 0.0 \\ & 2.25564 & 0.0 & 0.0 & 0.0 \\ & & 0.125 & 0.0 & 0.0 \\ & & & -0.3 & 0.0 \\ & & & & 0.3 \end{bmatrix} \qquad (2.18b)$$

$$B^3 = \begin{bmatrix} 0.16708 & 0.04177 & 0.0 & 0.0 & 0.0 \\ & 0.04177 & 0.0 & 0.0 & 0.0 \\ & & 0.08333 & 0.0 & 0.0 \\ & & & 0.0 & 0.0 \\ & & & & 0.0 \end{bmatrix} \qquad (2.18c)$$

$$B^4 = \begin{bmatrix} 4.26065 & 0.06265 & 0.0 & 0.0 & 0.0 \\ & 2.25564 & 0.0 & 0.0 & 0.0 \\ & & 0.125 & 0.0 & 0.0 \\ & & & 0.3 & 0.0 \\ & & & & -0.3 \end{bmatrix} \qquad (2.18d)$$

$$B^5 = \begin{bmatrix} 4.7711 & 0.04177 & 0.0 & 0.0 & 0.0 \\ & 0.16708 & 0.0 & 0.0 & 0.0 \\ & & 0.08333 & 0.0 & 0.0 \\ & & & 0.2 & 0.0 \\ & & & & 0.5 \end{bmatrix} \qquad (2.18e)$$

The elimination process consists of setting $B^3 = 0$ and then renaming

$B^4 \rightarrow B^3$ and $B^5 \rightarrow B^4$. In the same way we obtain the following D-matrices after elimination:

$$D^{11} = D^{44} = \begin{bmatrix} 2.78474 & 0.02784 & 0.0 & 0.0 & 0.0 \\ & 0.11139 & 0.0 & 0.0 & 0.0 \\ & & 0.05555 & 0.0 & 0.0 \\ & & & 0.6 & 0.0 \\ & & & & 1.5 \end{bmatrix} \quad (2.19a)$$

$$D^{12} = D^{21} = D^{34} = D^{43} = \begin{bmatrix} 1.39237 & 0.01392 & 0.0 & 0.0 & 0.0 \\ & 0.05569 & 0.0 & 0.0 & 0.0 \\ & & 0.02777 & 0.0 & 0.0 \\ & & & -0.6 & 0.0 \\ & & & & -1.5 \end{bmatrix} \quad (2.19b)$$

$$D^{22} = D^{33} = \begin{bmatrix} 2.84043 & 0.04177 & 0.0 & 0.0 & 0.0 \\ & 1.50376 & 0.0 & 0.0 & 0.0 \\ & & 0.08333 & 0.0 & 0.0 \\ & & & 3.6 & 0.0 \\ & & & & 2.7 \end{bmatrix} \quad (2.19c)$$

and $D^{23} = D^{32} = [0]$ because the nodes through the thickness number 2 and 3 are separated by the midplane.

2.3 Analytical Solutions

The development of analytical solutions to the layer-wise displacement theory is by no means simple, especially for boundary conditions other than simply-supported. The present work is in the same spirit as the works of Pagano [76,77], who presented analytical solutions of the well-known first-order shear deformation theory to investigate shear deformation effects in composite laminates.

In this study we use a finite-element approximation through the thickness based on the linear Lagrangian interpolation. In order to satisfy the conditions (2.2), we choose the midplane as an interface and set $U(x,y,0) = V(x,y,0) = 0$. A convenient way to accomplish this is to eliminate the variables u^j and v^j at the midplane; therefore the number

of necessary terms in (2.3) reduces to n = N, the number of layers, as explained in Section 2.2, Equations 2.5-6 and 2.12-15.

The coefficients A_{pq} have the same meaning as in the classical plate theory (CPT). The calculation of the coefficients B^j_{pq} involves only the properties of the layers adjacent to the j-th interface because the functions ϕ_j are identically zero at other interfaces. The same is true for the coefficients D^{ji}_{pq}.

Since the approximation through the thickness is built with a finite-element family of functions, a standard, one-dimensional finite-element procedure can be used to perform the integration. This makes the procedure very general with respect to the number of layers, thicknesses and properties that can be handled. The contributions of each layer to its adjacent nodes (located on the interfaces) are then assembled in the usual way [74]. The $[B^j]$ array has an entry for each interface. The array $[D^{ji}]$ has a half bandwidth of 2.

Here we consider analytical solutions for the case of cylindrical bending of a plate strip under various boundary conditions and for simply-supported cross-ply plates.

2.3.1 Cylindrical Bending

The plate equations (2.9) can be specialized to cylindrical bending by taking v = 0, v^j = 0, u = u(x), $u^j = u^j(x)$, w = w(x). The equivalent equations can be written as

$$A_{11} \frac{du^2}{dx^2} + \sum_{k=1}^{N} B^k_{11} \frac{d^2u^k}{dx^2} = 0$$

$$A_{55} \frac{d^2 w}{dx^2} + \sum_{k}^{N} B_{55}^{k} \frac{du^k}{dx} + q = 0$$

$$B_{11}^{j} \frac{d^2 u}{dx} - B_{55}^{j} \frac{dw}{dx} + \sum_{k=1}^{N} [D_{11}^{jk} \frac{d^2 u^k}{dx^2} - D_{55}^{jk} u^k] = 0 \qquad (2.20)$$

Equations (2.12) consist of N + 2 equations in u, w, u^1, u^2, ... u^N unknowns, where N denotes the number of layers. The coefficients A_{11}, B_{11}^{j}, A_{55}, B_{55}^{j}, D_{11}^{jk} and D_{55}^{jk} with j,k = 1,...,N+1 are computed for the N+1 interfaces according to Equations 2.12-15. Then the coefficients corresponding to the midplane interface are eliminated as explained in Section 2.2 and the remaining coefficients are renumbered with j,k = 1,...,N to correspond with the N superscripted variables in Equation (2.20).

We consider the case of N = 2 to illustrate the solution by the state-space procedure [78]. First we transform the system of Equations (2.20) to a system of first-order ordinary differential equations. Introducing the unknowns x_i through the relations

$$\begin{aligned} \alpha_1 &= u \quad & \alpha_3 &= w \quad & \alpha_5 &= u^1 \quad & \alpha_7 &= u^2 \\ \alpha_2 &= u' \quad & \alpha_4 &= w' \quad & \alpha_6 &= (u^1)' \quad & \alpha_8 &= (u^2)' \end{aligned} \qquad (2.21)$$

we obtain a system of ordinary differential equations from Equation (2.20),

$$\{\alpha'\} = [\bar{A}]\{\alpha\} + \{F\} \qquad (2.22a)$$

where

$$[\bar{A}] = [A]^{-1}[B]$$
$$\{F\} = [A]^{-1}\{q\} \qquad (2.22b)$$

$$[A] = \begin{bmatrix} 1 & 0 & 0 & 0 & 0 & 0 & 0 & 0 \\ 0 & 0 & 1 & 0 & 0 & 0 & 0 & 0 \\ 0 & 0 & 0 & 0 & 1 & 0 & 0 & 0 \\ 0 & 0 & 0 & 0 & 0 & 0 & 1 & 0 \\ 0 & A_{11} & 0 & 0 & 0 & B^1_{11} & 0 & B^2_{11} \\ 0 & 0 & 0 & A_{55} & 0 & 0 & 0 & 0 \\ 0 & B^1_{11} & 0 & 0 & 0 & D^{11}_{11} & 0 & D^{12}_{11} \\ 0 & B^2_{11} & 0 & 0 & 0 & D^{21}_{11} & 0 & D^{22}_{11} \end{bmatrix}$$

$$[B] = \begin{bmatrix} 0 & 1 & 0 & 0 & 0 & 0 & 0 & 0 \\ 0 & 0 & 0 & 1 & 0 & 0 & 0 & 0 \\ 0 & 0 & 0 & 0 & 0 & 1 & 0 & 0 \\ 0 & 0 & 0 & 0 & 0 & 0 & 0 & 1 \\ 0 & 0 & 0 & 0 & 0 & 0 & 0 & 0 \\ 0 & 0 & 0 & 0 & 0 & -B^1_{55} & 0 & -B^2_{55} \\ 0 & 0 & 0 & B^1_{55} & D^{11}_{55} & 0 & D^{12}_{55} & 0 \\ 0 & 0 & 0 & B^2_{55} & D^{21}_{55} & 0 & D^{22}_{55} & 0 \end{bmatrix} ; \{q\} = \begin{Bmatrix} 0 \\ 0 \\ 0 \\ 0 \\ 0 \\ -f(x) \\ 0 \\ 0 \end{Bmatrix}$$

(2.22c)

As a particular example, we consider a plate strip made of an isotropic material ($E = 30 \times 10^6$ psi, $E/G = 2.5$, $h = 2$ in.) in cylindrical bending. A uniformly distributed transverse load of intensity f_o is used. For this case $[\bar{A}]$ becomes

$$[\bar{A}] = \begin{bmatrix} 0 & 1 & 0 & 0 & 0 & 0 & 0 & 0 \\ 0 & 0 & 0 & 0 & -6/5 & 0 & -6/5 & 0 \\ 0 & 0 & 0 & 1 & 0 & 0 & 0 & 0 \\ 0 & 0 & 0 & 0 & 0 & 1/2 & 0 & -1/2 \\ 0 & 0 & 0 & 0 & 0 & 1 & 0 & 0 \\ 0 & 0 & 0 & -6/5 & 3 & 0 & 9/5 & 0 \\ 0 & 0 & 0 & 0 & 0 & 0 & 0 & 1 \\ 0 & 0 & 0 & 6/5 & 9/5 & 0 & 3 & 0 \end{bmatrix}; \quad \{F\} = \begin{Bmatrix} 0 \\ 0 \\ 0 \\ -f_o/24 \\ 0 \\ 0 \\ 0 \\ 0 \end{Bmatrix} \tag{2.23}$$

The eigenvalues of the matrix $[\bar{A}]$ are

$$\lambda_1 = \lambda_2 = \lambda_3 = \lambda_4 = \lambda_5 = \lambda_6 = 0$$
$$\lambda_7 \cong 2.19$$
$$\lambda_8 = -\lambda_7. \tag{2.24}$$

For this case we have only four linearly independent eigenvectors, which indicates that the matrix A is defective. For the eigenvalue $\lambda = 0$ the eigenvector is of the form

$$\{\xi_1\} = \{k_1, 0, k_2, 0, 0, 0, 0, 0\}^T$$

To obtain other linearly independent solutions, we use the solution procedure presented by Goldbery and Schwartz [78]. First we set

$$(\bar{A} - \lambda I)\{\xi_2\} = \{\xi_1\}$$

and find that $\lambda = 0$, and therefore

$$[\bar{A}]\{\xi_2\} = \{\xi_1\}.$$

This yields

$$\{\xi_2\} = \{k_3, k_1, k_4, k_2, k_2, 0, -k_2, 0\}^T.$$

Next we set $[\bar{A}]\{\xi_3\} = \{\xi_2\}$ and find

$$\{\xi_3\} = \{k_5, k_3, k_6, k_4, k_4, k_2, -k_4, -k_2\}^T \text{ and } k_1 = 0,$$

which annihilates one of the eigenvectors.

Repeating the procedure, we obtain

$$\{\xi_4\} = \{k_7, k_5, k_8, k_6, \tfrac{5}{6}(k_2 + \tfrac{6}{5} k_6), k_4, -\tfrac{5}{6}(k_2 + \tfrac{6}{5} k_6), -k_4\}^T, \; k_3 = 0$$

$$\{\xi_5\} = \{k_7, k_5, k_8, k_6, -\tfrac{4}{51}(5k_2 + 6k_6), k_4, \tfrac{4}{51}(5k_2 + 6k_6), -k_4\}^T.$$

Lastly, we set $[\bar{A}]\{\xi_6\} = \{\xi_5\}$, and arrive at the condition $k_2 = 0$, which annihilates the only eigenvector left, so the process is terminated. The particular solution of the problem is,

$$\{\alpha_p(x)\} = \int_0^x [\Phi(x - s) \cdot \Phi^{-1}(0)] \cdot \{F(s)\} ds \qquad (2.25)$$

where

$$\Phi(x) = \begin{bmatrix} 0 & 1 & 0 & x & 0 & 0 & & \\ 0 & 0 & 0 & 1 & 0 & 0 & & \\ 1 & 0 & x & 0 & x^2/2 & x^3/6 & & \\ 0 & 0 & 1 & 0 & x & x^2/2 & & \\ 0 & 0 & 1 & 0 & x & 5/6 + x^2/2 & \{\xi_7\}e^{\lambda_7 x} & \{\xi_8\}e^{\lambda_8 x} \\ 0 & 0 & 0 & 0 & 1 & x & & \\ 0 & 0 & -1 & 0 & -x & -5/6 - x^2/2 & & \\ 0 & 0 & 0 & 0 & -1 & -x & & \end{bmatrix}. \qquad (2.26)$$

The general solution is given by

$$\{\alpha(x)\} = \Phi(x) \cdot \{k\} + \{\alpha_p(x)\} \qquad (2.27)$$

where $\{k\}$ is the vector of constants, which can be found using the boundary conditions. For example, for a clamped-clamped case the

boundary conditions at $x = \pm a/2$ are:

$$u(-a/2) = u(a/2) = 0$$

$$w(-a/2) = w(a/2) = 0$$

$$u^1(-a/2) = u^1(a/2) = 0$$

$$u^2(-a/2) = u^2(a/2) = 0,$$

which give us eight equations to compute the eight constants in the vector $\{k\}$.

For the particular choice of $a = 20$ in. and uniformly distributed load of intensity $f_o = 1$ lb/in, the solution is given by

$$u(x) = (-5.94 \times 10^{-29} e^{-2.19x} - 3.07 \times 10^{-26} e^{2.19x}) \cdot 10^{-6}.$$

$$w(x) = \left(\frac{x^2}{48} - \frac{x^4}{480} + \frac{5}{12} x^2 - 22.9167\right) \cdot 10^{-6}$$

$$u^1(x) = \left(\frac{5}{6} x - \frac{x^3}{120} + 1.18 \times 10^{-28} e^{-2.19x} + 6.15 \times 10^{-26} e^{2.19x}\right) \cdot 10^{-6}$$

$$u^2(x) = \left(-\frac{5}{6} x + \frac{x^3}{120} + 1.18 \times 10^{-28} e^{-2.19x} + 6.15 \times 10^{-26} e^{2.19x}\right) \cdot 10^{-6} \tag{2.28}$$

Plots of the transverse deflection w as a function of the aspect ratio a/h are shown in Figure 2.3 for three types of boundary conditions: cantilever, simply supported, and clamped at both ends. For all cases a uniformly distributed load is used. Values for the exact 3-D solution [76] for the simply supported case are also shown. The deflections are normalized with respect to the CPT solution. The present solution is in excellent agreement with the 3-D elasticity

solution. We note that the clamped plate exhibits more shear deformation.

Similar results are presented in Figure 2.4 for a two-layer cross-ply [0°/90] plate strip. The material properties of a ply are taken to be those of a graphite-epoxy material:

$$E_1 = 19.2 \times 10^6 \text{ psi}$$
$$E_2 = 1.56 \times 10^6 \text{ psi}$$
$$G_{12} = G_{13} = 0.82 \times 10^6 \text{ psi}$$
$$G_{23} = 0.523 \times 10^6 \text{ psi}$$
$$\nu_{12} = \nu_{13} = 0.24$$
$$\nu_{23} = 0.49. \qquad (2.29)$$

Once again, it is clear that the present theory yields very accurate results.

2.3.2 Simply Supported Plates

Consider a rectangular (a x b) cross-ply laminate, not necessarily symmetric, composed of N layers. For such a plate the laminate constitutive equations (2.11) simplify, because $A_{16} = A_{26} = A_{45} = B^k_{16} = B^k_{26} = B^k_{45} = D^{jk}_{16} = D^{jk}_{26} = D^{jk}_{45} = 0$. The remaining coefficientsin the constitutive equations are computed for the N+1 interfaces according to Equations 2.12-15. Then the coefficients corresponding to the midplane interface are eliminated as explained in Section 2.2 and the remaining coefficients are renumbered with j,k = 1,...,N to correspond with the 2N superscripted variables used in Equation (2.30). The governing equations become

$$A_{11}u_{,xx} + A_{12}v_{,yx} + A_{66}(u_{,yy} + v_{,xy})$$

$$+ \sum_{k=1}^{N} [B_{11}^k u_{,xx}^k + B_{12}^k v_{,yx}^k + B_{66}^k (u_{,yy}^k + v_{,xy}^k)] = 0$$

$$A_{66}(u_{,yx} + v_{,xx}) + A_{12}u_{,xy} + A_{22}v_{,yy}$$

$$+ \sum_{k=1}^{N} [B_{66}^k (u_{,yx}^k + v_{,xx}^k) + B_{12}^k u_{,xy}^k + B_{22}^k v_{,yy}^k] = 0$$

$$A_{55}w_{,xx} + A_{44}w_{,yy} + \sum_{k=1}^{N} [B_{55}^k u_{,x}^k + B_{44}^k v_{,y}^k] + q = I_o \ddot{w}$$

$$B_{11}^j u_{,xx} + B_{12}^j v_{,yx} + B_{66}^j (v_{,yy} + v_{,xy}) - B_{55}^j w_{,x}$$

$$+ \sum_{k=1}^{N} [D_{11}^{jk} u_{,xx}^k + D_{12}^{jk} v_{,yx}^k + D_{66}^{jk} (u_{,yy}^k + v_{,xy}^k) - D_{55}^{jk} u^k] = 0$$

$$B_{66}^j (u_{,yx} + v_{,xx}) + B_{12}^j u_{,xy} + B_{22}^j v_{,yy} - B_{44}^j w_{,y}$$

$$+ \sum_{k=1}^{N} [D_{66}^{jk} (u_{,yx}^k + v_{,xx}^k) + D_{12}^{jk} u_{,xy}^k + D_{22}^{jk} v_{,yy}^k - D_{44}^{jk} v^k] = 0 \qquad (2.30)$$

for i,j = 1,2,...,N. These equations are subject to the boundary conditions,

$$v = w = v^k = N_x = N_x^k = 0 \; ; \; x = 0,a \; ; \; k = 1,\ldots,N$$

$$u = w = u^k = N_y = N_y^k = 0 \; ; \; y = 0,b \; ; \; k = 1,\ldots,N. \qquad (2.31)$$

These boundary conditions are identically satisfied by the following expressions for displacements (i.e., Navier's solution procedure is used):

$$u = \sum_{m,n}^{\infty} X_{mn} \cos \alpha x \sin \beta y$$

$$v = \sum_{m,n}^{\infty} Y_{mn} \sin \alpha x \cos \beta y$$

$$w = \sum_{m,n}^{\infty} W_{mn} \sin \alpha x \sin \beta y$$

$$u^k = \sum_{m,n}^{\infty} R^k_{mn} \cos \alpha x \sin \beta y$$

$$v^k = \sum_{m,n}^{\infty} S^k_{mn} \sin \alpha x \cos \beta y \qquad (2.32a)$$

where

$$\alpha = \frac{m\pi}{a} \; ; \; \beta = \frac{n\pi}{b} \; ; \; k = 1,\ldots,N.$$

The transverse load can be expanded in double Fourier series

$$f(x,y) = \sum_{m,n}^{\infty} q_{mn} \sin \alpha x \sin \beta y \qquad (2.32b)$$

Substitution of these expressions into the governing equations gives a system of 2N + 3 equations for each of the Fourier modes (m,n), from which we obtain the coefficients (X_{mn}, Y_{mn}, W_{mn}, R^k_{mn}, S^k_{mn}):

$$\begin{bmatrix} [K] & [K^j] \\ [K^j]^T & [D^{jk}] \end{bmatrix} \begin{Bmatrix} \{\Delta^1\} \\ \{\Delta^2\} \end{Bmatrix} = \begin{Bmatrix} 0 \\ 0 \\ q_{mn} \\ 0 \\ 0 \end{Bmatrix} \qquad (2.33)$$

where $\{\Delta^1\}^T = \{X_{mn}, Y_{mn}, W_{mn}\}$, $\{\Delta^2\}^T = \{R^k_{mn}, S^k_{mn}\}$, and the coefficients $[K]$, $[D^{jk}]$, and $[K^j]$ are given in Appendix 1.

Once the coefficients (X_{mn}, Y_{mn}, W_{mn}, R^k_{mn}, S^k_{mn}) are obtained, the inplane stresses can be computed from the constitutive equations as,

$$\sigma_x(x,y,z) = - \sum_{m,n}^{\infty} \{[Q_{11}\alpha(X_{mn} + \sum_{k=1}^{N} R^k_{mn}\phi^k(z)) + Q_{12}\beta(Y_{mn} + \sum_{k=1}^{N} S^k_{mn}\phi^k(z))]\sin \alpha x \sin \beta y\}$$

$$\sigma_y(x,y,z) = - \sum_{m,n}^{\infty} \{[Q_{12}\alpha(X_{mn} + \sum_{k=1}^{N} R^k_{mn}\phi^k(z)) + Q_{22}\beta(Y_{mn} + \sum_{k=1}^{N} S^k_{mn}\phi^k(z))]\sin \alpha x \sin \beta y\}$$

$$\sigma_{xy}(x,y,z) = Q_{66} \sum_{m,n}^{\infty} \{[\beta(X_{mn} + \sum_{k=1}^{N} R^k_{mn}\phi^k(z)) + \alpha(Y_{mn} + \sum_{k=1}^{N} S^k_{mn}\phi^k(z))]\cos \alpha x \cos \beta y\}. \qquad (2.34)$$

The shear stresses are computed integrating the equilibrium equations of 3-D elasticity through the thickness of each layer and enforcing continuity of stresses along the interfaces:

$$\sigma_{xz}(x,y,z) = \sum_{m,n}^{\infty} [\{[(Q_{11}\alpha^2 + Q_{66}\beta^2)X_{mn} + (Q_{12} + Q_{66})\alpha\beta Y_{mn}]z + \sum_{k=1}^{N} \{[(Q_{11}\alpha^2 + Q_{66}\beta^2)R^k_{mn} + (Q_{12} + Q_{66})\alpha\beta S^k_{mn}]\int \phi^k dz\} + H_i\}\cos \alpha x \sin \beta y]$$

$$\sigma_{yz}(x,y,z) = \sum_{m,n}^{\infty} [\{[(Q_{66} + Q_{12})\alpha\beta X_{mn} + (Q_{66}\alpha^2 + Q_{22}\beta^2)Y_{mn}]z$$

$$+ \sum_{k=1}^{N} \{[(Q_{66} + Q_{12})\alpha\beta R^k_{mn} + (Q_{66}\alpha^2 + Q_{22}\beta^2)S^k_{mn}]\int \phi^k dz\}$$

$$+ G_i\}\sin \alpha x \cos \beta y] \qquad (2.35)$$

where H_i, G_i are constants introduced to satisfy the continuity of stresses.

To assess the quality of the theory we consider a three-ply symmetric laminate, simply supported, and subjected to sinusoidal transverse load. This problem has the 3-D elasticity solution [77] and the classical plate theory (CPT) solution. The high quality of the solutions obtained with this theory can be fully appreciated considering the stress distributions through the thickness for σ_x, σ_y, σ_{xy}, σ_{yz} and σ_{xz} for a/h = 4 (see Figures 2.5-2.9), and a/h = 10 (see Figures 2.10-2.14). The material properties of each ply are:

$$E_1/E_2 = 25.0,\ G_{12} = 0.5\ E_2,\ G_{13} = G_{12},\ G_{23} = 0.2\ E_2$$

$$\nu_{12} = \nu_{13} = 0.25. \qquad (2.36)$$

Using these material properties, the coefficients in the constitutive equations are computed in the example presented in Section 2.2. All stresses are nondimensionalized with respect to the applied load.

The deflection w(x,y) obtained in the present theory coincides with the exact 3-D solution and is not shown here. In all cases the present solutions for stresses are in excellent agreement with the 3-D elasticity solutions, whereas the CPT solutions are considerably in error.

The analytical solutions of the generalized laminate plate theory are presented, and its accuracy is investigated by comparison with the

3-D elasticity theory. The agreement is found to be excellent even for very thick plates. The theory gives accurate interlaminar stress distributions, and should prove to be very useful in the failure analysis of composite laminates.

2.4. Natural Vibrations

The Generalized Laminated Plate Theory (GLPT) has been shown (Section 2.3) to provide excellent predictions of the local response, e.g., interlaminar stresses, inplane displacements and stresses, etc. This is due to the refined representation of the laminated nature of composite plates provided by GLPT and to the consideration of shear deformation effects. The global response of composite laminates with the inclusion of geometrical nonlinearity will be investigated in Chapter 4. Analytical solutions for natural vibrations of cylindrical shells will be presented in Chapter 5. The objective of this section is to investigate the natural vibrations of laminated composite plates using GLPT. Analytical solutions are constructed and compared to exact 3-D elasticity solutions when available. Results are presented for symmetric and unsymmetric cross-ply. The theory is shown to yield accurate predictions of fundamental frequencies compared to the 3-D elasticity solutions.

2.4.1 Formulation

We use the following approximation of the displacements through the thickness of the plate (2.1):

$$u_1(x,y,z) = u(x,y) + \sum_{j=1}^{N} u^j(x,y)\phi^j(z)$$

$$u_2(x,y,z) = v(x,y) + \sum_{j=1}^{N} v^j(x,y)\phi^j(z)$$

$$u_3(x,y,z) = w(x,y)$$

where N is the number of layers, u, v and w are the midplane displacements, u^j and v^j are the displacements at interfaces between layers, relative to the middle surface, and ϕ^j are linear interpolation functions (2.6),

$$\phi^j(z) = \begin{cases} \Psi_2^{j-1}(z) \; ; \; z_{j-1} \le z \le z_j \\ \Psi_1^{j}(z) \; ; \; z_j \le z \le z_{j+1} \end{cases}$$

$$\phi^j(0) = 0 \text{ for all } j = 1,2,\ldots,N.$$

and Ψ_i^j are the local Lagrange linear interpolation functions associated with the i-th node of the j-th layer. In this section we compute the inertia terms,

$$I^0 = \sum_{k=1}^{N} \int_{z_{k-1}}^{z_k} \rho^k dz$$

$$I^i = \sum_{k=1}^{N} \int_{z_{k-1}}^{z_k} \phi^i(z)\rho^k dz \qquad (2.37)$$

$$I^{ij} = \sum_{k=1}^{N} \int_{z_{k-1}}^{z_k} \phi^i(z)\phi^j(z)\rho^k dz$$

If the rotary inertia is neglected we have $I^i = I^{ij} = 0$ for all i,j = 1,...,N. This causes the mass matrix to be not positive definite. The degrees of freedom corresponding to the displacements u^j and v^j can be eliminated to reduce the order of the system and to recover a positive definite mass matrix.

If the inplane inertia is neglected then $I_1^o = I_2^o = 0$ and $I_3^o \neq 0$. The degrees of freedom corresponding to the displacements u and v can be eliminated to further reduce the size of the system and to obtain a positive definite mass matrix.

2.4.2 Numerical Results

The analytical solution of the free vibrations of laminated composite plates using GLPT can be developed for the case of rectangular cross-ply plates subjected to simply supported boundary conditions:

$$v = w = v^j = N_x = N_y^j = 0 \quad \text{at } x = 0,a. \tag{2.38}$$
$$u = w = u^j = N_y = N_x^j = 0 \text{ at } y = 0,b.$$

For this case we have $A_{16} = A_{26} = A_{45} = B_{16}^i = B_{26}^i = B_{45}^i = D_{16}^{ij} = D_{26}^{ij} = D_{45}^{ij} = 0$. Furthermore, the following displacement functions satisfy the boundary conditions and the governing equations (2.9):

$$(u(x,y);u^j(x,y)) = \sum_{m,n=1}^{\infty} (X_{mn};R_{mn}^j)e^{i\omega t} \cos\frac{m\pi x}{a} \sin\frac{m\pi y}{b}$$

$$(v(x,y);v^j(x,y) = \sum_{m,n=1}^{\infty} (Y_{mn};S_{mn}^j)e^{i\omega t} \sin\frac{m\pi x}{a} \cos\frac{m\pi y}{b} \tag{2.39}$$

$$w(x,y) = \sum_{m,n=1}^{\infty} W_{mn}e^{i\omega t} \sin\frac{m\pi x}{a} \sin\frac{m\pi y}{b}$$

Following a standard Navier procedure, the governing differential equations are transformed into an algebraic system for each of the modes (m,n),

$$([K] - \omega_{mn}^2[M])\{x\} = \{0\} \tag{2.40}$$

with

$$\{x_{mn}\}^T = \{X_{mn},Y_{mn},W_{mn},R_{mn}^j,S_{mn}^j\} \tag{2.41}$$

The eigenvalue problem can be solved to obtain the vibration frequencies ω_{mn} and mode shapes $\{\chi_{mn}\}$. The stress components can be computed for any mode shape by using the constitutive equations (2.11). Improved predictions of interlaminar stresses can be obtained using the equilibrium equations (2.35).

Comparison with the exact 3-D solution [79] is presented in Table 2.1 for three-ply laminates with orthotropic layers. The total thickness is $h = h_1 = h_2 = h_3 = 1$. The properties and thicknesses of individual layers are varied to illustrate the effect of the orthotropy in lines 1 to 4. Case 5 represents an unsymmetric laminate for which the inclusion of the inplane displacements and inertias is necessary, as it can be concluded from the results. This is due to the influence of the bending-extension coupling. It can be seen that the GLPT gives results much closer than CPT for all the cases considered. The influence of the shear correction factor is quite small for GLPT, due to the refined representation of the shear strains.

The exact 3-D solution [79] for a three-layer laminate is used in Table 2.2 to illustrate the accuracy of the GLPT solutions for different combinations of Poisson ratio, density ratio and elastic moduli ratio between different layers. All layers are isotropic and they have equal thickness. Analytical solutions of the GLPT for different combinations of shear correction factors and inplane inertias are listed in Table 2.2. Since all laminates considered are symmetric, there is no bending-extension coupling and therefore the inclusion of inplane inertias does not change the results much. As in the previous case, it can be seen that the GLPT results are not significantly affected by the value of the

shear correction factor. Solutions obtained using the finite element model are also reported for comparison. The frequencies predicted by the finite element model (Chapter 3) are slightly larger than the exact ones due to the stiffening effect introduced by the discretization. A 2 x 2 mesh of 9-node elements is used to model a quarter of a plate, with appropriate symmetry boundary conditions [80].

The vibration of ARALL Laminates and Aluminum plates are investigated using GLPT and CPT. ARALL Laminates are described in Section 3.4.5. The effects of rotary and inplane inertia on the vibration of simply-supported rectangular plates is investigated. Numerical results are presented for various values of the aspect ratio a/b and thickness ratio a/h. It can be seen from Table 2.3 that CPT gives closer results for isotropic materials, while larger differences between CPT and GLPT can be observed for ARALL Laminates. This is because the hybrid nature of ARALL is correctly represented in GLPT, while the different materials are smeared out in CPT.

Since ARALL Laminates are symmetric, the inclusion of inplane inertia does not affect the transverse natural frequency. This is because inplane and transverse deflections are uncoupled for symmetric laminates. The results sh own in Tables 2.3, 2.4 and 2.5 can be explained as follows. The frequency ω is related to the stiffness K and mass M by the relation,

$$\omega \sim \sqrt{\frac{K}{M}}$$

The fundamental frequency of an ARALL Laminate depends on the transverse stiffness (i.e. stiffness coefficients D_{22}), which is smaller than the

axial stiffness (i.e. stiffness coefficient D_{11}). Because of the specific construction of ARALL Laminates, it can be established that the following stiffness and mass inequalities hold:

$$K_{al} > K_{21} > K_{32} \; ; \; M_{al} > M_{21} > M_{32}$$

where subscripts 'al', '21' and '32' refer to aluminum, 2/1 Laminates and 3/2 Laminates, respectively. The above inequalities imply the following two cases of inequalities between 2/1 and 3/2 ARALL Laminates:

Case 1: $K_{21}K_{32} > K_{32}M_{21}$

Case 2: $K_{21}M_{32} < K_{32}M_{21}$

Similar inequalities hold for aluminum and 2/1 or 3/2 ARALL Laminates. If Case 1 holds then $\omega_{21} > \omega_{32}$ (i.e., the fundamental frequency of 2/1 Laminates is greater than that of 3/2 Laminates), and if Case 2 holds then $\omega_{21} < \omega_{32}$. Similarly, if we replace K_{32} and M_{32} by K_{al} and M_{al}, we arrive at the inequalities

$\omega_{21} > \omega_{al}$, when Case 1 holds

$\omega_{21} < \omega_{al}$, when Case 2 holds.

In the present study Case 1 is valid for thin laminates (i.e. $a/h \geq 20$) and Case 2 is valid for thick laminates (i.e., $a/h < 20$). For thick laminates, while mass remains the same as for thin laminates, the stiffness is reduced due to transverse shear deformation. Of course Case 2 holds in the classical plate theory for all side-to-thickness ratios. Tables 2.4 and 2.5 show that the differences between the

results of GLPT and CPT are more evident as the aspect ratios a/b increases. From the results it is evident that ARALL Laminates exhibit lower fundamental frequencies than Aluminum plates for moderate to large thickness ratios (i.e. a/h < 20). This is because the reduced flexural rigidity, due to the presence of layers with low shear moduli, outweighs the effect of the slightly lower density of ARALL Laminates. For large thickness ratios (i.e., a/h > 20), both effects cancel out, and the aluminum plates, 3/2 and 2/1 Laminates exhibit increasingly large frequencies.

In order to investigate the accuracy of CPT compared to GLPT in predicting natural frequencies other than the fundamental we present results for several values of the Fourier modes (n: mode number along the fiber direction, and m: mode number across the fiber direction). To investigate the effects of the material properties we consider ARALL 2/1 in Table 2.6, ARALL 3/2 in Table 2.7 and an Aluminum plate in Table 2.8. It can be seen that the difference between GLPT and CPT reduces as the thickness ratio a/h becomes large but significant differences persist over a broader range of thickness ratio for the higher modes. This can be attributed to the fact that shear deformation effects remain significant for the higher modes having a similar effect as the reduction of the thickness ratio. As it can be seen comparing Tables 2.6 to 2.8, the differences between GLPT and CPT are more pronounced for Hybrid Laminates than for isotropic plates.

Appendix 1

Coefficients of the matrices in Equation (2.33)

$$K_{11} = - A_{11}\alpha^2 - A_{66}\beta^2$$

$$K_{12} = -(A_{12} + A_{66})\alpha\beta \; ; \; k_{21} = k_{12}$$

$$K_{22} = -A_{22}\beta^2 - A_{66}\alpha^2 \; ; \; k_{13} = k_{31} = 0$$

$$K_{33} = -A_{44}\beta^2 - A_{55}\alpha^2 \; ; \; k_{23} = k_{32} = 0$$

$$K^j_{11} = -B^j_{11}\alpha^2 - B^j_{66}\beta^2$$

$$K^j_{12} = -(B^j_{12} + B^j_{66})\alpha\beta \; ; \; k^j_{21} = k^j_{12}$$

$$K^j_{22} = -B^j_{22}\beta^2 - B^j_{66}\alpha^2$$

$$K^j_{31} = -B^j_{55}\alpha$$

$$K^j_{32} = -B^j_{44}\beta$$

$$D^{jk}_{11} = -D^{jk}_{55} - D^{jk}_{11}\alpha^2 - D^{jk}_{66}\beta^2$$

$$D^{jk}_{12} = -(D^{jk}_{12} + D^{jk}_{66})\alpha\beta \; ; \; D_{21} = D_{12}$$

$$D^{jk}_{22} = -D^{jk}_{44} - D^{jk}_{22}\beta^2 - D^{jk}_{66}\alpha^2$$

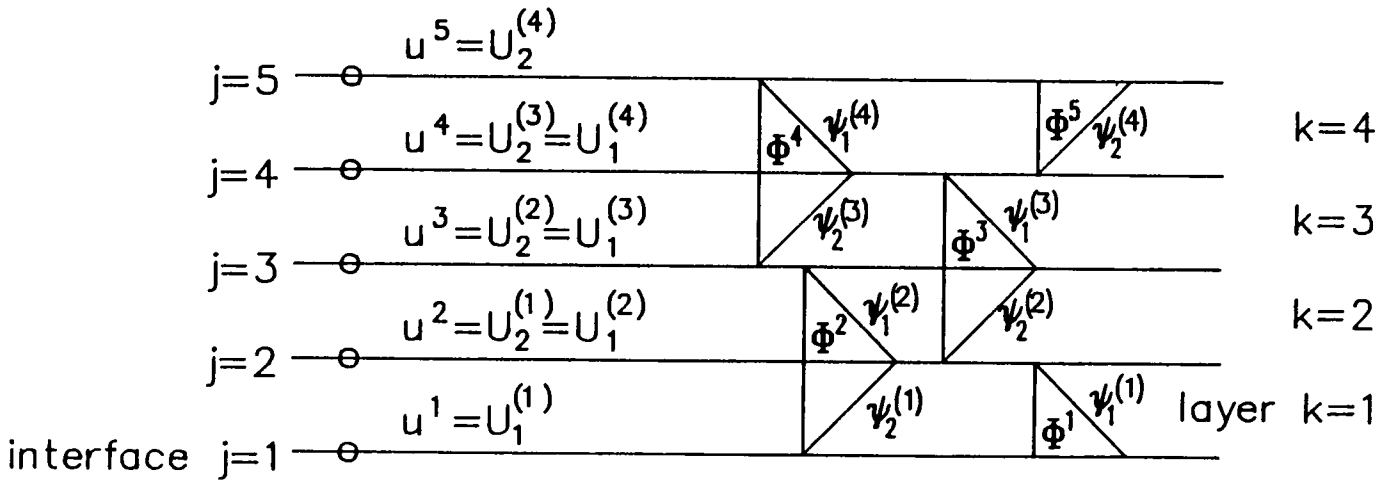

2.1 Variables and interpolation functions before elimination of the midplane quantities.

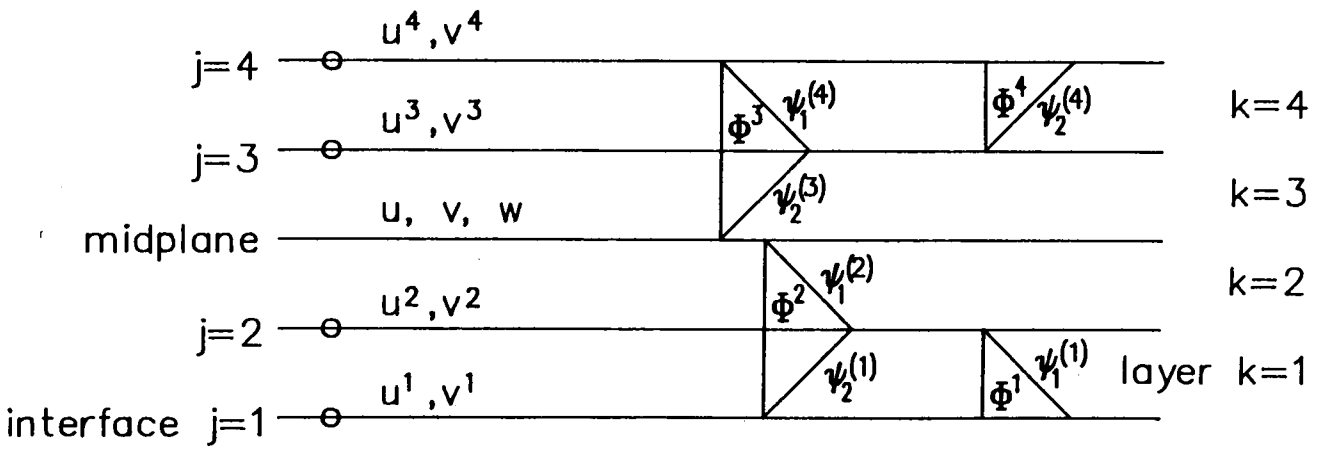

2.2 Variables and interpolation functions after elimination of the midplane quantities.

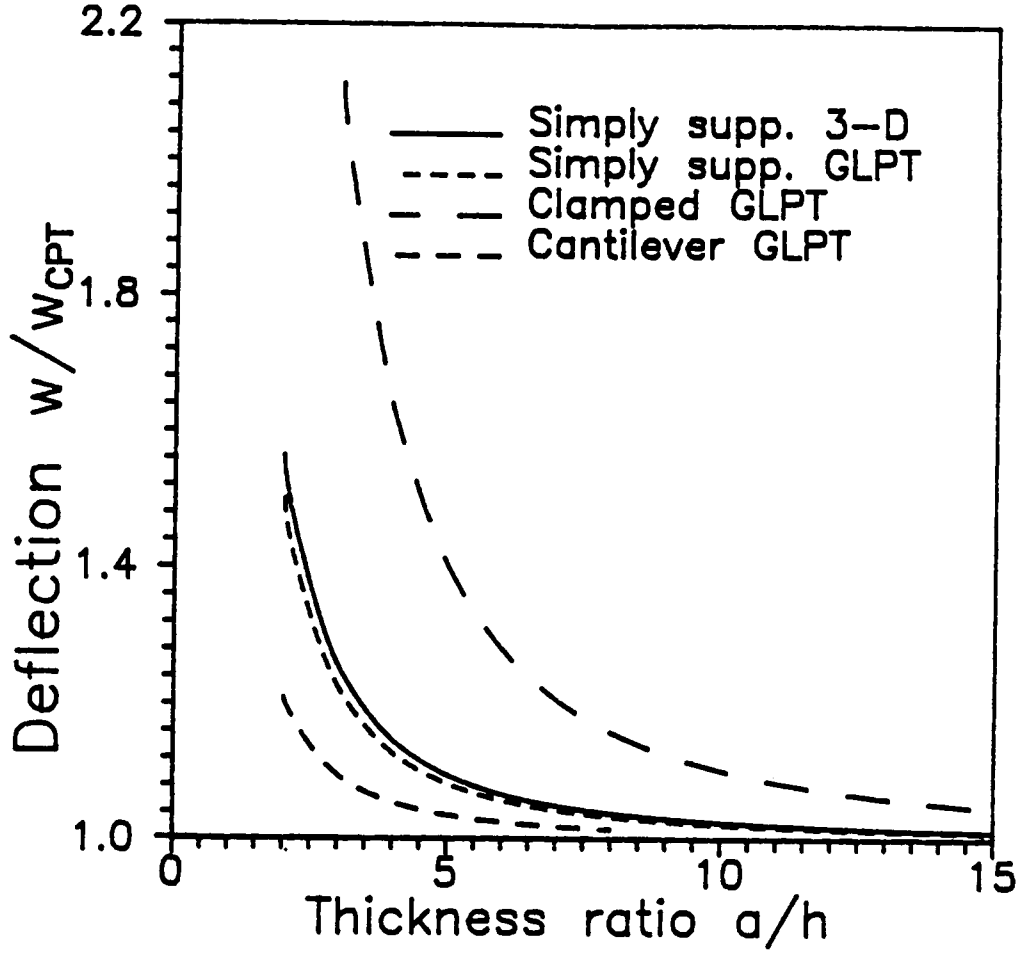

2.3 Normalized maximum deflection versus side to thickness ratio for an isotropic plate strip under uniform transverse load.

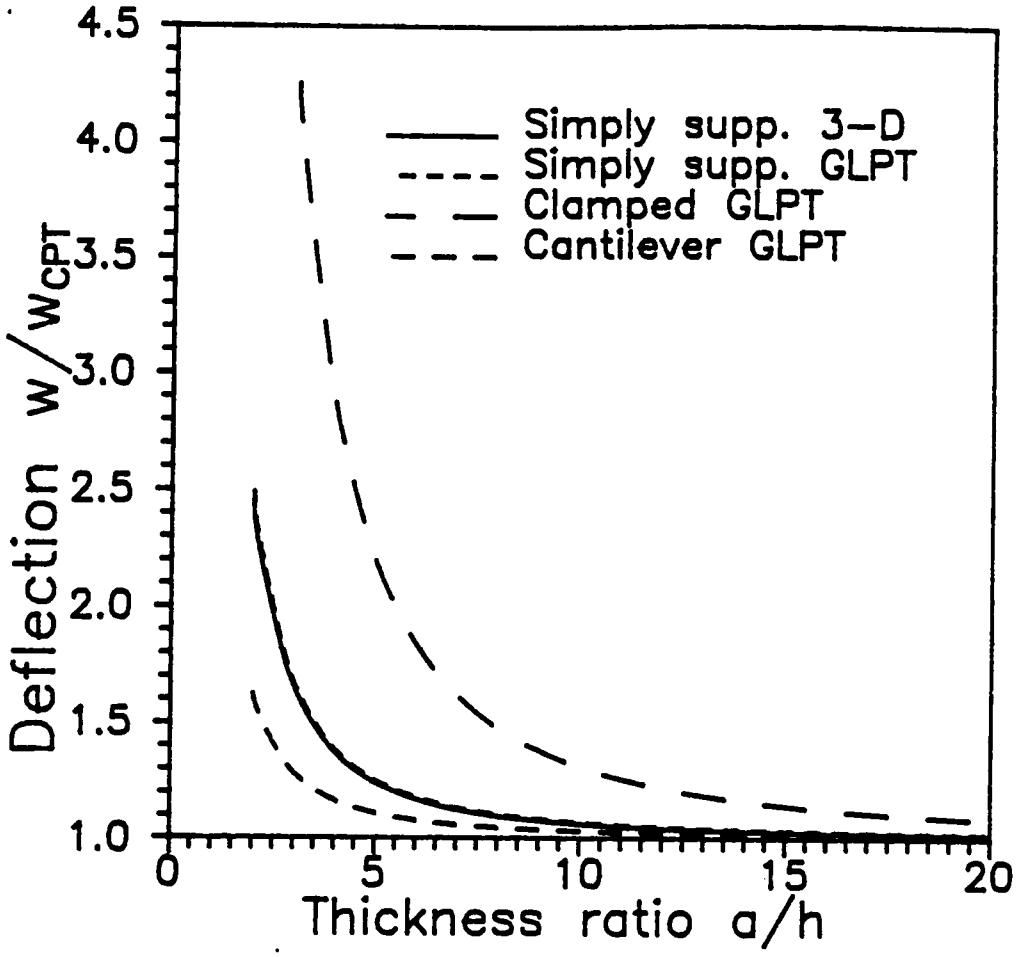

2.4 Normalized maximum deflection versus side to thickness ratio for two-layer cross-ply plate strip under uniform transverse load.

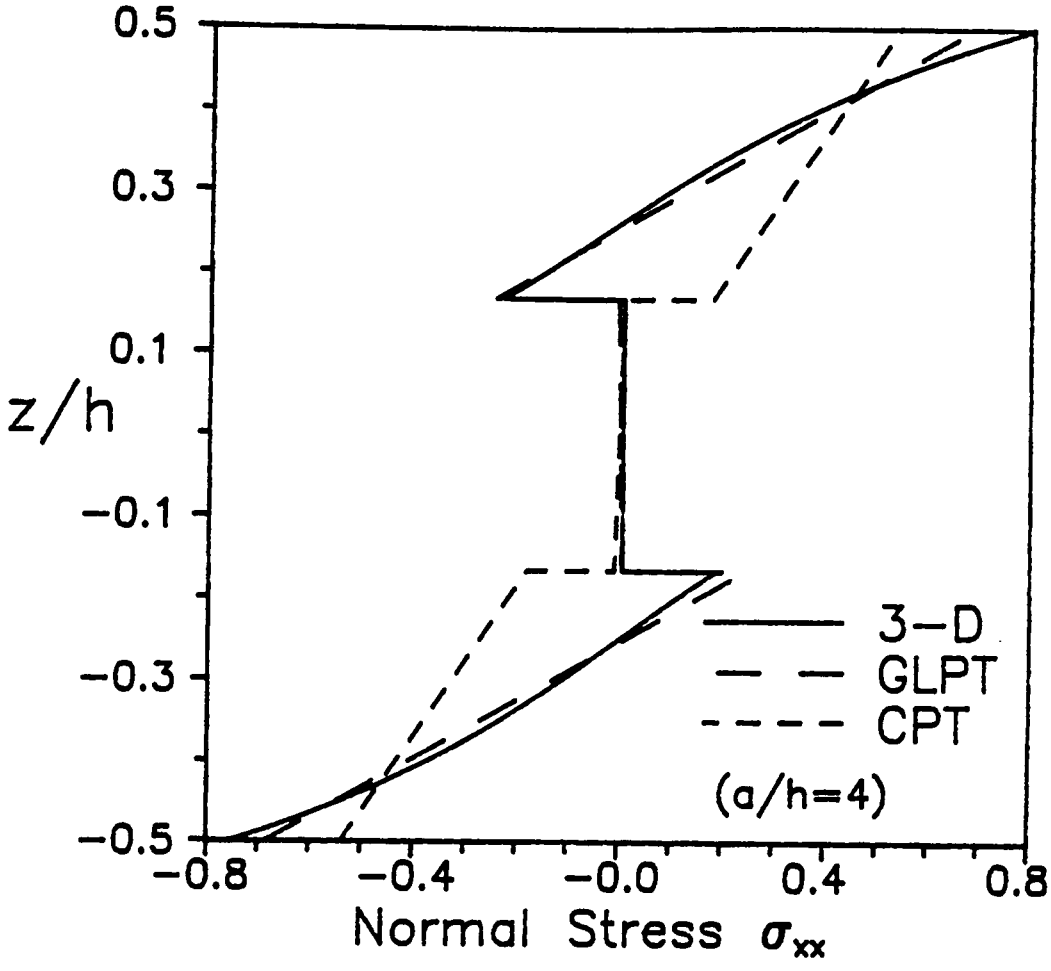

2.5 Variation of the axial stress through the thickness of three-layer cross-ply (0/90/0) laminate under sinusoidal varying transverse load.

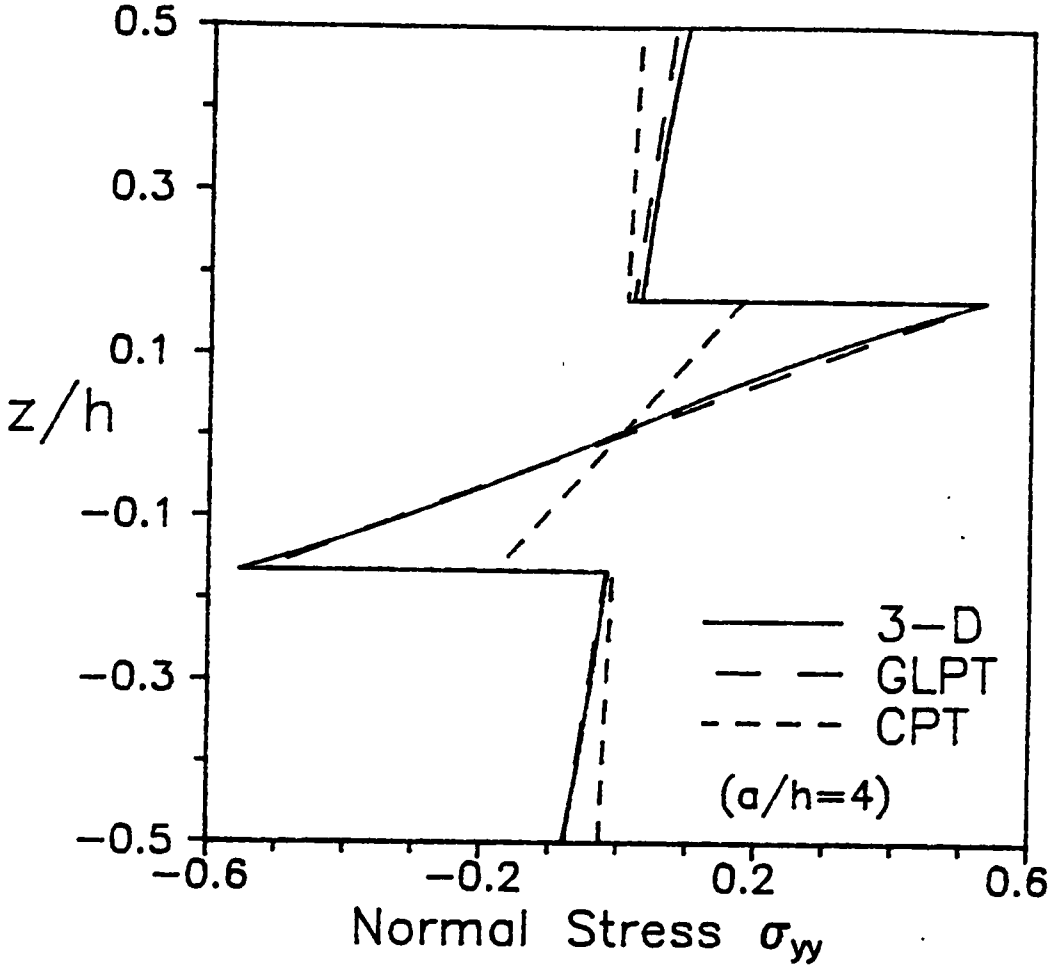

2.6 Variation of the axial stress through the thickness of a three-layer cross-ply (0/90/0) laminate under sinusoidal transverse load.

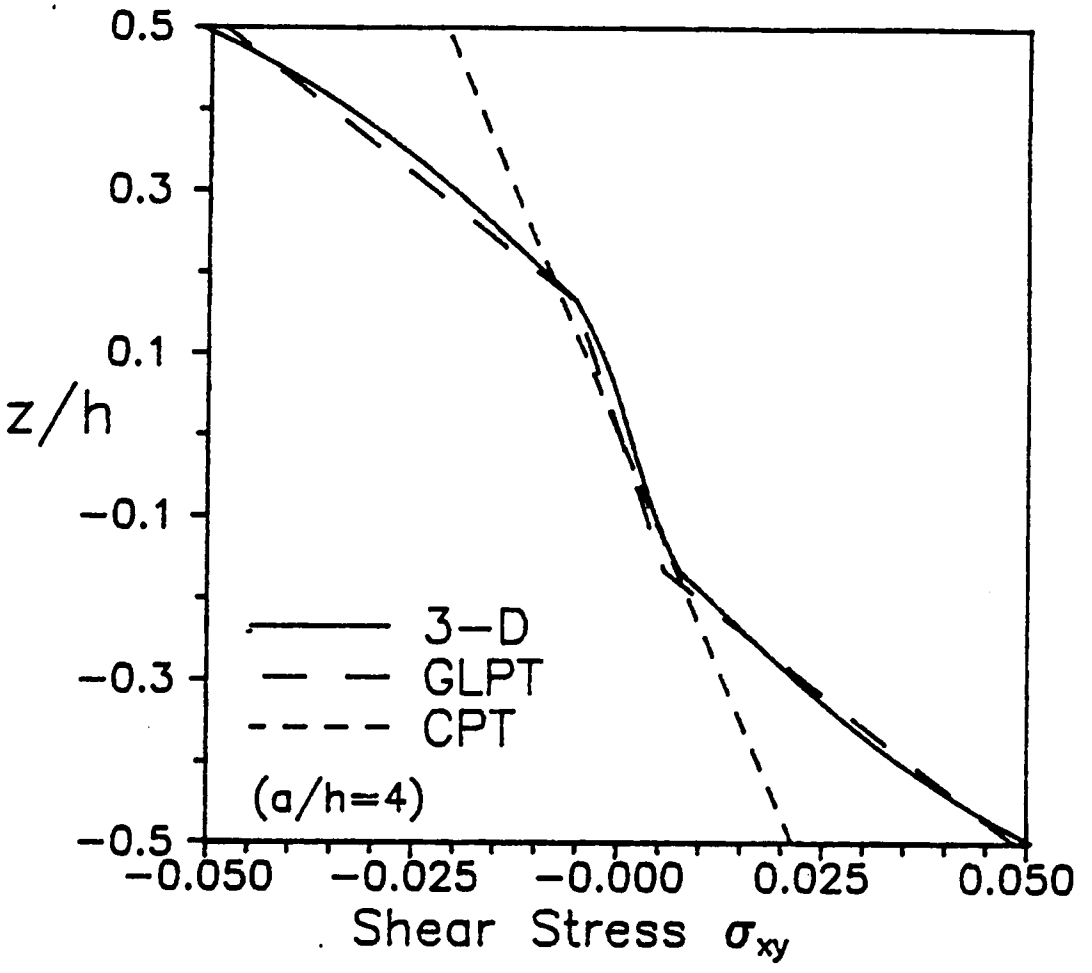

2.7 Variation of the shear stress σ_{xy} through the thickness of a three-layer cross-ply (0/90/0) laminate under sinusoidal transverse load.

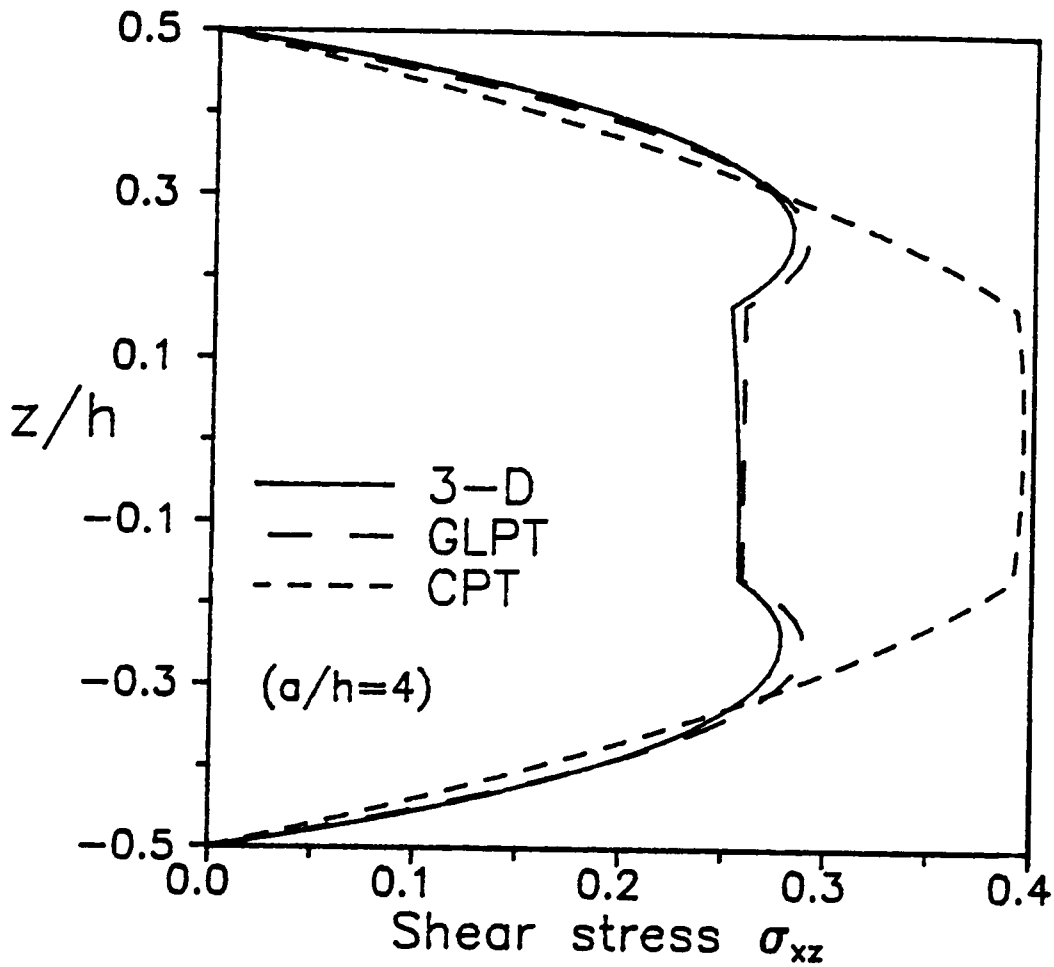

2.8 Variation of the transverse shear stress through the thickness of a three-layer cross-ply (0/90/0) laminate under sinusoidal transverse load.

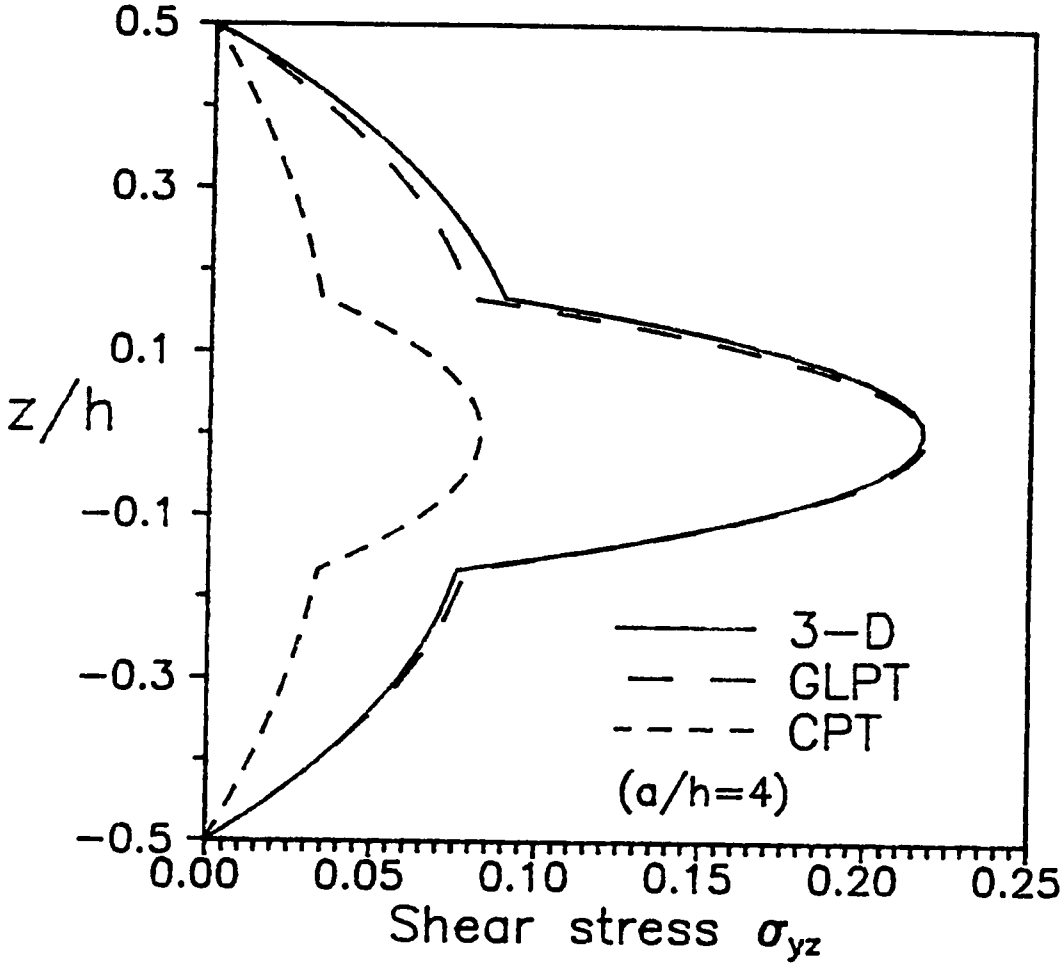

2.9 Variation of transverse shear stress σ_{yz} through the thickness of a three-layer cross-ply (0/90/0) laminate under sinusoidal transverse load.

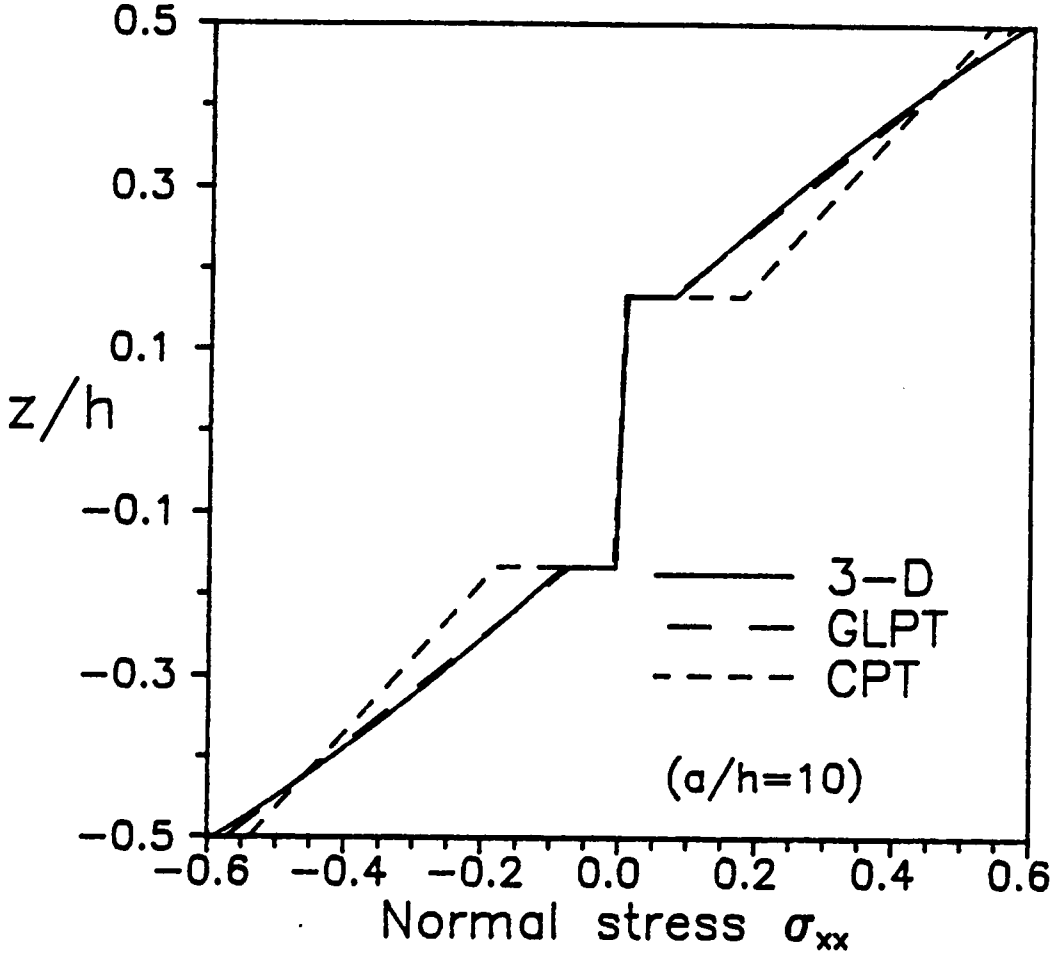

2.10 Variation of the normal stress σ_{xx} through the thickness of a three-layer cross-ply (0/90/0) laminate under sinusoidal transverse load.

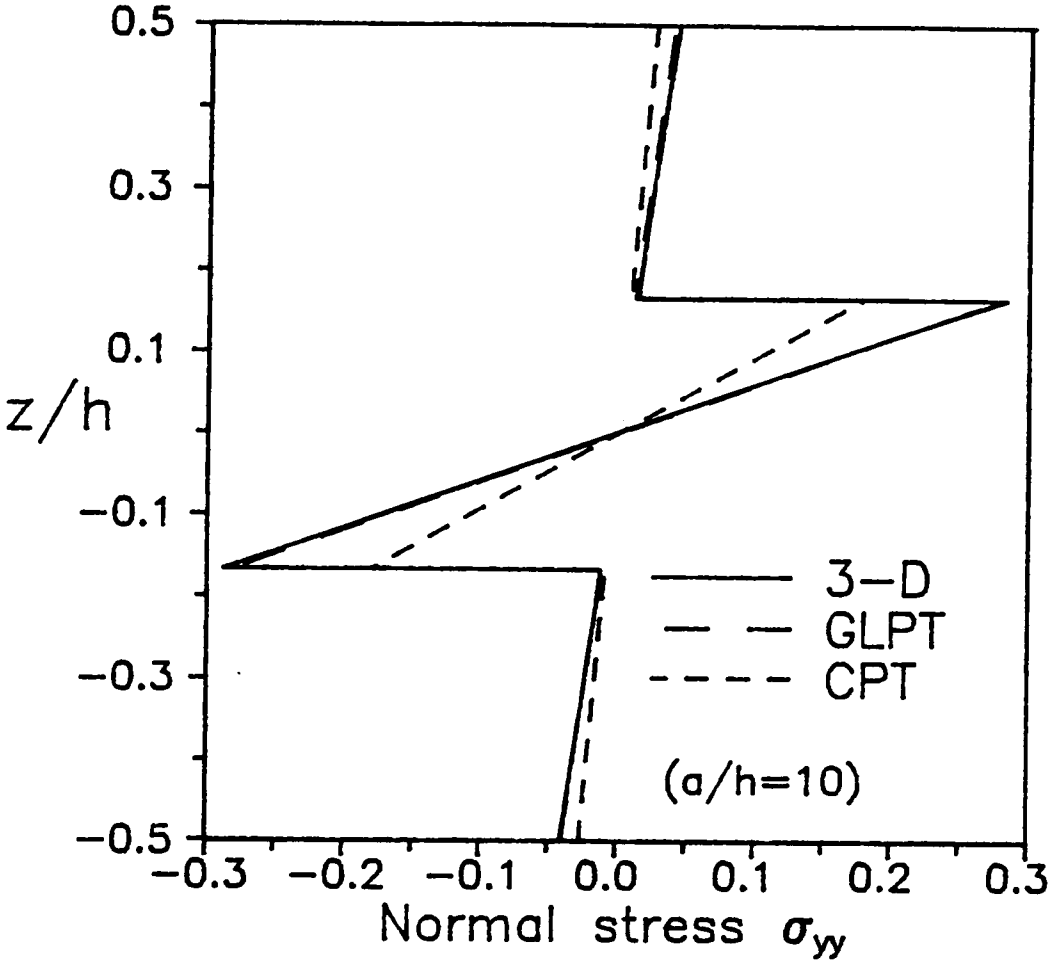

2.11 Variation of the normal stress σ_{yy} through the thickness of a three-layer cross-ply (0/90/0) laminate under sinusoidal transverse load.

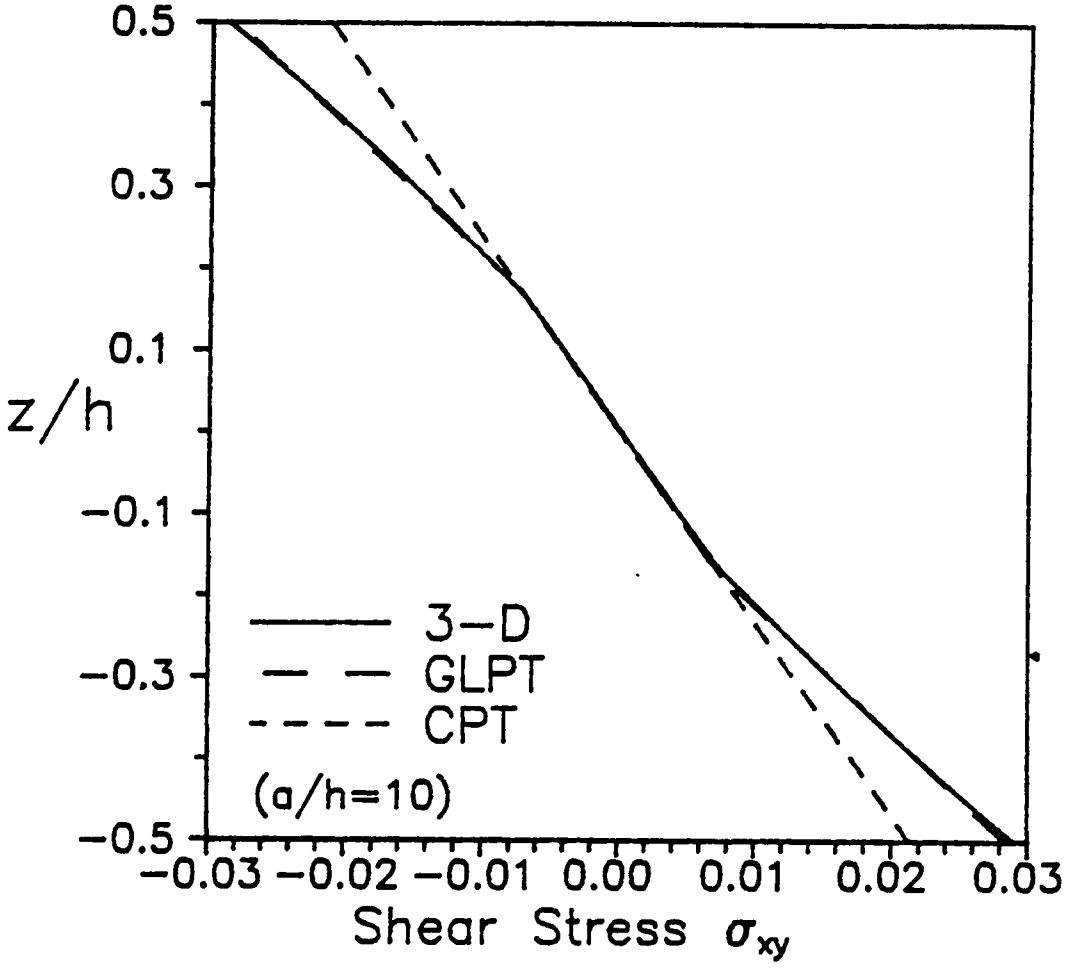

2.12 Variation of the shear stress σ_{xy} through the thickness of a three-layer cross-ply laminate under sinusoidal transverse load.

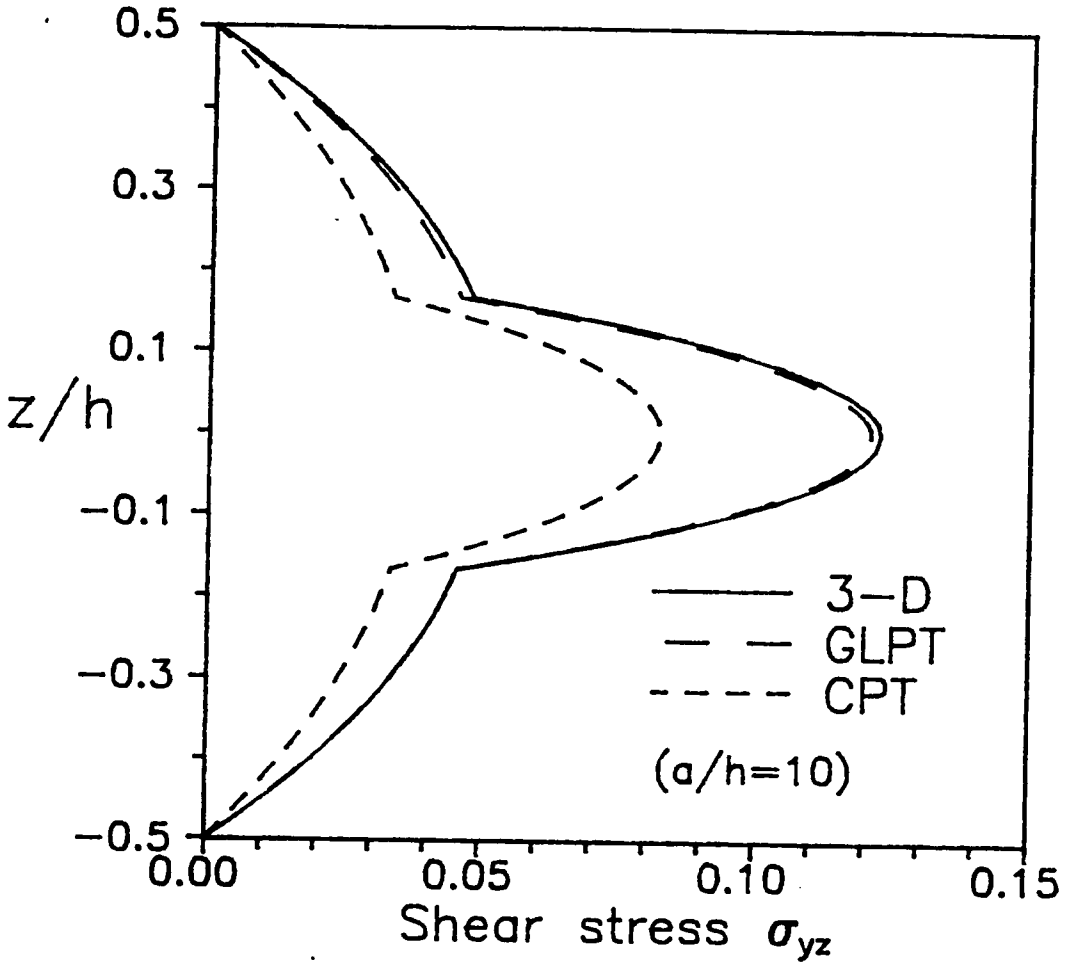

2.13 Variation of the transverse shear stress σ_{yz} through the thickness of a three-layer cross-ply laminate under sinusoidal transverse load.

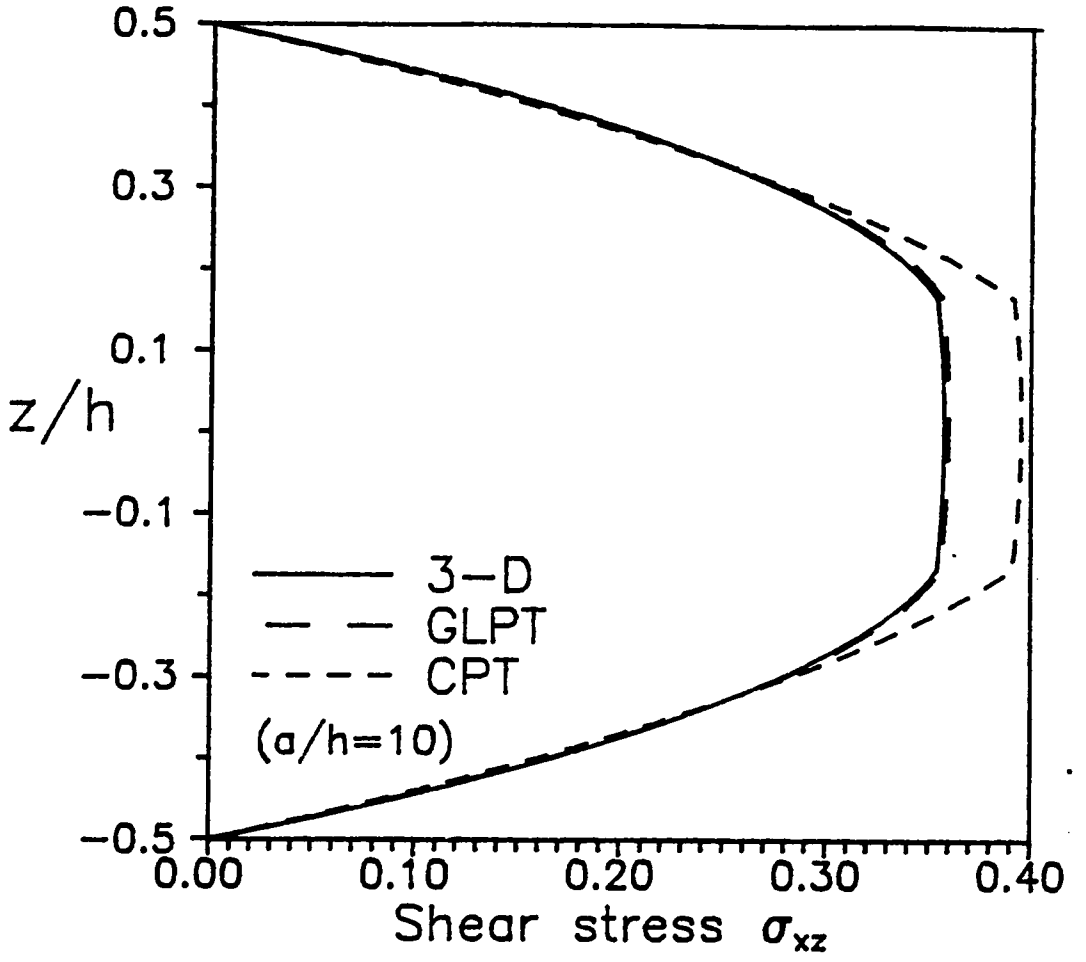

2.14 Variation of the transverse shear stress σ_{xz} through the thickness of a three-layer cross-ply laminate under sinusoidal transverse load.

Table 2.1 Fundamental frequency $\bar{\omega} = \omega h \sqrt{\rho/C_{66}(2)}$ for three-ply orthotropic laminate.

h_1/h	h_3/h	CPT $C_{66}(1)$ $C_{66}(2)$	CPT $C_{66}(3)$ $C_{66}(2)$	CPT $k^2=\pi^2/12$ IPI=yes	Exact 3-D	GLPT $k^2=\pi^2 12$ IPI=yes	GLPT $k^2=\pi^2/12$ IPI=no	GLPT $k^2=1$ IPI=yes	GLPT $k^2=1$ IPI=no
0.1	0.1	1	1	0.09686	0.09248	0.09198	0.09198	0.09267	0.92670
0.1	0.1	10	10	0.22491	0.19132	0.18647	0.18647	0.19160	0.19160
0.1	0.1	50	50	0.47951	0.29954	0.28341	0.28341	0.30060	0.30060
0.1	0.1	50	10	0.29305	0.23166	0.22360	0.23975	0.23211	0.25189
0.1	0.3	10	10	0.24736	0.21052	0.20519	0.21295	0.21095	0.21938

$C_{11} = 3.802$; $C_{12} = 0.879$; $C_{22} = 1.996$; $C_{44} = 1.05$; $C_{55} = 0.608$; $C_{66} = 1.0$;

$a/b = 1$; $a/h = 10$; IPI = inplane inertia included.

Table 2.2 Fundamental Eigenvalue $\bar{\omega} = \omega h\sqrt{\rho(2)/G(2)}$ for three-ply isotropic laminate.

ρ_1/ρ_1	ν_1	G_1/G_2	CPT $k^2=\pi^2/12$ IPI=yes	Exact 3-D	GLPT $k^2=\pi^2/12$ IPI=yes	GLPT $k^2=\pi^2/12$ IPI=no	GLPT $k^2=1$ IPI=yes	GLPT $k^2=1$ IPI=no	FEM $k^2=1$ IPI=yes
1	0.3	1	0.07705	0.07452	0.07415	0.07468	0.07454	0.07509	0.07458
1	0.3	2	0.09399	0.08998	0.08933	0.08994	0.08999	0.09062	0.09000
1	0.3	5	0.13239	0.12307	0.12146	0.12218	0.12305	0.12382	0.12300
1	0.3	15	0.21564	0.18366	0.17861	0.17928	0.18362	0.18440	0.18372
2	0.3	15	0.19685	0.16757	0.16290	0.16366	0.16744	0.16834	0.16753
3	0.3	15	0.18225	0.15508	0.15870	0.15152	0.15491	0.15585	0.15498
1	0.2	1	0.07466	0.07229	0.07264	0.07326	0.07311	0.07365	0.07237

$\rho_1 = \rho_3$; $G_1 = G_3$; $\nu_1 = \nu_3$; $\nu_2 = 0.3$; $h_1 = h_3 = 0.1h$; $a/b = 1$; $a/h = 10$;

IPI = inplane inertia included.

Table 2.3 Fundamental Frequency $\bar{\omega} = \omega \frac{ab}{h} \sqrt{\frac{\rho_{AL}}{E_{AL}}}$ for a/b = 1.

a/h	Theory	Rotary Inertia	Inplane Inertia	AL	ARALL 2/1	ARALL 3/2
10	GLPT	yes	yes	5.84530	5.06894	5.10272
		no	yes	5.88853	5.08869	5.12564
		yes	no	5.84530	5.06894	5.10272
		no	no	5.8853	5.08869	5.12564
	CPT	no	no	6.04287	6.32473	6.07226
5	GLPT	yes	yes	5.36859	3.70444	3.78094
		no	yes	5.48859	3.72641	3.80310
		yes	no	5.36859	3.70444	3.78094
		no	no	5.48859	3.72641	3.80310
	CPT	no	no	6.04287	6.32473	6.07226
20	GLPT	yes	yes	5.99115	5.90821	5.77432
		no	yes	6.00313	5.91849	5.78481
		yes	no	5.99115	5.90821	5.77432
		no	no	6.00313	5.91849	5.78481
	CPT	no	no	6.04287	6.32473	6.07226
50	GLPT	yes	yes	6.03448	6.25107	6.02150
		no	yes	6.03646	6.25324	6.02356
		yes	no	6.03448	6.25107	6.02150
		no	no	6.03646	6.25324	6.02356
	CPT	no	no	6.04287	6.32473	6.07226
100	GLPT	yes	yes	6.04077	6.30603	6.05974
		no	yes	6.04126	6.30660	6.06027
		yes	no	6.04077	6.30603	6.05974
		no	no	6.04126	6.30660	6.06027
	CPT	no	no	6.04287	6.32473	6.07226

Table 2.4 Fundamental Frequency $\bar{\omega} = \omega \frac{ab}{h} \sqrt{\frac{\rho_{Al}}{E_{Al}}}$ for a/b = 2

a/h	Theory	Rotary Inertia	Al	ARAL 2/1	ARAL 3/2
5	GLPT	yes	5.89692	3.58746	3.49686
	GLPT	no	6.10834	3.62144	3.51801
	CPT	no	7.55369	7.903253	7.49241
10	GLPT	yes	6.98593	5.22132	5.30423
	GLPT	no	7.09747	5.24796	5.33507
	CPT	no	7.55369	7.903253	7.49241
20	GLPT	yes	7.39581	6.78216	6.67933
	GLPT	no	7.43135	6.80344	6.70291
	CPT	no	7.55369	7.903253	7.49241
50	GLPT	yes	7.52759	7.67882	7.34018
	GLPT	no	7.53371	7.68505	7.34617
	CPT	no	7.55369	7.903253	7.49241
100	GLPT	yes	7.54714	7.34499	7.45338
	GLPT	no	7.54869	7.84672	7.45499
	CPT	no	7.55369	7.903253	7.49241

Table 2.5: Fundamental Frequency $\bar{\omega} = \omega \frac{ab}{h} \sqrt{\frac{\rho_{Al}}{E_{Al}}}$ for a/b = 5

a/h	Theory	Rotary Inertia	Al	ARALL 2/1	ARALL 3/2
	GLPT	yes	7.8585	4.9407	4.1486
5	GLPT	no	7.8525	2.8837	4.2060
	CPT	no	15.7120	16.4380	15.5454
	GLPT	yes	11.6442	6.9430	6.6198
10	GLPT	no	15.0222	7.0256	6.6620
	CPT	no	15.7120	16.4380	15.5454
	GLPT	yes	14.2346	10.1474	10.2947
20	GLPT	no	14.5105	10.2031	10.3555
	CPT	no	15.7120	16.4380	15.5353
	GLPT	yes	15.4370	14.4124	14.0980
50	GLPT	no	15.4994	14.4533	14.1423
	CPT	no	15.7120	16.4380	15.5454
	GLPT	yes	15.6415	15.8379	15.1381
100	GLPT	no	15.6580	15.8541	15.1538
	CPT	no	15.71201	16.4380	15.5454

Table 2.6: Natural Frequencies $\omega_{mn} = \frac{ab}{h}\sqrt{\frac{\rho_{AL}}{E_{AL}}}$ for ARALL 2/1 with a/b = 1, using GLPT, compared to CPT.

a/h	m=1 n=1	m=1 n=2	m=1 n=3	m=2 n=1	m=2 n=2	m=2 n=3	m=3 n=1	m=3 n=2	m=3 n=3
CPT	6.33	15.80	31.61	15.82	25.30	41.10	31.65	41.13	56.92
5	3.70	7.17	11.96	7.22	10.16	14.60	12.07	14.67	18.74
10	5.07	10.44	17.37	10.48	14.82	21.03	17.49	21.10	26.65
20	5.91	13.56	24.31	13.59	20.27	30.00	24.40	30.06	38.64
50	6.25	15.38	29.90	15.38	24.19	38.29	29.95	38.33	51.78
100	6.31	15.69	31.15	15.71	25.00	40.33	31.20	40.36	55.47

Table 2.7: Natural Frequencies $\omega_{mn} = \omega_{mn} \frac{ab}{h} \sqrt{\frac{\rho}{E_{AL}}}$ for ARALL 3/2 with a/b = 1, using GLPT, compared to CPT.

a/h	m=1 n=1	m=1 n=2	m=1 n=3	m=2 n=1	m=2 n=2	m=2 n=3	m=3 n=1	m=3 n=2	m=3 n=3
CPT	6.07	14.98	29.91	15.54	24.29	39.10	31.38	40.02	54.65
5	3.78	6.99	10.96	7.10	9.56	13.07	11.17	13.18	16.29
10	5.10	10.61	17.52	10.85	15.12	21.06	17.94	21.29	26.29
20	5.77	13.36	24.35	13.77	20.41	30.35	25.22	30.84	39.50
50	6.02	14.68	28.73	15.20	23.50	37.13	30.06	37.94	50.92
100	6.06	14.91	29.60	15.45	24.08	38.57	31.03	39.46	53.64

Table 2.8: Natural frequencies $\omega_{mn} = \omega_{mn} \frac{ab}{h} \sqrt{\frac{\rho}{E_{AL}}}$ for aluminum plates with a/b = 1 using GLPT, compared to CPT

a/h	m=1 n=1	m=1 n=2	m=1 n=3	m=2 n=1	m=2 n=2	m=2 n=3	m=3 n=1	m=3 n=2	m=3 n=3
CPT	6.04	15.11	30.21	15.11	24.17	39.28	30.21	39.28	54.39
5	5.37	11.79	20.24	11.79	24.17	24.50	20.24	24.50	30.76
10	5.84	13.97	26.19	13.97	21.47	32.90	26.19	32.90	43.27
20	5.99	14.79	29.00	14.79	23.38	37.27	29.00	37.27	50.65
50	6.03	15.05	30.00	15.05	24.04	38.93	30.00	38.93	53.72
100	6.04	15.09	30.16	15.09	24.14	39.19	30.16	39.19	54.22

Chapter 3

A PLATE BENDING ELEMENT BASED ON A GENERALIZED LAMINATE PLATE THEORY

3.1 Introduction

Laminated composite plates are often modelled using the classical laminate plate theory (CLPT) or the first-order shear deformation plate theory (FSDT). In both cases the laminate is treated as a single-layer plate with equivalent stiffnesses, and the displacements are assumed to vary through the thickness according to a single expression [17], not allowing for possible discontinuities in strains at an interface of dissimilar material layers.

The generalized laminate plate theory allows layerwise representation of inplane displacements, and an improved response of inplane and transverse shear deformations. In the generalized laminate plate theory (GLPT) the equations of three-dimensional elasticity are reduced to differential equations in terms of unknown functions in two dimensions by assuming layer-wise approximation of the displacements through the thickness. Consequently, the strains are different in different layers. Exact analytical solutions of the theory are developed in Chapter 2 to evaluate the accuracy of the theory compared to the 3-D elasticity theory. The results indicated that the generalized laminate plate theory allows accurate determination of interlaminar stresses.

This chapter deals with the finite-element formulation of the theory and its application to laminated composite plates. The accuracy

of the numerical results obtained using the present plate element are discussed in light of the exact solutions of the theory.

3.2 Finite-Element Formulation

The generalized displacements (u,v,w,u^j,v^j) are expressed, over each element, as a linear combination of the two-dimensional interpolation functions ψ_i and the nodal values $(u_i,v_i,w_i,u_i^j,v_i^j)$ as follows:

$$(u,v,w,u^j,v^j) = \sum_{i=1}^{m} (u_i,v_i,w_i,u_i^j,v_i^j)\psi_i \tag{3.1}$$

where m is the number of nodes per element.

Using Eq. (1), the strains can be expressed in the form

$$\{e\} = [B_L]\{\Delta\}, \quad \{e^j\} = [\overline{B}_L]\{\Delta^j\} \tag{3.2a}$$

where

$$\{\Delta\} = \begin{Bmatrix} \{u\} \\ \{v\} \\ \{w\} \end{Bmatrix}, \quad \{\Delta^j\} = \begin{Bmatrix} \{u^j\} \\ \{v^j\} \end{Bmatrix}, \tag{3.2b}$$

The matrices $[B_L]$ and $[\overline{B}_L]$ are given in Appendix 2 along with the strain vectors $\{e\}$ and $\{e^j\}$. The constitutive equations of the laminate are given by:

$$\begin{aligned} \{N\} &= [A]\{e\} + \sum_{k=1}^{N} [B^k]\{e^k\} \\ \{N^j\} &= [B^j]\{e\} + \sum_{k=1}^{N} [D^{jk}]\{e^k\} \end{aligned} \tag{3.3}$$

where the constitutive matrices are given in equation (2.11b). The coefficients in the constitutive matrices should be computed as explained in Section 2.2.

Using Eqs. (3.1) in the virtual work statement (2.7), we obtain the finite element model

$$\begin{bmatrix} [k^{11}] & [k_1^{12}] & \cdots & [k_N^{12}] \\ [k_1^{21}] & [k_{11}^{22}] & \cdots & \cdot \\ \cdot & & \cdots & \cdot \\ \cdot & & \cdots & \cdot \\ [k_N^{21}] & & \cdots & [k_{NN}^{22}] \end{bmatrix} \begin{Bmatrix} \{\Delta\} \\ \{\Delta^1\} \\ \cdot \\ \cdot \\ \{\Delta N\} \end{Bmatrix} = \begin{Bmatrix} \{q\} \\ \{0\} \\ 0 \\ 0 \\ \{0\} \end{Bmatrix} \tag{3.4a}$$

where the submatrices $[k^{11}]$, $[k_j^{12}]$, $[k_i^{21}]$ and $[k_y^{22}]$ are given by coefficients in the stiffness matrix equation (3.4)

$$[k^{11}] = \sum_e \int_{\Omega_e} [B_L]^T [A][B_L] d\Omega_e$$

$$[k_i^{12}] = [k_i^{21}] = \sum_e \int_{\Omega_e} [B_L]^T [B^j][B_L] d\Omega_e$$

$$[k_{ij}^{22}] = \sum_e \int_{\Omega_e} [\bar{B}_L]^T [D^{ij}][\bar{B}_L] d\Omega_e \tag{3.4b}$$

3.3 Interlaminar Stress Calculation

When a piecewise linear interpolation through the thickness is used, GLPT provides an excellent representation of the displacements, and accurate prediction of the in plane stresses ($\sigma_{xx}, \sigma_{yy}, \sigma_{xy}$) as was demonstrated in Chapter 2. Interlaminar stresses ($\sigma_{xz}, \sigma_{yz}, \sigma_{zz}$) can be computed, as was done in Chapter 2, from the equilibrium equations of 3D-elasticity when exact analytical solutions are available. An approximate technique is used in this study to integrate the equilibrium equations, using the inplane stress information provided by the finite element solution. The scheme as presented in [81] is

extended here to quadrilateral isoparametric elements. It approximates the shear stress distribution through each layer with a quadratic function, thus requiring 3n equations for each of the shear stresses (σ_{xz},σ_{yz}), where n is the number of layers; n equations are used to satisfy the n average shear stresses on each layer. Two equations are used to impose vanishing shear stresses at the surfaces of the plate. Then, (n - 1) equations are employed to satisfy continuity of the shear stresses at the interfaces between layers. Finally, the remaining (n - 1) equations are used to compute the jump in $\sigma_{xz,z}$ (or $\sigma_{yz,z}$) at each interface.

The average shear stresses on each layer are computed from the constitutive equations and the displacement field obtained in the finite-element analysis.

In this work, unlike Reference 81, the equilibrium equations

$$\begin{aligned} \sigma_{xz,z} &= -(\sigma_{xx,x} + \sigma_{xy,y}) \\ \sigma_{yz,z} &= -(\sigma_{xy,x} + \sigma_{yy,y}) \end{aligned} \tag{3.5}$$

are used to compute $\sigma_{xz,z}$ and $\sigma_{yz,z}$ directly from the finite-element approximation. The in-plane components of the stresses and their in-plane derivatives ($\sigma_{xx,x}$;$\sigma_{yy,y}$;$\sigma_{xy,x}$ and $\sigma_{xy,y}$) are computed from the constitutive equations for each layer, i.e.,

$$\begin{Bmatrix} \sigma_x \\ \sigma_y \\ \sigma_{xy} \end{Bmatrix} = \begin{bmatrix} Q_{11} & Q_{12} & Q_{13} \\ Q_{12} & Q_{22} & Q_{23} \\ Q_{13} & Q_{23} & Q_{33} \end{bmatrix} \begin{Bmatrix} \frac{\partial u}{\partial x} + \sum_{j=1}^{N} \frac{\partial u_j}{\partial x} \psi^j \\ \frac{\partial v}{\partial x} + \sum_{j=1}^{N} \frac{\partial v_j}{\partial x} \psi^j \\ \frac{\partial u}{\partial y} + \frac{\partial v}{\partial x} + \sum_{j=1}^{N} \left(\frac{\partial u_j}{\partial y} + \frac{\partial v_j}{\partial x}\right) \psi^j \end{Bmatrix} \tag{3.6}$$

The procedure thus requires computation of second derivatives of the displacements (u,v,u_j,v_j) as presented in Appendix 3.

3.4 Numerical Examples

Several numerical examples are presented to assess the quality of the finite element model and to display the features of the GLPT in the modeling of laminated composite plates. Whenever possible, comparison is made with 3D-elasticity solutions. Two problems of bending of composite laminates that can be analytically solved using the full 3D-elasticity equations are the cylindrical bending of cross-ply plates and the bending of simply-supported plates. The cylindrical bending problem is one in which one of the planar dimensions of the plate is much larger (in theory, of infinite length along the y-axis) than the other. The generalized plane-strain conditions prevail, and it is sufficient to consider only a unit width along the y-axis. The problem is then reduced to a one-dimensional beam problem. Only certain symmetric laminates can be analyzed in cylindrical bending because other lamination schemes would violate the generalized plane-strain condition.

Analytical solutions to the 3D-equations of elasticity for cylindrical bending exist for simply-supported boundary conditions [76]. Analytical solutions to the 3D-equations of elasticity for square plates also exist for simply-supported, cross-ply laminates [77]. For more general cases that do not admit analytical solutions to the 3D-elasticity equations, we can still compare the finite element solutions to closed form solutions of GLPT developed in Chapter 2. Navier type

solutions were presented in Chapter 2 for square plates and cylindrical bending. Since the Navier technique is restricted to simply-supported boundary conditions, closed-form solutions for cylindrical bending (using eigenvalue expansions [78]) that admit any combination of boundary conditions were developed in Chapter 2. Comparisons to other theories like the classical laminated plate theory are presented to demonstrate the accuracy of the new theory.

3.4.1 Cylindrical Bending of a (0/90) Plate Strip

Transverse deflections, normalized with respect to the classical laminated-plate theory solution, are plotted in Figure 3.1 for a (0/90) laminated-plate in cylindrical bending. The material properties used are those of graphite-epoxy:

$$E_1 = 19.2 \times 10^6 \text{ psi}, \; E_2 = 1.56 \times 10^6 \text{ psi},$$
$$G_{12} = G_{13} = 0.82 \times 10^6 \text{ psi},$$
$$G_{23} = 0.523 \times 10 \text{ psi}, \; \nu_{12} = \nu_{13} = 0.24,$$
$$\nu_{23} = 0.49. \tag{3.7}$$

A uniform load and three different boundary conditions were used (SS = simply supported at both ends, CC = clamped at both ends and CT = cantilever). The 3D elasticity solution [76] for the simply supported case and the closed form solutions of GLPT from Chapter 2 for the three types of boundary conditions are plotted for comparison. Five elements are used to represent one-half of the plate for the SS and CC cases, taking advantage of the symmetry of the problem and 10 elements are used for the CT case, which has no symmetry. Very good agreement is found between the finite-element solution and the exact solutions.

3.4.2 Cylindrical Bending of a (0/90/0) Plate Strip

A long, cross-ply (0/90/0) laminated plate (a/h = 4), simply-supported along the long edges and subjected to sinusoidal load is analyzed. The plate can be analyzed using any strip along the length. The underlying assumption is that every line along the length deforms into the same shape (called cylindrical bending). The problem becomes essentially one-dimensional (e.g., beam).

The material properties used are

$$E_1 = 25 \times 10^6 \text{ psi}, \; E_2 = 10^6 \text{ psi},$$

$$G_{12} = G_{13} = 0.5 \times 10^6 \text{ psi},$$

$$G_{23} = 0.2 \times 10^6 \text{ psi}, \; \nu_{12} = \nu_{13} = \nu_{23} = 0.25. \tag{3.8}$$

The displacements and stresses are normalized as follows:

$$\bar{u} = \frac{100E_2}{q_0 h s^3} u \; , \; \bar{w} = \frac{100E_2}{q_0 h s^4} w$$

$$\bar{\sigma}_{xz} = \frac{1}{s q_0} \sigma_{xz} \; , \; \bar{\sigma}_{xx} = \frac{1}{q_0} \sigma_{xx} \; , \tag{3.9}$$

where s = a/h, a = width and h = total thickness of the plate. Both one-dimensional and two-dimensional elements were used in this example, imposing the appropriate boundary conditions on the plate elements to simulate the generalized plane-strain (i.e., cylindrical bending) condition. Under these conditions, both elements gave exactly the same results.

Eight four-node linear elements were used to represent one-half of the span. Comparisons with the 3D elasticity solution are made in Figures 3.2 to 3.4. Through-the-thickness distributions of the in plane

displacements u obtained by various theories are shown in Figure 3.2. The GLPT solution is in excellent agreement with the 3D elasticity solution, whereas the CLPT solution is in considerable error. The inplane normal stress σ_{xx} computed in the CLPT (see Figure 3.3) differs even in sign at the interface of laminae.

Eight nine-node quadratic elements are used to obtain the through-the-thickness distribution of shear stress σ_{xz} from the equilibrium equations, and the result is shown in Figure 3.4. Note that the 3D elasticity solution is slightly unsymmetric because the load applied at the top surface is unsymmetric about the midplane, while the GLPT solution is symmetric because the load is assumed to be applied at the midplane, as is the case with all plate theories.

3.4.3 Cross-ply Laminates

Sinusoidal Load. Consider a simple supported (0/90/0) square laminate under sinusoidal load. This example is chosen because there exists an exact 3D elasticity solution [77]. The material properties used are the same as those used in Section 3.4.2 Due to symmetry (geometric as well as material), only one quarter of the laminate is modelled using a 4 x 4 uniform mesh of quadratic elements. A coordinate system with the origin at the center of the plate is used for reference. The simply-supported boundary conditions used are the same as those used to obtain the 3D elasticity solution:

$$w = u = u^j = 0 \text{ at } y = \pm a/2$$

$$w = v = v^j = 0 \text{ at } x = \pm a/2$$

The following normalizations of stresses are used in presenting the

results:

$$(\bar{u},\bar{v}) = \frac{100E_2}{q_o h s^3}(u,v)\ ,\ \bar{w} = \frac{100E_2}{q_o h s^4} w\ ,\ (\bar{\sigma}_{xz},\bar{\sigma}_{yz}) = \frac{1}{q_o s}(\sigma_{xz},\sigma_{yz})\ ,$$

$$(\bar{\sigma}_{xx},\bar{\sigma}_{yy},\bar{\sigma}_{xy}) = \frac{1}{q_o s^2}(\sigma_{xx},\sigma_{yy},\sigma_{xy}) \qquad (3.10)$$

where s = a/h, a is the length of the square plate and h is the thickness of the plate. The stresses were computed at the following locations, which are the center points of the elements:

$$\sigma_{xx}(\tfrac{a}{16}, \tfrac{a}{16}),\ \sigma_{yy}(\tfrac{a}{16}, \tfrac{a}{16}) \text{ and } \sigma_{xy}(\tfrac{7a}{16}, \tfrac{7a}{16}). \qquad (3.11)$$

The stress distributions through laminate thickness are shown in Figures 3.5-3.7 for s = 4. The quality of the GLPT solution and the accuracy of the finite-element solutions are apparent from the figures.

Uniform Load. Next we consider the case of a simply-supported [0/90/0] plate under uniformly distributed transverse load. The material properties used are those of a graphite-epoxy material given in Eq. (3.7). The plate is simply-supported on all four sides. Due to symmetry, only a quarter of the plate is modelled. The appropriate boundary conditions for a simply-supported cross-ply laminate, with symmetry axes along x = 0 and y = 0, are:

on x = 0: $u = u^j = 0$

on y = 0: $v = v^j = 0$

on x = a: $v = w = v^j = 0$

on y = b: $u = w = u^j = 0$ (3.12)

The through-the-thickness distribution of the inplane normal stress σ_{xx}, for aspect ratio a/h = 10, is shown in Figure 3.8. The

stresses were computed at the Gauss point x = 0.0528a and y = 0.0528a. Figures 3.9 and 3.10 contain similar plots of the interlaminar shear stresses σ_{yz} and σ_{xz}, respectively. In Figure 3.9, σ_{yz} is computed at the point x = 0.0528a and y = 0.9472a, in Figure 3.10, σ_{xz} is computed at the point x = 0.9472a and y = 0.0528a. In these plots, broken lines represent stresses obtained from the constitutive equations, while the smooth solid line represents the stress distribution obtained using the equilibrium equations. Stresses obtained using the GLPT and FSDT are compared in these figures. In this case, the GLPT admits an analytical solution; the finite element solution agrees with the analytical solution. The stress components predicted by the GLPT are in close agreement with the 3D elasticity solution. The differences between the stresses computed in the FSDT and GLPT theories are significant for a/h = 10, but the difference reduces as the a/h ratio increases.

3.4.4 Angle-ply Laminates

While the inplane stresses obtained using FSDT and GLPT in a cross-ply plate are reasonably close, the stresses differ significantly for an antisymmetric angle-ply laminate. This is illustrated in this example. Consider the case of an anti-symmetric angle-ply (45/-45/45/-45) plate under uniformly distributed transverse load. The material properties are the same as those in the previous example.

The plate is simply-supported on all four sides. Due to symmetry, only a quarter of the plate is modelled. The appropriate boundary conditions for a simply-supported antisymmetric angle-ply rectangular laminate, with symmetry axes at x = 0 and y = 0, are:

$$\text{on } x = 0: \quad v = u^j = 0$$

$$\text{on } y = 0: \quad u = v^j = 0$$

$$\text{on } x = a: \quad v = w = v^j = 0$$

$$\text{on } y = b: \quad u = w = u^j = 0 \tag{3.13}$$

Figures 3.11 and 3.12 contain plots of through-the-thickness distribution of the inplane stresses σ_{xx} and σ_{xy}, respectively, for aspect ratio a/h = 10. Both figures correspond to the Gauss point x = y = 0.0528a. The shear correction factors used for the FSDT and GLPT are 1.0. The difference between the stresses computed by the FSDT and GLPT still persist, however reduced, even for thin laminates. For example, Figure 3.13 contains a plot of σ_{xx} for aspect ratio a/h = 50.

Figures 3.14 and 3.15 contain plots of σ_{xz} through the thickness of the same laminate at x = 0.9472a, y = 0.0528a for aspect ratios of 10 and 100. The results show striking differences between FSDT and GLPT. The difference does not vanish as the aspect ratio grows. It can be seen that the nondimensional shear stress distribution predicted by the FSDT remains almost unchanged as the aspect ratio is changed from 10 to 100. The reason for the difference can be attributed to the GLPT's ability to accurately predict interlaminar stresses, even at the free edge.

Figure 3.16 contains a plot of the nondimensional maximum transverse deflection w as a function of the aspect ratio of the plate. The difference between the two theories can be attributed to the different representation of the shear deformation. In this case the shear correction factor used in both theories is one. It is well known that the FSDT requires a shear correction factor smaller than one to

produce the correct transverse deflection. Convergence of the stresses provided by the FEM solution to the analytical solution of Chapter 2 can be inferred from Figure 3.17, where the maximum value of σ_{xx}, normalized with respect to the analytical solution, is shown for different discretizations. Convergence results for both linear and quadratic elements are shown. The convergence of linear elements is almost as fast as the convergence of quadratic elements, but only quadratic elements can be used to compute interlaminar shear stresses (see Section 3.3).

The generalized laminate theory yields accurate results for both displacements and stresses. The applicability of the GLPT element to problems with dissimilar materials and problems without analytical solutions is demonstrated. While the GLPT plate bending element is computationally expensive compared to the FSDT plate element (or the Mindlin plate element), it yields very accurate results for all stresses and it is less expensive compared to a three-dimensional finite element analysis of laminated composite plates.

3.4.5 Bending of ARALL 2/1 and 3/2 Hybrid Composites

In this section, the application of the GLPT element to a class of hybrid composite laminates is demonstrated. ARALL is a hybrid laminate in which layers of Aramid-Epoxy are placed between Aluminum layers. The designations 2/1 and 3/2 correspond to (Al/Ar/Al) and (Al/Ar/Al/Ar/Al), respectively. Each Aramid layer is modelled as three layers. The middle layer represents the fiber-rich part of the Aramid layer, and the layers on either side represent resin-rich parts that bond the Aramid

fiber to the Aluminum layer. In this study, aluminum layers are taken to be 0.03048 mm thick, fiber-rich layers 0.0144 mm thick and resin-rich layers 0.0072 mm thick. Thus, ARALL 2/1 is modelled as a six-layer laminate $(A\ell/resin/Ar)_s$. ARALL 3/2 is modelled using 10 layers $(A\ell/resin/Ar/resin/A\ell)_s$.

The material properties used are,

Aluminum:

$$E = 10.4 \times 10^6 \text{ psi}, \quad \nu = 0.333 \tag{3.14a}$$

Resin rich Aramid:

$$E_1 = 2.1976 \times 10^6 \text{ psi}, \quad E_2 = 4.8219 \times 10^5 \text{ psi},$$
$$G_{12} = 1.5717 \times 10^5 \text{ psi}, \quad G_{23} = 1.5576 \times 10^5 \text{ psi}$$
$$\nu_{12} = 0.3749, \quad \nu_{23} = 0.5479 \tag{3.14b}$$

Fiber rich Aramid:

$$E_1 = 1.2549 \times 10^7 \text{ psi}, \quad E_2 = 7.6525 \times 10^5 \text{ psi}$$
$$G_{12} = 2.8955 \times 10^5 \text{ psi}, \quad G_{23} = 2.6462 \times 10^5 \text{ psi}$$
$$\nu_{12} = 0.3458, \quad \nu_{23} = 0.4459 \tag{3.14c}$$

A simply-supported square-plate under uniform load is considered. Due to symmetry only a quarter (upper right quadrant) of the plate is modelled using the 4 by 4 mesh of eight-node isoparametric elements (see Figure 3.23). The simply supported boundary conditions used are:

$$w(0,y) = w(a,y) = v(0,y) = v(a,y) = v^j(0,y) = v^j(a,y) = 0$$
$$w(x,0) = w(x,b) = u(x,0) = u(x,b) = u^j(x,0) = u^j(x,b) = 0 \tag{3.15a}$$

The symmetry along the centerline implies that,

$$u(a/2,y) = u^j(a/2,y) = 0$$
$$v(x,b/2) = v^j(x,b/2) = 0 \tag{3.15b}$$

where $j = 1,\ldots,N$, and N is the number of layers in the laminate.

Both inplane and interlaminar shear stresses can be computed using either the constitutive equations or equilibrium equations. Inplane stresses are linear in each layer and they approximate closely the exact solution. Interlaminar shear stresses are constant in each layer, their values being approximately the average of the exact solution. It is also possible to obtain the actual distribution of interlaminar shear stresses by a postprocessing algorithm (see Section 3.3) if the solution is obtained using quadratic elements.

For all cases the stresses are presented as a function of the nondimensional thickness z/h. The results shown correspond to values at the Gauss points closest to the points where the solution has a maximum, i.e., $\sigma_{xx}(\alpha,\alpha,z)$, $\sigma_{yy}(\alpha,\alpha z)$, $\sigma_{xy}(\beta,\beta,z)$, $\sigma_{xz}(\beta,\alpha,z)$, $\sigma_{yz}(\alpha,\beta,z)$, with $\alpha = 0.526\ a$ and $\beta = 0.973\ a$. The following nondimensionalizations are used:

$$(\bar{\sigma}_x, \bar{\sigma}_y, \bar{\sigma}_{xy}) = (\sigma_x, \sigma_y, \sigma_{xy}) \frac{1}{qs^2}$$

$$(\bar{\sigma}_{yz}, \bar{\sigma}_{xz}) = (\sigma_{yz}, \sigma_{xz}) \frac{1}{qs}$$

$$\bar{w} = \frac{100E_{A\ell}}{qhs^4} w, \tag{3.16}$$

where q is the intensity of the uniform transverse load.

From the distribution of interlaminar transverse shear stresses (Figures 3.18 and 3.19), we can observe that the maximum occurs in the aluminum layers, either at the outer layers for ARALL 2/1 or at the center layer for ARALL 3/2. This may be an advantageous factor because the matrix material has low strength in shear. The first-order shear deformation theory (FSDT) predicts even lower shear stresses at the

Aramid layers because unlike GLPT, FSDT does not account for variable shear strain through the thickness. For hybrid composites like ARALL, the shear strain distribution is not a constant, contrary to the assumption made in FSDT. Therefore, large shear strains do occur in the more compliant Aramid layers, thus relaxing the shear stresses through the laminate. However, shear stresses do not reach high values in the compliant layers due to the low shear modulus of the Aramid. As a result, an optimization with respect to shear failure can be accomplished by the use of compliant layers.

The transverse shear stress σ_{xz} computed from equilibrium equations (continuous curves in Figure 3.20) and those computed from constitutive equations (discontinuous lines in Figure 3.20) are compared in Figure 3.20. Quadratic elements are used to obtain both stress fields. Of course, to obtain the transverse shear stresses from the constitutive equations one can even use linear finite elements. Figure 3.21 contains a comparison of σ_{xz} computed from the constitutive equations using linear finite elements with that obtained using equilibrium equations using quadratic elements. It is observed that the discontinuous stress fields computed from the constitutive equations agree very closely with those computed from equilibrium at the center of each layer.

The maximum transverse deflections versus side to thickness ratio are shown in Figure 3.22. Distributions through the thickness of the inplane normal stresses are shown in Figures 3.23 to 3.25. The deflections obtained by the FSDT are lower than those predicted by the GLPT. In general, the GLPT gives a more flexible model than the FSDT

because GLPT accounts for the different behavior of stiff and compliant layers.

3.4.6 Influence of the Boudary Conditions on the Bending of ARALL 3/2

Four different boundary conditions, called SS1, SS2, SS3 and SS4 are used to represent a simply supported boundary of a square ARALL 3/2 plate under uniform transverse load. For simplicity, the Aramid layers are represented by a simgle layer with the properties of the fiber-rich material. Consequently the ARALL 3/2 is modelled as a 6 layer assembly, where the Aluminum middle layer is represented as two layers, one above and one below the middle surface. For all cases, the same symmetry boundary conditions are applied along the x- and y-axis. On the boundary of the plate, the following boundary conditions are used:

SS1: $w(x, \frac{a}{2}) = w(\frac{a}{2}, y) = 0$

SS2: $u(x, \frac{a}{2}) = w(x, \frac{a}{2}) = 0$

$v(\frac{a}{2}, y) = w(\frac{a}{2}, y) = 0$

SS3: $u^j(x, \frac{a}{2}) = w(x, \frac{a}{2}) = 0$

$v^j(\frac{a}{2}, y) = w(\frac{a}{2}, y) = 0$

SS4: $u(x, \frac{a}{2}) = u^j(x, \frac{a}{2}) = w(x, \frac{a}{2}) = 0$

$v(\frac{a}{2}, y) = v^j(\frac{a}{2}, y) = w(\frac{a}{2}, y) = 0$

In Figures 3.26 to 3.30 we plot the distribution through the thickness of the stresses σ_x, σ_y, σ_{xy}, and σ_{xz} and σ_{yz}. It can be seen that the

influence of the boundary conditions is minimal. In particular, note that the results are not affected by constraining the inplane displacements u = v = 0. This is because the inplane displacements (u,v) do not play an important role in the linear analysis of symmetric laminates, such as ARALL 3/2.

3.5 Natural Vibrations

The Generalized Laminated Plate Theory (GLPT) has been shown in Chapter 2 to provide excellent predictions of the local response, e.g., interlaminar stresses, inplane displacements and stresses, etc. This is due to the refined representation of the laminated nature of composite plates provided by GLPT and to the consideration of shear deformation effects. The global response of composite laminates with the inclusion of geometrical nonlinearity will be investigated in Chapter 4. Analytical solutions for natural vibrations of plates were presented in Section 2.4. The objective of this section is to investigate the natural vibrations of laminated composite plates using GLPT. Results are presented for symmetric and unsymmetric cross-ply and angle-ply laminates. The effects of symmetry boundary conditions, lamination angle, orthotropy and thickness ratio are investigated. The theory and associated finite element model are shown to yield accurate predictions of fundamental frequencies compared to the 3-D elasticity solutions.

3.5.1 Formulation

The approximation of the displacements through the thickness of the plate was given in Section 2.1. The form of the variational statement used to derive the finite element model, and the corresponding Euler-

Lagrange equations and boundary conditions, can be found in Section 2.2. The finite element model can be found in Section 3.2 for the static linear case, and in Section 4.3 for the static nonlinear case. In this section we compute the inertia terms,

$$I^0 = \sum_{k=1}^{N} \int_{z_{k-1}}^{z_k} \rho^k dz$$

$$I^i = \sum_{k=1}^{N} \int_{z_{k-1}}^{z_k} \phi^i(z)\rho^k dz$$

$$I^{ij} = \sum_{k=1}^{N} \int_{z_{k-1}}^{z_k} \phi^i(z)\phi^j(z)\rho^k dz$$

In the finite element model the generalized displacements (u,v,w,u^j,v^j) are expressed over each element as a linear combination of the two-dimensional interpolation functions ψ_i as follows:

$$(u,v,w,u^j,v^j) = \sum_{i=1}^{m} (u_i,v_i,w_i,u_i^j,v_i^j)\psi_i$$

where m is the number of nodes per element. The finite element model advanced in Section 3.2 is complemented here by the mass matrix to give,

$$\{[K] - \omega^2[M]\}\{\delta\} = \{0\} \tag{3.17}$$

with

$$[M] = \begin{bmatrix} [m^{11}] & [m_1^{12}] & \cdots & [m_N^{12}] \\ [m_1^{21}] & [m_{11}^{22}] & \cdots & \cdot \\ \cdot & \cdot & \cdots & \cdot \\ \cdot & \cdot & \cdots & \cdot \\ \cdot & \cdot & \cdots & \cdot \\ [m_N^{21}] & \cdot & \cdots & [m_{NN}^{22}] \end{bmatrix}; \quad \{\delta\} = \begin{Bmatrix} \{\Delta\} \\ \{\Delta^1\} \\ \cdot \\ \cdot \\ \cdot \\ \{\Delta^N\} \end{Bmatrix} \tag{3.18}$$

and

$$\{\Delta\}^T = \{u_1, v_1, w_1, \ldots, u_m, v_m, w_m\}$$

$$\{\Delta^j\}^T = \{u_1^j, v_1^j, \ldots, u_m^j, v_m^j\}$$

$$[m^{11}] = \sum_e \int_{\Omega_e} I^o [H]^T [H] dA_e$$

$$[m_i^{12}] = [m_i^{21}]^T = \sum_e \int_{\Omega_e} I^i [H]^T [H] dA_e \qquad (3.19)$$

$$[m_{ij}^{22}] = \sum_e \int_{\Omega_e} I^{ij} [H]^T [H] dA_e$$

with

$$(u, v, w, u^j, v^j) = [H]\{\delta\} \qquad (3.20)$$

If the rotary inertia is neglected we have $I^i = I^{ij} = 0$ for all $i,j = 1,\ldots,N$. This causes the mass matrix to be not positive definite. The degrees of freedom corresponding to the displacements u^j and v^j can be eliminated at the element level to reduce the order of the system and to recover a positive definite mass matrix.

If the inplane inertia is neglected, then $I_1^o = I_2^o = 0$ and $I_3^o \neq 0$. The degrees of freedom corresponding to the displacements u and v can be eliminated to further reduce the size of the system and to obtain a positive definite mass matrix.

3.5.2 Numerical Examples

Cross-Ply Plates. To study the influence of the number of layers and the degree of orthotropy on the accuracy of the GLPT, a comparison is presented in Tables 3.1 and 3.2 with the 3-D solution [82] for cross-ply, simply supported plates. Symmetric laminates are considered in Table 3.1 and unsymmetric laminates in Table 3.2. In all cases the

total thickness of the 0°-layers is the same as that of the 90°-layers while layers of the same class have the same thickness. The GLPT solution is obtained with a 2 x 2 mesh of 9-node elements in a quarter of the plate. The inplane inertias are included and the shear correction factor is taken to be $k^2 = 1.0$. The CPT solution and the corresponding errors with respect to the 3-D solution are included for comparison. Very good correlation between the GLPT and the 3-D solutions is observed.

Antisymmetric angle ply plates. Antisymmetric, simply supported laminates with all layers having the same thickness are considered. The nondimensional fundamental frequency is defined as $\bar{\omega} = \omega\, a^2 \sqrt{\rho/E_2}$. In all cases the GLPT solution is compared with the analytical CPT solution. Two- and six-layer laminates are considered with $G_{12}/E_2 = 0.5$, $G_{23}/E_2 = 0.2$, $\nu_{12} = 0.25$ and $h = 1.0$, regardless of the number of layers. The finite element solutions are obtained using a 2 x 2 mesh of 9-node elements in a quarter of a plate with the symmetry boundary conditions. A similar study to the one presented in Section 4.5 for the influence of the symmetry boundary conditions on the bending under transverse loads is carried out here to study the influence on the vibration frequencies. A 4 x 4 mesh is used to model the full plate and to compare with the quarter plate model. It is concluded that the symmetry boundary conditions are identically satisfied in the full plate model and identical vibration frequencies are obtained.

The effect of the thickness ratio a/h is shown in Figure 3.31 for $E_1/E_2 = 40$ and $\theta = 45°$. It is evident that shear deformation plays an important role for low values of the thickness ratio. The effect of the

lamination angle θ is considered in Figure 3.32 for a/h = 10 and E_1/E_2 = 40. The natural frequencies predicted by the GLPT are consistently lower than those predicted by CPT. The variation of $\bar{\omega}$ with the lamination angle θ is not as important as predicted by CPT. This is because the shear deformation effects are more important for the thickness considered in Figure 3.32. The effect of the degree of orthotropy (E_1/E_2) is investigated in Figure 3.33 for a/h = 10 and θ = 45°. The fundamental frequency ω is normalized by the frequency ω_o of the orthotropic plate (or, the number of layers approaches ∞), which eliminates the coupling terms B_{ij}.

Symmetric angle-ply laminates. No analytical solutions are available for symmetric angle-ply laminates due to the coupling introduced by the coefficients D_{16} and D_{26}. In the following example the total thickness of the $+\theta°$ layers is the same as for the $-\theta°$ layers, while all layers in the same class have the same thickness. Both a 4 x 4 mesh in the full plate and a 2 x 2 mesh in a quarter of the plate give similar results. The nondimensional frequencies $\bar{\omega}$ are computed as in the previous example and the same material properties are used for 3-, 5- and 9-ply laminates.

The effect of the thickness ratio a/h on the fundamental frequencies is examined in Figure 3.34 for θ = 45° and E_1/E_2 = 40. Shear deformation exerts an important influence for the lower range of thickness ratio, lowering the free vibration frequencies because of the reduced rigidity of the plate. The effect of the lamination angle $\theta°$ is displayed in Figure 3.35 for a/h = 10 and E_1/E_2 = 40. Significantly higher frequencies are observed for the ±45° lamination. The effect of

increasing the number of layers is to reduce the bending-extension coupling B_{ij} which in turn increases the value of the free vibration frequencies. The effect of the orthotropy, E_1/E_2, of individual layers is illustrated in Figure 3.36 for varying numbers of layers with a/h = 10 and $\theta = 45°$. In general, increasing the longitudinal modulus E_1 increases the rigidity of the plate; consequently, the value of the natural frequencies also increases. The effect is more pronounced for a high number of layers for which the coupling B_{ij} is small.

The Generalized Laminated Plate Theory is shown to be accurate for predicting free vibration frequencies of laminated composite plates on any range of thickness ratio, orthotropy of the material, or lamination angles. The theory can produce excellent representation of local effects as well. The importance of the laminated nature of the plate and the shear deformation effects are evident from the examples presented. It is shown that symmetry boundary conditions can be used for the linear analysis of angle-ply plates.

3.6 Implementation into ABAQUS Computer Program

3.6.1 Description of the GLPT Element

The degrees of freedom (d.o.f.) used in the GLPT element are:

- two inplane displacements (u,v) of the middle surface;
- the transverse displacement (w) of the middle surface;
- 2*NLAYER inplane relative displacements (u^j, v^j) at the interface between layers, where NLAYER is the number of layers in the laminate.

The theory requires that the middle surface coincide with an

interface. If such an interface does not exist at the middle surface, then we must model the middle layer as a two-layer assembly. In this way we introduce an interface at the midplane of the plate. The variables (u,v,w) completely describe the displacements at the midplane, and no additional variables (u^j, v^j) are necessary at the midplane. We measure the displacements (u,v,w) with respect to global (i.e., structural) coordinates. However, we measure the relative displacements of the interfaces (u^j, v^j) with respect to the midplane.

For each node we arrange the degrees of freedom as follows: u, v, w, u_1, v_1, u_2, v_2, ..., u_n, v_n. Figure 3.31 depicts the relationship between the various displacements and their corresponding degree of freedom. Both linear and quadratic elements are used for approximation of u, v, w,..., in the plane (see Figure 3.37).

3.6.2 Input Data to ABAQUS

In this section we describe the minimum set of option-cards necessary to run a problem using the GLPT element.

*NODE

Under the *NODE option card, the nodal data of a 2D planar mesh is listed in the usual way, giving the x and y coordinates of the modes in the mesh.

*USER ELEMENT

The *USER ELEMENT card must be specified immediately after completion of the *NODES option. This is because the *USER ELEMENT card defines the GLPT element and makes it available to subsequent options in

the input data. The necessary parameters are:

- NODES = 4 or 8 or 9 depending on the element being used
- TYPE = U1
- COORDINATES = 2 (3.21)
- VARIABLES = 2
- PROPERTIES = 5 + 3*NLAYER + 6*NMATS

The second card in the *USER ELEMENT option must list the degrees of freedom starting with 1 and up to NDOF, the number of d.o.f. per node computed as

- NDOF = 3 + 2*NLAYER (3.22)

*UEL PROPERTY

Following the *UEL PROPERTY option there must be as much parameters as declared in the PROPERTIES suboption of the *USER ELEMENT option. - NLAYER: number of layers of the laminate

- NMATS: number of materials to be used
- NGAUS: full integration rule
- NGPRD: reduced integration rule
- SCF: shear correction factor
- θ_K t_k, m_k, with k = 1, NLAYER
- E_1^j, E_2^j, G_{12}^j, G_{23}^j, ν_{12}^j, ν_{23}^j with j = 1, NMATS

The subscript k indicates the number of layer counting from the bottom up. θ_k is the angle between the material coordinate system and the structural coordinate system. t_k the thickness of the k-th layer and m_k is the material property set number of the k-th layer. The superscript j goes over all the material property sets.

*ELEMENT

The connectivities are given with a *ELEMENT card using TYPE=U1 for the 4-, 8-, and 9-node elements.

The specification of the boundary conditions may involve:

- the inplane displacements of the middle surface (u,v) which correspond to d.o.f. 1 and 2.
- the transverse deflection of the middle surface (w) which corresponds to d.o.f. 3.
- the inplane relative displacements of the interfaces, usually employed to specify rotations.

*BOUNDARY

Under *BOUNDARY the specified degrees of freedom (DOF) of the structure are listed. In Figure 3.37 we show the relationship between the number of DOF and the displacements for a typical node. In the following we describe how to specify the various DOF to model commonly encountered boundary conditions for plates. As an example consider a four-layer laminate as depicted in Figure 3.37. Furthermore assume that the plate is square and simply-supported on all four sides. In this case only one quarter of the plate need to be modelled as shown in Figure 3.38. The boundary conditions used are [80],

$$\text{at } x = 0: \quad u_1(y) = \psi_x(y) = 0$$

$$\text{at } y = 0: \quad u_2(x) = \psi_y(x) = 0$$

$$\text{at } x = a/2: \quad u_3(y) = u_2(y) = \psi_y(y) = 0$$

$$\text{at } y = a/2: \quad u_3(x) = u_1(x) = \psi_x(x) = 0$$

For the four-layer laminate these translate to:

at x = 0: set d.o.f. 1,4,6,8,10 to zero

at y = 0: set d.o.f. 2,5,7,9,11 to zero

at x = a/2: set d.o.f. 2,3,5,7,9,11 to zero

at y = a/2: set d.o.f. 1,3,4,6,8,10 to zero

We will extend on the treatment of the specification of boundary conditions in the examples in the following section.

Loading

Two types of load are implemented. Transverse load, bilinear over each element, is specified by the 4 values at the corner nodes. Inplane lateral load, linear on the side, is specified by its two components on each end-node defining side 1 of the element (i.e., the side limited by the local nodes 1 and 2). Loads are specified as,

$$\text{ELEMENT, } q1,q2,q3,a4,f_x^1,f_y^1,f_x^2,f_y^2$$

where q_i = pressure at node i

f_x^1 = x-component of the lateral pressure at local node 1

3.6.3 Output Files and Postprocessing

To complete the discussion on the use of the GLPT element in ABAQUS we describe the output files and how the output can be further post-processed.

The ABAQUS computer program produces its standard output. This file lists, among other things, the displacements (u,v,w) in the first 3 columns of the section labeled NODE OUTPUT. The column labeled U1 corresponds to u, U2 to v and U3 to w.

During a normal execution using the GLPT element, the USER SUBROUTINE writes a temporary file. Useful information can be retrieved from it using the post-processor program.

The structure of the temporary file is described here.

For each element we have:

1st card (4I5) IEL NGP NLAYER ID

where

- IEL: element number
- NGP: number of Gauss points at which the stresses are stored
- NLAYER: number of layers
- ID: element type (1 = GLPT)

Next, NLAYER + 1 cards follow with the z-coordinate of the interfaces (1PE13.5).

Next, for each Gauss point (a total of NGP*NGP) we have:

One card with the Gauss point coordinates (2(1PE13.5))

2*NLAYER cards, each couple of them gives the stresses at the bottom and top surfaces respectively, for each layer. Each card gives the stresses computed from constitutive equations (6(1PE13.5)):

$z, \sigma_{xx}, \sigma_{yy}, \sigma_{xy}, \sigma_{xy}, \sigma_{yz}, \sigma_{xz}$

Finally we have a list of the coefficients in the third-order approximation of the interlaminar shear stresses, as computed from equilibrium equations. These coefficients can be used by the post-processor program to give a series of values of σ_{yz} and σ_{xz} through the thickness, suitable for plotting.

The post-processor uses the temporary file to produce an output file in which the distribution of stresses is shown at user specified points or at points where the stresses have a maximum. The post-processing program can be easily modified to suit the needs of the analyst without having to modify the USER ELEMENT subroutine.

3.6.4 One-element Test Example

As a first example we model a simply supported plate using one GLPT element. The plate is uniformly loaded in the transverse direction (w). For element number 1, the magnitude of the transverse load at the nodes 1 to 4 is 1, 1, 1, 1. The x- and y-components of the lateral load on node 1 of side 1 are equal to 0,0 and the two components at node 2 are 0,0.

Due to symmetry of the geometry, load and material properties, only 1/4 of the plate need to be modelled. The appropriate boundary conditions in terms of displacements and rotations for a simply supported, cross-ply plate, with symmetry at x = 0 and y = 0 are [80]:

- on x = 0: $u = \phi_x = 0$
- on y = 0: $v = \phi_y = 0$
- on x = a/2: $v = w = \phi_y = 0$
- on y = a/2: $u = w = \phi_x = 0$

The *BOUNDARY option card describes the boundary conditions for this example. On each card, one node and the specified d.o.f. are given. According to Figure 3.37, d.o.f. 1 represents u, d.o.f. 2 represents v, d.o.f. 3 represents w. For this example NLAYER = 4, then according to Equation 3.21, the number of d.o.f. per node is NDOF = 11.

Consequently, the relative inplane displacements in the x-direction correspond to d.o.f. number 4, 6, 8, 10 and those in the y-direction to d.o.f. number 5, 7, 9, 11.

The SS boundary condition on x = a/2 is satisfied setting to zero the d.o.f. 2, 3, 5, 7, 9, 11 for nodes 2, 6, 3 (see Figure 3.39). On y = a/2, d.o.f. 1, 3, 4, 6, 8, 10 are set to zero for nodes 4, 7, 3.

The symmetry condition along x = 0 is satisfied by setting d.o.f. 1, 4, 6, 8, 10 to zero for nodes 1, 8, 4. Similarly, on y = 0 we set d.o.f. 2, 5, 7, 9, 11 to zero for nodes 1, 5, 2.

The plate is laminated as [0/90/0]t with thicknesses $[0.833/0.833/0.833]_T$. Since we must specify an interface at the middle surface, we model the plate as a $[0/90]_S$ with thicknesses $[0.833/0.417]_S$ which is equivalent. We use a single material (NMATS = 1) with properties:

- E_1 = 1.2549E7
- E_2 = 7.6525E5
- G_{12} = 2.8955E5
- G_{23} = 2.6462E5
- ν_{12} = 0.3458
- ν_{23} = 0.4459

Immediately after the *NODES option is completed, we declare the *USER ELEMENT option. We specify:

- NODES = 8
- TYPE = U1
- COORDINATES = 2
- PROPERTIES = 23

- VARIABLES = 1 (This value is fixed for any problem)

Since NDOF = 11 is this example, the next card lists the d.o.f., i.e., 1, 2, 3, 4, 5, 6, 7, 8, 9, 10, 11.

To specify all the necessary parameters to the model we need, according to Equation 3.21, PROPERTIES = 23. The 23 parameters are given with a *UEL PROPERTY card for the ELSET = CUBE. According to Equation 3.22 we have:

- NLAYER = 4
- NMATS = 1
- NGAUS = 2
- NGPRD = 2
- SCF = 1
- $\theta_1 = 0$
- $t_1 = 0.833$
- $m_1 = 1$
- $\theta_2 = 90$
- $t_2 = 0.417$
- $m_2 = 1$
- $\theta_3 = 90$
- $t_3 = 0.417$
- $m_3 = 1$
- $\theta_4 = 0$
- $t_4 = 0.833$
- $m_4 = 1$
- $E_1 = 1.2549E7$
- $E_2 = 7.6525E5$

- G_{12} = 2.8955E5
- G_{23} = 2.6462E5
- G_{23} = 2.6462E5
- ν_{12} = 0.3458
- ν_{23} = 0.4459

The *ELEMENT option uses element TYPE = U1 and declares all the elements as belonging to the named ELSET = CUBE.

Finally, the *USER SUBROUTINES,INPUT = 15 card is required to allow proper link with the main ABAQUS program. A complete report of the stresses can be obtained by using the postprocessing program.

Appendix 2

Strain-Displacement Matrices and Laminate Stiffnesses Equations

The strains $\{e\}$ and $\{e^k\}$ appearing in Equation (3.2) are

$$\{e\} = \begin{Bmatrix} \frac{\partial u}{\partial x} \\ \frac{\partial v}{\partial y} \\ \frac{\partial u}{\partial y} + \frac{\partial v}{\partial x} \\ \frac{\partial w}{\partial x} \\ \frac{\partial w}{\partial y} \end{Bmatrix}, \quad \{e^k\} = \begin{Bmatrix} \frac{\partial u^k}{\partial x} \\ \frac{\partial v^k}{\partial y} \\ \frac{\partial u^k}{\partial y} + \frac{\partial v^k}{\partial x} \\ u^k \\ v^k \end{Bmatrix}$$

The matrices $[H]$ and $[\bar{H}]$ appearing in the strain-displacement relations (3.2) are

$$[B_L]_{(5\times 3m)} = \begin{bmatrix} \frac{\partial \psi_1}{\partial x} & 0 & 0 & \frac{\partial \psi_2}{\partial x} & 0 & 0 & \cdots & \frac{\partial \psi_m}{\partial x} & 0 & 0 \\ 0 & \frac{\partial \psi_1}{\partial y} & 0 & 0 & \frac{\partial \psi_2}{\partial y} & 0 & \cdots & 0 & \frac{\partial \psi_m}{\partial y} & 0 \\ \frac{\partial \psi_1}{\partial y} & \frac{\partial \psi_1}{\partial x} & 0 & \frac{\partial \psi_2}{\partial y} & \frac{\partial \psi_2}{\partial x} & 0 & \cdots & \frac{\partial \psi_m}{\partial y} & \frac{\partial \psi_m}{\partial x} & 0 \\ 0 & 0 & \frac{\partial \psi_1}{\partial x} & 0 & 0 & \frac{\partial \psi_2}{\partial x} & \cdots & 0 & 0 & \frac{\partial \psi_m}{\partial x} \\ 0 & 0 & \frac{\partial \psi_1}{\partial y} & 0 & 0 & \frac{\partial \psi_{12}}{\partial y} & \cdots & 0 & 0 & \frac{\partial \psi_m}{\partial y} \end{bmatrix}$$

$$[\overline{B}_L] = \text{(5x2m)} \begin{bmatrix} \frac{\partial \psi_1}{\partial x} & 0 & \frac{\partial \psi_2}{\partial x} & 0 & \cdots & \frac{\partial \psi_m}{\partial x} & 0 \\ 0 & \frac{\partial \psi_1}{\partial y} & 0 & \frac{\partial \psi_2}{\partial y} & \cdots & 0 & \frac{\partial \psi_m}{\partial y} \\ \frac{\partial \psi_1}{\partial y} & \frac{\partial \psi_1}{\partial x} & \frac{\partial \psi_2}{\partial y} & \frac{\partial \psi_2}{\partial x} & \cdots & \frac{\partial \psi_m}{\partial y} & \frac{\partial \psi_m}{\partial x} \\ \psi_1 & 0 & \psi_2 & 0 & \cdots & \psi_m & 0 \\ 0 & \psi_1 & 0 & \psi_2 & \cdots & 0 & \psi_m \end{bmatrix}$$

Appendix 3

Computation of Higher-Order Derivatives

The computation of the second- and higher-order derivatives of the interpolation functions with respect to the global coordinates involves additional computations.

The first-order derivatives with respect to the global coordinates are related to those with respect to the local (or element) coordinates according to

$$\begin{Bmatrix} \frac{\partial \psi_i}{\partial x} \\ \\ \frac{\partial \psi_i}{\partial y} \end{Bmatrix} = \begin{bmatrix} \frac{\partial x}{\partial \xi} & \frac{\partial y}{\partial \xi} \\ \\ \frac{\partial x}{\partial \eta} & \frac{\partial y}{\partial \eta} \end{bmatrix}^{-1} \begin{Bmatrix} \frac{\partial \psi_i}{\partial \xi} \\ \\ \frac{\partial \psi_i}{\partial \eta} \end{Bmatrix} \equiv [J]^{-1} \begin{Bmatrix} \frac{\partial \psi_i}{\partial \xi} \\ \\ \frac{\partial \psi_i}{\partial \eta} \end{Bmatrix} \qquad \text{(a)}$$

where the Jacobian matrix [J] is evaluated using the approximation of the geometry:

$$x = \sum_{j=1}^{r} x_j \phi_j(\xi,\eta)$$

$$y = \sum_{j=1}^{r} y_j \phi_j(\xi,\eta) \qquad \text{(b)}$$

where ϕ_j are the interpolation functions used for the geometry and (ξ,η) are the element natural coordinates. For the isoparametric formulation $r = m$ and $\phi_j = \psi_j$. The second-order derivatives of ψ_i with respect to the global coordinates (x,y) are given by

$$\begin{Bmatrix} \frac{\partial^2 \psi_i}{\partial x^2} \\ \frac{\partial^2 \psi_i}{\partial y^2} \\ \frac{\partial^2 \psi_i}{\partial x \partial y} \end{Bmatrix} = [J_1]^{-1} \left\{ \begin{Bmatrix} \frac{\partial^2 \psi_i}{\partial \xi^2} \\ \frac{\partial^2 \psi_i}{\partial \eta^2} \\ \frac{\partial^2 \psi_i}{\partial \xi \partial \eta} \end{Bmatrix} - [J_2] \begin{Bmatrix} \frac{\partial \psi_i}{\partial x} \\ \\ \frac{\partial \psi_i}{\partial y} \end{Bmatrix} \right\} \tag{c}$$

where

$$[J_1] = \begin{bmatrix} (\frac{\partial x}{\partial \xi})^2 & (\frac{\partial y}{\partial \xi})^2 & 2 \frac{\partial y}{\partial \xi} \frac{\partial x}{\partial \xi} \\ (\frac{\partial x}{\partial \eta})^2 & (\frac{\partial y}{\partial \eta})^2 & 2 \frac{\partial x}{\partial \eta} \frac{\partial y}{\partial \eta} \\ \frac{\partial x}{\partial \eta} \frac{\partial x}{\partial \xi} & \frac{\partial y}{\partial \eta} \frac{\partial y}{\partial \xi} & \frac{\partial x}{\partial \eta} \frac{\partial y}{\partial \xi} + \frac{\partial y}{\partial \eta} \frac{\partial x}{\partial \xi} \end{bmatrix} \tag{d}$$

$$[J_2] = \begin{bmatrix} \frac{\partial^2 x}{\partial \xi^2} & \frac{\partial^2 y}{\partial \xi^2} \\ \frac{\partial^2 x}{\partial \eta^2} & \frac{\partial^2 y}{\partial \eta^2} \\ \frac{\partial^2 x}{\partial \eta \partial \xi} & \frac{\partial^2 y}{\partial \xi \partial \eta} \end{bmatrix} \tag{e}$$

The matrices $[J_1]$ and $[J_2]$ are computed using Equation (b).

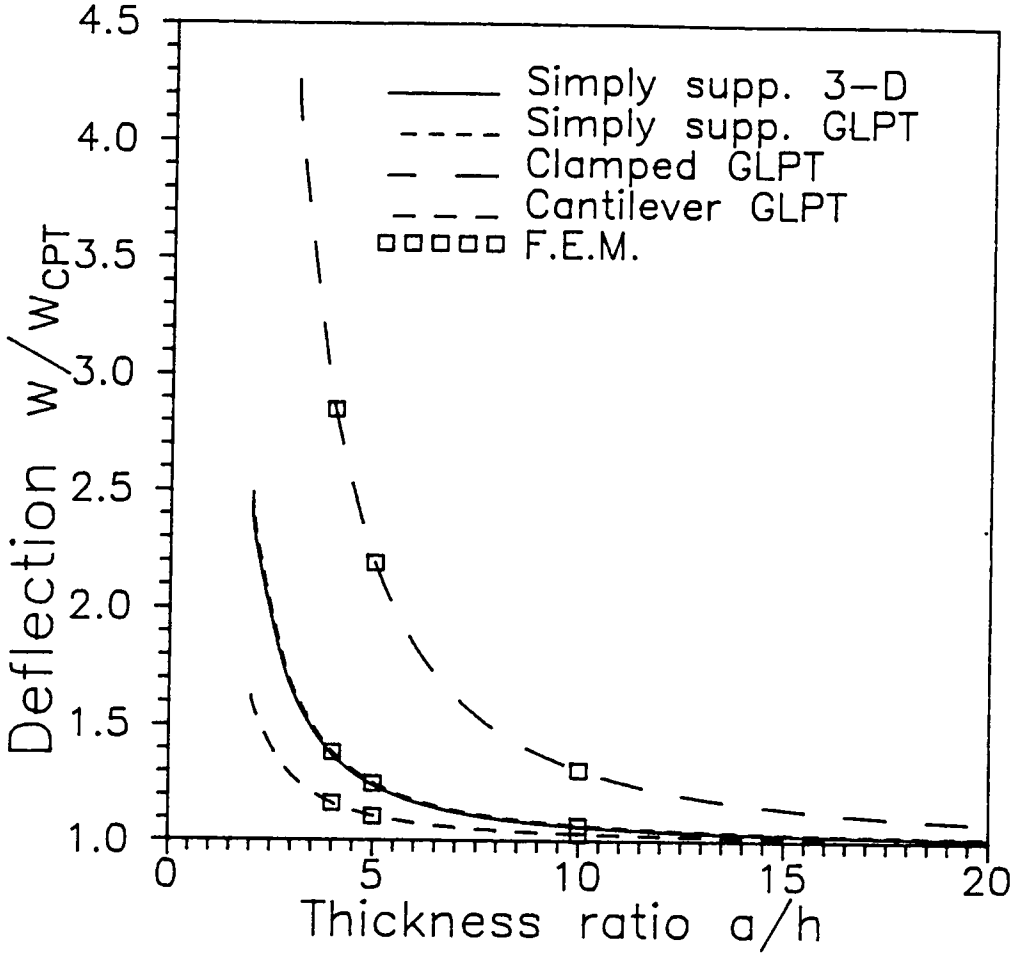

3.1 Comparison between the 3D analytical solution, GLPT analytical solutions and GLPT finite element solutions for a (0/90) laminated plate in cylindrical bending. The transverse load is uniformly distributed and three boundary conditions (SS = simply supported, CC = clamped, and CT = cantilever) are considered.

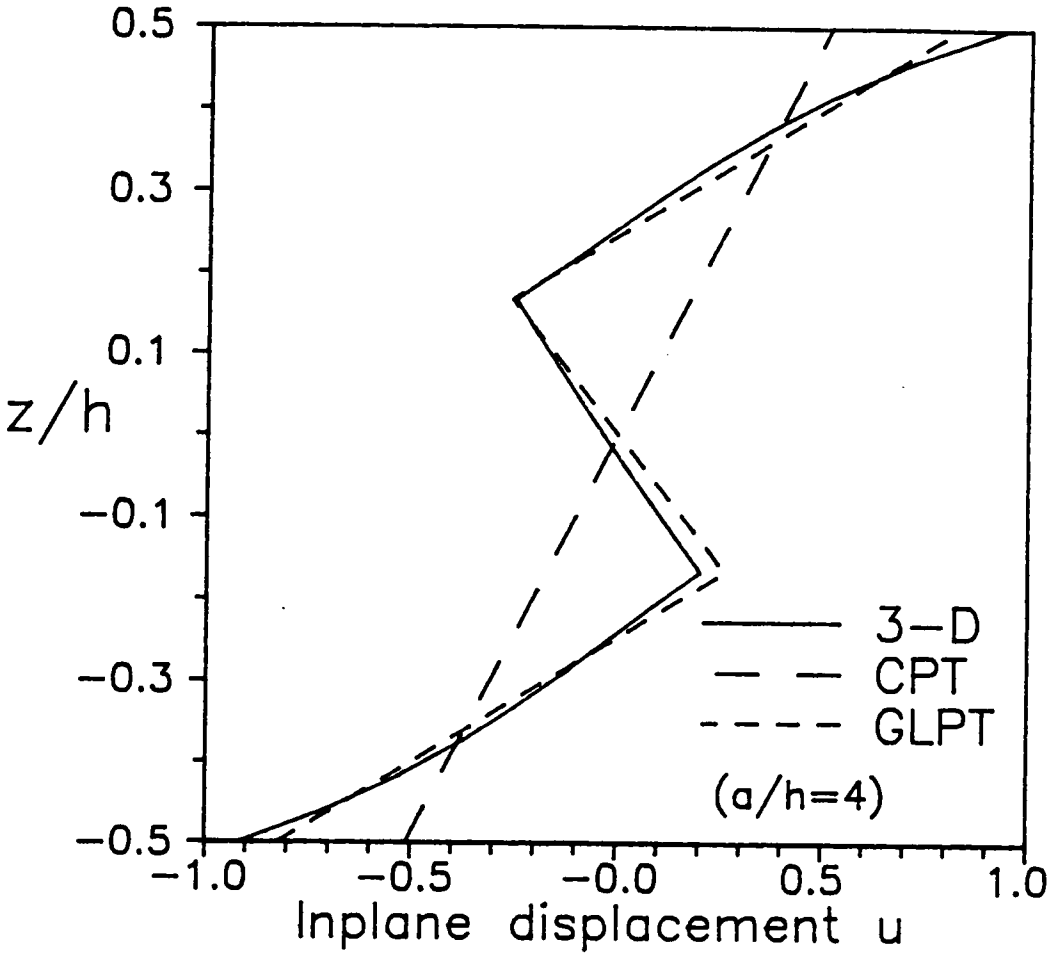

3.2 Through-the-thickness distribution of the in-plane displacement u for a simply supported, (0/90/0) laminate under sinusoidal load, a/h = 4.

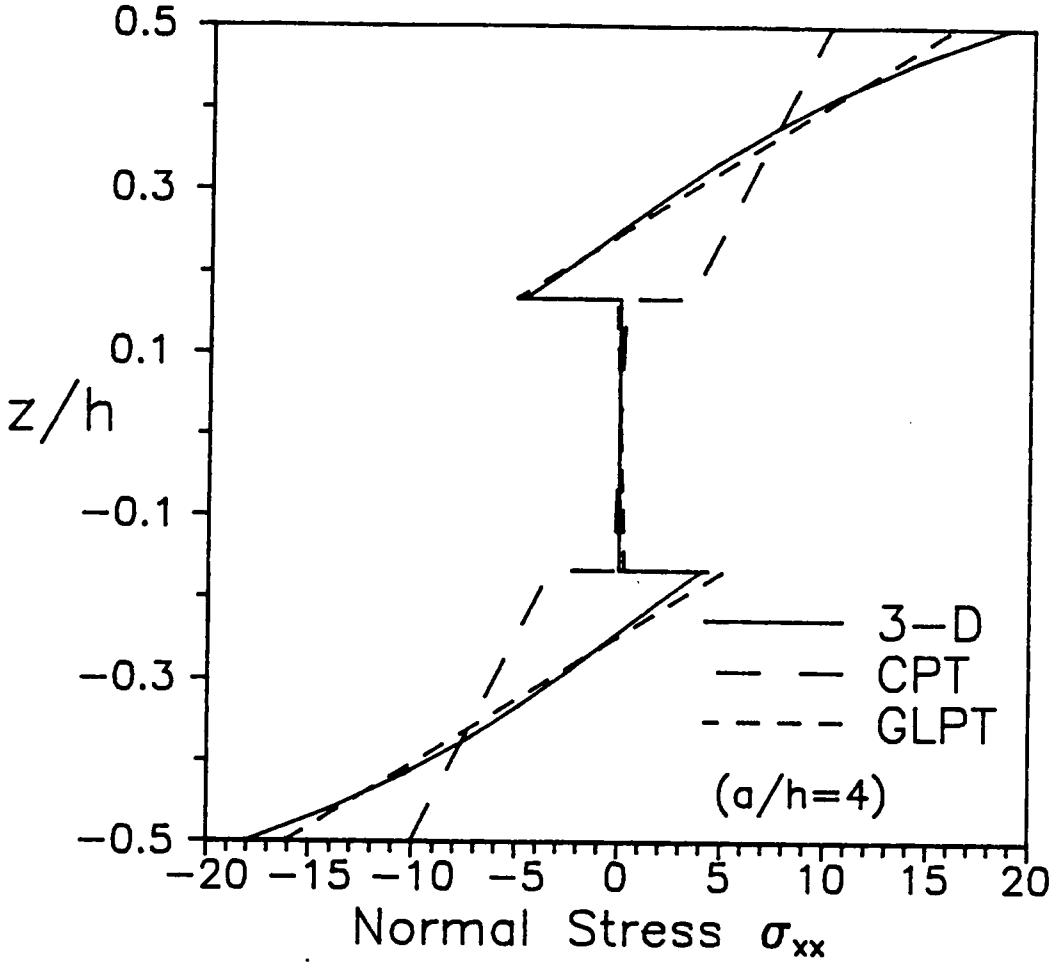

3.3 Through-the-thickness distribution of the in-plane normal stress σ_{xx} for a simply supported, (0/90/0) laminate under sinusoidal load, a/h = 4.

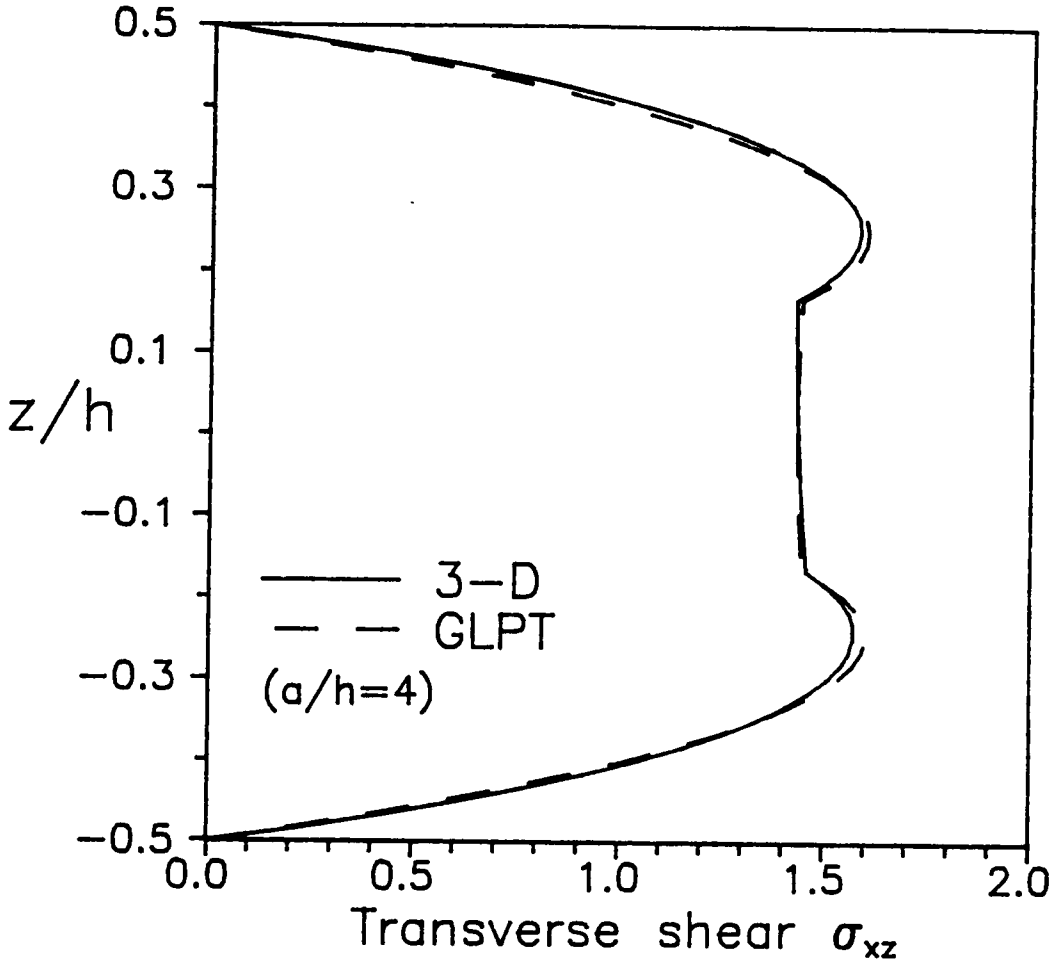

3.4 Through-the-thickness distribution of the transverse shear stress σ_{xz} for a simply supported, (0/90/0) laminate under sinusoidal load, a/h = 4.

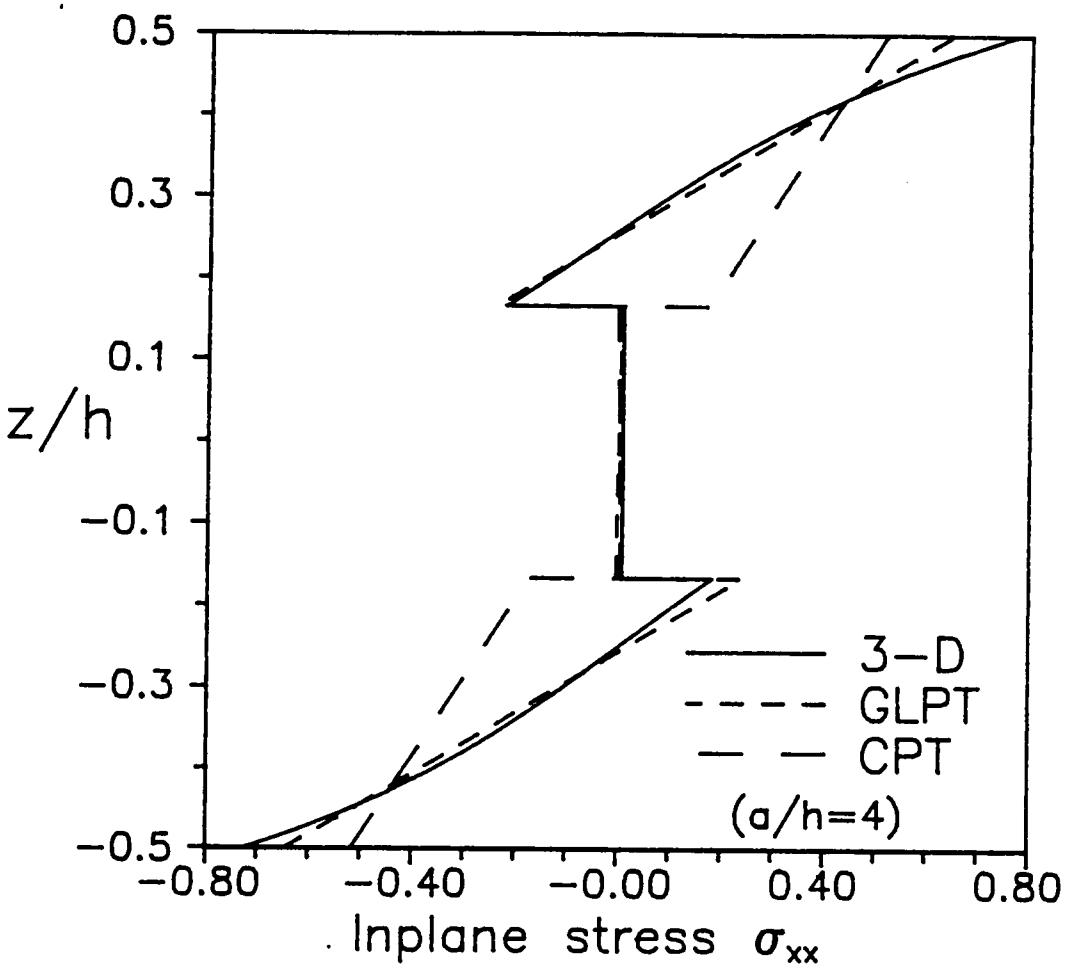

3.5 Through-the-thickness distribution of the in-plane normal stress σ_{xx} at (x,y) = (a/16, a/16) for a simply-supported, (0/90/0) laminated square plate under double-sinusoidal load, a/h = 4.

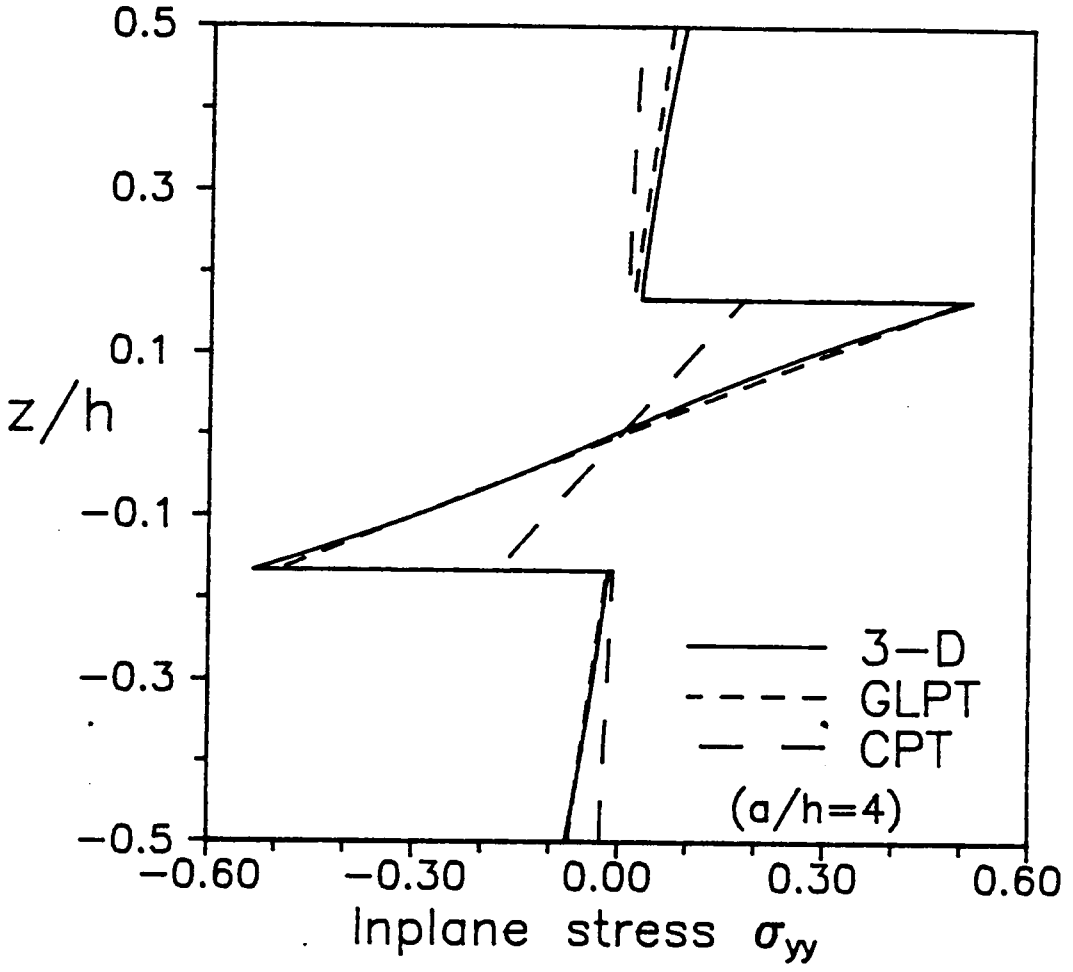

3.6 Through-the-thickness distribution of the in-plane normal stress σ_{yy} at (x,y) = (a/16, a/16) for a simply supported, (0/90/0) laminated square plate under double-sinusoidal load, a/h = 4.

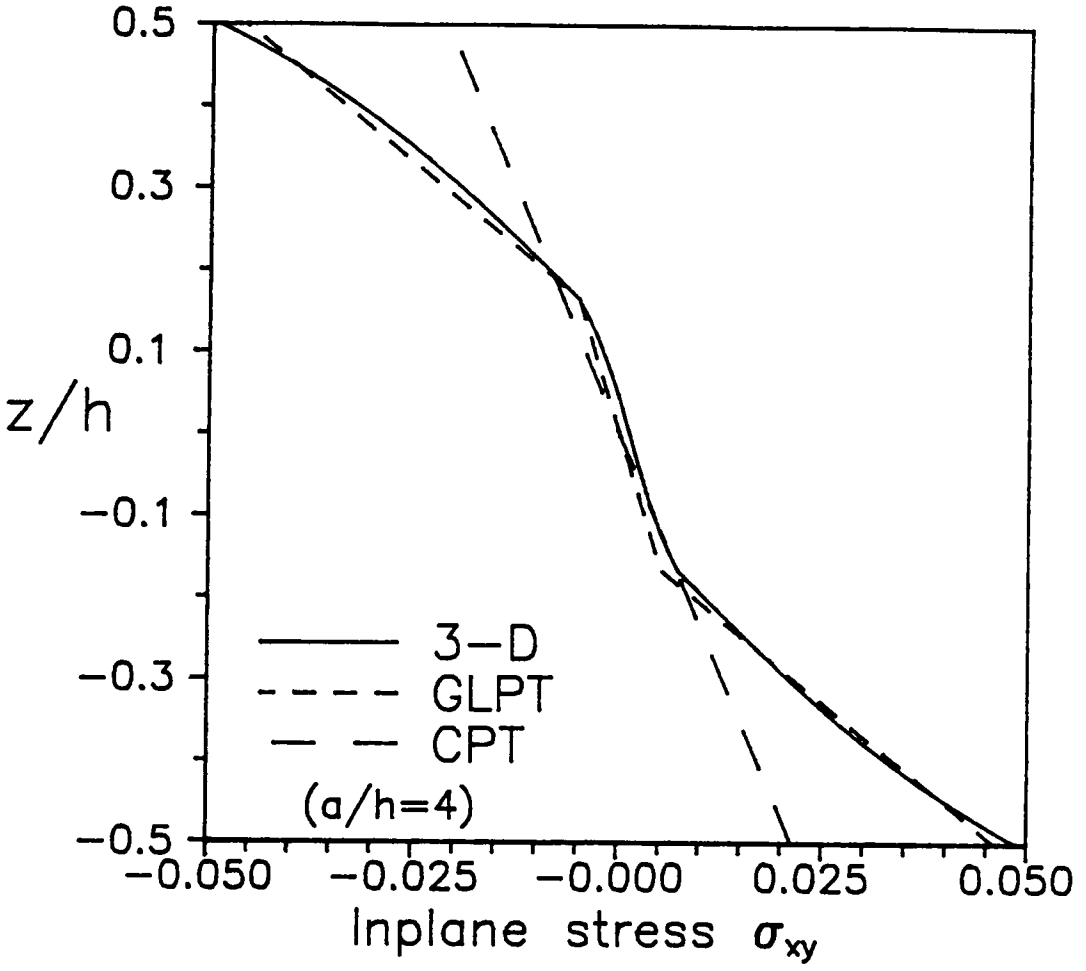

3.7 Through-the-thickness distribution of the in-plane shear stress σ_{xy} at (x,y) = (7a/17, 7a/16) for a simply supported, (0/90/0) laminated square plate under double-sinusoidal load, a/h = 4.

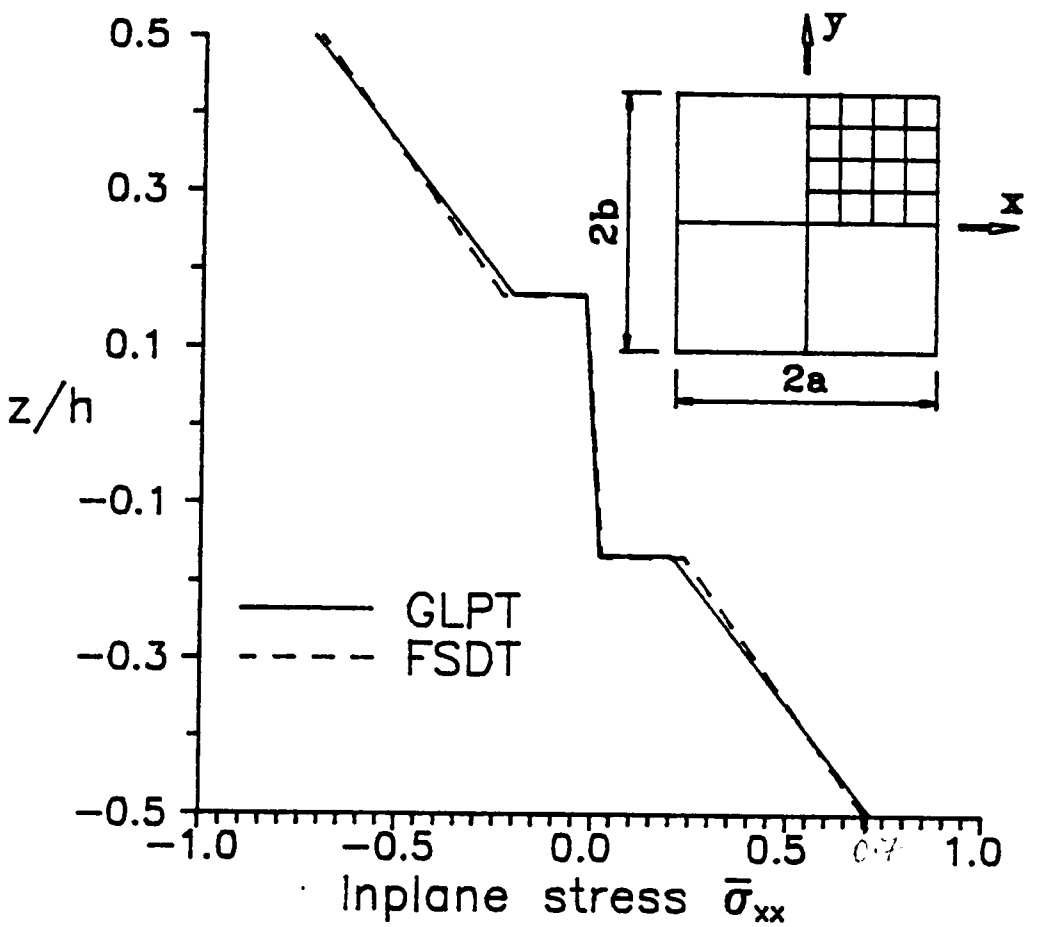

3.8 Through-the-thickness distribution of the in-plane normal stress σ_{xx} for a simply-supported, (0/90/0) laminated square plate under uniform load, (a/h = 10) as computed using the GLPT and FSDT.

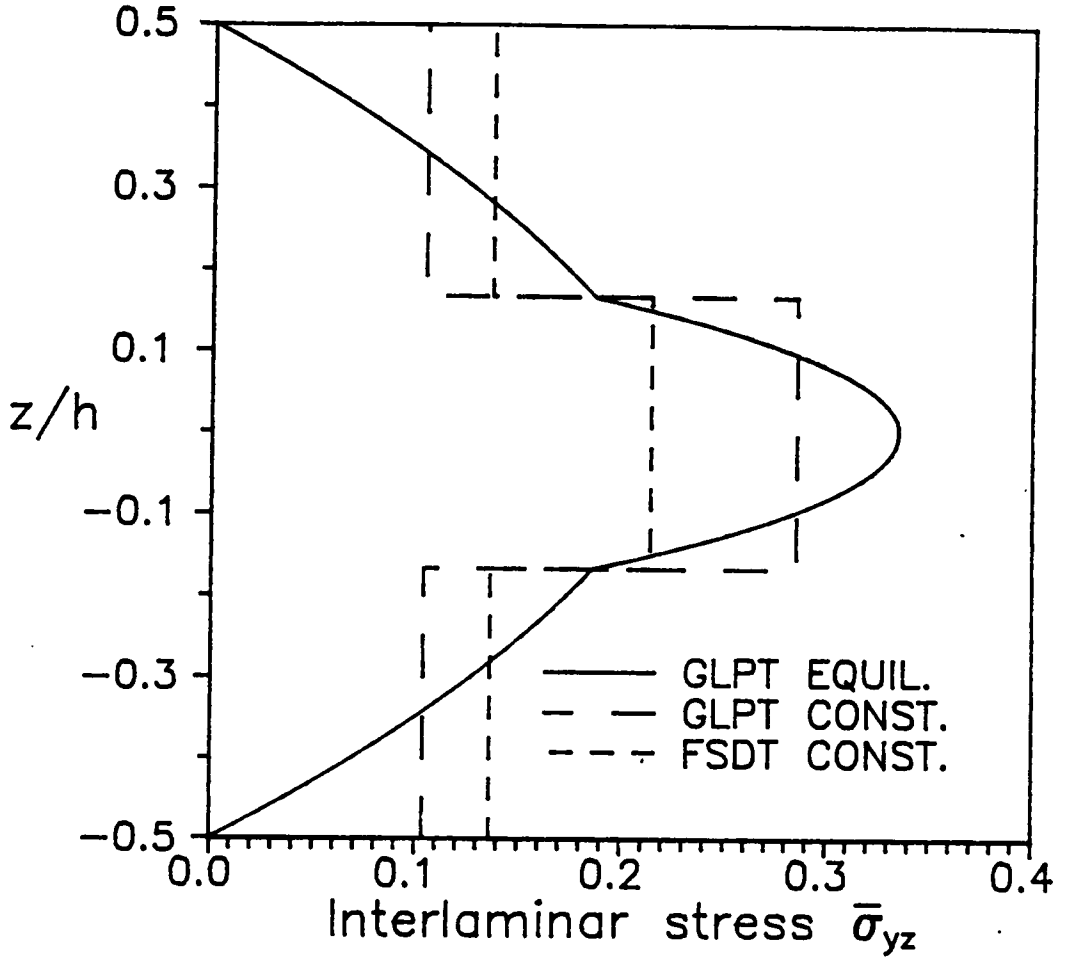

3.9 Through-the-thickness distribution of the transverse shear stress σ_{yz} for a simply-supported, (0/90/0) laminated square plate under uniform load, (a/h = 10) as computed using the GLPT and FSDT.

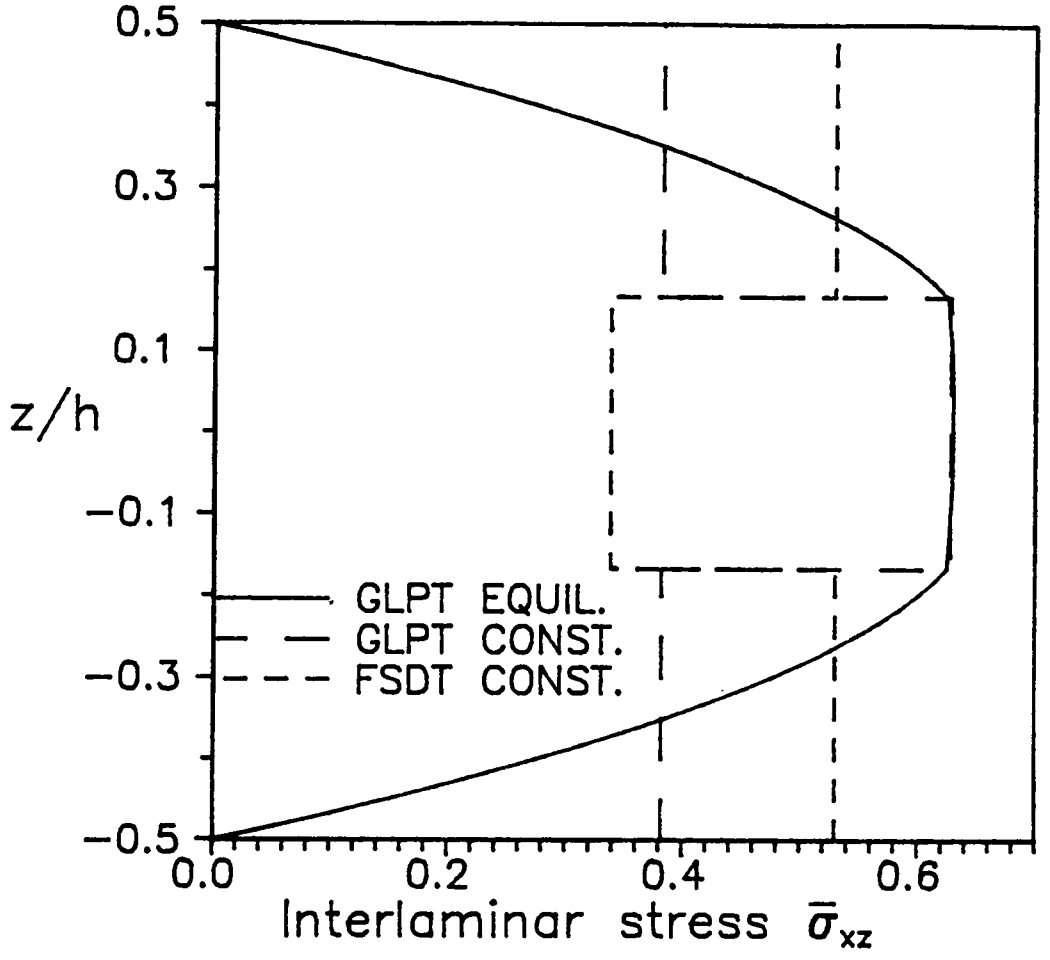

3.10 Through-the-thickness distribution of the transverse shear stress σ_{xz} for a simply-supported, (0/90/0) laminated square plate under uniform load, (a/h = 10) as computed using the GLPT and FSDT.

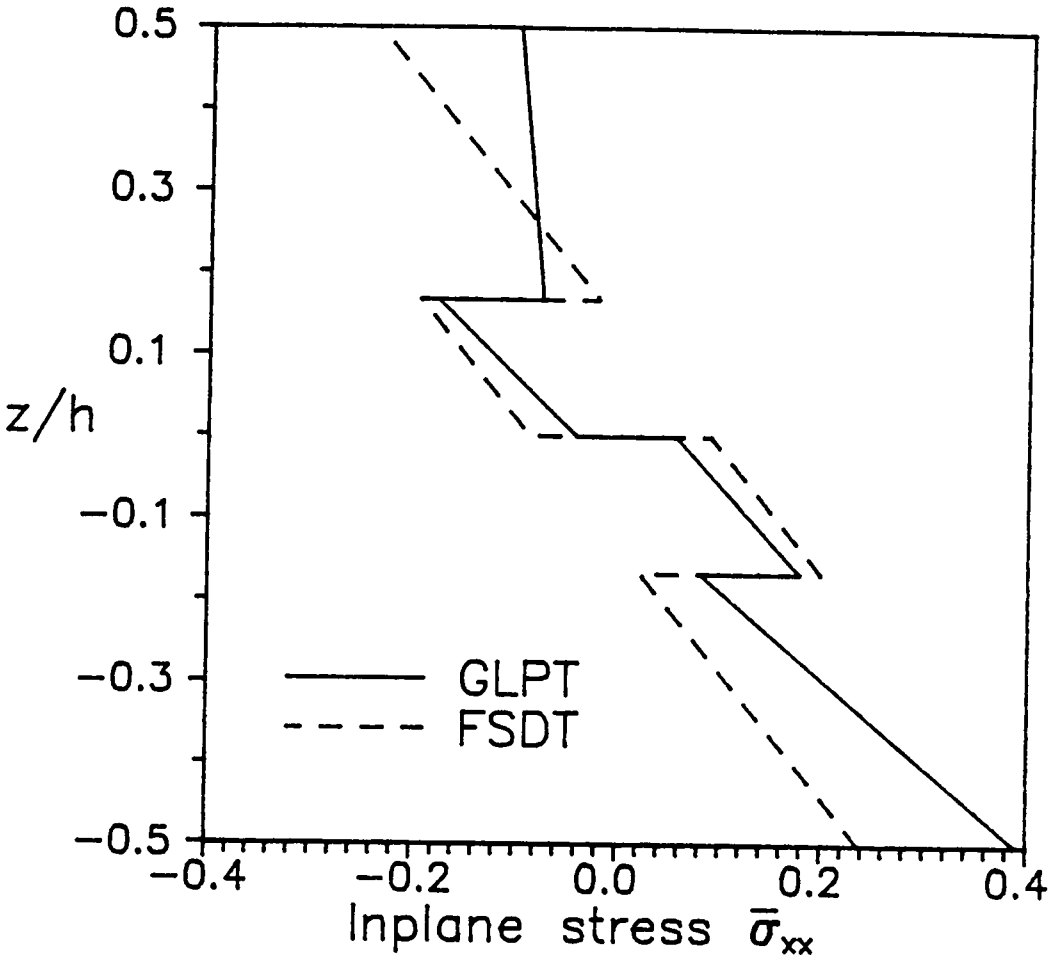

3.11 Through-the-thickness distribution of the stress σ_{xx} for a simply supported (45/-45/45/-45) laminated square plate under uniform load (a/h = 10).

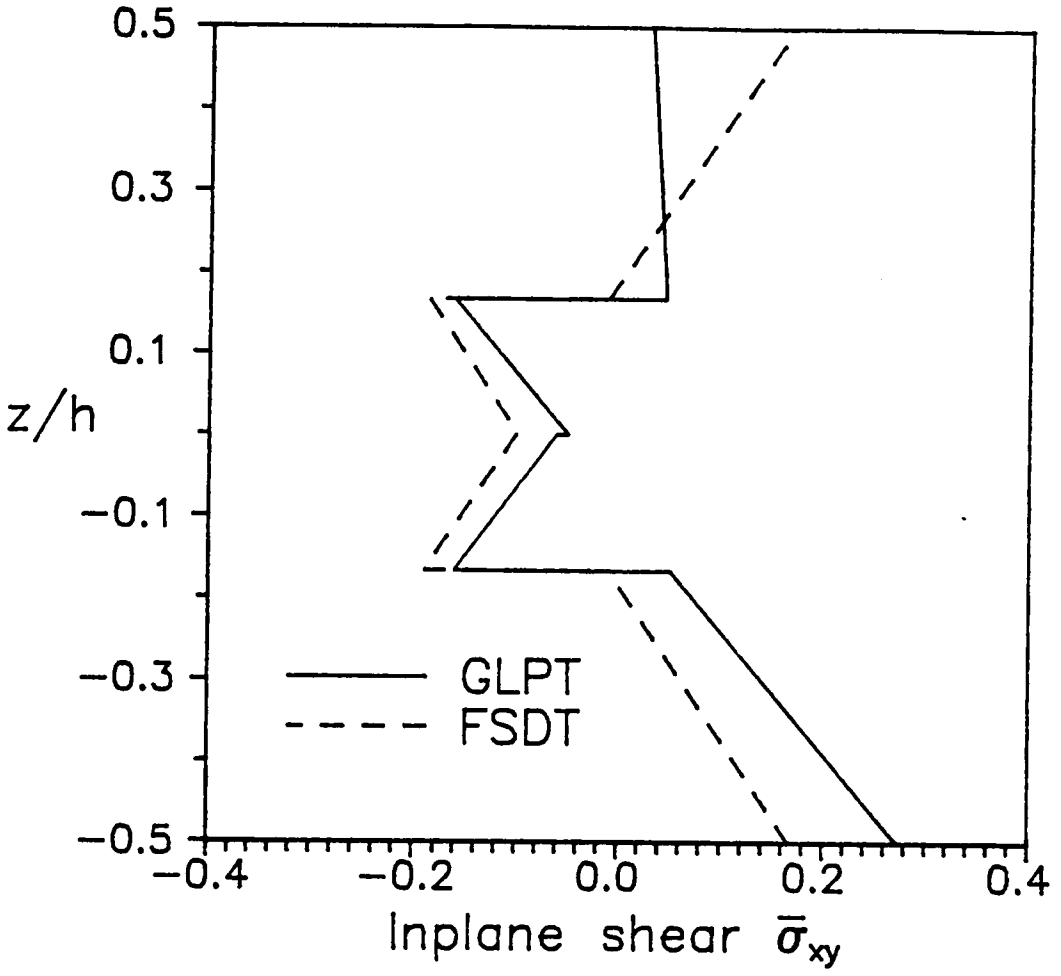

3.12 Through-the-thickness distribution of the stress σ_{xy} for a simply supported (45/-45/45/-45) laminated square plate under uniform load (a/h = 10).

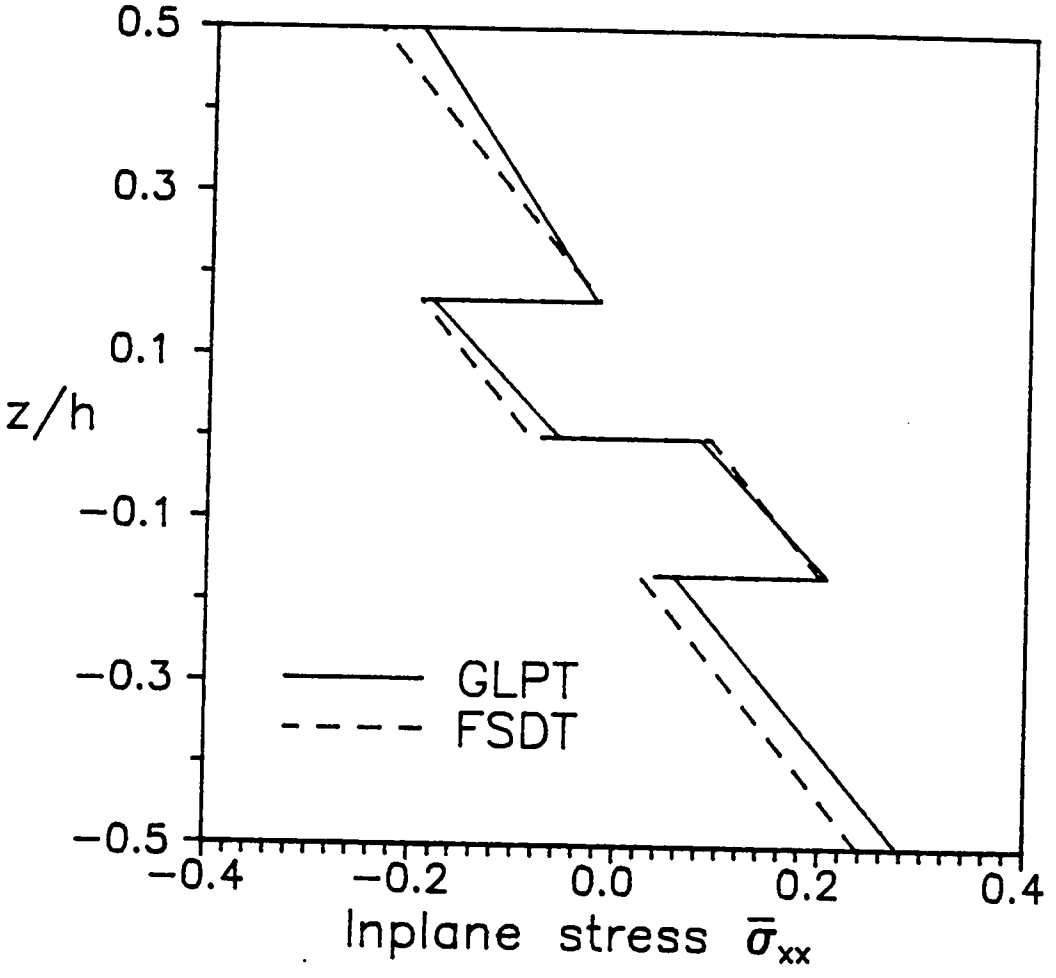

3.13 Through-the-thickness distribution of the in-plane shear stress σ_{xy} for a simply supported (45/-45/45/-45) laminated square plate under uniform load (a/h = 50).

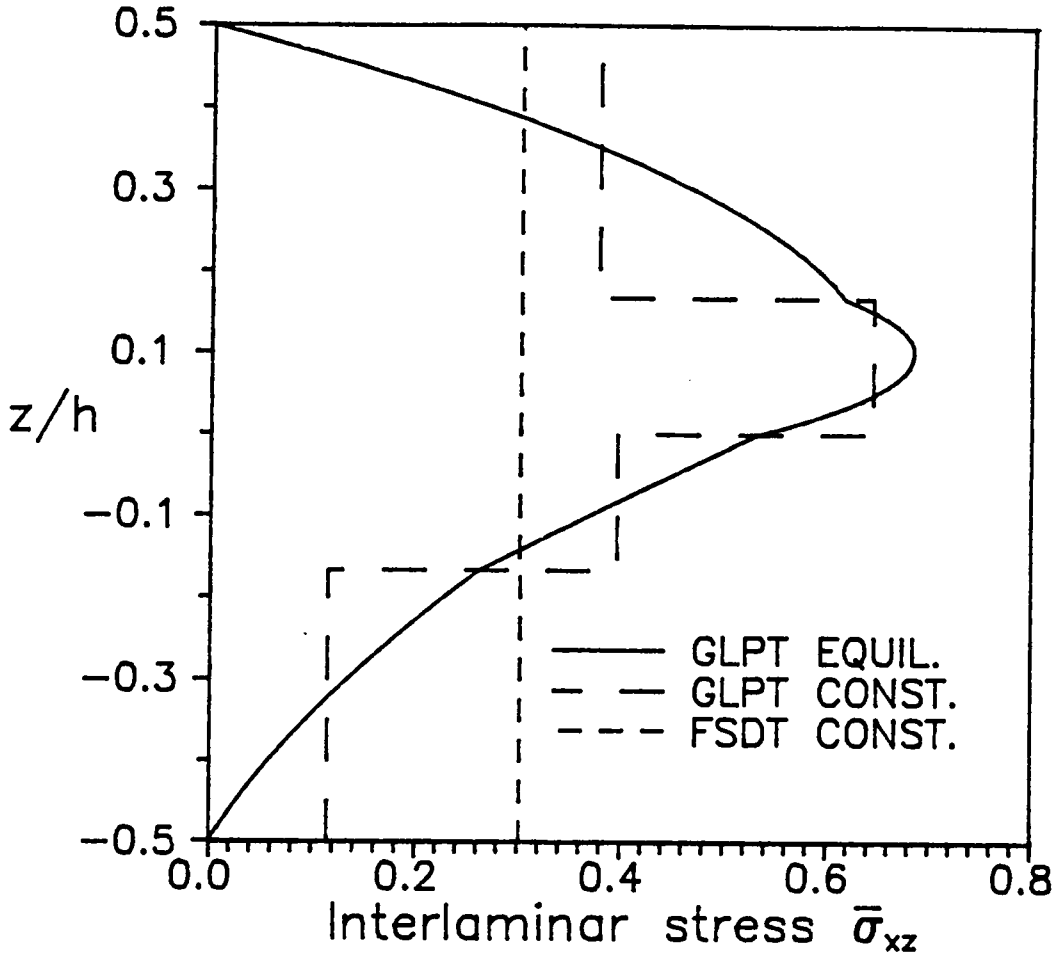

3.14 Through-the-thickness distribution of the transverse shear stress σ_{xz} for a simply supported (45/-45/45/-45) laminated square plate under uniform load (a/h = 10).

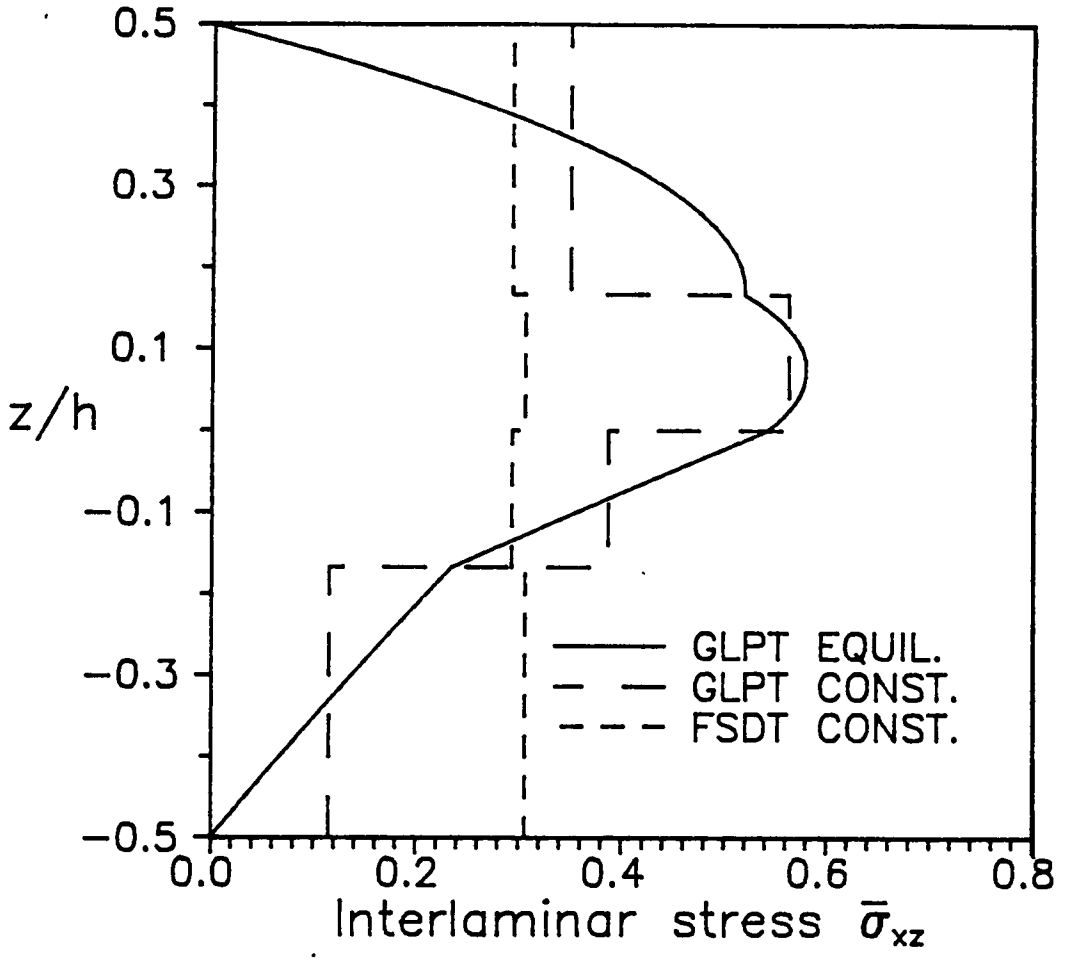

3.15 Through-the-thickness distribution of the transverse stress σ_{xz} for a simply supported (45/-45/45/-45) laminated square plate under uniform load (a/h = 100).

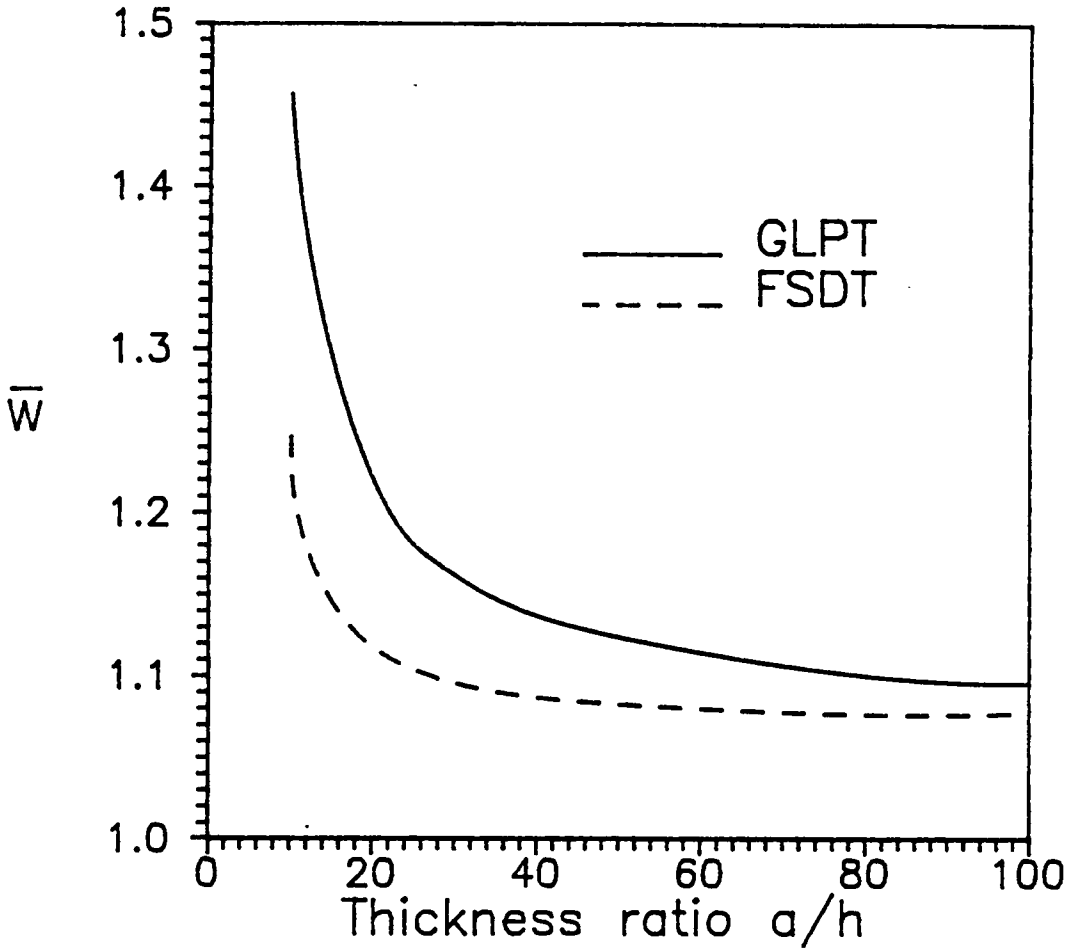

3.16 Normalized transverse deflection versus aspect ratio for the antisymmetric angle-ply (45/-45/45/-45) square plate under uniform load.

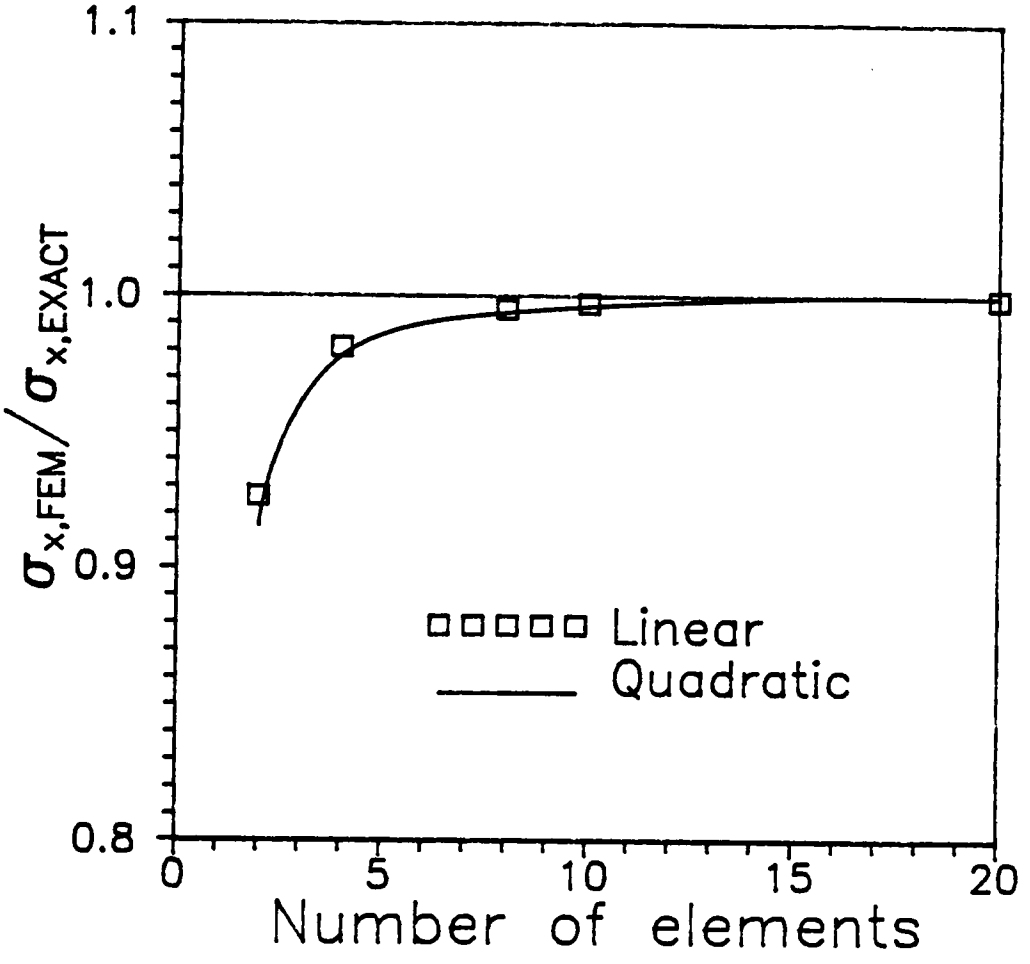

3.17 Convergence of stresses obtained using two-dimensional linear and eight-node quadratic elements for cylindrical bending of beams (a/h = 4).

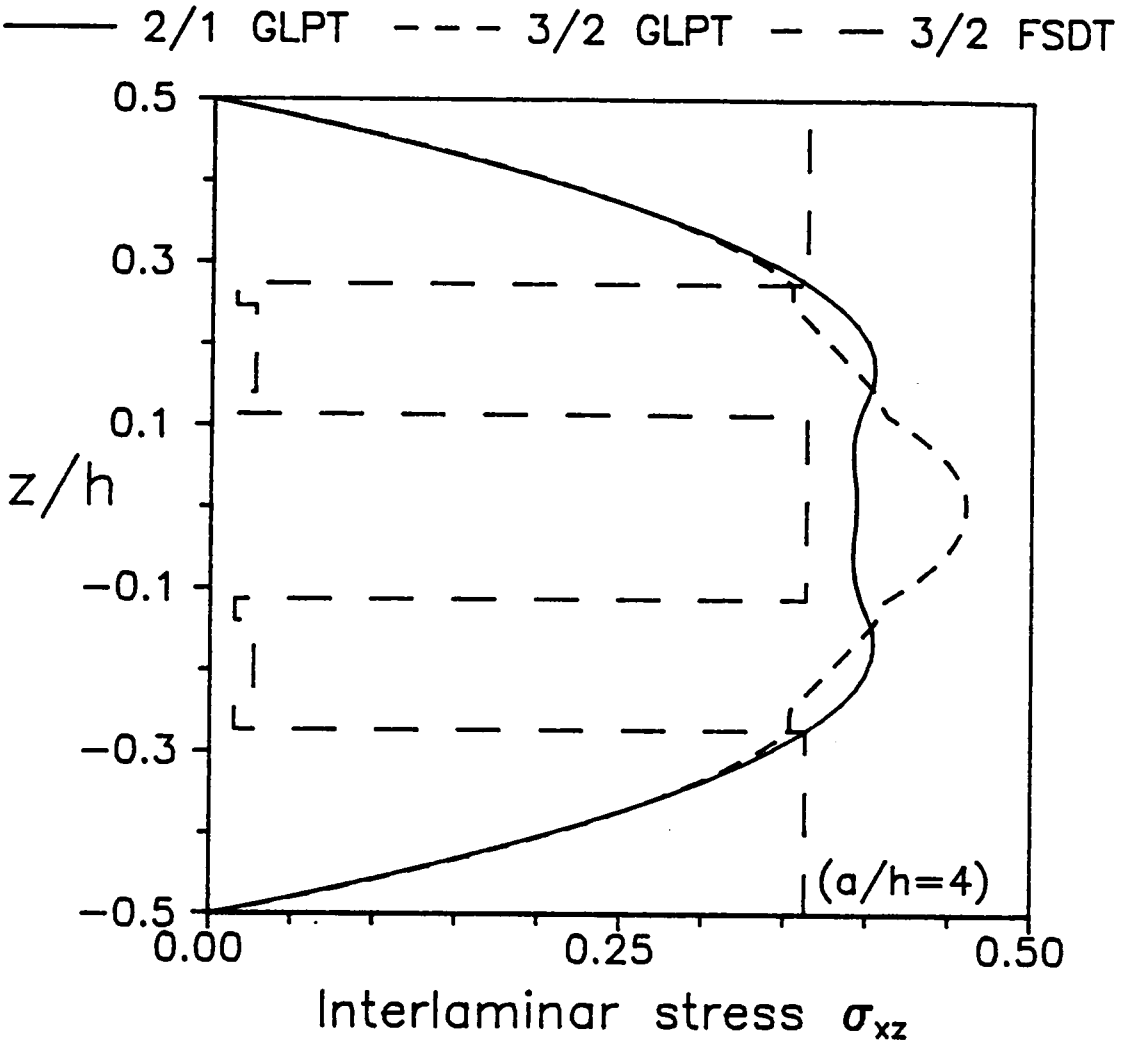

3.18 Comparison of the transverse shear stress distributions σ_{xz} from GLPT and FSDT for ARALL 3/2 laminates. The geometry and boundary conditions are depicted in Figure 3.38. The distribution of σ_{xz} for ARALL 2/1 is also depicted for comparison.

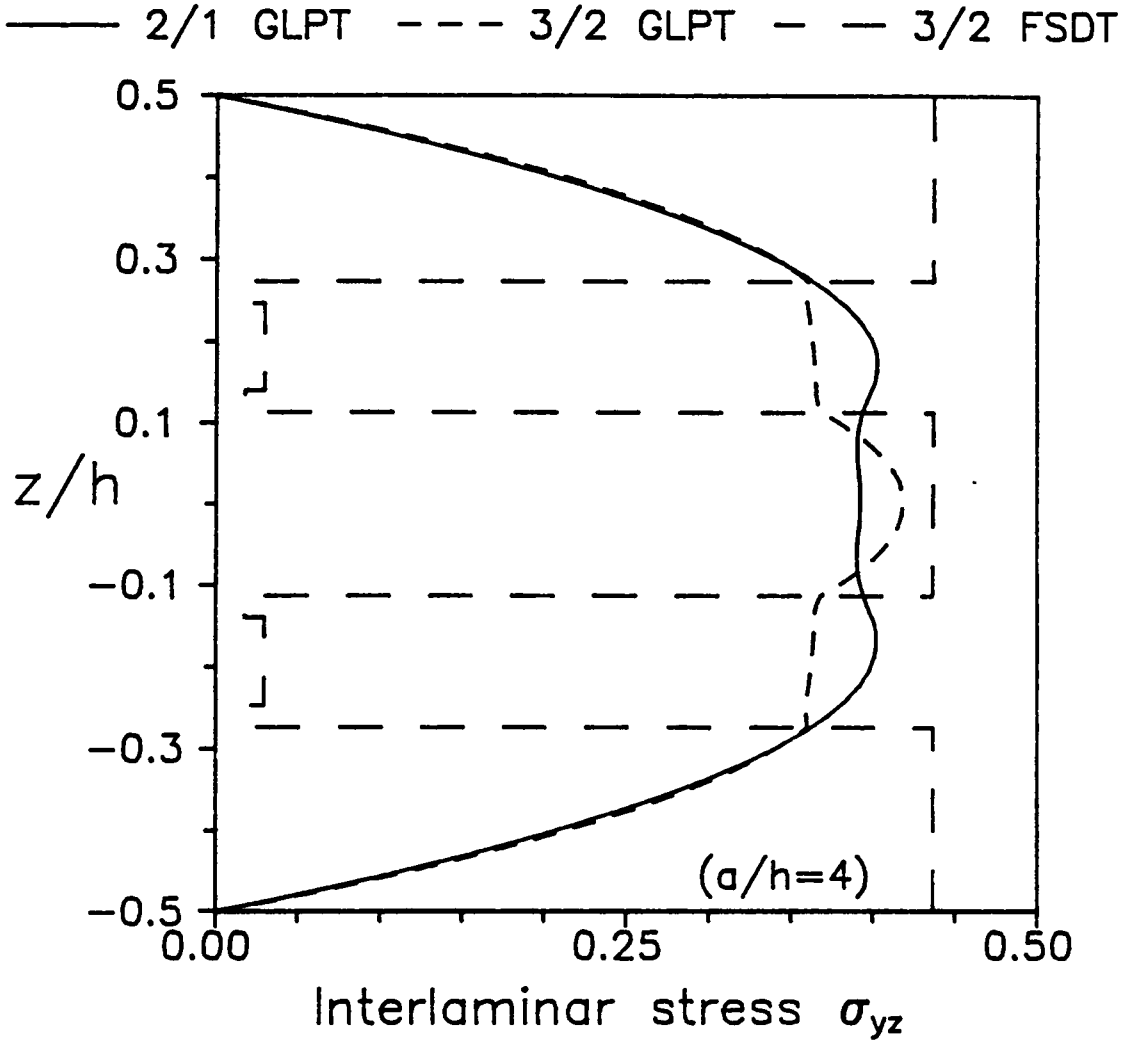

3.19 Comparison of the transverse shear stress distribution σ_{yz} from GLPT and FSDT for ARALL 3/2 laminates. The geometry and boundary conditions are depicted in Figure 3.38. The distribution of σ_{yz} for ARALL 2/1 is also depicted for comparison.

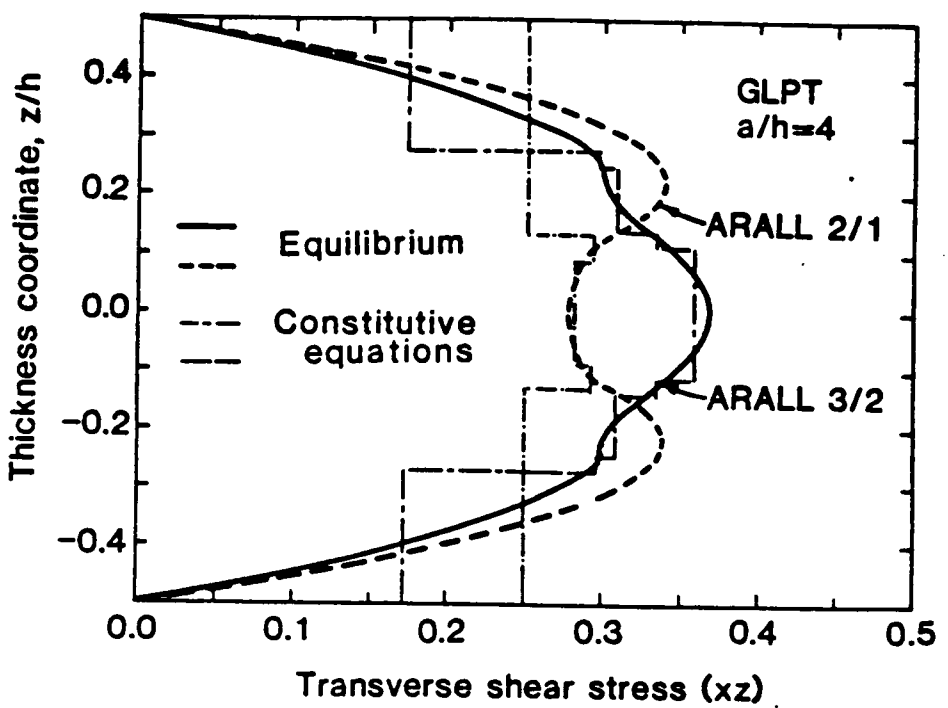

3.20 Comparison between the transverse shear stress σ_{xz} distributions obtained from equilibrium and constitutive equations for ARALL 2/1 and 3/2 laminates. The geometry and boundary conditions are depicted in Figure 3.38. 8-node quadratic elements are used to obtain all the results shown.

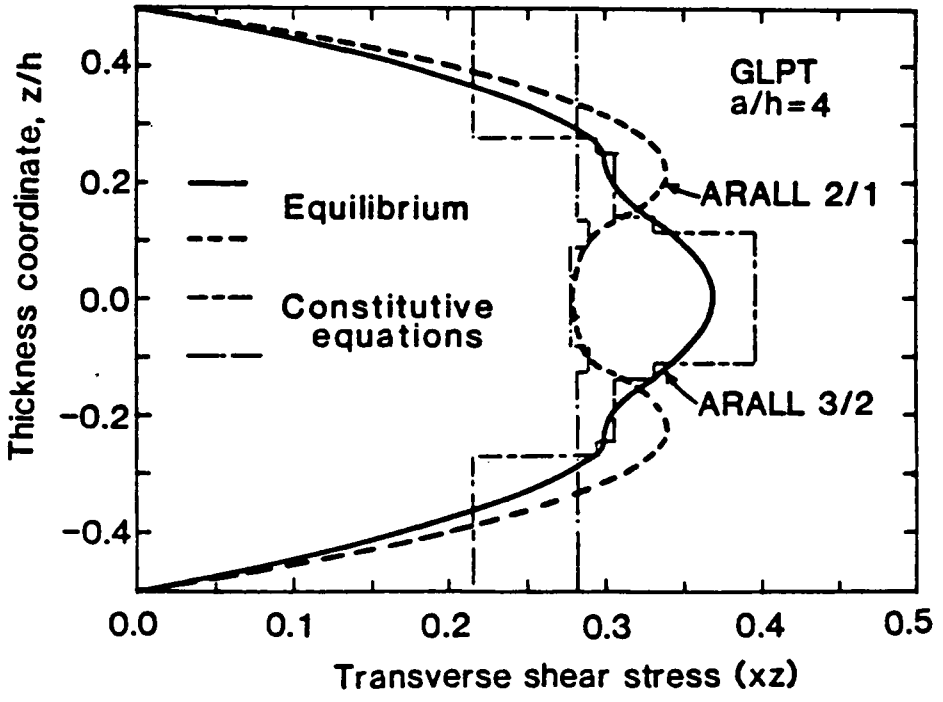

3.21 Smooth lines show the transverse shear stress σ_{xz} distributions obtained from equilibrium equations and quadratic elements. Broken lines represent the transverse shear stress σ_{xz} distributions obtained from constitutive equations and linear elements. ARALL 2/1 and 3/2, and the geometry and boundary conditions of Figure 3.38 are used.

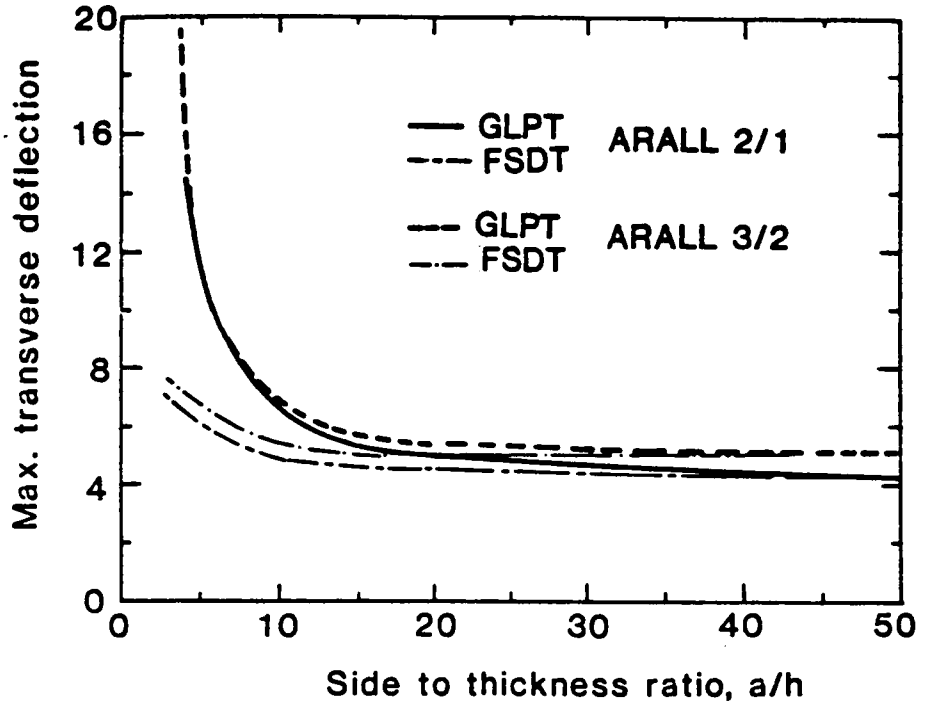

3.22 Maximum transverse deflection versus side to thickness ratio. Comparison between results from GLPT and FSDT for ARALL 2/1 and 3/2 laminates. Simply supported square plates under doubly-sinusoidal load as shown in Figure 3.38 are considered.

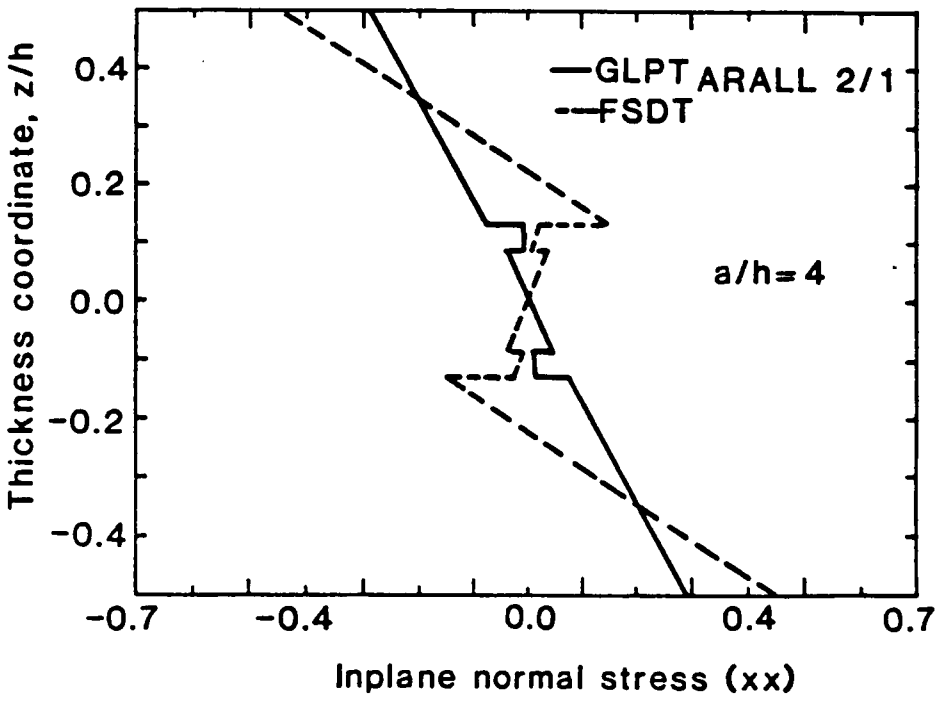

3.23 Comparison of the inplane normal stress distribution σ_{xx} from GLPT and FSDT for ARALL 2/1 laminate. The geometry and boundary conditions are depicted in figure 3.38.

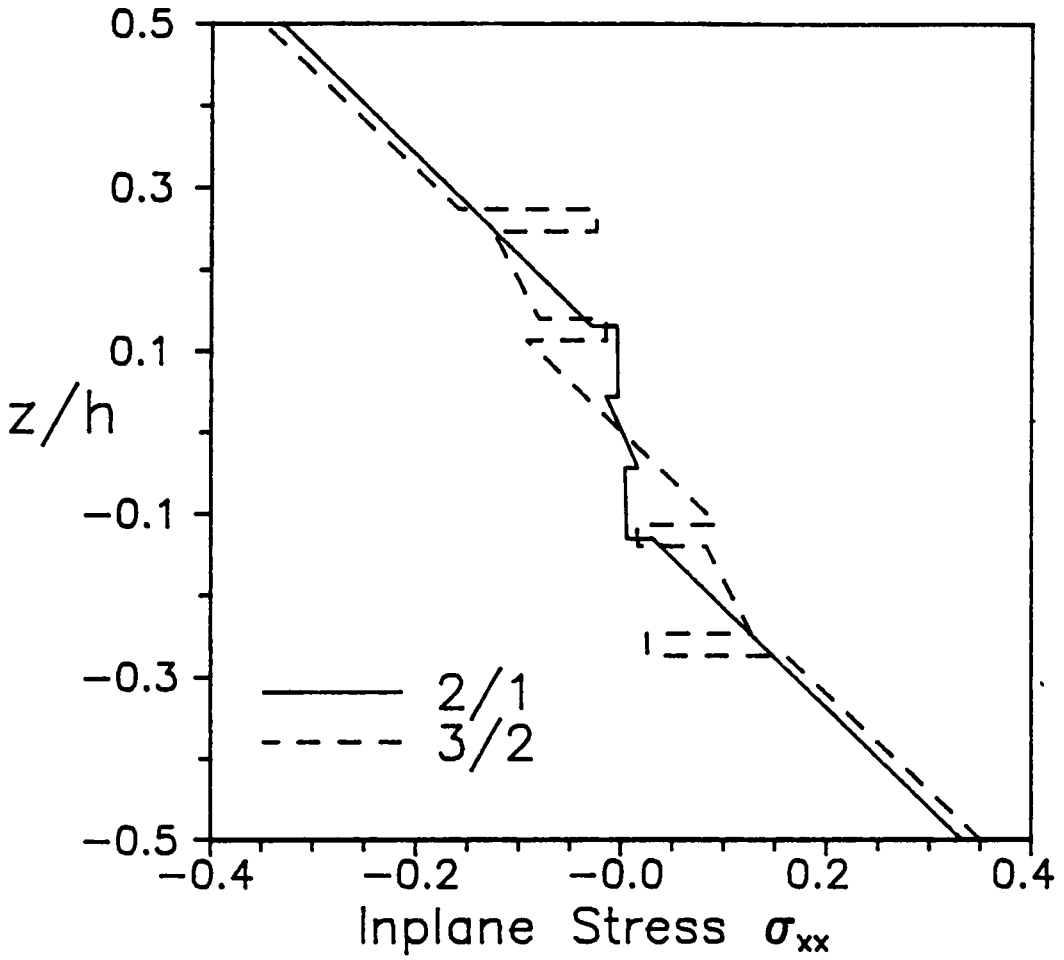

3.24 Through the thickness distribution of the inplane normal stress σ_{xx} for ARALL 2/1 and ARALL 3/2 laminates. The geometry and boundary conditions are depicted in figure 3.38.

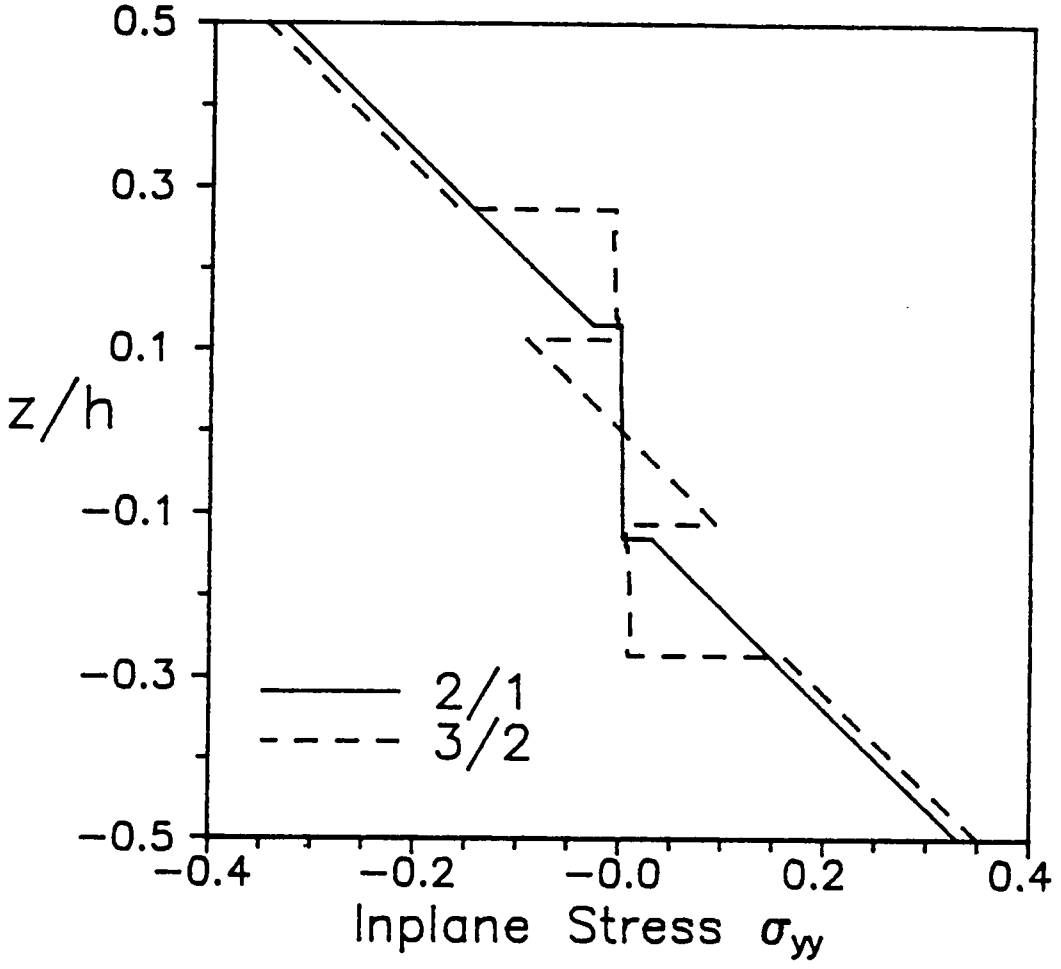

3.25 Through the thickness distribution of the inplane normal stress σ_{yy} for ARALL 2/1 and ARALL 3/2 laminates. The geometry and boundary conditions are depicted in figure 3.38.

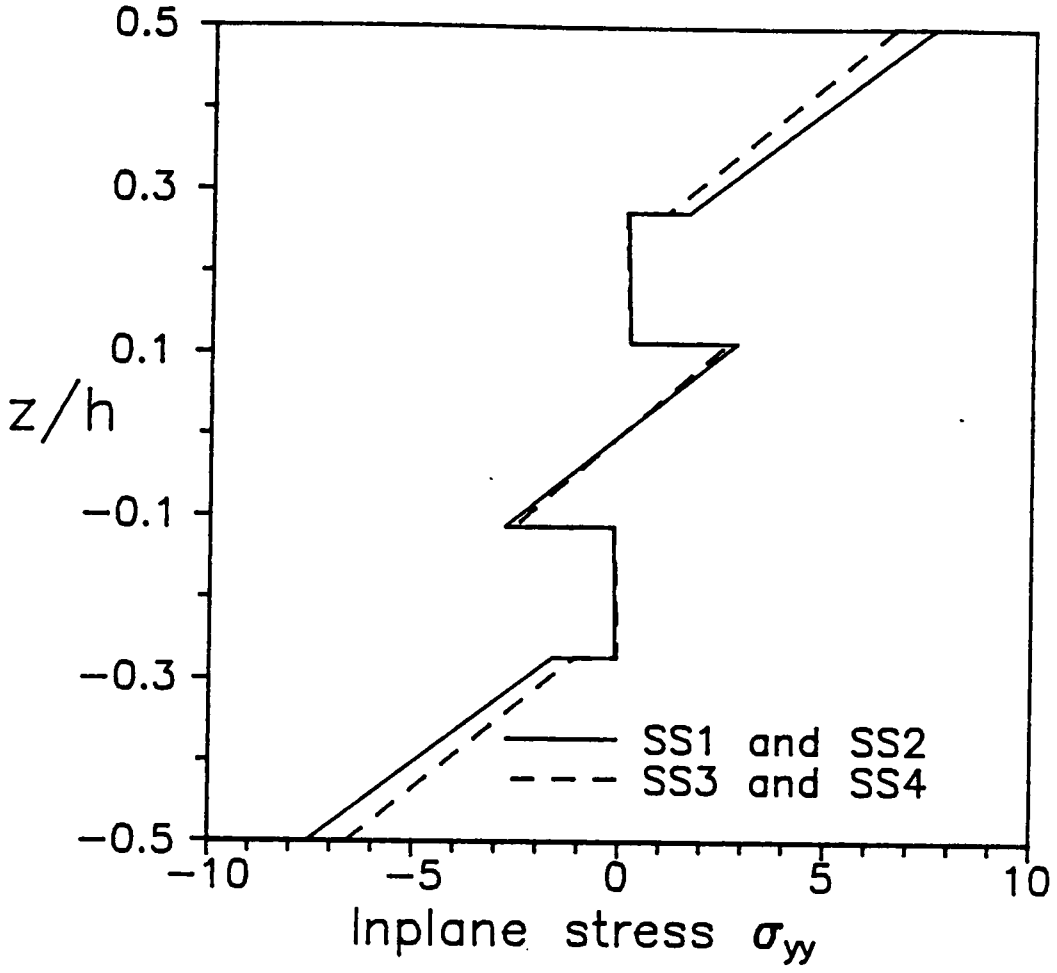

3.26 Influence of the boundary conditions (SS1 to SS4) on the stress distribution σ_{yy} in ARALL 3/2 laminate under uniform transverse load for a/h = 4.

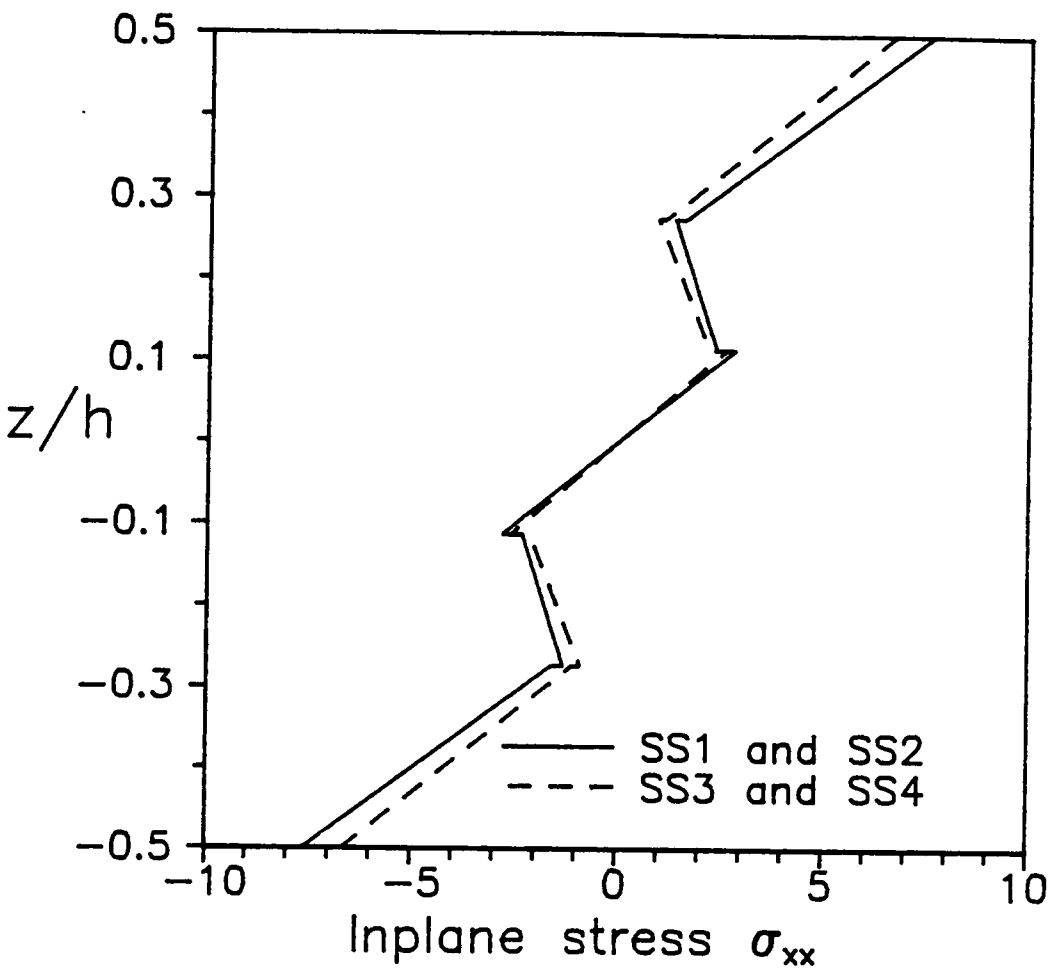

3.27 Influence of the boundary conditions (SS1 to SS4) on the stress distribution σ_{xx} in ARALL 3/2 laminate under uniform transverse load for a/h = 4,

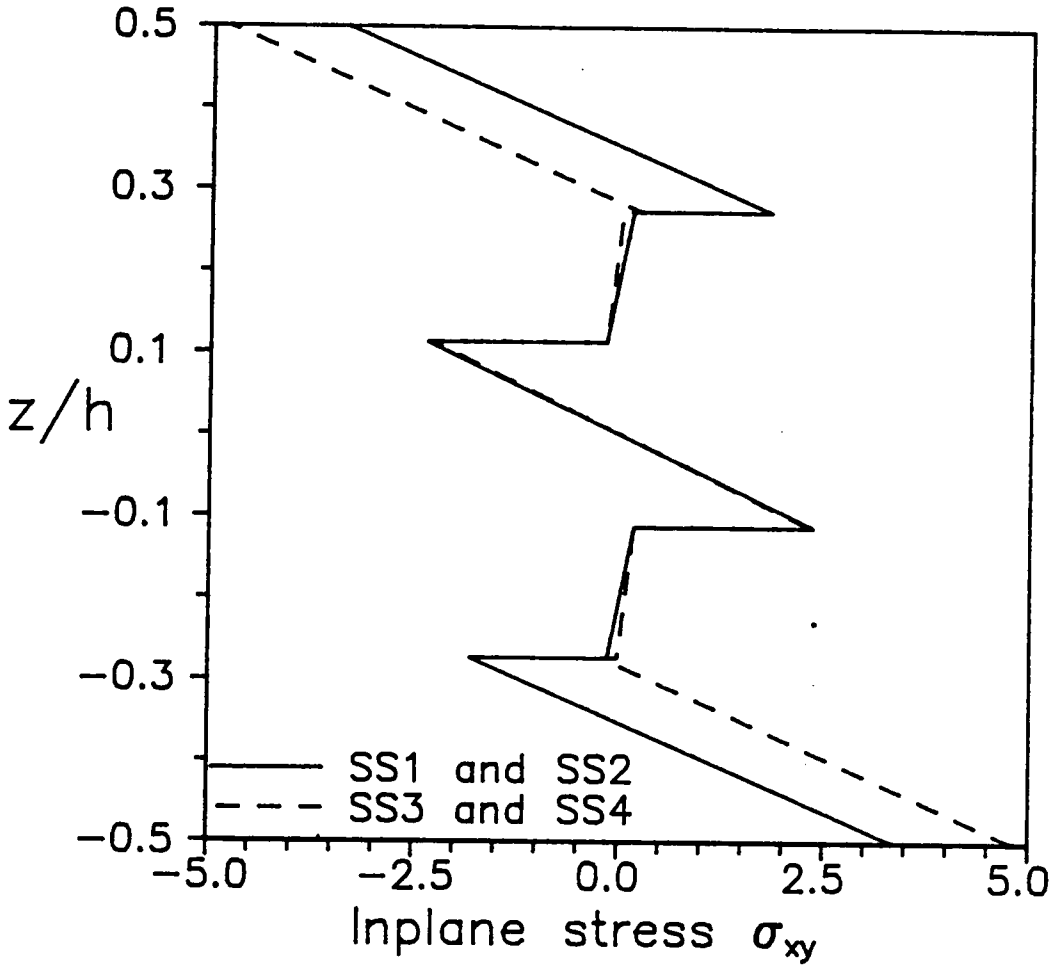

3.28 Influence of the boundary conditions (SS1 to SS4) on the stress distribution σ_{xy} in ARALL 3/2 laminate under uniform transverse load for a/h = 4.

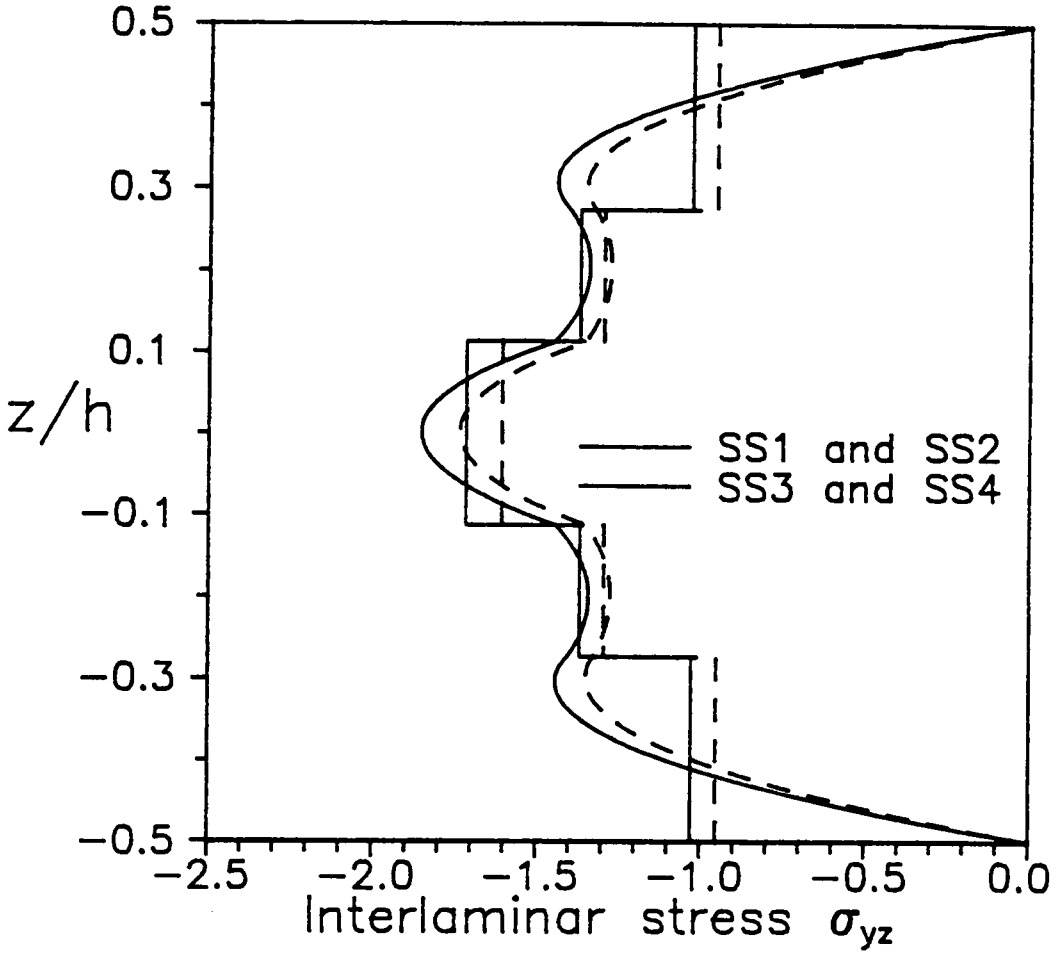

3.29 Influence of the boundary conditions (SS1 to SS4) on the stress distribution σ_{yz} in ARALL 3/2 laminate under uniform transverse load for a/h = 4. Smooth curves reprsent results obtained from equilibrium equations, and broken lines from constitutive equations.

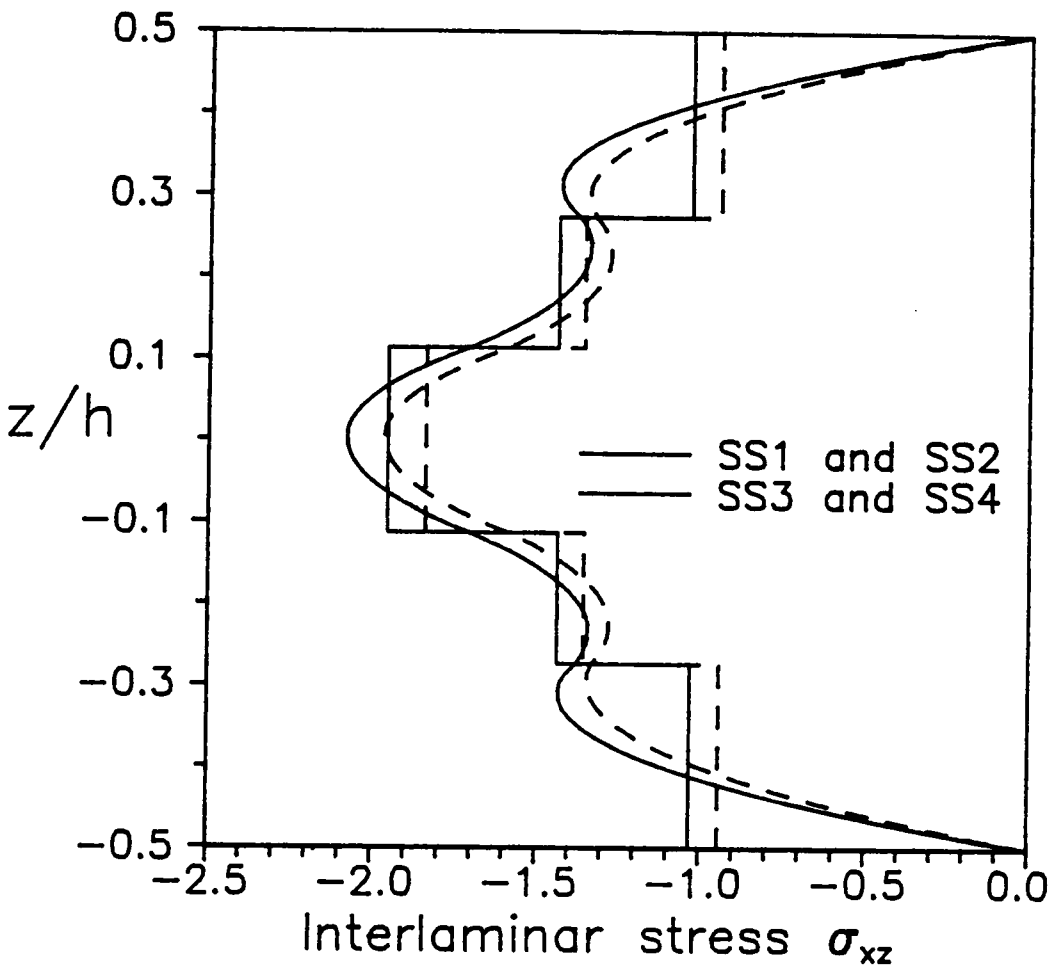

3.30 Influence of the boundary conditions (SS1 to SS4) on the stress distribution σ_{xz} in ARALL 3/2 laminate under uniform transverse load for a/h = 4. Smooth curves represent results obtained from equilibrium equations, and broken lines from constitutive equations.

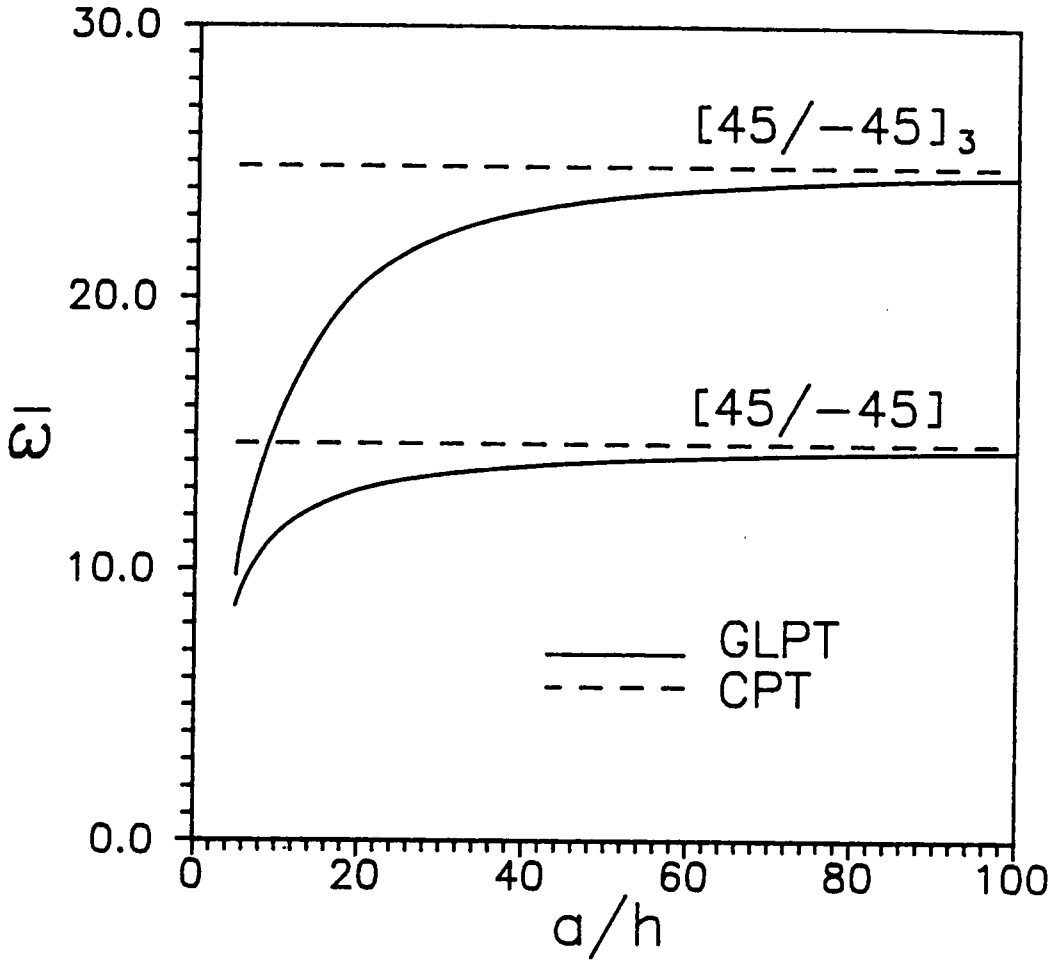

3.31 Fundamental frequencies as a function of the thickness ratio for 2- and 6-layer antisymmetric angle-ply laminates.

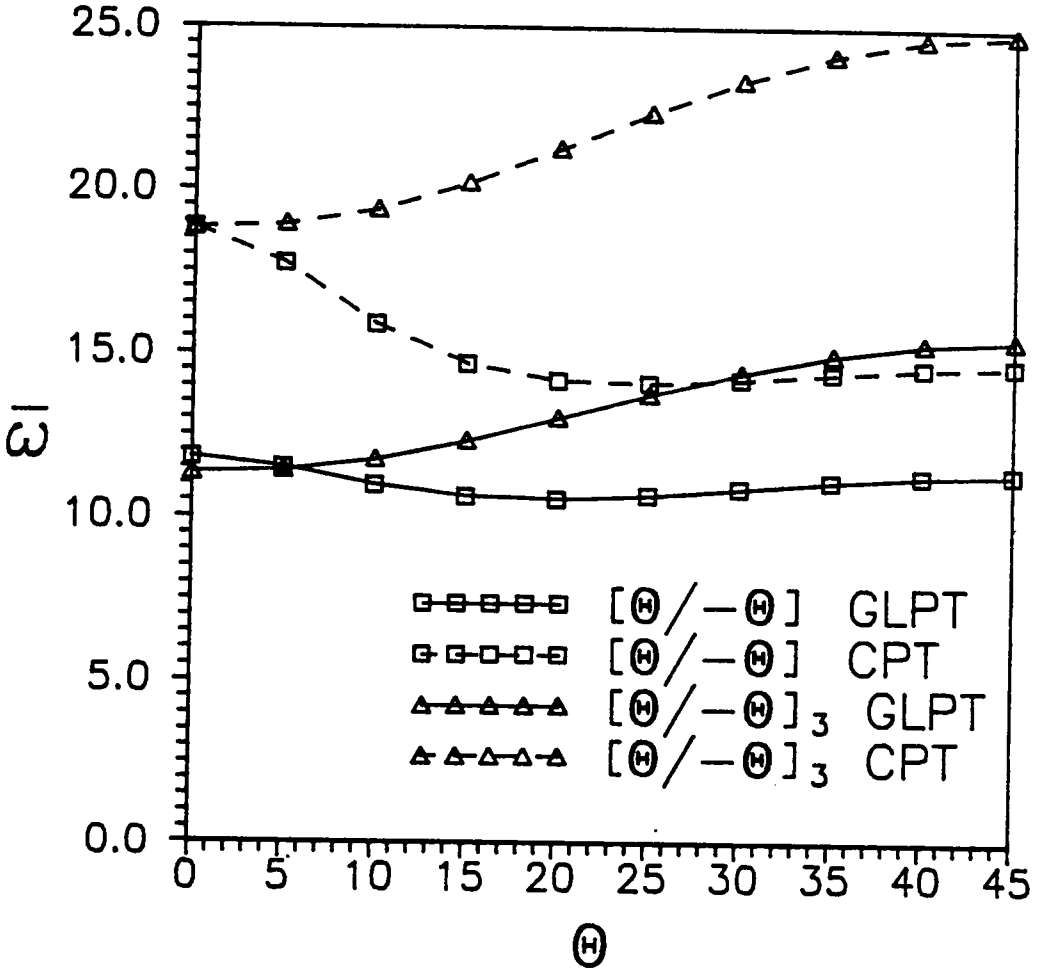

3.32 Fundamental frequencies as a function of the lamination angle θ for 2- and 6-layer antisymmetric angle-ply laminates.

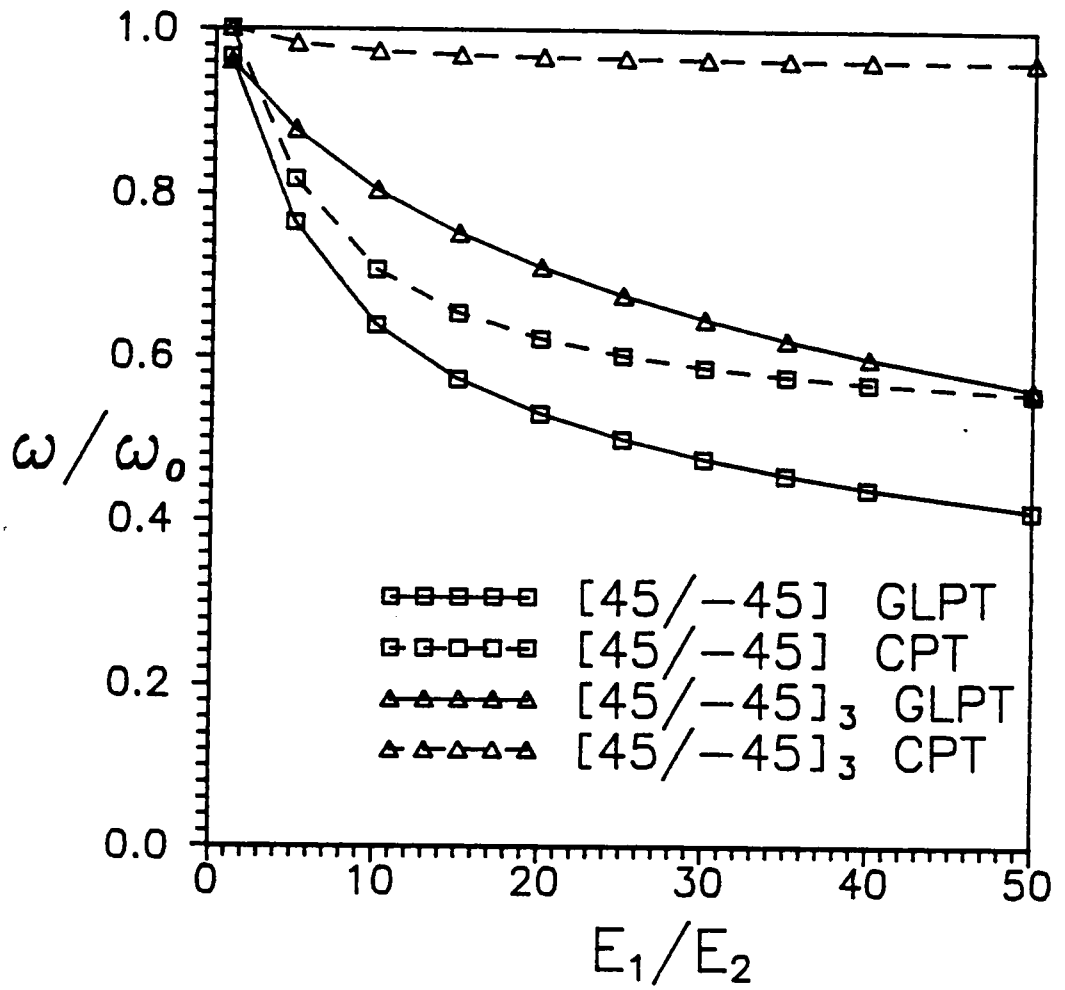

3.33. Fundamental frequencies as a function of the orthotropicity ratio E_1/E_2 for 2- and 6-layer antisymmetric angle-ply laminates.

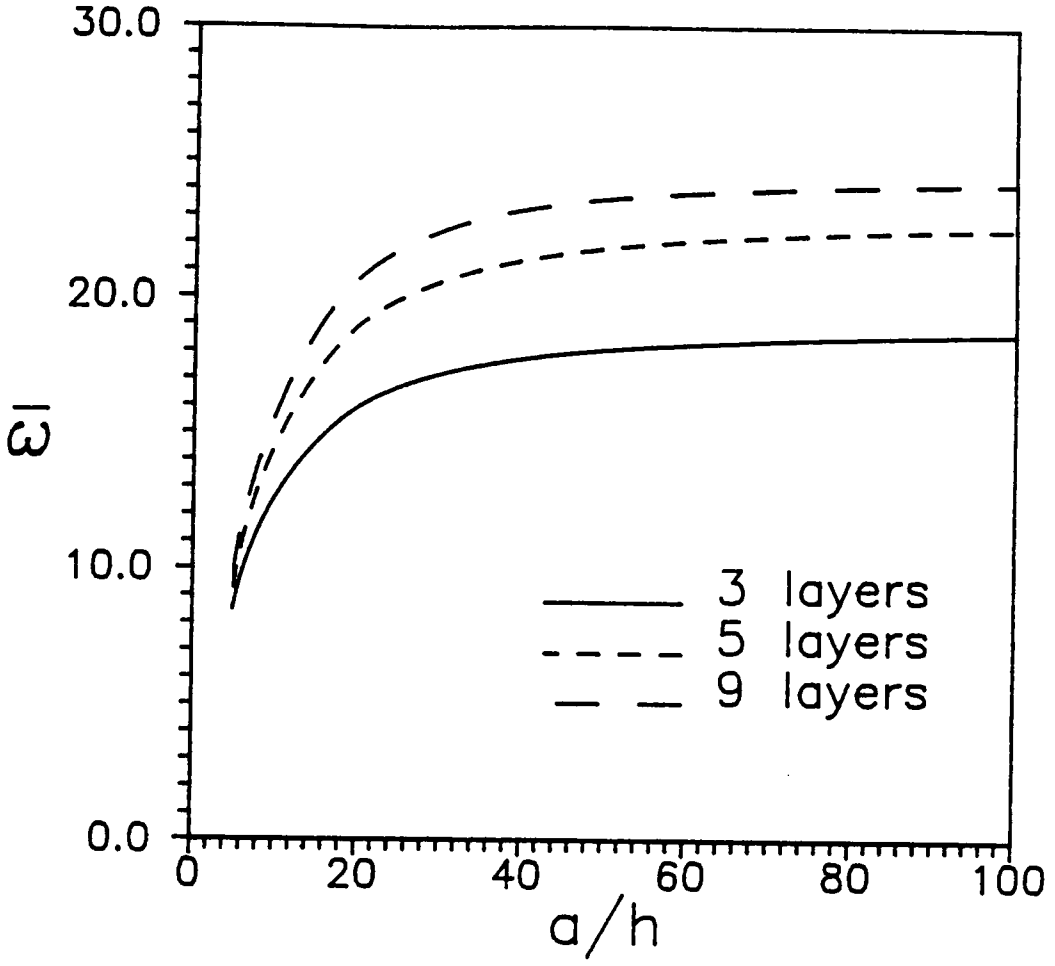

3.34 Effect of the number of layers and the thickness ratio on the fundamental frequencies of symmetric angle-ply laminates.

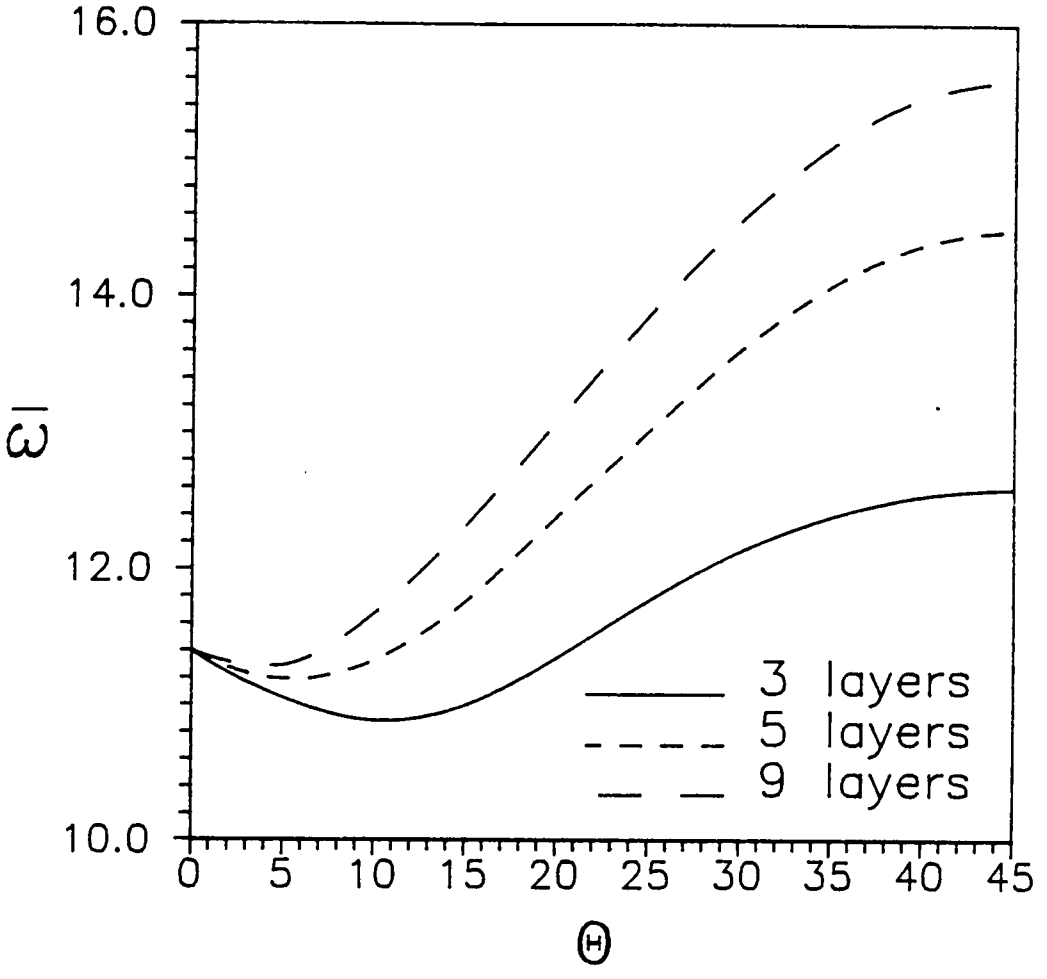

3.35 Effect of the number of layers and the lamination angle θ on the fundamental frequencies of symmetric angle-ply laminates.

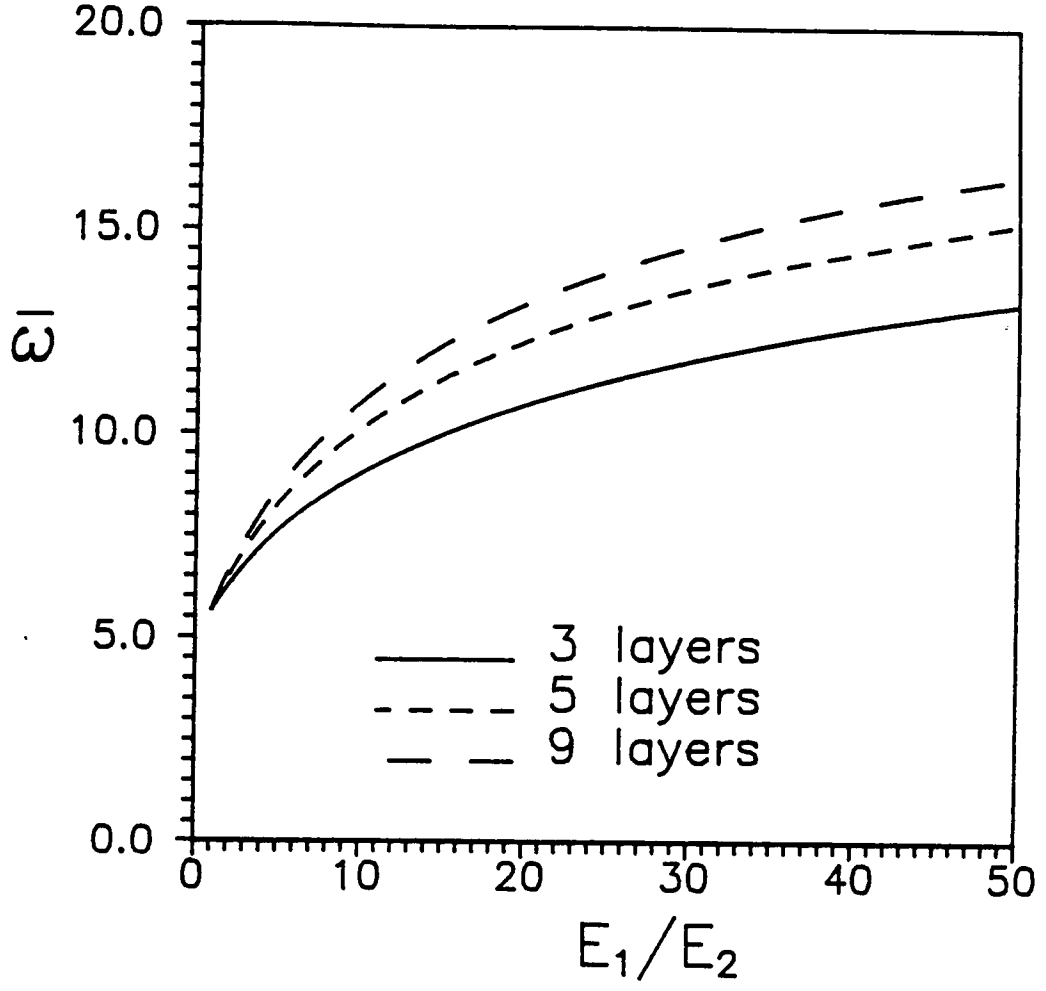

3.36 Effect of the number of layers and the orthotropicity ratio E_1/E_2 on the fundamental frequencies of symmetric angle-ply laminates.

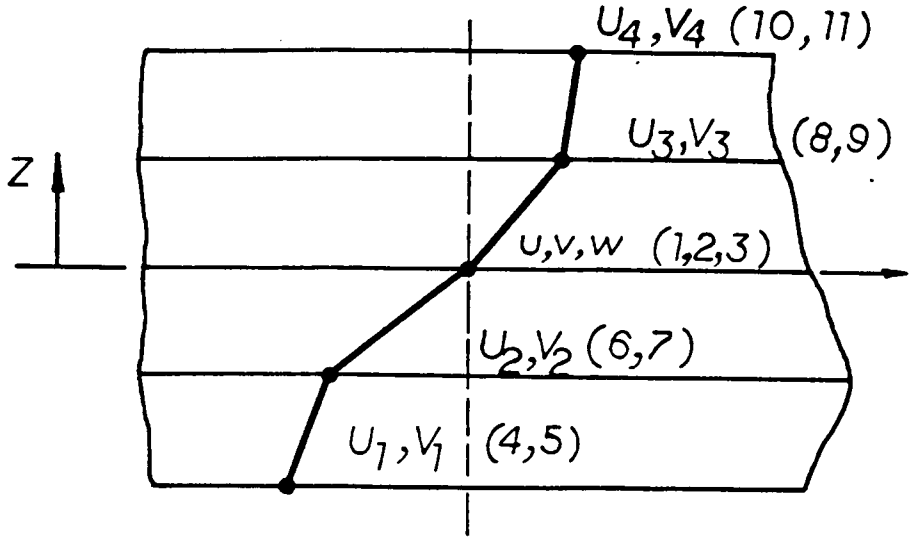

3.37 Displacements and degrees of freedom in GLPT.

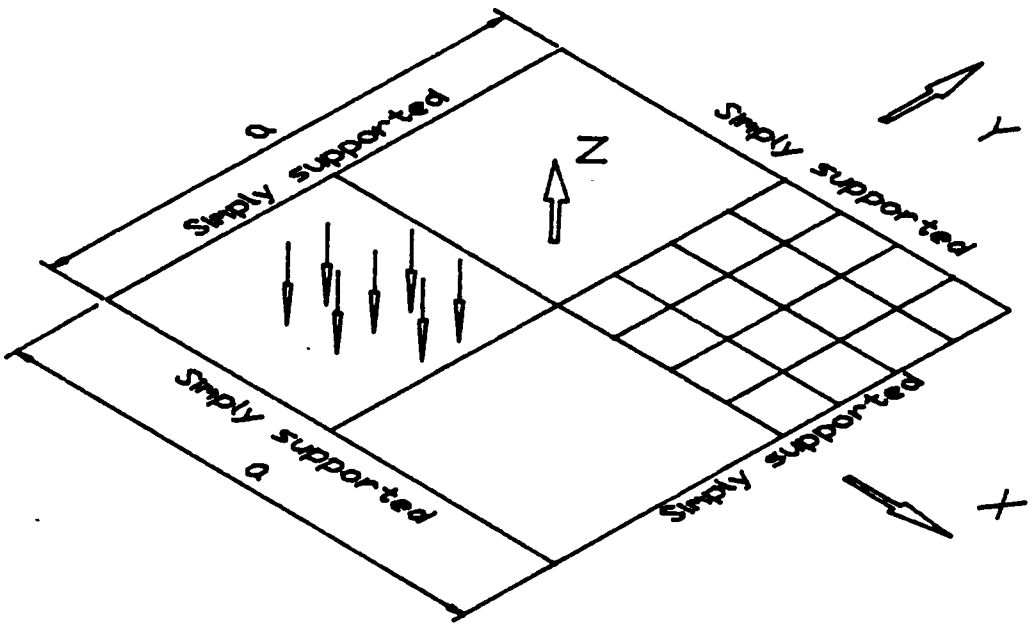

3.38 Finite element mesh on a quarter of a simply-supported plate modelled using the symmetry boundary conditions along x = 0 and y = 0.

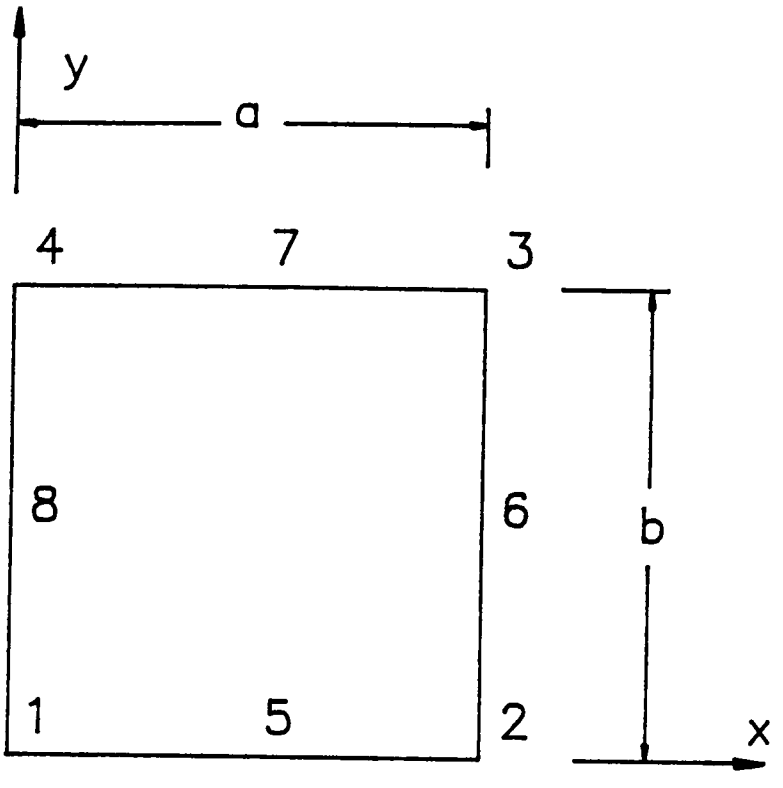

3.39 One element model.

Table 3.1: Fundamental frequency $\bar{\omega} = \omega(\rho h^2/E_2)^{1/2}$ for symmetric cross-ply laminates.

Source	Layers	E_1/E_2 = 3	10	20	30	40
Noor		0.26474	0.32841	0.38241	0.41089	0.43006
GLPT		0.26453	0.33677	0.38977	0.42055	0.44114
Error	3	0.08%	2.55%	1.92%	2.35%	2.58%
CPT		0.29198	0.41264	0.54043	0.64336	0.73196
Error		10.29%	25.65%	41.32%	56.58%	70.20%
Noor		0.26587	0.34089	0.39972	0.43140	0.45374
GLPT		0.26450	0.34146	0.40119	0.43667	0.46067
Error	5	0.52%	0.17%	0.37%	1.22%	1.53%
CPT		0.29198	0.41264	0.54043	0.64336	0.73196
Error		9.82%	21.05%	35.20%	49.13%	61.32%
Noor		0.26640	0.34432	0.40547	0.44210	0.46679
GLPT		0.26415	0.34233	0.40416	0.44142	0.46666
Error	9	0.84%	0.58%	0.32%	0.15%	0.03%
CPT		0.29187	0.41264	0.54043	0.64336	0.73196
Error		9.60%	19.84%	33.28%	45.52%	56.81%

$G_{12}/E_2 = 0.6$; $G_{23}/E_2 = 0.5$; $\nu_{12} = 0.25$, $a/h = 10$.

Table 3.2: Fundamental frequencies $\bar{\omega} = \omega(\rho h^2/E_2)^{1/2}$ for antisymmetric cross-ply laminates.

Source	Layers	E_1/E_2 = 2	10	20	30	40
Noor		0.25031	0.27938	0.30698	0.32705	0.34250
GLPT		0.25133	0.27897	0.30517	0.32429	0.33905
Error	2	0.41%	0.15%	0.59%	0.84%	1.01%
CPT		0.27082	0.30968	0.35422	0.39355	0.42884
Error		8.19%	10.85%	15.39%	20.33%	25.21%
Noor		0.26182	0.32578	0.37622	0.40660	0.42719
GLPT		0.26094	0.32702	0.38058	0.41337	0.43572
Error	4	0.34%	0.38%	1.16%	1.67%	2.00%
CPT		0.28676	0.38877	0.49907	0.58911	0.66691
Error		9.53%	19.34%	32.65%	44.89%	56.12%
Noor		0.26440	0.33657	0.39359	0.42783	0.45091
GLPT		0.26262	0.33566	0.39420	0.42974	0.45385
Error	6	0.67%	0.27%	0.15%	0.45%	0.65%
CPT		0.28966	0.40215	0.52234	0.61963	0.70359
Error		9.55%	19.48%	32.71%	44.83%	56.04%
Noor		0.26583	0.34250	0.40337	0.44011	0.46498
GLPT		0.26348	0.34011	0.40134	0.43848	0.46372
Error	10	0.88%	0.70%	0.50%	0.37%	0.27%
CPT		0.29115	0.40889	0.53397	0.63489	0.72185
Error		9.52%	19.38%	32.38%	44.26%	55.24%

$G_{12}/E_2 = 0.6$; $G_{23}/E_2 = 0.5$; $\nu_{12} = 0.5$, $a/h = 10$.

Chapter 4

NONLINEAR ANALYSIS OF COMPOSITE LAMINATES

4.1 Introduction

In the following sections the nonlinear version of the Generalized Laminated Plate Theory is formulated, and it is used to investigate nonlinear effects in composite laminates. A plate bending finite element based on the theory is developed and its accuracy is investigated by comparison with exact and approximate solutions to conventional plate theories. The element has improved description of the in plane as well as the transverse deformation response. The theory is further applied to study various aspects of the geometrically nonlinear analysis of composite plates. It is shown that inclusion of the geometric nonlinearity relaxes stress distributions, and that composite laminates with bending-extensional coupling do not exhibit bifurcation buckling.

4.2 Formulation of the Nonlinear Theory

4.2.1 Displacements and Strains

The displacements (u_1,u_2,u_3) at a point (x,y,z) in the laminate are assumed to be of the form (2.1)

$$u_1(x,y,z) = u(x,y) + U(x,y,z)$$
$$u_2(x,y,z) = v(x,y) + V(x,y,z)$$
$$u_3(x,y,z) = w(x,y), \qquad (4.1)$$

where (u,v,w) are the displacements of a point $(x,y,0)$ on the reference plane of the laminate, and U and V are functions which vanish on the

reference plane:

$$U(x,y,0) = V(x,y,0) = 0. \tag{4.2}$$

The von Kármán strains associated with the displacements in Equation (4.1) are given by

$$\varepsilon_x = \frac{\partial u}{\partial x} + \frac{\partial U}{\partial x} + \frac{1}{2}\left(\frac{\partial w}{\partial x}\right)^2, \quad \varepsilon_y = \frac{\partial v}{\partial y} + \frac{\partial V}{\partial y} + \frac{1}{2}\left(\frac{\partial w}{\partial y}\right)^2$$

$$2\varepsilon_{xy} = \left(\frac{\partial u}{\partial y} + \frac{\partial v}{\partial x}\right) + \left(\frac{\partial U}{\partial y} + \frac{\partial V}{\partial x}\right) + \frac{\partial w}{\partial x}\frac{\partial w}{\partial y},$$

$$2\varepsilon_{xz} = \frac{\partial U}{\partial z} + \frac{\partial w}{\partial x}, \quad 2\varepsilon_{yz} = \frac{\partial V}{\partial z} + \frac{\partial w}{\partial y}. \tag{4.3}$$

The principle of virtual displacements is used to derive a consistent set of differential equations governing the equilibrium of a laminate composed of N constant-thickness orthotropic lamina, the material axes of each lamina being arbitrarily oriented with respect to the laminate coordinates.

4.2.2 Thickness Approximation

In order to reduce the three-dimensional theory to a two-dimensional theory, it is necessary to make an assumption concerning the variation of U and V with respect to the thickness coordinate, z. To keep the flexibility of the degree of variation of the displacements through thickness, we assume that U and V are approximated as (2.3)

$$U(x,y,z) = \sum_{j=1}^{n} u^j(x,y)\phi_j(z)$$

$$V(x,y,z) = \sum_{j=1}^{n} v^j(x,y)\phi_j(z), \tag{4.4}$$

where u^j and v^j are undetermined coefficients and ϕ_j are any continuous functions that satisfy the condition

$$\phi_j(0) = 0 \text{ for all } j = 1,2,\ldots,n. \tag{4.5}$$

The approximation in Equation (4) can also be viewed as the global semi-discrete finite-element approximations of U and V through the thickness. In that case, ϕ_j denote the global interpolation functions, and u^j and v^j are the nodal values of U and V at the nodes through the thickness of the laminate.

4.2.3 Governing Equations

The nonlinear equations relating u, v, w, u^j and v^j can be derived using the virtual work principle. Substituting Equation (4.4) into the virtual work principle, we obtain the weak (or variational) statement of the present theory,

$$\begin{aligned} 0 = \int_\Omega \{ & N_x\left(\frac{\partial \delta u}{\partial x} + \frac{\partial w}{\partial x}\frac{\partial \delta w}{\partial x}\right) + N_y\left(\frac{\partial \delta v}{\partial y} + \frac{\partial w}{\partial y}\frac{\partial \delta w}{\partial y}\right) + N_{xy}\left(\frac{\partial \delta u}{\partial y} + \frac{\partial \delta v}{\partial x}\right. \\ & \left. + \frac{\partial w}{\partial x}\frac{\partial \delta w}{\partial y} + \frac{\partial \delta w}{\partial x}\frac{\partial w}{\partial y}\right) + Q_x\frac{\partial \delta w}{\partial x} + Q_y\frac{\partial \delta w}{\partial y} \\ & + \sum_{j=1}^{n}\left[N_x^j\frac{\partial \delta u^j}{\partial x} + N_y^j\frac{\partial \delta v^j}{\partial y} + N_{xy}^j\left(\frac{\partial \delta u^j}{\partial y} + \frac{\partial \delta v^j}{\partial x}\right)\right. \\ & \left. + Q_x^j u^j + Q_y^j v^j\right] - p\delta w\} dA, \end{aligned} \tag{4.6a}$$

where p is the distributed transverse load, and

$$(N_x, N_y, N_{xy}) = \int_{-h/2}^{h/2} (\sigma_x, \sigma_y, \sigma_{xy}) dz$$

$$(Q_x, Q_y) = \int_{-h/2}^{h/2} (\sigma_{xz}, \sigma_{yz}) dz$$

$$(N_x^j, N_y^j, N_{xy}^j) = \int_{-h/2}^{h/2} (\sigma_x, \sigma_y, \sigma_{xy}) \phi_j(z) dz$$

$$(Q_x^j, Q_y^j) = \int_{-h/2}^{h/2} (\sigma_{xz}, \sigma_{yz}) \frac{d\phi_j}{dz} (z) dz. \tag{4.6b}$$

The Euler-Lagrange equations of the theory are:

$$\begin{aligned}
&N_{x,x} + N_{xy,y} = 0 \\
&N_{xy,x} + N_{y,y} = 0, \\
&Q_{x,x} + Q_{y,y} + N(w) + p = 0, \\
&N_{x,x}^j + N_{xy,y}^j - Q_x^j = 0, \\
&N_{xy,x}^j + N_{y,y}^j - Q_y^j = 0,
\end{aligned} \qquad j = 1,2,\ldots,n \tag{4.7a}$$

where N(w) is due to the inclusion of the von Kármán nonlinearity in the theory:

$$N(w) = \frac{\partial}{\partial x} \left(N_x \frac{\partial w}{\partial x} + N_{xy} \frac{\partial w}{\partial y}\right) + \frac{\partial}{\partial y} \left(N_{xy} \frac{\partial w}{\partial x} + N_y \frac{\partial w}{\partial y}\right) \tag{4.7b}$$

There are (2n + 3) differential equations in (2n + 3) variables (u, v, w, u^j, v^j). The form of the geometric and force boundary conditions is given below:

Geometric (Essential)	Force (Natural)
u	$N_x n_x + N_{xy} n_y$
v	$N_{xy} n_x + N_y n_y$
w	$Q_x n_x + Q_y n_y$
u^j	$N_x^j n_x + N_{xy}^j n_y$
v^j	$N_{xy}^j n_x + N_y^j n_y$

(4.8)

where (n_x, n_y) denote the direction cosines of a unit normal to the boundary of the midplane Ω.

4.2.4 Constitutive Equations

The constitutive equations of an orthotropic lamina in the laminate coordinate system are given by

$$\begin{Bmatrix} \sigma_x \\ \sigma_y \\ \sigma_{xy} \\ \sigma_{yz} \\ \sigma_{xz} \end{Bmatrix}_{(k)} = \begin{bmatrix} \bar{Q}_{11} & \bar{Q}_{12} & Q_{16} & 0 & 0 \\ \bar{Q}_{12} & \bar{Q}_{22} & Q_{26} & 0 & 0 \\ \bar{Q}_{16} & \bar{Q}_{26} & Q_{66} & 0 & 0 \\ 0 & 0 & 0 & \bar{Q}_{55} & \bar{Q}_{45} \\ 0 & 0 & 0 & \bar{Q}_{45} & \bar{Q}_{44} \end{bmatrix}_{(k)} \begin{Bmatrix} \varepsilon_x \\ \varepsilon_y \\ 2\varepsilon_{xy} \\ 2\varepsilon_{xz} \\ 2\varepsilon_{yz} \end{Bmatrix}_{(k)} \tag{4.9}$$

Substitution of Equation (4.9) into Equation (4.6b) gives the following laminate constitutive equations:

$$\begin{Bmatrix} N_x \\ N_y \\ N_{xy} \\ Q_x \\ Q_y \end{Bmatrix} = \begin{bmatrix} A_{11} & A_{12} & A_{16} & 0 & 0 \\ A_{12} & A_{22} & A_{26} & 0 & 0 \\ A_{16} & A_{26} & A_{66} & 0 & 0 \\ 0 & 0 & 0 & A_{55} & A_{45} \\ 0 & 0 & 0 & A_{45} & A_{44} \end{bmatrix} \begin{Bmatrix} \frac{\partial u}{\partial x} + \frac{1}{2}\left(\frac{\partial w}{\partial x}\right)^2 \\ \frac{\partial v}{\partial y} + \frac{1}{2}\left(\frac{\partial w}{\partial y}\right)^2 \\ \frac{\partial u}{\partial y} + \frac{\partial v}{\partial x} + \frac{\partial w}{\partial x}\frac{\partial w}{\partial y} \\ \frac{\partial w}{\partial x} \\ \frac{\partial w}{\partial y} \end{Bmatrix}$$

$$+\sum_{j=1}^{n}\begin{bmatrix} B_{11}^{j} & B_{12}^{j} & B_{16}^{j} & 0 & 0 \\ B_{22}^{j} & B_{22}^{j} & B_{26}^{j} & 0 & 0 \\ B_{16}^{j} & B_{26}^{j} & B_{66}^{j} & 0 & 0 \\ 0 & 0 & 0 & \bar{B}_{55}^{j} & \bar{B}_{45}^{j} \\ 0 & 0 & 0 & \bar{B}_{45}^{j} & \bar{B}_{44}^{j} \end{bmatrix} \begin{Bmatrix} \frac{\partial u^{j}}{\partial x} \\ \frac{\partial v^{j}}{\partial y} \\ \frac{\partial u^{j}}{\partial y} + \frac{\partial v^{j}}{\partial x} \\ u^{j} \\ v^{j} \end{Bmatrix} \tag{4.10a}$$

$$\begin{Bmatrix} N_x^j \\ N_y^j \\ N_{xy}^j \\ Q_x^j \\ Q_y^j \end{Bmatrix} = \begin{bmatrix} B_{11}^{j} & B_{12}^{j} & B_{16}^{j} & 0 & 0 \\ B_{12}^{j} & B_{22}^{j} & B_{26}^{j} & 0 & 0 \\ B_{16}^{j} & B_{26}^{j} & B_{66}^{j} & 0 & 0 \\ 0 & 0 & 0 & \bar{B}_{55}^{j} & \bar{B}_{45}^{j} \\ 0 & 0 & 0 & \bar{B}_{45}^{j} & \bar{B}_{44}^{j} \end{bmatrix} \begin{Bmatrix} \frac{\partial u}{\partial x} + \frac{1}{2}\left(\frac{\partial w}{\partial x}\right)^2 \\ \frac{\partial v}{\partial y} + \frac{1}{2}\left(\frac{\partial w}{\partial y}\right)^2 \\ \frac{\partial u}{\partial y} + \frac{\partial v}{\partial x} + \frac{\partial w}{\partial x}\frac{\partial w}{\partial y} \\ \frac{\partial w}{\partial x} \\ \frac{\partial w}{\partial y} \end{Bmatrix}$$

$$+\sum_{k=1}^{n}\begin{bmatrix} D_{11}^{jk} & D_{12}^{jk} & D_{16}^{jk} & 0 & 0 \\ D_{12}^{jk} & D_{22}^{jk} & D_{26}^{jk} & 0 & 0 \\ D_{16}^{jk} & D_{26}^{jk} & D_{66}^{jk} & 0 & 0 \\ 0 & 0 & 0 & \bar{D}_{55}^{jk} & \bar{D}_{45}^{jk} \\ 0 & 0 & 0 & \bar{D}_{45}^{jk} & \bar{D}_{44}^{jk} \end{bmatrix} \begin{Bmatrix} \frac{\partial u^{k}}{\partial x} \\ \frac{\partial v^{k}}{\partial y} \\ \frac{\partial u^{k}}{\partial y} + \frac{\partial v^{k}}{\partial y} \\ u^{k} \\ v^{k} \end{Bmatrix} \tag{4.10b}$$

where the stiffness coefficients were given in Equation 2.11b. They should be computed as explained in Section 2.2 when linear interpolation functions are used [see Equation (2.6)].

4.3 Finite-Element Formulation

The generalized displacements (u,v,w,u^j,v^j) are expressed over each element as a linear combination of the two-dimensional interpolation functions ψ_i and the nodal values $(u_i,v_i,w_i,u_i^j,v_i^j)$ as follows:

$$(u,v,w,u^j,v^j) = \sum_{i=1}^{m} (u_i,v_i,w_i,u_i^j,v_i^j)\psi_i \tag{4.11}$$

where m is the number of nodes per element. Using Equation (4.11), the linear components of the strains can be expressed in the form

$$\begin{aligned} \{e\} &= [B]\{\Delta\} \\ \{e^j\} &= [\bar{B}]\{\Delta^j\} \end{aligned} \tag{4.12a}$$

where

$$\begin{aligned} \{\Delta\}^T &= \{u_1,v_1,w_1,\ldots,u_m,v_m,w_m\} \\ \{\Delta^j\}^T &= \{u_1^j,v_1^j,\ldots,u_m^j,v_m^j\} \end{aligned} \tag{4.12b}$$

Similarly, the nonlinear component of the strains can be written in the form

$$\{\eta\} = [B_{NL}]\{\Delta\} \tag{4.12c}$$

The matrices [B], $[\bar{B}]$ and $[B_{NL}]$ are given in Appendix 4. Using Equation (4.12) in the virtual work statement (4.6a), we obtain

$$\begin{aligned} 0 = \int_\Omega & (\{\delta\Delta\}^T[B]^T[A][B]\{\Delta\} + \{\delta\Delta\}^T[B]^T[A][B_{NL}]\{\Delta\} \\ & + 2\{\delta\Delta\}^T[B_{NL}]^T[A][B]\{\Delta\} + 2\{\delta\Delta\}^T[B_{NL}]^T[A][B_{NL}]\{\Delta\} \\ & + \sum_j^N [\{\delta\Delta\}^T[B]^T[B^j][\bar{B}]\{\Delta^j\} + 2\{\delta\Delta\}^T[B_{NL}]^T[B^j][\bar{B}]\{\Delta^j\} \\ & + \{\delta\Delta^j\}^T[\bar{B}]^T[B^j][B]\{\Delta\} + \{\delta\Delta^j\}^T[\bar{B}]^T[B^j][B_{NL}]\{\Delta\} \end{aligned}$$

$$+ \sum_{r}^{N} [\{\delta\Delta^j\}^T[\bar{B}]^T[D^{jr}][\bar{B}]\{\Delta^r\}]] - p\delta w)dA.$$

The finite element model is given by

$$\begin{bmatrix} [k^{11}] & [k_1^{12}] & \cdots & [k_N^{12}] \\ [k_1^{21}] & [k_{11}^{22}] & \cdots & \cdot \\ \vdots & & \ddots & \vdots \\ [k_N^{21}] & & \cdots & [k_{NN}^{22}] \end{bmatrix} \begin{Bmatrix} \{\Delta\} \\ \{\Delta^1\} \\ \vdots \\ \{\Delta^N\} \end{Bmatrix} = \begin{Bmatrix} \{q\} \\ \{q^1\} \\ \vdots \\ \{q^N\} \end{Bmatrix} \tag{4.13}$$

where the submatrices $[k^{11}]$, $[k_j^{12}]$, $[k_j^{21}]$, $[k_{ji}^{22}]$ with i,j = 1,...,N are given in Appendix 4.2. The load vectors $\{q\}$, $\{q^1\}...\{q^N\}$ are analogous to $\{\Delta\}$, $\{\Delta^1\}$, ... $\{\Delta^N\}$ in Equation (4.12b). The nonlinear algebraic system is solved by the Newton-Raphson algorithm. The components of the Jacobian matrix are given in Appendix 5.

The inplane components of the stresses (σ_x,σ_y,σ_{xy}) and their inplane derivatives ($\sigma_{x,x}$; $\sigma_{y,y}$; $\sigma_{xy,z}$; $\sigma_{xy,y}$) are computed from the constitutive equations for each layer, i.e.,

$$\begin{Bmatrix} \sigma_x \\ \sigma_y \\ \sigma_{xy} \end{Bmatrix} = \begin{bmatrix} Q_{11} & Q_{12} & Q_{13} \\ Q_{12} & Q_{22} & Q_{23} \\ Q_{13} & Q_{23} & Q_{33} \end{bmatrix} \begin{Bmatrix} \frac{\partial u}{\partial x} + \frac{1}{2}(\frac{\partial w}{\partial x})^2 + \sum_{j=1}^{N} \frac{\partial u^j}{\partial x}\psi_j \\ \frac{\partial v}{\partial y} + \frac{1}{2}(\frac{\partial w}{\partial y})^2 + \sum_{j=1}^{N} \frac{\partial v^j}{\partial y}\psi_j \\ \frac{\partial u}{\partial y} + \frac{\partial v}{\partial x} + \frac{\partial w}{\partial x}\frac{\partial w}{\partial y} + \sum_{j=1}^{N} (\frac{\partial u^j}{\partial y} + \frac{\partial v^j}{\partial x})\psi_j \end{Bmatrix} \tag{4.14}$$

Next, the interlaminar shear stresses (σ_{xz} and σ_{yz}) are recovered (see Section 3.2) from the equilibrium equations

$$\sigma_{xz,z} = -(\sigma_{x,x} + \sigma_{xy,y})$$

$$\sigma_{yz,z} = -(\sigma_{xy,x} + \sigma_{y,y}). \tag{4.15}$$

The nonlinear equations are also linearized to formulate the eigenvalue problem associated with bifurcation (buckling) analysis,

$$([K_D] - \lambda[K_G])\cdot\underset{\sim}{\Phi} = \underset{\sim}{0} \tag{4.16}$$

where $[K_D]$ is the linear part of the direct stiffness matrix (4.13) and $[K_G]$ is the geometric stiffness matrix, obtained from the nonlinear part of Equation (4.13) by perturbation of the nonlinear equations around the equilibrium position (see Section 4.6).

4.4 Numerical Examples

The first couple of sample problems are intended to validate the nonlinear finite element model developed herein. The problems of composite laminates are selected to illustrate certain aspects of the solution that are not often seen in isotropic plates or even in symmetric laminates.

4.4.1 Clamped Isotropic (ν = 0.3) Plate

Consider a clamped square plate of side a = 1000 mm, thickness h = 2 mm, isotropic and subjected to uniformly distributed transverse load, $p = \lambda p_o (p_o = 100 N/m^2)$. Figure 4.1 shows the variation of σ_{xx}/p at the top, bottom and middle surface of the plate as a function of the load parameter λ. A 2 x 2 mesh of nine-node quadratic elements is used in a quarter plate. The stress is obtained at the Gauss point, x = 0.973a, y = 0.527a. It is clear that the effect of the geometric nonlinearity is to reduce the maximum stress from the value predicted by the linear theory. As can be seen from Figure 4.1, the membrane effects dominate over the bending effects as the load is increased. The linear theory

overestimates the stress at the surface and underestimates at the middle surface. Composite materials, usually stronger in tension than in shear, can be used more efficiently in situations where membrane forces are significant.

Figure 4.2 contains the transverse deflection as a function of the load parameter, which compares well with that of Reference [83]. For isotropic plates, the distribution of stresses and displacements through the thickness is linear, as shown in Figure 4.3. The maximum stress, at the surface of the plate, is due to bending. The effect of the nonlinearity is to reduce the value of stress at the top and bottom surfaces and to increase at the middle surface of the plate. The stress results presented in Figure 4.3 correspond to the point: $x = 0.973a$, $y = 0.527a$.

4.4.2 Cross-Ply (0/90) Simply-Supported Plate

A simply-supported cross-ply (0/90) laminate under uniform transverse load is analyzed. The geometry used is the same as in the previous example. The following material properties and boundary conditions are used:

$$E_1 = 250 \text{ GPa}, \; E_2 = 20 \text{ GPa}, \; G_{12} = G_{13} = 10 \text{ GPa},$$

$$G_{23} = 4 \text{ GPa}, \; \nu_{12} = 0.25$$

$$v = w = \phi_2 = 0 \text{ at } x = a/2$$

$$u = w = \phi_1 = 0 \text{ at } y = a/2$$

$$u = \phi_1 = 0 \text{ at } x = 0$$

$$v = \phi_2 = 0 \text{ at } y = 0 \tag{4.17}$$

where $\phi_1(x,y)$ and $\phi_2(x,y)$ are the rotations about the y and x-axes, respectively. These rotations can be expressed in terms of the u^j and v^j at the nodes. For example, $\phi_2(x,y) = 0$ is satisfied by setting all $v^j = 0$ through the thickness at that (x,y) location.

In order to investigate the effect of the symmetry boundary conditions, results on both a 2 x 2 quarter-plate and a 4 x 4 full-plate model are reported in Figure 4.4. For cross-ply plates, the symmetry boundary conditions used in the quarter-plate model are found to be identical to the corresponding values obtained from the full-plate model. Therefore, the maximum transverse deflections as a function of the load parameter λ, shown in Figure 4.4, are identical for both models. This turns out not to be the case for angle-ply laminates as we shall see in the next example. The distribution of the inplane normal stress σ_{xx} at x = y = 0.526a is shown in Figure 4.5, and the distribution of the interlaminar shear stress σ_{xz} at x = 0.973a, y = 0.526a is shown in Figure 4.6. The values of stresses reduce with increasing load. The reduction of interlaminar stresses is of definite significance for composite materials, usually stronger in tension than in shear.

4.5 Symmetry Boundary Conditions for Angle-Ply Plates

Consider a simply-supported angle-ply (45/-45) plate under uniform load. In order to investigate the effect of the symmetry boundary

conditions for angle-ply laminates we consider a 2 x 2 mesh to model a quarter of a plate and a 4 x 4 mesh to model the full plate. The nine-node quadratic element is used. The material properties, load, and geometry are the same as in the Example 4.4.2. Load-deflection curves obtained from both models are shown in Figure 4.7. A discrepancy between the load-deflection curves of the two models is observed, the full model being more rigid. In order to explain this discrepancy, it must be noted that the symmetry boundary conditions used in the quarter-plate model were derived [80] using the exact solution to the linear problem formulated in terms of the first order shear deformation theory (FSDT). For the angle-ply case, the assumed (GLPT) solution is

$$u = U \sin\frac{x\pi}{a}\cos\frac{y\pi}{b}$$

$$v = V \cos\frac{x\pi}{a}\sin\frac{y\pi}{b}$$

$$w = W \sin\frac{x\pi}{a}\sin\frac{y\pi}{b}$$

$$v^j = V^j \cos\frac{x\pi}{a}\sin\frac{y\pi}{b}$$

$$u^j = U^j \sin\frac{x\pi}{a}\cos\frac{y\pi}{b}, \qquad (4.18)$$

which satisfies both the displacement and stress symmetry boundary conditions at the center lines (x = a/2 and y = b/2) of the plate for the linear case:

$$v(a/2,y) = u^j(a/2,y) = 0 \; ; \; N_1(a/2,y) = N_2^j(a/2,y) = 0$$
$$u(x,b/2) = v^j(x,b/2) = 0 \; ; \; N_2(x,b/2) = N_1^j(x,b/2) = 0 \qquad (4.19)$$

However, once the nonlinear terms are incorporated into the stress resultants, Equation (4.10a), the force boundary conditions are no

longer satisfied:

$$N_1(a/2,y) = A_{12}\frac{\pi^2 W^2}{2b^2}\cos^2(y\pi/b) \neq 0$$
$$N_2(x,b/2) = A_{12}\frac{\pi^2 W^2}{2a^2}\cos^2(x\pi/a) \neq 0 \qquad (4.20)$$

Since the force boundary conditions are automatically set to zero in a finite element model in which corresponding displacements are not specified, the problem solved is not the one in which Equations (4.20) are valid. Since a plate with nonzero inplane forces is stiffer than with zero inplane forces, the associated transverse deflections will be different, with the quarter-plate model yielding larger deflections.

It can be shown that the normal to the middle plane does not remain straight after deformation, as is assumed in FSDT. The distribution of inplane displacements of the point $x = 0$, $y = 3a/4$ (relative to the middle surface displacement) through the thickness of the laminate is shown in Figure 4.8. With increasing load, the importance of the bending effect reduces compared to the membrane deformations. Therefore, the departure of the distribution of inplane displacements from a straight line reduces for increasing values of the load as shown in Figure 4.8.

4.6 Buckling and Post-Buckling of Laminated Plates

In this section we derive the eigenvalue problem to compute the bifurcation load and corresponding buckling mode for plates modelled using the GLPT. It is assumed that equilibrium states (primary path) can be found using the linear theory (Chapters 2 and 3) and that those equilibrium states are stable up to a certain amplitude of the applied

load. Consequently, a perturbation of the nonlinear governing equations (4.7) around an equilibrium state will provide us with an eigenvalue problem for the limit of stability (intersection with a secondary path).

Although the full nonlinear equations (4.7) are extensively used in this chapter to compute nonlinear equilibrium states, the following analysis assumes that a linear analysis gives a good approximation of the behavior of the structure up to the limit of stability. This assumption leads to an elegant and efficient formulation of the buckling problem [84] that provides reliable results for a wide variety of cases. However, for certain lamination stacking sequences it is not possible to uncouple the linear prebuckling solution from the perturbed nonlinear equations and therefore a standard eigenvalue problem cannot be formulated. In particular this is the case for composite laminates having bending-extension coupling because even the linear prebuckling solution shows nonvanishing transverse deflections that prevent us from uncoupling the prebuckling solution from the perturbed nonlinear equations as we shall see in Section 4.6.2. More complex buckling analyses can still be formulated without resorting to a full nonlinear analysis [85, 86]. Particularly, an eigenvalue problem can be formulated at each equilibrium solution of a full nonlinear analysis to check for the stability of that equilibrium state.

Writing down the complex set of nonlinear governing equations and applying a perturbation around the equilibrium state (see Section 4.6.2) will prove to be a lengthy process. Instead, in this section we use an energy approach in combination with the finite element formulation to derive the eigenvalue problem and corresponding matrices.

The finite element approximation to the first variation to the total potential energy gives the conditions for equilibrium

$$\delta\pi(\underset{\sim}{u}) = \int_V [\hat{B}^T]\underset{\sim}{\sigma}dv - \underset{\sim}{f} = \underset{\sim}{0} \tag{4.19}$$

where the strains are related to the displacements by

$$\underset{\sim}{\varepsilon} = [\hat{B}]\underset{\sim}{u} \tag{4.20}$$

and we can always write the strain-displacement matrix $[\hat{B}]$ as the sum of a linear part $[\hat{B}_L]$ and a nonlinear part $[\hat{B}_{NL}]$

$$[\hat{B}] = [\hat{B}_L] + [\hat{B}_{NL}(\underset{\sim}{u})] \tag{4.21}$$

While the first variation $\delta\pi(\underset{\sim}{u}) = 0$ indicates equilibrium, the second variation $\delta^2\pi(\underset{\sim}{u}) = 0$ indicates a critical point on the equilibrium path

$$\delta^2\pi(\underset{\sim}{u}) = \int_V [\delta\hat{B}^T]\underset{\sim}{\sigma}dv + \int_V [\hat{B}^T]\delta\underset{\sim}{\sigma}dv = \underset{\sim}{0} \tag{4.22}$$

From the constitutive equations

$$\underset{\sim}{\sigma} = [C](\underset{\sim}{\varepsilon} - \underset{\sim}{\varepsilon}_o) + \underset{\sim}{\sigma}_o \tag{4.23}$$

we obtain

$$\delta\underset{\sim}{\sigma} = [C]\delta\underset{\sim}{\varepsilon} = [C][\hat{B}]\delta\underset{\sim}{u} \tag{4.24}$$

and from Equation (4.21) we obtain

$$[\delta\hat{B}] = [\delta\hat{B}_{NL}] \tag{4.25}$$

Therefore

$$0 = \delta^2\pi(\underset{\sim}{u}) = \int_V [\delta\hat{B}_{NL}^T]\underset{\sim}{\sigma}dv + \left(\int_V [\hat{B}_L^T][C][\hat{B}_L]dv\right)\delta\underset{\sim}{u}$$

$$+ \left(\int_V \{[\hat{B}_L^T][C][\hat{B}_L] + [\hat{B}_{NL}^T][C][\hat{B}_{NL}] + [\hat{B}_{NL}^T][C][\hat{B}_L]\}dv\right)\delta\underset{\sim}{u} \tag{4.26}$$

or

$$0 = \delta^2\pi(\underset{\sim}{u}) = ([K_\sigma] + [K_L] + [K_{NL}])\delta\underset{\sim}{u} \tag{4.27}$$

or

$$[K_T]\delta\underset{\sim}{u} = 0 \tag{4.28}$$

Equation (4.28) indicates that a zero eigenvalue in the tangent stiffness matrix $[K_T]$ indicates unstable equilibrium, although not necessarily a birfurcation. On the other hand, Equation (4.28) can be used in a predictor-corrector algorithm until $\delta\underset{\sim}{u} = 0$, and simultaneous satisfaction of Equation (4.19) will indicate convergence to an equilibrium position.

If the prebuckling deformations can be accurately predicted by a linear solution and that linear solution renders the nonlinear stiffness matrix $[K_{NL}] = 0$, then for a fixed load p_o

$$\delta^2\pi = ([K_L] + [K_\sigma])\delta\underset{\sim}{u} = \underset{\sim}{0} \tag{4.29}$$

Since a linear solution is used for the prebuckling deformations, and as we shall see the geometric stiffness matrix $[K_\sigma]$ depends linearly on the load, for any load level λp_o, with λ an unknown constant, we have

$$\delta^2\pi = ([K_L] + \lambda[K_\sigma])\delta\underset{\sim}{u} = 0 \tag{4.30}$$

If any nontrivial perturbation $\delta\underset{\sim}{u}$ exists and Equation (4.30) is still satisfied, then λp_o is the buckling load, λ obtained from the eigenvalue problem (4.30). For the particular case of plates, the condition $[K_{NL}] = 0$ is satisfied whenever the linear prebuckling solution exhibits zero transverse deflections. For that reason the buckling behavior of laminated plates having bending-extension coupling cannot be accurately

predicted by a standard bifurcation buckling analysis (see also Section 4.6.2). The linear stiffness matrix $[K_L]$ is presented in Chapter 3, Equation 3.4. The geometric stiffness matrix $[K_\sigma]$ involves the stresses obtained from a linear solution and the nonlinear strains of Equation (4.12c) and Appendix 4. From Equation (4.26) we can write

$$[K_\sigma]\delta\underset{\sim}{u} = \int_V \underset{\sim}{\sigma}[\delta\hat{B}_{NL}]dr \tag{4.31}$$

and using the plate variables

$$[K_\sigma]\delta\underset{\sim}{u} = \int_\Omega \{N_x \frac{\partial}{\partial x}\frac{\partial \delta w}{\partial x} + N_y \frac{\partial}{\partial y}\frac{\partial \delta w}{\partial y} + N_{xy}\frac{\partial}{\partial x}\frac{\partial \delta w}{\partial y} + N_{xy}\frac{\partial}{\partial y}\frac{\partial \delta w}{\partial x}\}d\Omega \tag{4.32}$$

where V is the volume and Ω is the surface of the plate. Equation (4.32) can be written as

$$[K_\sigma]\delta\underset{\sim}{u} = \int_\Omega \{\frac{\partial}{\partial x}, \frac{\partial}{\partial y}\}\begin{bmatrix} N_x & N_{xy} \\ N_{xy} & N_y \end{bmatrix}\begin{Bmatrix} \frac{\partial \delta w}{\partial y} \\ \frac{\partial \delta w}{\partial x} \end{Bmatrix} d\Omega \tag{4.33}$$

$$[K_\sigma] = \int_\Omega [G]^T[N][G]d\Omega \tag{4.34}$$

where

$$[G] = \begin{bmatrix} 0 & 0 & \frac{\partial \psi_i}{\partial x} \\ 0 & 0 & \frac{\partial \psi_i}{\partial y} \end{bmatrix} \quad ; \quad \delta\underset{\sim}{u} = \begin{Bmatrix} \delta u \\ \delta v \\ \delta w \end{Bmatrix} \tag{4.35}$$

where ψ_i are the finite element interpolation functions. The matrix of the stresses is known from the linear solution,

$$[N] = \begin{bmatrix} N_x & N_{xy} \\ N_{xy} & N_y \end{bmatrix} \tag{4.36}$$

which completely defines the eigenvalue problem (4.30). The postbuckling solution is found using a full nonlinear analysis and the Newton-Raphson method as described in Section 4.3.

4.6.1 Angle-Ply (45/-45) Laminates

The same geometry as in Section 4.5 (a = b = 1000 mm, h = 2 mm) is used to analyze a (45/-45) simply-supported laminate under uniform inplane compressive load $N_y = \lambda \cdot N_{yo}$ (N_{yo} = 10.85 N/m). The material properties used are:

$$E_1/E_2 = 40;\ E_2 = 6.25\ \text{GPa};\ G_{12}/E_2 = 0.82;\ G_{13} = G_{12};$$
$$G_{23}/E_2 = 0.52\ ;\ \nu_{12} = 0.24.$$

Although an exact solution of the eigenvalue problem associated with the buckling equations exists for this case [87], the boundary conditions used to obtain that solution cannot be used for the nonlinear analysis. For the nonlinear analysis, the boundary conditions have to allow an applied load, $N_x = 0$ and $N_y = \lambda \cdot N_{yo}$. Both a bifurcation (eigenvalue) analysis and a nonlinear bending analysis are performed using a 4 x 4 full-plate model, and the nonlinear response is shown in Figure 4.9. Both the nonlinear and eigenvalue analyses estimate the critical load accurately.

The eigenvalue problem, which leads to an accurate prediction of the critical load for laminates without bending-extension coupling, is formulated with the assumption that pre-buckling deformations do not

include nonzero transverse deflections. This assumption is not satisfied in the next example.

4.6.2 Antisymmetric Cross-Ply Laminates

An antisymmetric cross-ply laminate under inplane load $N_y = \lambda \cdot N_{yo}$ (N_{yo} = 6.25 N/m) is considered next. In this case the pre-buckling transverse deflections are important. The geometry and material properties are the same as in the previous example. The simply-supported boundary conditions of cross-ply laminates, Equations (4.17), are used for the 4 x 4 full-plate model (although the 2 x 2 mesh in a quarter plate would be all right in this case). In order to assess the effect of the number of layers, four laminates are analyzed as shown in Figure 4.10. The values of the critical buckling load given by the exact solution of the eigenvalue problem [87] are depicted on the corresponding load-deflection curves for comparison. It is evident that in this case the eigenvalues are not representative of any bifurcation points of the structure. The structure behaves nonlinearly for all values of the load. The observed behavior can be explained as follows.

The complete set of governing equations for the nonlinear behavior of composite plates, during pre- and post-buckling regime, can be formally written as

$$\underset{\sim}{F}(\underset{\sim}{x},p) = \underset{\sim}{0} \tag{4.37}$$

where p is the load and

$$\begin{aligned} \underset{\sim}{x} &= (u,v,w,\phi_1,\phi_2) \text{ for FSDT} \\ \underset{\sim}{x} &= (u,v,w,u^j,v^j) \text{ for GLPT with } j = 1, \ldots, N. \end{aligned} \tag{4.38}$$

An eigenvalue analysis is usually formulated to compute the critical

load under which the structure will undergo large deflections without substantial changes in the applied load. The eigenvalue analysis looks for a situation on which the structure has multiple equilibrium positions (bifurcation) for the same load state. Assuming that at least one equilibrium state (i.e., $\underset{\sim}{x}_0$) can be found solving Equation (4.37), a small perturbation is introduced in the displacements (i.e., $\underset{\sim}{x} = \underset{\sim}{x}_0 + \underset{\sim}{x}_1$) to see if a new equilibrium state is found. Since the perturbation is small, it is possible to expand Equation (4.37) around the primary (prebuckled) equilibrium position,

$$\underset{\sim}{F}(\underset{\sim}{x},p) = \underset{\sim}{F}(\underset{\sim}{x}_0,p) + \left.\frac{\partial \underset{\sim}{F}(\underset{\sim}{x},p)}{\partial \underset{\sim}{x}}\right|_{\underset{\sim}{x}_0} \cdot \underset{\sim}{x}_1 = \underset{\sim}{0} \tag{4.39}$$

Since $\underset{\sim}{x}_0$ is an equilibium state, we have,

$$\underset{\sim}{F}(\underset{\sim}{x}_0,p) = \underset{\sim}{0} \tag{4.40}$$

Therefore,

$$\left.\frac{\partial \underset{\sim}{F}(\underset{\sim}{x},p)}{\partial \underset{\sim}{x}}\right|_{\underset{\sim}{x}_0} \cdot \underset{\sim}{x}_1 = \underset{\sim}{0} \tag{4.41}$$

which, for the sake of simplicity can be written as

$$[J(\underset{\sim}{x}_0,p)] \cdot \underset{\sim}{x}_1 = \underset{\sim}{0} \tag{4.42}$$

which is the condition for a secondary (buckled) equilibrium state to exist. This leads to an eigenvalue problem for the critical load in the following way: If $\underset{\sim}{F}(\underset{\sim}{x},p) = \underset{\sim}{0}$, Equation (4.37), can be linearized, then it is possible to compute the pre-buckling solution for a reference load, say p_0, and then obtain the pre-buckling solution for any load by scaling the reference load and the the reference solution by a parameter λ,

$$p = \lambda \cdot p_{ref}$$

$$\underset{\sim}{x}_o = \lambda \cdot \underset{\sim}{x}_{ref} \tag{4.43}$$

Substituting Equation (4.23) into Equation (4.42), the nonlinear dependence on $\underset{\sim}{x}_o$ is eliminated,

$$[J(\lambda, \underset{\sim}{x}_{ref}, p_{ref})] \cdot \underset{\sim}{x}_1 = \underset{\sim}{0} \tag{4.44}$$

The Jacobian [J] does not depend on $\underset{\sim}{x}_1$ because $\underset{\sim}{x}_1$ is small, and therefore nonlinear terms in $\underset{\sim}{x}_1$ are neglected in Equation (4.42). Since there are terms in Equation (4.24) that do not depend on the load, Equation (4.44) leads to the usual eigenvalue problem,

$$([K_D] + \lambda \cdot [K_G])\underset{\sim}{x}_1 = \underset{\sim}{0} \tag{4.45}$$

where the lowest eigenvalue λ gives the critical load.

The plate equations can be linearized, as required to arrive at Equation (4.43), if the pre-buckled deformations do not include transverse deflections. This is because the use of the von-Karman nonlinear strains limits all the nonlinearity to the transverse deflection w. But for laminates having bending-extension coupling, the pre-buckling transverse deflections (i.e., w_o) are non-vanishing for any load. Linearization (i.e., to consider $w_o = 0$) introduces substantial errors into the analysis and the predicted critical loads are not representative of any substantial change in the behavior of the structure, as can be seen in Figure 4.9.

An attempt to perform an eigenvalue analysis by the finite element method would produce an unsymmetric geometric stiffness matrix $[K_D]$, with associated complex eigenvalues and eigenvectors. Furthermore, the geometric stiffness $[K_D]$ would depend nonlinearly on the reference load. In this way we further demonstrate the limitations of eigenvalue analysis for laminated plates having bending-extension coupling. An

approximation would be to arbitrarily set to zero the transverse deflections obtained in the pre-buckling analysis in order to compute the geometric stiffness $[K_D]$, but the results to be obtained would be of questionable usefulness.

An eigenvalue problem can still be formulated if the linearization is performed at each load step with respect to the deformed configuration [85,86].

Appendix 4

Strain-displacement matrices

The strains $\{e\}$, $\{\eta\}$, and $\{e^j\}$ appearing in Equation (4.12) are

$$\{e\} = \begin{Bmatrix} \frac{\partial u}{\partial x} \\ \frac{\partial v}{\partial y} \\ \frac{\partial u}{\partial y} + \frac{\partial v}{\partial x} \\ \frac{\partial w}{\partial x} \\ \frac{\partial w}{\partial y} \end{Bmatrix}, \quad \{e^j\} = \begin{Bmatrix} \frac{\partial u^j}{\partial x} \\ \frac{\partial v^j}{\partial y} \\ \frac{\partial u^j}{\partial y} + \frac{\partial v^j}{\partial x} \\ u^j \\ v^j \end{Bmatrix}; \quad \{\eta\} = \begin{Bmatrix} \frac{1}{2}\left(\frac{\partial w}{\partial x}\right)^2 \\ \frac{1}{2}\left(\frac{\partial w}{\partial y}\right)^2 \\ \frac{\partial w}{\partial x}\frac{\partial w}{\partial y} \\ 0 \\ 0 \end{Bmatrix}$$

The matrices $[B]$, $[\bar{B}]$ and $[B_{NL}]$ appearing in the strain-displacement relations (4.12) are

$$[B]_{(5x3m)} = \begin{bmatrix} \frac{\partial \psi_i}{\partial x} & 0 & 0 \\ 0 & \frac{\partial \psi_i}{\partial y} & 0 \\ \frac{\partial \psi_i}{\partial y} & \frac{\partial \psi_i}{\partial x} & 0 \\ 0 & 0 & \frac{\partial \psi_i}{\partial x} \\ 0 & 0 & \frac{\partial \psi_i}{\partial y} \end{bmatrix}$$

$$[\bar{B}]_{(5x2m)} = \begin{bmatrix} \frac{\partial \psi_i}{\partial x} & 0 \\ 0 & \frac{\partial \psi_i}{\partial y} \\ \frac{\partial \psi_i}{\partial y} & \frac{\partial \psi_i}{\partial x} \\ \psi_i & 0 \\ 0 & \psi_i \end{bmatrix}$$

$$[B_{NL}]_{(5x3m)} = \frac{1}{2} \begin{bmatrix} 0 & 0 & \frac{\partial w}{\partial x} & \frac{\partial \psi_i}{\partial x} & \\ 0 & 0 & \frac{\partial w}{\partial y} & \frac{\partial \psi_i}{\partial y} & \\ 0 & 0 & \frac{\partial w}{\partial x} & \frac{\partial \psi_i}{\partial y} & + \frac{\partial w}{\partial y} \frac{\partial \psi_i}{\partial x} \\ 0 & 0 & 0 & & \\ 0 & 0 & 0 & & \end{bmatrix}$$

with (i = 1,...,m).

Appendix 5

Stiffness matrices

$$[k^{11}] = \sum_e \int_{\Omega_e} ([B]^T[A][B] + [B]^T[A][B_{NL}] + 2[B_{NL}]^T[A][B] + 2[B_{NL}]^T[A][B_{NL}])d\Omega_e$$

$$[k_j^{12}] = \sum_e \int_{\Omega_e} ([B]^T[B^j][\bar{B}] + 2[B_{NL}]^T[B^j][\bar{B}])d\Omega_e$$

$$[k_j^{21}] = \sum_e \int_{\Omega_e} ([\bar{B}]^T[B^j][B] + [\bar{B}]^T[B^j][B_{NL}])d\Omega_e$$

$$[k_{jr}^{22}] = \sum_e \int_{\Omega_e} ([\bar{B}]^T[D^{jr}][\bar{B}])d\Omega_e$$

Jacobian Matrix

$$[J] = \begin{bmatrix} [\frac{\partial\{R^o\}}{\partial\{\Delta\}}] & [\frac{\partial\{R^o\}}{\partial\{\Delta^1\}}] & \cdots & [\frac{\partial\{R^o\}}{\partial\{\Delta^N\}}] \\ [\frac{\partial\{R^1\}}{\partial\{\Delta\}}] & [\frac{\partial\{R^1\}}{\partial\{\Delta^1\}}] & \cdots & [\frac{\partial\{R^1\}}{\{\partial\Delta^N\}}] \\ \vdots & \vdots & \vdots\vdots & \vdots \\ [\frac{\partial\{R^N\}}{\partial\{\Delta\}}] & [\frac{\partial\{R^N\}}{\partial\{\Delta^1\}}] & \cdots & [\frac{\partial\{R^N\}}{\partial\{\Delta^N\}}] \end{bmatrix}$$

where

$$\{R^o\} = [k^{11}]\{\Delta\} + \sum_j^N [k_j^{12}]\{\Delta^j\}$$

$$[R^j\} = [k_j^{21}]\{\Delta\} + \sum_r^N [k_{jr}^{22}]\{\Delta^r\};\ (j = 1,\ldots,N)$$

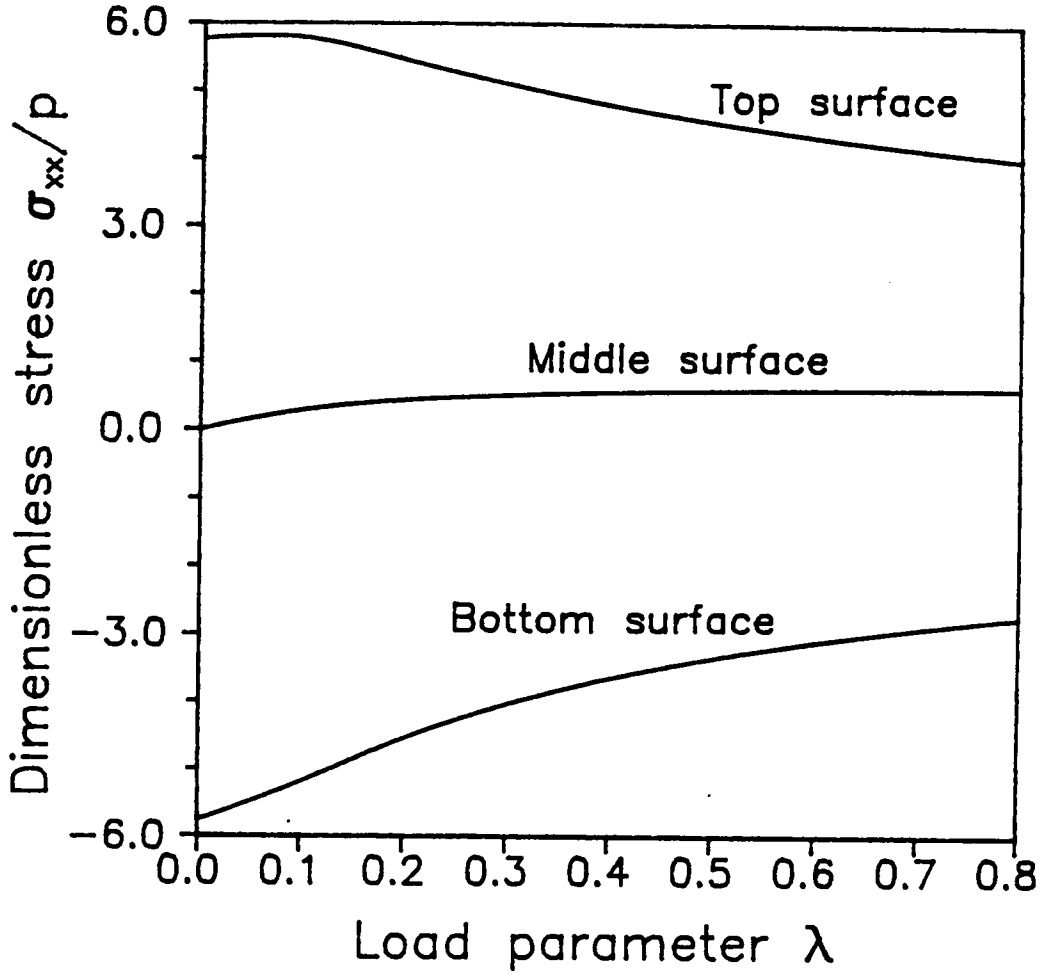

4.1 Maximum stress as a function of the load for a clamped isotropic plate under uniformly distributed transverse load shows the stress relaxation as the membrane effect becomes dominant.

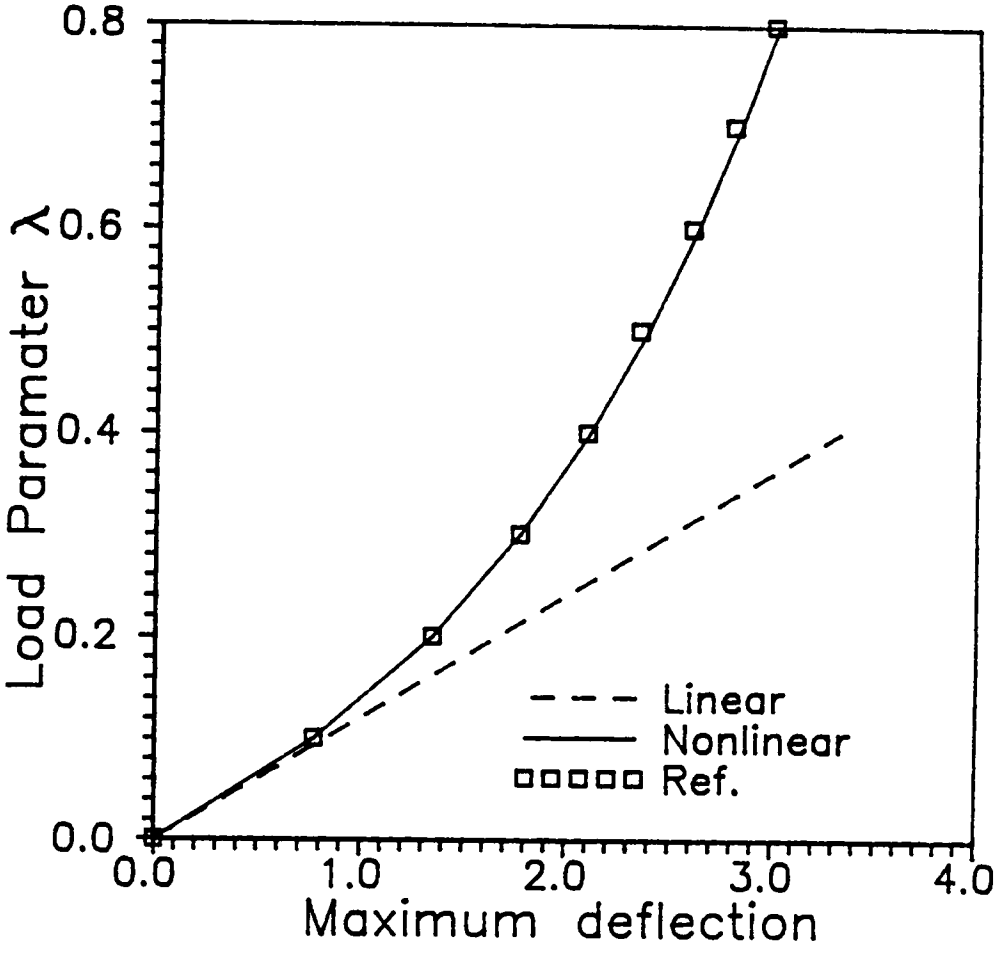

4.2 Load deflection curve for a clamped isotropic plate under transverse load.

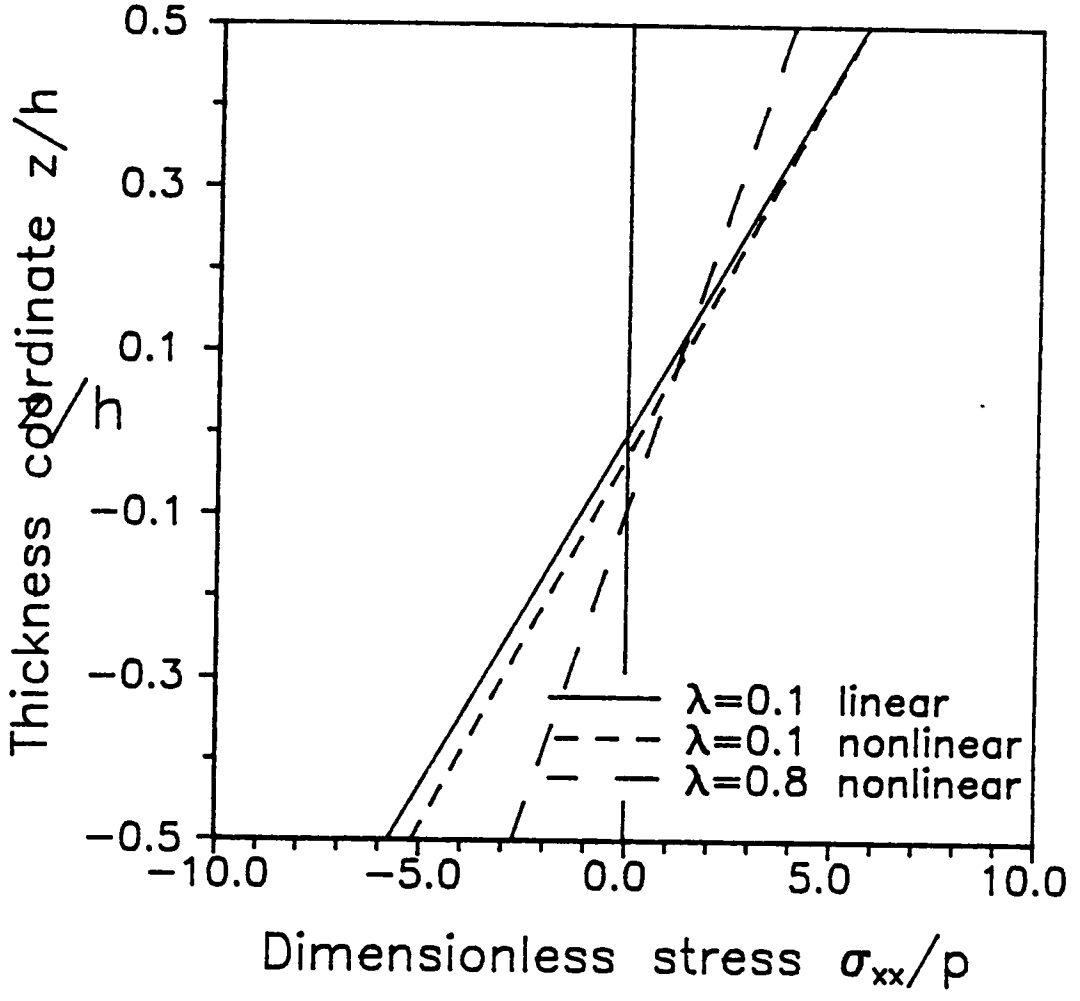

4.3 Through-the-thickness distribution of the inplane normal stress σ_{xx} for a clamped isotropic plate under transverse load for several values of the load, showing the stress relaxation as the load increases.

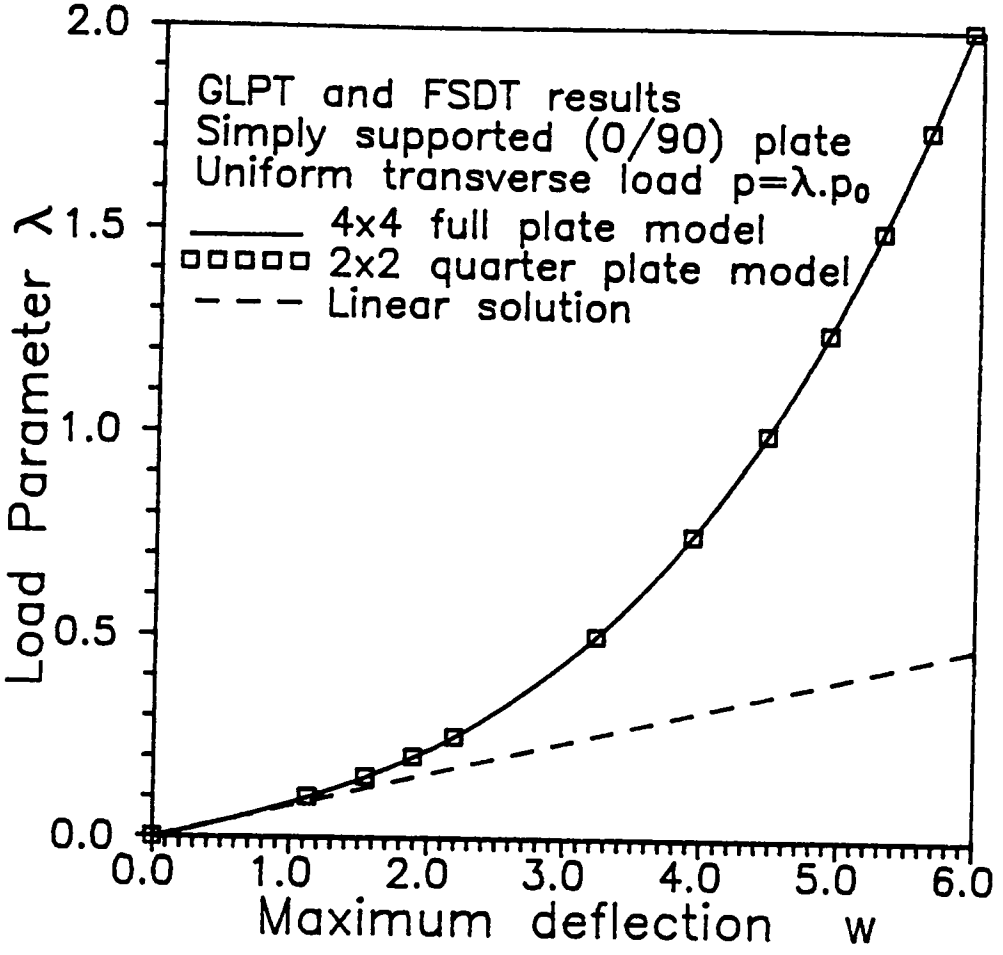

4.4 Load deflection curves for a simply-supported cross-ply (0/90) plate under transverse load. Both theories, GLPT and FSDT, and both models, 2 x 2 quarter-plate and 4 x 4 full plate produce the same transverse deflections.

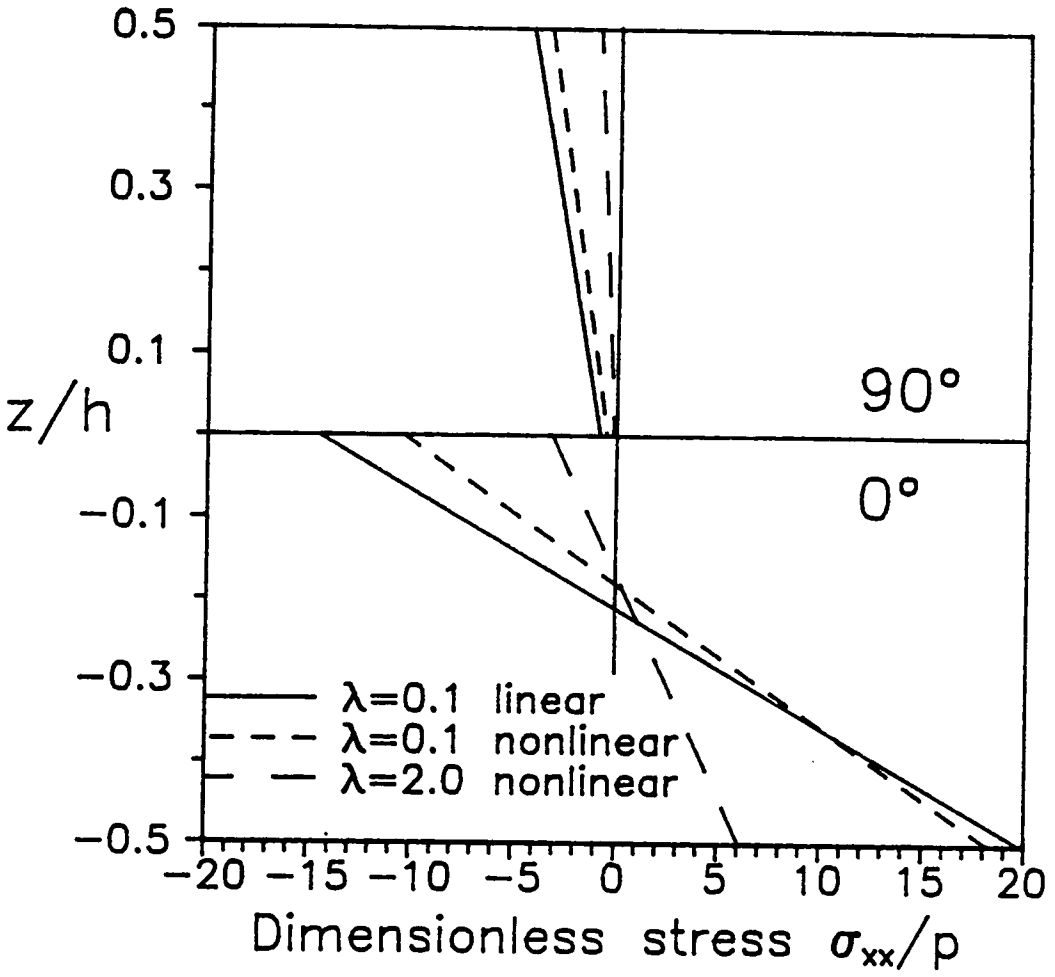

4.5 Through-the-thickness distribution of the inplane normal stress σ_{xx} for a simply-supported cross-ply (0/90) plate for several values of the load.

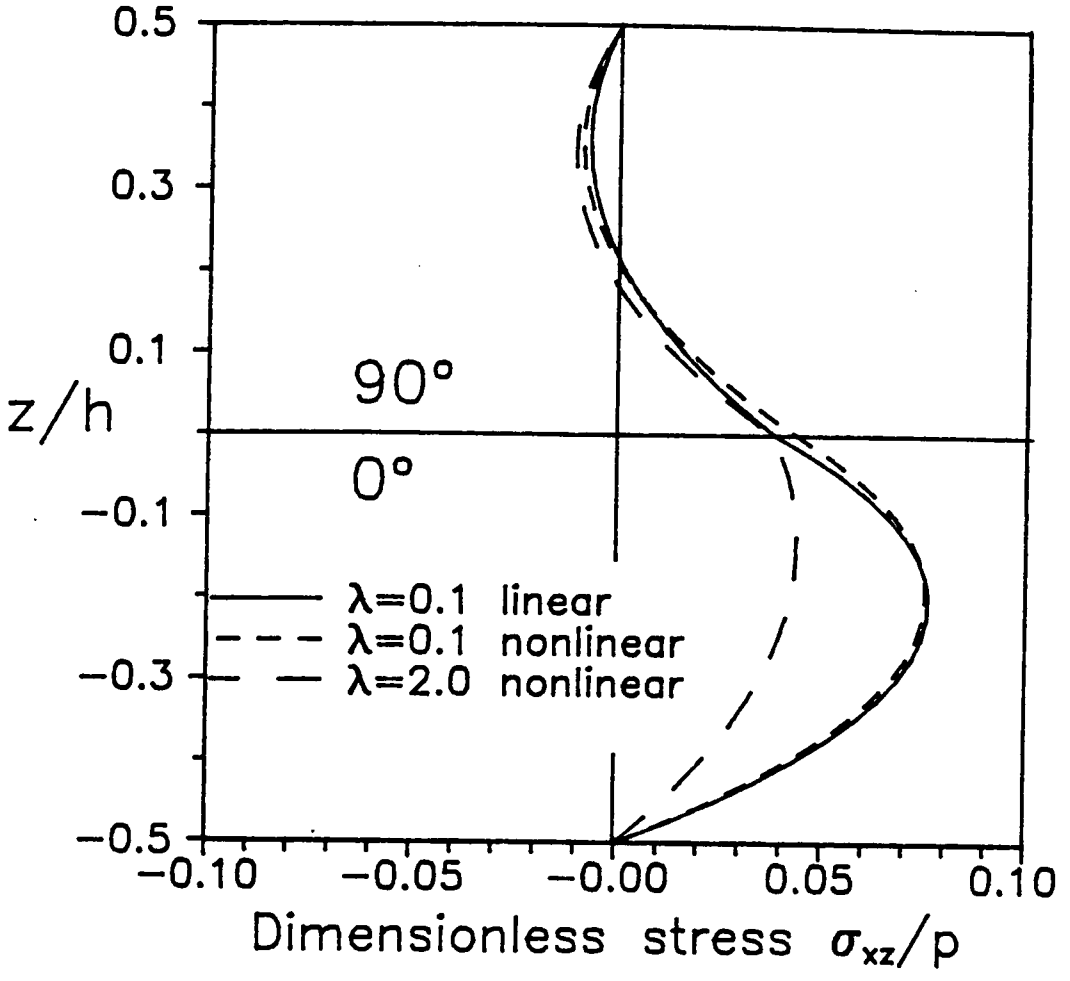

4.6 Through-the-thickness distribution of the interlaminar shear stress σ_{xz} for a simply-supported cross-ply (0/90) plate for several values of the load.

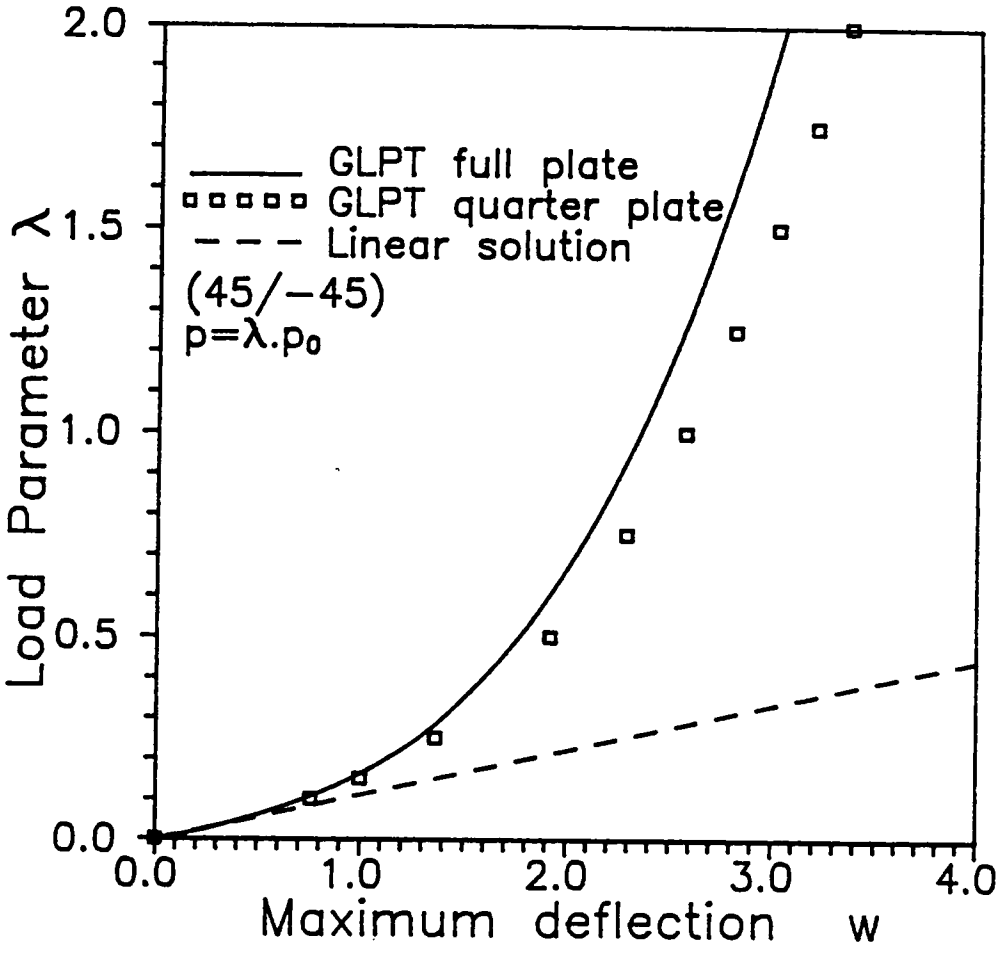

4.7 Load deflection curves for a simply-supported angle-ply (45/-45) plate under transverse load, obtained from a 2 x 2 quarter-plate model and a 4 x 4 full-plate model using GLPT.

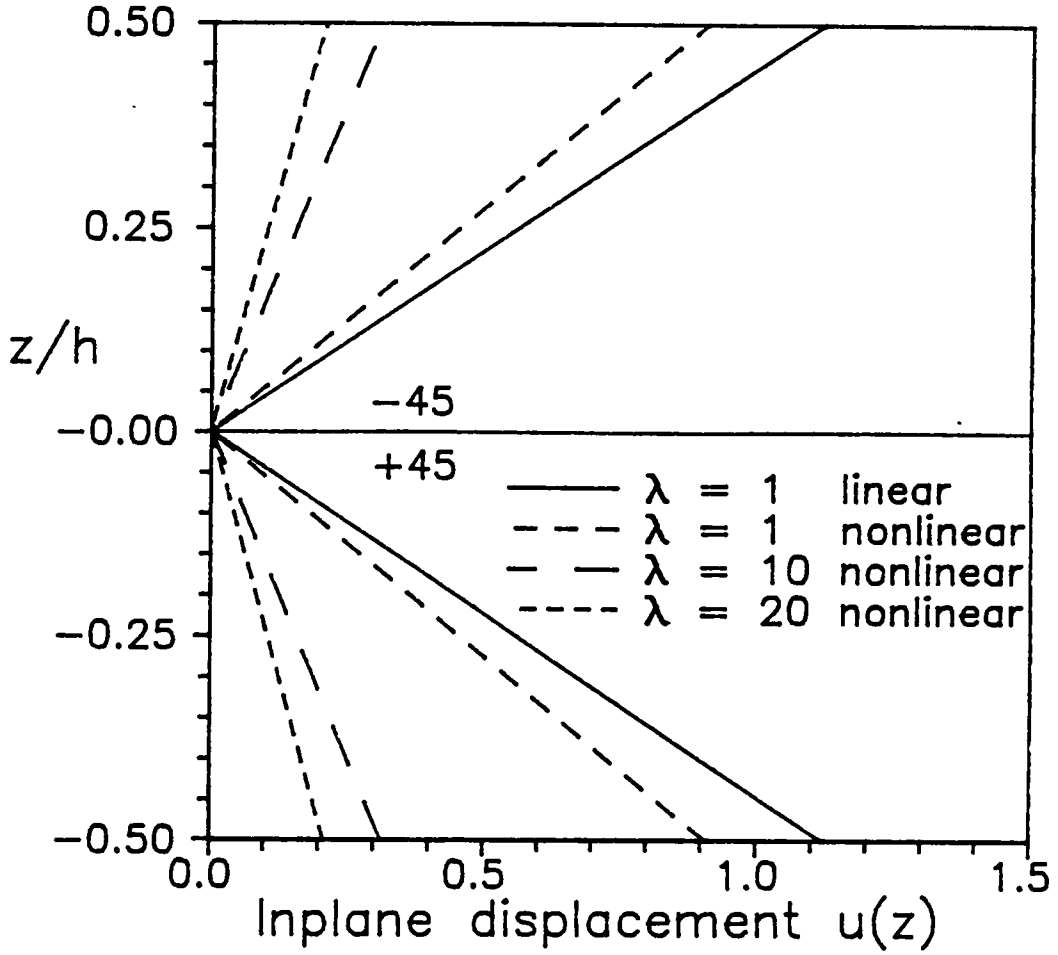

4.8 Through-the-thickness distribution of inplane displacements $[u(z/h) - \bar{u}]\cdot 20/v_{max}$, at x = a/2, y = 3b/4 for a (45/-45) laminated plate under uniformly distributed transverse load, where $\bar{u}$ is the middle surface displacement.

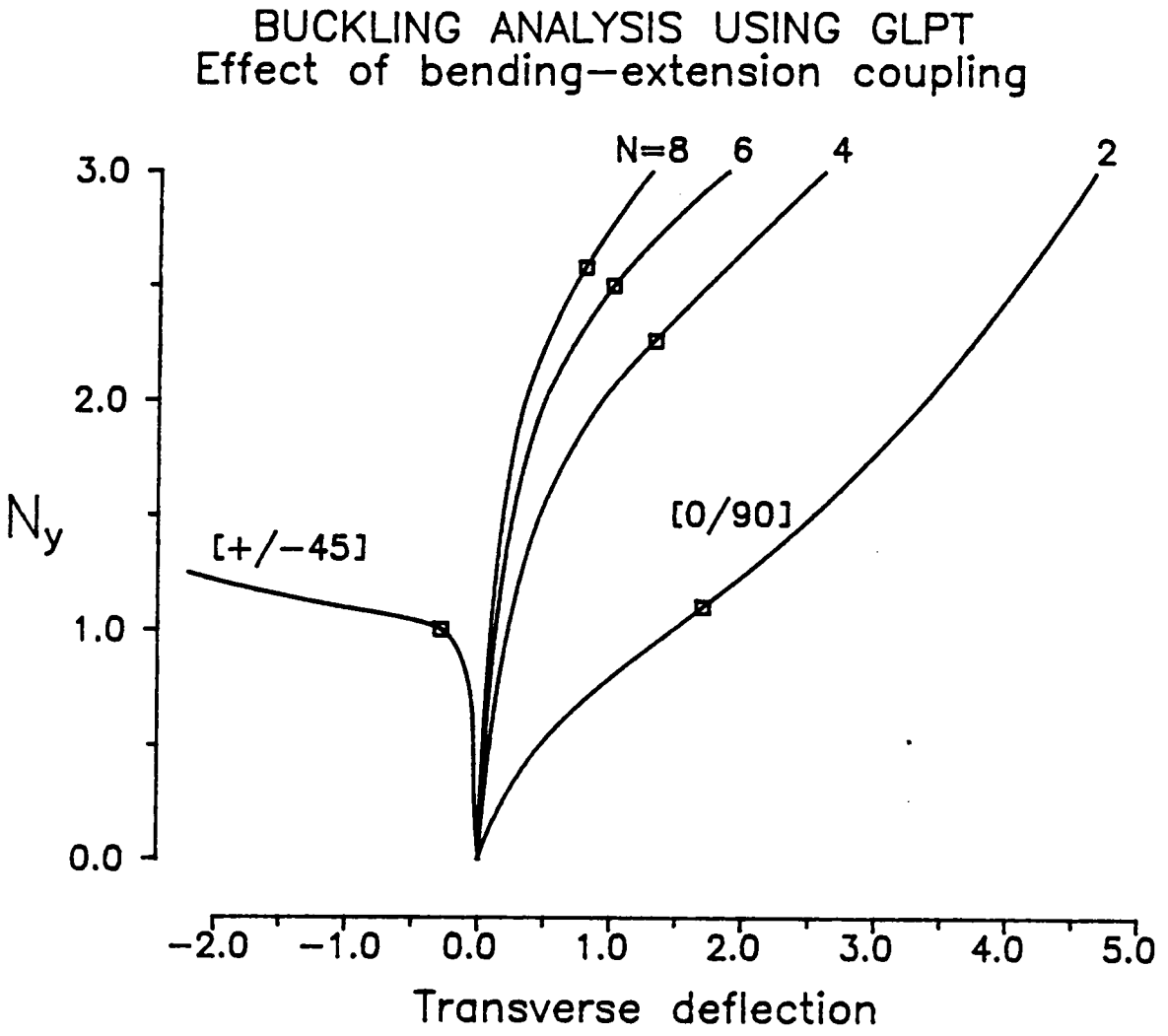

4.9 Load-deflection curve and critical loads for angle-ply (45/-45) and antisymmetric cross-ply laminates, simply supported and subjected to an inplane load N_y. The critical loads from a closed-form solution (eigenvalues) are shown on the corresponding load deflection curves.

Chapter 5

AN EXTENSION OF THE GLPT TO LAMINATED CYLINDRICAL SHELLS

5.1 Introduction

Laminated cylindrical shells are often modelled as equivalent single-layer shells using classical, i.e., Love-Kirchhoff shell theory in which straight lines normal to the undeformed middle surface remain straight, inextensible and normal to the deformed middle surface. Consequently, transverse normal strains are assumed to be zero and transverse shear deformations are neglected [88-90]. The classical theory of shells is expected to yield sufficiently accurate results when (i) the lateral dimension-to-thickness ratio (s/h) is large; (ii) the dynamic excitations are within the low-frequency range; (iii) the material anisotropy is not severe. However, application of such theories to layered anisotropic composite shells could lead to as much as 30% or more errors in deflections, stresses, and natural frequencies [91-93].

As pointed out by Koiter [94], refinements to Love's first approximation theory of thin elastic shells are meaningless, unless the effects of transverse shear and normal stresses are taken into account in a refined theory. The transverse normal stress is, in general, of order h/a (thickness-to-radius) times a bending stress, whereas the transverse shear stresses obtained from equilibrium conditions are of order h/ℓ (thickness-to-length along the side of the panel) times a bending stress. Therefore, for $a/\ell > 10$, the transverse normal stress is negligible compared to the transverse shear stresses.

The effects of transverse shear and normal stresses in shells were considered by Hildebrand, Reissner, and Thomas [95], Luré [96], and Reissner [97], among others. Exact solutions of the 3-D equations and approximate solutions using a piece-wise variation of the displacements through the thickness were presented by Srinivas [98], where significant discrepancies were found between the exact solutions and the classical shell theory solutions.

The present study deals with a generalization of the shear deformation theories of laminated composite shells. The theory is based on the idea that the thickness approximation of the displacement field can be accomplished via a piece-wise approximation through each individual lamina. In particular, the use of a polynomial expansion with compact support (i.e., finite-element approximation) through the thickness proves to be convenient as was shown in previous chapters for laminated plates.

5.2 Formulation of the Theory

5.2.1 Displacements and Strains

The displacements (u_x, u_θ, u_z) at a point (x,θ,z) (see Figure 5.1) in the laminated shell are assumed to be of the form

$$\begin{aligned} u_x(x,\theta,z,t) &= u(x,\theta,t) + U(x,\theta,z,t) \\ u_\theta(x,\theta,z,t) &= v(x,\theta,t) + V(x,\theta,z,t) \\ u_z(x,\theta,z,t) &= w(x,\theta,t) + W(x,\theta,z,t), \end{aligned} \tag{5.1}$$

where (u,v,w) are the displacements of a point $(x,\theta,0)$ on the reference surface of the shell at time t, and U, V, W are as yet arbitrary functions that vanish on the reference surface:

$$U(x,\theta,0) = V(x,\theta,0) = W(x,\theta,0) = 0. \tag{5.2}$$

In developing the governing equations, the von Kármán type strains are considered [84], in which strains are assumed to be small, rotations with respect to the shell reference surface are assumed to be moderate, and rotations about normals to the shell reference surface are considered negligible. The nonlinear strain-displacement equations in an orthogonal cartesian coordinate system (Figure 5.1) become:

$$\varepsilon_{xx} = \frac{\partial u_x}{\partial x} + \frac{1}{2}(\beta_x^2) \quad ; \quad \beta_x = -\frac{\partial u_z}{\partial x}$$

$$\varepsilon_{\theta\theta} = \frac{1}{(a+z)}\left[\frac{\partial u_\theta}{\partial \theta} + u_z\right] + \frac{1}{2}\beta_\theta^2 \quad ; \quad \beta_\theta = -\frac{1}{(a+z)}\frac{\partial u_z}{\partial \theta}$$

$$\varepsilon_{zz} = \frac{\partial u_z}{\partial z}$$

$$\gamma_{x\theta} = \frac{1}{(a+z)}\frac{\partial u_x}{\partial \theta} + \frac{\partial u_\theta}{\partial x} + \beta_x\beta_\theta$$

$$\gamma_{xz} = \frac{\partial u_x}{\partial z} + \frac{\partial u_z}{\partial x}$$

$$\gamma_{\theta z} = \frac{1}{(a+z)}\left[\frac{\partial u_z}{\partial \theta} - u_\theta\right] + \frac{\partial u_\theta}{\partial z}, \tag{5.3}$$

where a is the radius of curvature of the shell. Introducing Donnell's approximation [99], i.e., $z \ll a$, strains $\varepsilon_{\theta\theta}$, $\gamma_{x\theta}$ and $\gamma_{\theta z}$ can be simplified as

$$\varepsilon_{\theta\theta} = \frac{1}{a}\left(\frac{\partial u_\theta}{\partial \theta} + u_z\right) + \frac{1}{2}\beta_\theta^2 \; ; \; \beta_\theta = -\frac{1}{a}\frac{\partial u_z}{\partial \theta}$$

$$\gamma_{x\theta} = \frac{1}{a}\frac{\partial u_x}{\partial \theta} + \frac{\partial u_\theta}{\partial x} + \beta_x\beta_\theta$$

$$\gamma_{\theta z} = \frac{1}{a}\left[\frac{\partial u_z}{\partial \theta} - u_\theta\right] + \frac{\partial u_\theta}{\partial z}. \tag{5.4}$$

Substituting for u_x, u_θ and u_z from Equation (5.1) into Equations (5.3)

and (5.4), we obtain

$$\varepsilon_{xx} = \frac{\partial u}{\partial x} + \frac{\partial U}{\partial x} + \frac{1}{2}\beta_x^2$$

$$\varepsilon_{\theta\theta} = \frac{1}{a}\left[\frac{\partial v}{\partial \theta} + \frac{\partial V}{\partial \theta} + w + W\right] + \frac{1}{2}\beta_\theta^2$$

$$\varepsilon_{zz} = \frac{\partial W}{\partial z}$$

$$\gamma_{x\theta} = \frac{\partial v}{\partial x} + \frac{\partial V}{\partial x} + \frac{1}{a}\left[\frac{\partial u}{\partial \theta} + \frac{\partial U}{\partial \theta}\right] + \beta_x\beta_\theta$$

$$\gamma_{xz} = \frac{\partial U}{\partial z} + \frac{\partial w}{\partial x} + \frac{\partial W}{\partial x}$$

$$\gamma_{\theta z} = \frac{1}{a}\left[\frac{\partial w}{\partial \theta} + \frac{\partial W}{\partial \theta} - v - V\right] + \frac{\partial V}{\partial z}$$

$$\beta_x = -\left[\frac{\partial w}{\partial x} + \frac{\partial W}{\partial x}\right]$$

$$\beta_\theta = -\frac{1}{a}\left[\frac{\partial w}{\partial \theta} + \frac{\partial W}{\partial \theta}\right]. \qquad (5.5)$$

5.2.2 Variational Formulation

The Hamilton variational principle is used to derive the equations of motion of a cylindrical laminate composed of N constant-thickness orthotropic lamina, whose principal material coordinates are arbitrarily oriented with respect to the laminate coordinates. The principle can be stated, in the absence of body forces and specified tractions, as:

$$0 = \int_0^T \Big[\int_V (\sigma_x\delta\varepsilon_{xx} + \sigma_\theta\delta\varepsilon_{\theta\theta} + \sigma_z\delta\varepsilon_{zz} + \sigma_{xz}\delta\gamma_{xz} + \sigma_{\theta z}\delta\gamma_{\theta z} + \sigma_{x\theta}\delta\gamma_{x\theta})dV - \int_\Omega q\delta u_z d\Omega - \int_V \rho(\dot{u}_x\delta\dot{u}_x + \dot{u}_\theta\delta\dot{u}_\theta + \dot{u}_z\delta\dot{u}_z)dV\Big]dt. \qquad (5.6)$$

where σ_x, σ_θ, σ_z, σ_{xz} and $\sigma_{\theta z}$ are the stresses, q is the distributed

transverse load, ρ is the density, V is the total volume of the laminate, Ω is the reference surface of the laminate (assumed to be the middle surface of the shell), the superposed dot denotes differentiation with respect to time, and δ denotes the variational symbol.

Substituting the strain-displacement relations (5.5) into Equation (5.6), we obtain

$$
\begin{aligned}
0 = \int_0^T \Big[\int_{-\frac{h}{2}}^{\frac{h}{2}} \int_\Omega \Big\{ & \sigma_x \Big(\frac{\partial \delta u}{\partial x} + \frac{\partial \delta U}{\partial x} + \beta_x \delta \beta_x \Big) \\
& + \frac{\sigma_\theta}{a} \Big(\frac{\partial \delta v}{\partial \theta} + \frac{\partial \delta V}{\partial \theta} + \delta w + \delta W + \beta_\theta \delta \beta_\theta \Big) \\
& + \sigma_z \frac{\partial \delta W}{\partial z} + \sigma_{xz} \Big(\frac{\partial \delta w}{\partial x} + \frac{\partial \delta U}{\partial z} + \frac{\partial \delta W}{\partial x} \Big) \\
& + \frac{\sigma_{\theta z}}{a} \Big(\frac{\partial \delta w}{\partial \theta} - \delta v + \frac{\partial \delta W}{\partial \theta} - \delta V + a \frac{\partial \delta V}{\partial z} \Big) \\
& + \frac{\sigma_{x\theta}}{a} \Big(a \frac{\partial \delta v}{\partial x} + \frac{\partial \delta u}{\partial \theta} + a \frac{\partial \delta V}{\partial x} + \frac{\partial \delta U}{\partial \theta} + a \beta_x \delta \beta_\theta + a \beta_\theta \delta \beta_x \Big) \\
& - \rho \big[(\dot{u} + \dot{U}) \delta (\dot{u} + \dot{U}) + (\dot{v} + \dot{V}) \delta (\dot{v} + \dot{V}) \\
& + (\dot{w} + \dot{W}) \delta (\dot{w} + \dot{W}) \big] \Big\} dA dz \\
& - \int_\Omega q \delta (w + W) dA \Big] dt
\end{aligned}
\tag{5.7}
$$

where the following additional approximation, consistent with the Donnell approximation, is used:

$$
\int_V f(x,\theta,z) dz = \int_{r_i}^{r_o} \int_\Omega f \, r dr d\Omega = \int_{-\frac{h}{2}}^{\frac{h}{2}} \int_\Omega f \cdot \Big(1 + \frac{z}{a}\Big) dz dA
$$

$$\approx \int_{-\frac{h}{2}}^{\frac{h}{2}} \int_{\Omega} f \cdot dz dA \quad \text{for } z << a, \tag{5.8}$$

where (r_i, r_o) denote the inner and outer radius, respectively, of the cylindrical shell, and z is a coordinate measured along the normal to the shell surface with origin at the reference surface.

5.2.3 Approximation Through Thickness

In order to reduce the three-dimensional theory to a two-dimensional one, we use a Kantorovich-type approximation [17] where the functions U, V, and W are approximated by

$$\begin{aligned} U(x,\theta,z,t) &= \sum_{j=1}^{n} u^j(x,\theta,t)\phi^j(z), \\ V(x,\theta,z,t) &= \sum_{j=1}^{n} v^j(x,\theta,t)\phi^j(z), \\ W(x,\theta,z,t) &= \sum_{j=1}^{m} w^j(x,\theta,t)\psi^j(z), \end{aligned} \tag{5.9}$$

where u^j, v^j, w^j are undetermined coefficients and $\phi^j(z)$, $\psi^j(z)$ are any continuous functions that satisfy the conditions [c.f. Equation (5.2)]

$$\begin{aligned} \phi^j(0) &= 0 \quad ; \quad j = 1,2,\ldots n \\ \psi^j(0) &= 0 \quad ; \quad j = 1,2,\ldots m. \end{aligned} \tag{5.10}$$

5.2.4 Governing Equations

To complete the theory, we derive the equations relating the (3 + 2n + m) variables (u, v, w, u^j, v^j, w^j). Substituting Equation (5.9) into Equation (5.7) and integrating through the thickness, we obtain

$$0 = \int_0^T \int_\Omega \{[N_x(\frac{\partial \delta u}{\partial x} + \frac{\partial w}{\partial x}\frac{\partial \delta w}{\partial x}) + \frac{1}{a} N_\theta(\frac{\partial \delta v}{\partial \theta} + \delta w + \frac{1}{a}\frac{\partial w}{\partial \theta}\frac{\partial \delta w}{\partial \theta})$$

$$+ \frac{1}{a} N_{x\theta}(a\frac{\partial \delta v}{\partial x} + \frac{\partial \delta u}{\partial \theta} + \frac{\partial w}{\partial x}\frac{\partial \delta w}{\partial \theta} + \frac{\partial w}{\partial \theta}\frac{\partial \delta w}{\partial x}) + Q_{xz}\frac{\partial \delta w}{\partial x}$$

$$- \frac{1}{a} Q_{\theta z}(\frac{\partial \delta w}{\partial \theta} + \delta v)]$$

$$+ \sum_{j=1}^{n} [M_x^j \frac{\partial \delta u^j}{\partial x} + \frac{1}{a} M_\theta^j \frac{\partial \delta v^j}{\partial \theta} + Q_{xz}^j \delta u^j - \frac{1}{a} M_{\theta z}^j \delta v^j + Q_{\theta z}^j \delta v^j$$

$$+ M_{x\theta}^j \frac{\partial \delta v^j}{\partial x} + \frac{1}{a} M_{x\theta}^j \frac{\partial \delta u^j}{\partial \theta}) + \sum_{j=1}^{m} (\frac{\hat{M}_\theta^j}{a} \delta w^j$$

$$+ \hat{Q}_z^j \delta w^j + \hat{M}_{xz}^j \frac{\partial \delta w^j}{\partial x} + \frac{\hat{M}_{\theta z}^j}{a}\frac{\partial \delta w^j}{\partial \theta})$$

$$+ \sum_{j=1}^{m} [\hat{M}_x^j (\frac{\partial w}{\partial x}\frac{\partial \delta w^j}{\partial x} + \frac{\partial \delta w}{\partial x}\frac{\partial w^j}{\partial x})$$

$$+ \frac{\hat{M}_\theta^j}{a^2} (\frac{\partial w}{\partial \theta}\frac{\partial \delta w^j}{\partial \theta} + \frac{\partial \delta w}{\partial \theta}\frac{\partial w^j}{\partial \theta}) + \frac{\hat{M}_{x\theta}^j}{a} (\frac{\partial w}{\partial x}\frac{\partial \delta w^j}{\partial \theta}$$

$$+ \frac{\partial \delta w}{\partial x}\frac{\partial w^j}{\partial \theta} + \frac{\partial \delta w}{\partial \theta}\frac{\partial w^j}{\partial x} + \frac{\partial w}{\partial \theta}\frac{\partial \delta w^j}{\partial x})$$

$$+ \sum_{j=1}^{m}\sum_{k=1}^{m} (L_x^{jk}\frac{\partial w^j}{\partial x}\frac{\partial \delta w^k}{\partial x} + \frac{1}{a^2} L_\theta^{jk}\frac{\partial w^j}{\partial \theta}\frac{\partial \delta w^k}{\partial \theta}$$

$$+ \frac{1}{a} L_{x\theta}^{jk}\frac{\partial w^j}{\partial x}\frac{\partial \delta w^k}{\partial \theta} + \frac{1}{a} L_{x\theta}^{jk}\frac{\partial \delta w^j}{\partial x}\frac{\partial w^k}{\partial \theta}]$$

$$- [I^o(\dot{u}\delta\dot{u} + \dot{v}\delta\dot{v} + \dot{w}\delta\dot{w}) + \sum_{j=1}^{n} I^j(\dot{u}\delta\dot{u}^j + \dot{v}\delta\dot{v}^j$$

$$+ \dot{u}^j\delta\dot{u} + \dot{v}^j\delta\dot{v}) + \sum_{j=1}^{m} \hat{I}^j(\dot{w}\delta\dot{w}^j + \dot{w}^j\delta\dot{w})$$

$$+ \sum_{j=1}^{n}\sum_{k=1}^{n} I^{jk}(\dot{u}^j\delta\dot{u}^k + \dot{v}^j\delta\dot{v}^k)$$

$$+ \sum_{j=1}^{m}\sum_{k=1}^{m} \hat{I}^{jk}\dot{w}^j\delta\dot{w}^k] - q\delta w\}dAdt. \qquad (5.11)$$

Here N_x, N_θ, etc. denote the stress resultants,

$$(N_x, N_\theta, N_{x\theta}, Q_{xz}, Q_{\theta z}) = \int_{-\frac{h}{2}}^{\frac{h}{2}} (\sigma_x, \sigma_\theta, \sigma_{x\theta}, \sigma_{xz}, \sigma_{\theta z})dz$$

$$(M_x^j, M_\theta^j, M_{x\theta}^j, M_{\theta z}^j) = \int_{-\frac{h}{2}}^{\frac{h}{2}} (\sigma_x, \sigma_\theta, \sigma_{x\theta}, \sigma_{\theta z})\phi^j dz$$

$$(Q_{xz}^j, Q_{\theta z}^j) = \int_{-\frac{h}{2}}^{\frac{h}{2}} (\sigma_{xz}, \sigma_{\theta z}) \frac{d\phi^j}{dz} dz$$

$$(\hat{M}_x^j, \hat{M}_\theta^j, \hat{M}_{x\theta}^j, \hat{M}_{xz}^j, \hat{M}_{\theta z}^j) = \int_{-\frac{h}{2}}^{\frac{h}{2}} (\sigma_x, \sigma_\theta, \sigma_{x\theta}, \sigma_{xz}, \sigma_{\theta z})\psi^j dz$$

$$\hat{Q}_z^j = \int_{-\frac{h}{2}}^{\frac{h}{2}} \sigma_z \frac{d\psi^j}{dz} dz$$

$$(L_x^{jk}, L_\theta^{jk}, L_{x\theta}^{jk}) = \int_{-\frac{h}{2}}^{\frac{h}{2}} (\sigma_x, \sigma_\theta, \sigma_{x\theta})\psi^j\psi^k dz$$

and I_o, I^j, and $\hat{I}^j$ are the inertias,

$$I^o = \int_{-\frac{h}{2}}^{\frac{h}{2}} \rho dz \quad ; \quad (I^j, \hat{I}^j) = \int \rho(\phi^j, \psi^j)dz$$

$$(I^{jk},\hat{I}^{jk}) = \int\rho(\phi^j\phi^k,\psi^j\psi^k)dz. \tag{5.12}$$

Equations of Motion. The Euler-Lagrange equations of the theory are obtained by integrating the derivatives of the varied quantities by parts and collecting the coefficients of $\delta u,\delta v,\delta w,\delta u^j,\delta v^j$, and δw^j:

$$N_{x,x} + \frac{1}{a}N_{x\theta,\theta} = I^0\ddot{u} + \sum_{j=1}^{n} I^j\ddot{u}^j$$

$$\frac{1}{a}N_{\theta,\theta} + \frac{1}{a}Q_{\theta z} + N_{x\theta,x} = I^0\ddot{v} + \sum_{j=1}^{n} I^j\ddot{v}^j$$

$$-\frac{1}{a}N_\theta + Q_{xz,x} + \frac{1}{a}Q_{\theta z,\theta} + \underline{[N_x\frac{\partial w}{\partial x}]_{,x} + [\frac{1}{a^2}N_\theta\frac{\partial w}{\partial\theta}]_{,\theta}}$$

$$+ \underline{[\frac{1}{a}N_{x\theta}\frac{\partial w}{\partial x}]_{,\theta} + [\frac{1}{a}N_{x\theta}\frac{\partial w}{\partial\theta}]_{,x} + \sum_{j=1}^{m}([\hat{M}_x^j\frac{\partial w^j}{\partial x}]_{,x}}$$

$$\underline{+ [\frac{1}{a^2}\hat{M}_\theta^j\frac{\partial w^j}{\partial\theta}]_{,\theta} + [\frac{1}{a}\hat{M}_{x\theta}^j\frac{\partial w^j}{\partial x}]_{,\theta} + [\frac{1}{a}\hat{M}_{x\theta}^j\frac{\partial w^j}{\partial\theta}]_{,x})}$$

$$= I\ddot{w} + \sum_{j=1}^{m}\ddot{w}^j\hat{I}^j - q$$

$$M_{x,x}^j - Q_{xz}^j + \frac{1}{a}M_{x\theta,\theta}^j = I^j\ddot{u} + \sum_{k=1}^{n} I^{jk}\ddot{u}^k$$

$$\frac{1}{a}M_{\theta,\theta}^j + \frac{1}{a}M_{\theta z}^j - Q_{\theta z}^j + M_{x\theta,x}^j = I^j v + \sum_{k=1}^{n} I^{jk}\ddot{v}^k$$

$$-\frac{1}{a}\hat{M}_\theta^j - \hat{Q}_z^j + \hat{M}_{xz,x}^j + \frac{1}{a}\hat{M}_{\theta z,\theta}^j + \underline{[\hat{M}_x^j\frac{\partial w}{\partial x}]_{,x} + [\frac{1}{a^2}\hat{M}_\theta^j\frac{\partial w}{\partial\theta}]_{,\theta}}$$

$$\underline{+ [\frac{1}{a}\hat{M}_{x\theta}^j\frac{\partial w}{\partial x}]_{,\theta} + [\frac{1}{a}\hat{M}_{x\theta}^j\frac{\partial w}{\partial\theta}]_{,x} + \sum_{k=1}^{m}\{[L_x^{jk}\frac{\partial w^k}{\partial x}]_{,x} + [\frac{1}{a^2}L_\theta^{jk}\frac{\partial w^k}{\partial\theta}]_{,\theta}}$$

$$+ \underline{\left[\frac{1}{a} L^{jk}_{x\theta} \frac{\partial w^k}{\partial x}\right]_{,\theta} + \left[\frac{1}{a} L^{jk}_{x\theta} \frac{\partial w^k}{\partial \theta}\right]_{,x}} = \hat{I}^j \ddot{w} + \sum_{k=1}^{m} \hat{I}^{jk} \ddot{w}^k \qquad (5.13)$$

where underscored terms denote the nonlinear terms due to the von Kármán strains.

Boundary conditions. The virtual work principle gives the following geometric and force boundary conditions for the theory:

Geometric (essential)	Force (natural)
u	$aN_x n_x + N_{x\theta} n_\theta = 0$
v	$aN_{x\theta} n_x + N_\theta n_\theta = 0$
w	$aQ_{xz} n_x + Q_{\theta z} n_\theta = 0$
u^j	$aM^j_x n_x + M^j_{x\theta} n_\theta = 0$
v^j	$aM^j_{x\theta} n_x + M^j_\theta n_\theta = 0$
w^j	$a\hat{M}^j_{xz} n_x + \hat{M}^j_{\theta z} n_\theta = 0$ (5.14)

where (n_x, n_θ) denote the direction cosines of a unit normal to the boundary of the reference surface Ω.

5.2.5 Further Approximations

The theory can be easily simplified for linear behavior and/or zero normal strain $\varepsilon_{zz} = 0$. The term $\frac{1}{a} Q_{\theta z}$ in Equation (5.13) is neglected in Donnell's quasi-shallow shell equations, and it can be neglected here. To be consistent, the term $\frac{1}{a} M^j_{\theta z}$ should also be neglected simultaneously in this theoery.

Consistent with the assumptions made in the derivation of the kinematic equations for intermediate class of deformations, we can assume that the transverse normal strain is small and neglect the products of the derivatives of the interface transverse displacements,

$$\frac{\partial w^j}{\partial \alpha}\frac{\partial w^j}{\partial \beta} \approx 0 \text{ with } \alpha, \beta = x,\theta. \tag{5.15}$$

In this form we keep a nonlinear coupling between the transverse deflection of the middle surface (w) and the transverse deflections of the interfaces. All but the last Equation (5.13) remain unchanged, and the last equation in Equation (5.13) reduces to

$$-\frac{1}{a}\hat{M}^j_\theta - \hat{Q}^j_z + \hat{M}^j_{xz,x} + \frac{1}{a}\hat{M}^j_{\theta z,\theta} + [\hat{M}^j_x \frac{\partial w}{\partial x}]_{,x} + [\frac{1}{a^2}\hat{M}^j_\theta \frac{\partial w}{\partial \theta}]_{,\theta}$$

$$+ [\frac{1}{a}\hat{M}^j_{x\theta}\frac{\partial w}{\partial x}]_{,\theta} + [\frac{1}{a}\hat{M}^j_{x\theta}\frac{\partial w}{\partial \theta}]_{,x} = \hat{I}^j\ddot{w} + \sum_{k=1}^{m}\hat{I}^{jk}\ddot{w}^k. \tag{5.16}$$

In addition, we can assume that the normal strains in the transverse direction ($\frac{\partial w^j}{\partial x}$) are very small, and neglect the products $\frac{\partial w}{\partial \alpha}\frac{\partial w^j}{\partial \beta}$. In this case the third and sixth of Equations (5.13) reduce to

$$-\frac{1}{a}N_\theta + Q_{xz,x} + \frac{1}{a}Q_{\theta z,\theta} + [N_x\frac{\partial w}{\partial x}]_{,x} + [\frac{1}{a^2}N_\theta\frac{\partial w}{\partial \theta}]_{,\theta}$$

$$+ [\frac{1}{a}N_{x\theta}\frac{\partial w}{\partial x}]_{,\theta} + [\frac{1}{a}N_{x\theta}\frac{\partial w}{\partial \theta}]_{,x} = I^0\ddot{w} + \sum_{j=1}^{m}\ddot{w}^j\hat{I}^j - q$$

$$-\frac{1}{a}\hat{M}^j_\theta - \hat{Q}^j_z + \hat{M}^j_{xz,x} + \frac{1}{a}\hat{M}^j_{\theta z,\theta} = \hat{I}^j\ddot{w} + \sum_{k=1}^{m}\hat{I}^{jk}\ddot{w}^k. \tag{5.17}$$

Obviously, there is a range of applicability for each of the cases discussed above.

5.2.6 Constitutive Equations

The constitutive equations of an arbitrarily oriented, orthotropic lamina in the laminate coordinate system are

$$\begin{Bmatrix} \sigma_x \\ \sigma_\theta \\ \sigma_z \\ \sigma_{xz} \\ \sigma_{\theta z} \\ \sigma_{x\theta} \end{Bmatrix} = \begin{bmatrix} C_{11} & C_{12} & C_{13} & 0 & 0 & C_{16} \\ C_{12} & C_{22} & C_{23} & 0 & 0 & C_{26} \\ C_{13} & C_{23} & C_{33} & 0 & 0 & C_{36} \\ 0 & 0 & 0 & C_{55} & C_{45} & 0 \\ 0 & 0 & 0 & C_{45} & C_{44} & 0 \\ C_{16} & C_{26} & C_{36} & 0 & 0 & C_{66} \end{bmatrix} \begin{Bmatrix} \frac{\partial u}{\partial x} + \frac{1}{2}\left(\frac{\partial w}{\partial x}\right)^2 \\ \frac{1}{a}\frac{\partial v}{\partial \theta} + \frac{w}{a} + \frac{1}{2}\left(\frac{1}{a}\frac{\partial w}{\partial \theta}\right)^2 \\ 0 \\ \frac{\partial w}{\partial x} \\ \frac{1}{a}\frac{\partial w}{\partial \theta} - \frac{v}{a} \\ \frac{\partial v}{\partial x} + \frac{1}{a}\frac{\partial u}{\partial \theta} + \frac{\partial w}{\partial x}\frac{1}{a}\frac{\partial w}{\partial \theta} \end{Bmatrix}$$

$$+ \sum_{j=1}^{n} \begin{Bmatrix} \frac{\partial u^j}{\partial x}\phi^j \\ \frac{1}{a}\frac{\partial v^j}{\partial \theta}\phi^j \\ 0 \\ u^j \frac{d\phi^j}{dz} \\ v^j\left(\frac{d\phi^j}{dz} - \frac{1}{a}\phi^j\right) \\ \left(\frac{1}{a}\frac{\partial u^j}{\partial \theta} + \frac{\partial v^j}{\partial x}\right)\phi^j \end{Bmatrix} + \sum_{j=1}^{m} \begin{Bmatrix} \frac{\partial w}{\partial x}\frac{\partial w^j}{\partial x}\psi^j \\ \frac{1}{a}\left(w^j + \frac{1}{a}\frac{\partial w}{\partial \theta}\frac{\partial w^j}{\partial \theta}\right)\psi^j \\ w^j \frac{d\psi^j}{dz} \\ \frac{\partial w^j}{\partial x}\psi^j \\ \frac{1}{a}\frac{\partial w^j}{\partial \theta}\psi^j \\ \frac{1}{a}\left(\frac{\partial w}{\partial x}\frac{\partial w^j}{\partial \theta} + \frac{\partial w}{\partial \theta}\frac{\partial w^j}{\partial x}\right)\psi^j \end{Bmatrix} \tag{5.18}$$

where C_{ij} denote the elastic constants. Here the nonlinear strains used are those consistent with an intermediate class of deformations and correspond with the simplifications made to arrive at Equation (5.16).

Substitution of Equations (5.18) into Equation (5.12) gives the following laminate constitutive equations:

$$\begin{Bmatrix} N_x \\ N_\theta \\ Q_{xz} \\ Q_{\theta z} \\ N_{x\theta} \end{Bmatrix} = \begin{bmatrix} A_{11} & A_{12} & 0 & 0 & A_{16} \\ A_{12} & A_{22} & 0 & 0 & A_{26} \\ 0 & 0 & A_{55} & A_{54} & 0 \\ 0 & 0 & A_{45} & A_{44} & 0 \\ A_{16} & A_{26} & 0 & 0 & A_{66} \end{bmatrix} \begin{Bmatrix} \frac{\partial u}{\partial x} + \frac{1}{2}\left(\frac{\partial w}{\partial x}\right)^2 \\ \frac{1}{a}\frac{\partial v}{\partial \theta} + \frac{w}{a} + \frac{1}{2}\left(\frac{1}{a}\frac{\partial w}{\partial \theta}\right)^2 \\ \frac{\partial w}{\partial x} \\ \frac{1}{a}\frac{\partial w}{\partial \theta} - \frac{v}{a} \\ \frac{1}{a}\frac{\partial u}{\partial \theta} + \frac{\partial v}{\partial x} + \frac{\partial w}{\partial x}\frac{1}{a}\frac{\partial w}{\partial \theta} \end{Bmatrix}$$

$$+ \sum_{j=1}^{n} \begin{bmatrix} B_{11} & B_{12} & 0 & 0 & B_{16} \\ B_{12} & B_{22} & 0 & 0 & B_{26} \\ 0 & 0 & B_{55} & B_{54} & 0 \\ 0 & 0 & B_{45} & B_{44} & 0 \\ B_{16} & B_{26} & 0 & 0 & B_{66} \end{bmatrix}^{(j)} \begin{Bmatrix} \frac{\partial u^j}{\partial x} \\ \frac{1}{a}\frac{\partial v^j}{\partial \theta} \\ u^j \\ v^j \\ \frac{1}{a}\frac{\partial u^j}{\partial \theta} + \frac{\partial v^j}{\partial x} \end{Bmatrix}$$

$$+ \sum_{j=1}^{m} \begin{bmatrix} \hat{B}_{11} & \hat{B}_{12} & \hat{B}_{13} & 0 & 0 & \hat{B}_{16} \\ \hat{B}_{12} & \hat{B}_{22} & \hat{B}_{23} & 0 & 0 & \hat{B}_{26} \\ 0 & 0 & 0 & \hat{B}_{55} & \hat{B}_{54} & 0 \\ 0 & 0 & 0 & \hat{B}_{45} & \hat{B}_{44} & 0 \\ \hat{B}_{16} & \hat{B}_{26} & \hat{B}_{63} & 0 & 0 & \hat{B}_{66} \end{bmatrix}^{(j)} \begin{Bmatrix} \frac{\partial w}{\partial x} \frac{\partial w^j}{\partial x} \\ \frac{1}{a} \left(w^j + \frac{1}{a} \frac{\partial w}{\partial \theta} \frac{\partial w^j}{\partial \theta}\right) \\ w^j \\ \frac{\partial w^j}{\partial x} \\ \frac{1}{a} \frac{\partial w^j}{\partial \theta} \\ \frac{1}{a} \left(\frac{\partial w}{\partial x} \frac{\partial w^j}{\partial \theta} + \frac{\partial w}{\partial \theta} \frac{\partial w^j}{\partial x}\right) \end{Bmatrix} \tag{5.19}$$

$$\begin{Bmatrix} M_x^j \\ M_\theta^j \\ Q_{xz}^j \\ Q_{\theta z}^j \\ M_{x\theta}^j \end{Bmatrix} = \begin{bmatrix} F_{11} & F_{12} & 0 & 0 & F_{16} \\ F_{12} & F_{22} & 0 & 0 & F_{26} \\ 0 & 0 & F_{55} & F_{54} & 0 \\ 0 & 0 & F_{45} & F_{44} & 0 \\ F_{16} & F_{26} & 0 & 0 & F_{66} \end{bmatrix}^{(j)} \begin{Bmatrix} \frac{\partial u}{\partial x} + \frac{1}{2} \left(\frac{\partial w}{\partial x}\right)^2 \\ \frac{1}{a} \left(\frac{\partial v}{\partial \theta} + w + \frac{1}{2} \frac{\partial w}{\partial \theta}\right) \\ \frac{\partial w}{\partial x} \\ \frac{1}{a} \left(\frac{\partial w}{\partial \theta} - v\right) \\ \frac{1}{a} \left(\frac{\partial u}{\partial \theta} + a \frac{\partial v}{\partial x} + \frac{\partial w}{\partial x} \frac{\partial w}{\partial \theta}\right) \end{Bmatrix}$$

$$+\sum_{k=1}^{n}\begin{bmatrix} D_{11} & D_{12} & 0 & 0 & D_{16} \\ D_{12} & D_{22} & 0 & 0 & D_{26} \\ 0 & 0 & D_{55} & D_{54} & 0 \\ 0 & 0 & D_{45} & D_{44} & 0 \\ D_{16} & D_{26} & 0 & 0 & D_{66} \end{bmatrix}^{(j,k)} \begin{Bmatrix} \frac{\partial u^j}{\partial x} \\ \frac{1}{a}\frac{\partial v^j}{\partial \theta} \\ u^j \\ v^j \\ \frac{1}{a}\frac{\partial u^j}{\partial \theta} + \frac{\partial v^j}{\partial x} \end{Bmatrix}$$

$$+\sum_{k=1}^{m}\begin{bmatrix} \hat{D}_{11} & \hat{D}_{12} & \hat{D}_{13} & 0 & 0 & \hat{D}_{16} \\ \hat{D}_{12} & \hat{D}_{22} & \hat{D}_{23} & 0 & 0 & \hat{D}_{26} \\ 0 & 0 & 0 & \hat{D}_{55} & \hat{D}_{54} & 0 \\ 0 & 0 & 0 & \hat{D}_{45} & \hat{D}_{44} & 0 \\ \hat{D}_{16} & \hat{D}_{26} & \hat{D}_{63} & 0 & 0 & \hat{D}_{66} \end{bmatrix}^{(j,k)} \begin{Bmatrix} \frac{\partial w}{\partial x}\frac{\partial w^j}{\partial x} \\ \frac{1}{a}\left(w^j + \frac{1}{a}\frac{\partial w}{\partial \theta}\frac{\partial w^j}{\partial \theta}\right) \\ w^j \\ \frac{\partial w^j}{\partial x} \\ \frac{1}{a}\frac{\partial w^j}{\partial \theta} \\ \frac{1}{a}\left(\frac{\partial w}{\partial x}\frac{\partial w^j}{\partial \theta} + \frac{\partial w}{\partial \theta}\frac{\partial w^j}{\partial x}\right) \end{Bmatrix}$$

(5.20)

$$
\begin{Bmatrix} \hat{M}_x \\ \hat{M}_\theta \\ \hat{Q}_z \\ \hat{M}_{xz} \\ \hat{M}_{\theta z} \\ \hat{M}_{x\theta} \end{Bmatrix}^{(j)} = \begin{bmatrix} H_{11} & H_{12} & 0 & 0 & H_{16} \\ H_{12} & H_{22} & 0 & 0 & H_{26} \\ H_{31} & H_{32} & 0 & 0 & H_{36} \\ 0 & 0 & H_{55} & H_{54} & 0 \\ 0 & 0 & H_{45} & H_{44} & 0 \\ H_{16} & H_{26} & 0 & 0 & H_{66} \end{bmatrix}^{(j)} \begin{Bmatrix} \frac{\partial u}{\partial x} + \frac{1}{2}\left(\frac{\partial w}{\partial x}\right)^2 \\ \frac{1}{a}\left(\frac{\partial v}{\partial \theta} + w + \frac{1}{2}\frac{1}{a}\left(\frac{\partial w}{\partial \theta}\right)^2\right) \\ \\ \\ \frac{\partial w}{\partial x} \\ \frac{1}{a}\left(\frac{\partial w}{\partial \theta} - v\right) \\ \frac{1}{a}\left(\frac{\partial u}{\partial \theta} + a\frac{\partial v}{\partial x} + \frac{\partial w}{\partial x}\frac{\partial w}{\partial \theta}\right) \end{Bmatrix}
$$

$$
+ \sum_{k=1}^{n} \begin{bmatrix} Q_{11} & Q_{12} & 0 & 0 & Q_{16} \\ Q_{12} & Q_{22} & 0 & 0 & Q_{26} \\ Q_{31} & Q_{32} & 0 & 0 & Q_{36} \\ 0 & 0 & Q_{55} & Q_{54} & 0 \\ 0 & 0 & Q_{45} & Q_{44} & 0 \\ Q_{16} & Q_{26} & 0 & 0 & Q_{66} \end{bmatrix}^{(j,k)} \begin{Bmatrix} \frac{\partial u^j}{\partial x} \\ \frac{1}{a}\frac{\partial v^j}{\partial \theta} \\ \\ \\ u^j \\ v^j \\ \frac{1}{a}\frac{\partial u^j}{\partial \theta} + \frac{\partial v^j}{\partial x} \end{Bmatrix}
$$

$$+ \sum_{k=1}^{m} \begin{bmatrix} \hat{Q}_{11} & \hat{Q}_{12} & \hat{Q}_{13} & 0 & 0 & \hat{Q}_{16} \\ \hat{Q}_{12} & \hat{Q}_{22} & \hat{Q}_{23} & 0 & 0 & \hat{Q}_{26} \\ 0 & \hat{Q}_{32} & \hat{Q}_{33} & 0 & 0 & 0 \\ 0 & 0 & 0 & \hat{Q}_{55} & \hat{Q}_{54} & 0 \\ 0 & 0 & 0 & \hat{Q}_{45} & \hat{Q}_{44} & 0 \\ \hat{Q}_{16} & \hat{Q}_{26} & \hat{Q}_{63} & 0 & 0 & \hat{Q}_{66} \end{bmatrix}^{(j,k)} \begin{Bmatrix} \frac{\partial w}{\partial x} \frac{\partial w^j}{\partial x} \\ \frac{1}{a} \left(w^j + \frac{1}{a} \frac{\partial w}{\partial \theta} \frac{\partial w^j}{\partial \theta}\right) \\ w_j \\ \frac{\partial w^j}{\partial x} \\ \frac{1}{a} \frac{\partial w^j}{\partial \theta} \\ \frac{1}{a} \left(\frac{\partial w}{\partial x} \frac{\partial w^j}{\partial \theta} + \frac{\partial w}{\partial \theta} \frac{\partial w^j}{\partial x}\right) \end{Bmatrix} \tag{5.21}$$

$$M_{\theta z}^j = \bar{H}_{45}^j \left(\frac{\partial w}{\partial x}\right) + \bar{H}_{44}^j \left(\frac{1}{a} \frac{\partial w}{\partial \theta} - \frac{v}{a}\right) + \sum_{k}^{n} \left(\bar{Q}_{45}^{jk} u^k + \bar{Q}_{44}^{jk} v^k\right) + \sum_{k}^{m} \left(\bar{Q}_{45}^{jk} \frac{\partial w^k}{\partial x} + \bar{Q}_{44}^{jk} \frac{1}{a} \frac{\partial w}{\partial \theta}^k\right) \tag{5.22}$$

$$\begin{Bmatrix} L_x \\ L_\theta \\ L_{x\theta} \end{Bmatrix}^{(j,k)} = \begin{bmatrix} E_{11} & E_{12} & E_{16} \\ E_{12} & E_{22} & E_{26} \\ E_{16} & E_{26} & E_{66} \end{bmatrix}^{(j,k)} \begin{Bmatrix} \frac{\partial u}{\partial x} + \frac{1}{2} \left(\frac{\partial w}{\partial x}\right)^2 \\ \frac{1}{a} \left(\frac{\partial v}{\partial \theta} + w + \frac{1}{2} \frac{1}{a} \left(\frac{\partial w}{\partial \theta}\right)^2\right) \\ \frac{1}{a} \left(\frac{\partial u}{\partial \theta} + a \frac{\partial v}{\partial x} + \frac{\partial w}{\partial x} \frac{\partial w}{\partial \theta}\right) \end{Bmatrix}$$

$$
+\sum_{r=1}^{n}\begin{bmatrix} G_{11} & G_{12} & G_{16} \\ G_{12} & G_{22} & G_{26} \\ G_{16} & G_{26} & G_{36} \end{bmatrix}^{(j,k,r)} \begin{Bmatrix} \frac{\partial u^r}{\partial x} \\ \frac{1}{a}\frac{\partial v^r}{\partial \theta} \\ \frac{1}{a}\frac{\partial u^r}{\partial \theta} + \frac{\partial v^r}{\partial x} \end{Bmatrix}
$$

$$
+\sum_{r=1}^{m}\begin{bmatrix} \hat{G}_{11} & \hat{G}_{12} & \hat{G}_{16} & \hat{G}_{13} \\ \hat{G}_{12} & \hat{G}_{22} & \hat{G}_{26} & \hat{G}_{23} \\ \hat{G}_{61} & \hat{G}_{62} & \hat{G}_{66} & \hat{G}_{63} \end{bmatrix}^{(j,k,r)} \begin{Bmatrix} \frac{\partial w}{\partial x}\frac{\partial w^r}{\partial x} \\ \frac{1}{a}\left(w^r + \frac{1}{a}\frac{\partial w}{\partial \theta}\frac{\partial w^r}{\partial \theta}\right) \\ \frac{1}{a}\left(\frac{\partial w}{\partial x}\frac{\partial w^r}{\partial \theta} + \frac{\partial w}{\partial \theta}\frac{\partial w^r}{\partial x}\right) \\ w^r \end{Bmatrix} \tag{5.23}
$$

where A's, B's, F's, etc. are the laminate stiffness defined by

$$
A_{pq} = \int_{-\frac{h}{2}}^{\frac{h}{2}} C_{pq}\,dz \qquad (p,q = 1,2,6)
$$

$$
B^j_{pq} = \int_{-\frac{h}{2}}^{\frac{h}{2}} C_{pq}\phi^j\,dz \qquad (p,q = 1,2,6)
$$

$$
(B^j_{55}, B^j_{45}) = \int_{-\frac{h}{2}}^{\frac{h}{2}} (C_{55}, C_{45})\frac{d\phi^j}{dz}\,dz
$$

$$
(B^j_{54}, B^j_{44}) = \int_{-\frac{h}{2}}^{\frac{h}{2}} (C_{54}, C_{44})\left(\frac{d\phi^j}{dz} - \frac{\phi^j}{a}\right)dz
$$

$$
\hat{B}^j_{pq} = \int_{-\frac{h}{2}}^{\frac{h}{2}} C_{pq}\psi^j\,dz \qquad (p,q = 1,2,6,4,5)
$$

$$F_{pq}^{j} = \int_{-\frac{h}{2}}^{\frac{h}{2}} C_{pq}\phi^{j}dz \qquad (p,q = 1,2,6)$$

$$F_{pq}^{j} = \int_{-\frac{h}{2}}^{\frac{h}{2}} C_{pq}\frac{d\phi^{j}}{dz}\,dz \qquad (p,q = 4,5)$$

$$D_{pq}^{jk} = \int_{-\frac{h}{2}}^{\frac{h}{2}} C_{pq}\phi^{j}\phi^{k}dz \qquad (p,q = 1,2,6)$$

$$(D_{55}^{jk},D_{45}^{jk}) = \int_{-\frac{h}{2}}^{\frac{h}{2}} (C_{55},C_{45})\frac{d\phi^{j}}{dz}\frac{d\phi^{k}}{dz}\,dz$$

$$(D_{54}^{jk},D_{44}^{jk}) = \int_{-\frac{h}{2}}^{\frac{h}{2}} (C_{54},C_{44})\frac{d\phi^{j}}{dz}\left(\frac{d\phi^{k}}{dz} - \frac{\phi^{k}}{a}\right)dz$$

$$\hat{D}_{pq}^{jk} = \int_{-\frac{h}{2}} C_{pq}\phi^{j}\psi^{k}dz \qquad (p,q = 1,2,6)$$

$$(\hat{D}_{13}^{jk},\hat{D}_{23}^{jk},\hat{D}_{63}^{jk}) = \int_{-\frac{h}{2}}^{\frac{h}{2}} (C_{13},C_{23},C_{63})\phi^{j}\frac{d\psi^{k}}{dz}\,dz$$

$$\hat{D}_{pq}^{jk} = \int_{-\frac{h}{2}}^{\frac{h}{2}} C_{pq}\frac{d\phi^{j}}{dz}\psi^{k}dz \qquad (p,q = 4,5)$$

$$H_{pq}^{j} = \int_{-\frac{h}{2}}^{\frac{h}{2}} C_{pq}\psi^{j}dz \qquad (p,q = 1,2,4,5,6)$$

$$Q_{pq}^{jk} = \int_{-\frac{h}{2}}^{\frac{h}{2}} C_{pq}\psi^{j}\phi^{k}dz \qquad (p,q = 1,2,6)$$

$$(Q_{55},Q_{45})^{jk} = \int_{-\frac{h}{2}}^{\frac{h}{2}} (C_{55},C_{45})\psi^j \frac{d\phi^k}{dz}\, dz$$

$$(Q_{54},Q_{44})^{jk} = \int_{-\frac{h}{2}}^{\frac{h}{2}} (C_{45},C_{44})\psi^j(\frac{d\phi^k}{dz} - \frac{\phi^k}{a})dz$$

$$\hat{Q}_{pq}^{jk} = \int_{-\frac{h}{2}}^{\frac{h}{2}} C_{pq}\psi^j{}_\psi{}^k dz \qquad (p,q = 1,2,6,4,5)$$

$$(\hat{Q}_{13},\hat{Q}_{23},\hat{Q}_{63})^{jk} = \int_{-\frac{h}{2}}^{\frac{h}{2}} (C_{13},C_{23},C_{63})\psi^j \frac{d\psi^k}{dz}$$

$$(H_{31},H_{32},H_{36})^j = \int_{-\frac{h}{2}}^{\frac{h}{2}} (C_{31},C_{32},C_{36}) \frac{d\psi^j}{dz}\, dz$$

$$(Q_{31},Q_{32},Q_{36})^{jk} = \int_{-\frac{h}{2}}^{\frac{h}{2}} (C_{31},C_{32},C_{36}) \frac{d\psi^j}{dz}\, \phi^k dz$$

$$\hat{Q}_{32} = \int_{-\frac{h}{2}}^{\frac{h}{2}} C_{32} \frac{d\psi^j}{dz}\, \psi^k dz$$

$$\hat{Q}_{33} = \int_{-\frac{h}{2}}^{\frac{h}{2}} C_{33} \frac{d\psi^j}{dz} \frac{d\psi^k}{dz}\, dz$$

$$(\bar{H}_{45}^j,\bar{H}_{44}^j) = \int_{-\frac{h}{2}}^{\frac{h}{2}} (C_{45},C_{44})\phi^j dz$$

$$\bar{Q}_{45}^{jk} = \int_{-\frac{h}{2}}^{\frac{h}{2}} C_{45}\phi^j \frac{d\phi^k}{dz}\, dz$$

$$\bar{Q}_{44}^{jk} = \int_{-\frac{h}{2}}^{\frac{h}{2}} C_{44}\phi^j\left(\frac{d\phi^k}{dz} - \frac{\phi^k}{a}\right)dz$$

$$(\bar{Q}_{45}^{jk}, \bar{Q}_{44}^{jk}) = \int_{-\frac{h}{2}}^{\frac{h}{2}} (C_{45}, C_{44})\phi^j\psi^k dz$$

$$E_{pq}^{jk} = \int_{-\frac{h}{2}}^{\frac{h}{2}} C_{pq}\psi^j\psi^k dz \qquad (p,q = 1,2,6)$$

$$G_{pq}^{jkr} = \int_{-\frac{h}{2}}^{\frac{h}{2}} C_{pq}\psi^j\psi^k\phi^r dz \qquad (p,q = 1,2,6)$$

$$\hat{G}_{pq}^{jkr} = \int_{-\frac{h}{2}}^{\frac{h}{2}} C_{pq}\psi^j\psi^k\psi^r dz \qquad (p,q = 1,2,6)$$

$$(\hat{G}_{13}, \hat{G}_{23}, \hat{G}_{63})^{jkr} = \int_{-\frac{h}{2}}^{\frac{h}{2}} (C_{13}, C_{23}, C_{63})\psi^j\psi^k \frac{d\psi^r}{dz} dz. \qquad (5.24)$$

The theory presented so far is general in the sense that the interpolation functions ϕ^j and ψ^j can be chosen arbitrarily as long as they satisfy the conditions in Equation (5.10). The coefficients in Equations (5.24) are simplified when linear polynomials (Equation 2.6) are used for $\psi^j = \phi^j$. In this case the coefficients should be computed for all the interfaces j, k = 1,..., N + 1 as shown in Figure 2.1 (also see Section 2.2). The condition (5.2) is satisfied by eliminating the variables (u^r, v^r, w^r) at the middle surface interface according to Equation (5.10). The remaining variables are then renumbered from 1 to N as shown in Figure 2.2. Note that the model must include an interface

at the middle surface. If the middle surface does not coincide with an interface of the laminate, then the center layer is modelled as two layers in order to satisfy the condition (5.2).

5.3 Analytical Solutions

In order to produce an actual solution, we choose here linear Lagrange polynomials for both ϕ^j and ψ^j (see Equation 2.6). In this particular case the coefficients u^j, v^j, w^j are identified as the displacements of each (j-th) interface between layers. In order to be able to obtain an analytical solution and to compare the results with existing solutions of the 3D elasticity theory, we must restrict ourselves to the linear equations, which are obtained by eliminating the underscored terms in Equations (5.13). The solution of equations of even the linear theory is by no means trivial. These equations of motion combined with the constitutive relations are solved exactly for the case of orthotropic, simply supported laminated shells. Using a Navier-type solution method, a set of kinematically admissible solutions is assumed:

$$u(x,\theta,t) = \sum_m \sum_n X_{mn} \cos m\theta \cos \alpha x \, T_{mn}(t)$$

$$v(x,\theta,t) = \sum_m \sum_n \Gamma_{mn} \sin m\theta \sin \alpha x \, T_{mn}(t)$$

$$w(x,\theta,t) = \sum_m \sum_n \Pi_{mn} \cos m\theta \sin \alpha x \, T_{mn}(t)$$

$$u^j(x,\theta,t) = \sum_m \sum_n \Upsilon^j_{mn} \cos m\theta \cos \alpha x \, T_{mn}(t)$$

$$v^j(x,\theta,t) = \sum_m \sum_n I^j_{mn} \sin m\theta \sin \alpha x \, T_{mn}(t)$$

$$w^j(x,\theta,t) = \sum_m \sum_n \Omega^j_{mn} \cos m\theta \sin \alpha x \, T_{mn}(t)$$

$$T_{mn}(t) = e^{i\omega_{mn}} \tag{5.25}$$

where $\alpha = \frac{n\pi}{b}$ and b is the length of the cylinder.

After substitution into the constitutive equations and equations of motion, we get a system of 3N + 3 equations which relate the 3N + 3 unknowns $\{\xi\} = (X_{mn}, \Gamma_{mn}, \Pi_{mn}, \gamma^j_{mn}, I^j_{mn}, \Omega^j_{mn})$, $j = 1,\ldots,N$.

$$[k]\{\xi\} = \omega^2_{mn}[M]\{\xi\} \tag{5.26}$$

for each of the modes (m,n). The solution of the eigenvalue problem (5.26) gives 3N + 3 frequencies for each mode (m,n).

As an example, a three-ply laminate with orthotropic layers is analyzed. The stiffnesses of the inner layer are assumed to be: $C_{11} = 0.08$, $C_{12} = 0.05$, $C_{13} = 0.07$, $C_{22} = 0.19$, $C_{23} = 0.32$, $C_{33} = 1.0$, $C_{44} = 0.04$, $C_{55} = 0\ 03$, $C_{66} = 0.34$, and the outer layers are assumed to have stiffnesses 20 times those of the inner layers. The results are presented in terms of a non-dimensional parameter λ,

$$\lambda = \omega \, r_o \left(\frac{\sum_{i=1}^{N} \rho^i (r^2_{i+1} - r^2_i)}{\sum_{i=1}^{N} C^i_{33} (r^2_{i+1} - r^2_i)} \right)^{1/2} \tag{5.27}$$

where r_i is the radius of the i-th interface and r_o is the outer radius of the cylinder.

Results for a thin laminate ($r_1 = 0.95\ r_o$, $r_2 = 0.955\ r_o$, $r_3 = 0.995\ r_o$) are presented in Table 5.1. Similar results for a thick laminate ($r_1 = 0.8\ r_o$, $r_2 = 0.82\ r_o$, $r_3 = 0.98\ r_o$) are presented in

Table 5.2. The exact results using 3-D elasticity are taken from Srinivas [98]. In Table 5.3, results for a two-ply cylindrical shell are presented. The material properties used are those of a graphite-epoxy material (E_1 = 19.6 msi, E_2 = 1.56 msi, ν_{12} = 0.24, ν_{23} = 0.47, G_{12} = 0.82 msi, G_{23} = 0.523 msi), and the thickness of each layer is 0.05 in. The three lowest frequencies are presented in Table 5.3 in non-dimensional form as before. While neglecting the rotary inertia, the inplane inertias still need to be considered for cylindrical shells because the displacements tangential to the reference surface, mainly u_θ, play an important role in the behavior of the shell. This is in contrast to plate theory, where the in-plane inertias are usually neglected along with rotary inertia. Results obtained for zero transverse normal strain are also presented. They were obtained using the reduced stiffness matrix instead of the 3-D stiffness matrix. The present results are, in general, in good agreement with those presented by Srinivas [98].

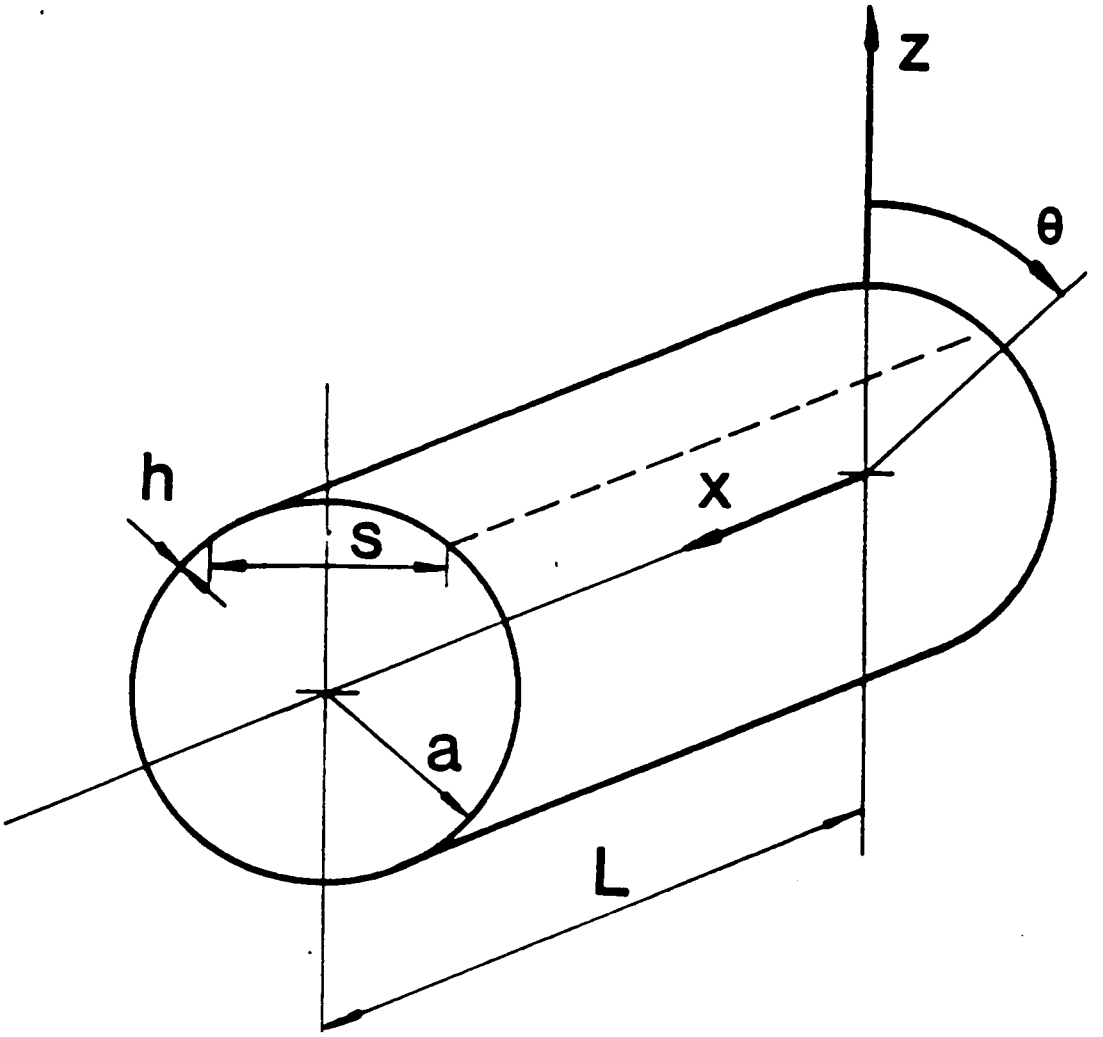

Figure 5.1 Shell coordinate system.

Table 5.1. Nondimensional Frequencies for a Three-Layer Thin Laminate

b/na	m	First Frequency		Second Frequency		Third Frequency	
		Exact*	GLST‡	Exact	GLST	Exact	GLST
1	0	.32461	.32706	1.8186	1.8074	3.0037	2.9666
	1	.33631	.33855	1.7031	1.6939	3.1438	3.1003
	2	.36737	.36917	1.4689	1.4529	3.4615	3.4020
	3	.40447	.40603	1.2612	1.2571	3.8451	3.7631
	4	.42507	.42687	1.1822	1.17873	4.2502	4.1407
2	0	.28282	.28354	.91614	.91301	1.5441	1.5389
	1	.30591	.30549	.73938	.73762	1.7807	1.7725
	2	.30838	.30897	.60419	.60273	2.2071	2.1913
	3	.21959	.22066	.80118	.79792	2.6748	2.6466
	4	.20414	.20527	1.1467	1.1396	3.1559	3.1098
8	0	.20999	.20989	.22904	.22898	.51742	.51708
	1	.07054	.07052	.41957	.41930	.84128	.83941
	2	.03594	.03638	.78928	.78801	1.3559	1.3476
	3	.06940	0.06966	1.1956	1.1900	1.9113	1.8887
	4	.12237	.12254	1.6058	1.5909	2.4841	2.4354

* Exact Results from Srinivas [91]
‡ GLST: Generalized Laminate Shell Theory (present)
a: radius; b: length; m: circumferential and n: longitudinal mode number.

Table 5.2 Nondimensional Frequencies for a Three-Layer Thick Laminate

b/na	m	First Frequency		Second Frequency		Third Frequency	
		Exact	GLSDT	Exact	GLSDT	Exact	GLSDT
1	0	.40438	.40838	1.6205	1.5064	1.7475	1.9271
	1	.42140	.42401	1.5294	1.4333	1.7530	1.9478
	2	.46495	.46524	1.3354	1.2710	1.7633	1.9850
	3	.50904	.51186	1.1742	1.1233	1.7626	2.0148
	4	.52631	.53482	1.1540	1.1003	1.7309	1.9960
2	0	.31807	.32042	.89129	.87015	1.4316	1.3733
	1	.35573	.35501	.71061	.69823	1.4242	1.5282
	2	.33947	.34297	.62782	.61531	1.3608	1.5689
	3	.28099	.28233	.85051	.84972	1.5134	1.7085
	4	.33070	.32851	1.1398	1.1460	1.7260	1.9032
8	0	.21844	.21680	.22955	.22916	.54260	.53637
	1	.06638	.06696	.46207	.46070	.86049	.85054
	2	.08773	.08718	.82383	.82943	1.3288	1.2941
	3	.18459	.18276	1.1547	1.1553	1.6937	1.6713
	4	.28616	.28404	1.3692	1.3842	1.9282	1.9686

Table 5.3 Nondimensional Frequencies of a Two-Ply Graphite-Epoxy Cylinder

		First Frequency				Second Frequency				Third Frequency			
		rotary inertia included		no rotary inertia		rotary inertia included		no rotary inertia		rotary inertia included		no rotary inertia	
b/na	m	$e_z \neq 0$	$e_z = 0$	$e_z \neq 0$	$e_z = 0$	$e_z \neq 0$	$e_z = 0$	$e_z \neq 0$	$e_z = 0$	$e_z \neq 0$	$e_z = 0$	$e_z \neq 0$	$e_z = 0$
1	0	.6370	.6370	.6353	.6353	.7716	.7809	.7725	.7838	2.2094	2.2102	2.1558	2.1594
	1	.4153	.4163	.4152	.4170	1.202	1.212	1.195	1.207	2.2208	2.2219	2.1657	2.1698
	2	.2936	.2938	.2937	.2947	1.818	1.834	1.788	1.804	2.2582	2.2619	2.1978	2.2052
	3	.2666	.2660	.2667	.2673	2.272	2.268	2.214	2.210	2.5134	2.5444	2.4253	2.4612
	4	.3109	.3092	.3111	.3115	2.357	2.355	2.287	2.289	3.1302	3.1670	3.9841	3.0258
2	0	.3185	.3185	.3186	.3186	.7606	.7692	.7610	.7700	1.1360	1.1360	1.1273	1.1277
	1	.2133	.2135	.2133	.2136	1.108	1.112	1.104	1.108	1.1678	1.1748	1.1579	1.1667
	2	.1397	.1398	.1397	.1400	1.211	1.209	1.200	1.199	1.7587	1.7785	1.7314	1.7524
	3	.1518	.1510	.1518	.1515	1.302	1.300	1.287	1.286	2.4325	2.4602	2.3586	2.3879
	4	.2313	.2291	.2314	.2303	1.419	1.418	1.399	1.398	3.0777	3.1126	2.9432	2.9816
8	0	.0797	.0797	.0798	.0977	.2864	.2863	.2863	.2862	.7601	.7684	.7603	.7685
	1	.0439	.0439	.0439	.0439	.3585	.3583	.3582	.3580	1.0958	1.1078	1.0923	1.1045
	2	.0454	.0451	.0454	.0451	.5145	.5144	.5134	.5132	1.7338	1.7530	1.7086	1.7285
	3	.1147	.1133	.1147	.1136	.7015	.7014	.6984	.6983	2.4132	2.4404	2.3421	2.3706
	4	.2133	.2105	.2133	.2115	.9004	.9003	.8937	.8936	3.0623	3.0968	2.9310	2.9686

Chapter 6

THE JACOBIAN DERIVATIVE METHOD FOR THREE-DIMENSIONAL FRACTURE MECHANICS

6.1 Introduction

The Fracture Mechanics algorithm developed in this chapter will be employed (Chapter 7) for the evaluation of fracture mechanics parameters at the boundary of delaminations in laminated composite plates.

The finite element method is well established as a tool for determination of stress intensity factors in fracture mechanics. Isoparametric elements are among the most frequently used elements due to their ability to model the geometry of complex domains. The quarter-point element [61,62] became very popular in linear elastic fracture mechanics (LEFM) because it can accurately represent the singularities in those problems. Its use has been extended to other problems as well [63].

Two main areas have received attention in fracture mechanics analyses: first, to model accurately the singular behavior near the crack front; second, to compute the stress intensity factor from the solution to the finite element model of the problem. The following sections deal with the second problem, with emphasis on the use of isoparametric elements. The method presented here has its origins in the virtual crack extension method of Hellen [72] and the stiffness derivative method of Parks [73]. Similar but different methods have been developed [100-103]. But in contrast to the VCEM, the Jacobian derivative method presented herein does not require an arbitrary choice of a "virtual" extension that in the VCEM becomes an "actual"

extension. We take advantage of the isoparametric formulation to compute the strain energy release rates directly from the displacement field.

The Jacobian derivative method is a true post processor algorithm. In this method the stress intensity factors are computed from an independently obtained displacement solution. Therefore, the displacement solution can be obtained with a program without any fracture mechanics capability, although adequate representation of the singular behavior near the crack front is necessary.[1] The displacement field may even be obtained by experimental techniques. Furthermore, the proposed technique does not require computation of stresses, thus reducing computational cost and increasing accuracy. The Jacobian derivative method also provides the distribution of the strain energy release rate along the crack front, $G = G(s)$, without any two-dimensional hypothesis (here s denotes a curvilinear coordinate along the crack front).

The present study is motivated by delamination type problems in composite laminates. These problems exhibit planar growth, that is, the crack grows in its original plane. However, the shape of the crack may vary with time. For example, a initially elliptic crack usually grows with variable aspect ratio. Therefore we cannot in general assume self

---

[1]The Saint Venant principle does not apply for reentrant corners (cracks). In other words, a reentrant corner singularity influences the displacement field all over the domain.

similar crack growth. The algorithm presented is simple, inexpensive, reliable and robust.

Numerous methods for the calculation of stress intensity factors have appeared over the years. The direct methods are those in which the stress intensity factors are computed as a part of the solution. The direct methods require special elements that incorporate the crack tip singularity [65]. The indirect methods are those in which the stress intensity factors are computed from displacements or stresses that are obtained independently. The more popular indirect methods are: extrapolation of displacements or stresses around the crack tip [66] and the nodal-force method [67,68]. Integral methods like the J-integral method [69], the modified crack closure integral [70,71], and the virtual crack extension method [72,73] are also used. The indirect methods can be used with conventional elements or with special elements that incorporate the singularity at the crack front.

The virtual crack extension method (VCEM) is appealing because it does not require computation of stresses, and therefore is inexpensive and accurate. However, the VCEM requires two computations for two slightly different configurations. Improved versions of the VCEM [72] or the stiffness derivative method [73] eliminate the second run but require the specification of a "virtual" crack extension (VCE), a small quantity that must be chosen arbitrarily. Rounding errors may appear if the VCE is too small, and badly distorted elements may result if the VCE is too large [72].

The virtual crack extension method postulates that the strain energy release rate can be computed as

$$G(s) = \frac{\partial U}{\partial a} \tag{6.1}$$

where U is the strain energy and a is the representative crack length. In the actual implementation of VCE, however, one approximates Equation (6.1) by the quotient $\Delta U/\Delta a$; in the limit $\Delta a \to 0$ this gives the desired value of G.

The Jacobian derivative method proposed here computes G(s) according to Equation (6.1) exactly. The method does not require the approximation of the derivative, and therefore the choice of the magnitude of the "virtual" crack extension does not arise. The concept has been already applied in other fields [104]. The basic idea of the method can be summarized as follows. In the isoparametric formulation the geometry and the solutions are approximated with the same interpolation (or finite elements). Therefore, the total potential energy depends both on the displacements and on the nodal coordinates that ultimately represent the shape of the domain. Once the displacements have been found for a fixed configuration, the potential energy depends only on the nodal coordinates of the boundary. Consequently, we can compute the strain energy release rate due to a virtual crack extension simply by differentiating with respect to the nodal coordinates on the crack front. The nodal coordinates can be treated as variables in the isoparametric formulation of the problem. In the next section we formally develop this idea.

6.2 Theoretical Formulation

The objective of the algorithm is to compute the strain energy release rate G(s) by Equation (6.1). Consider the total potential

energy functional,

$$\Pi = \int_{\Omega} \left(\int_{0}^{\varepsilon_{ij}} \sigma_{ij} d\varepsilon_{ij} \right) d\Omega + \int_{\Omega} f_i \cdot u_i d\Omega + \int_{\partial\Omega} t_i \cdot n_i dS \qquad (6.2)$$

Without loss of generality we consider a linear elastic material for which the strain energy, U, is

$$U = \int_{0}^{\varepsilon_{ij}} \sigma_{ij} d\varepsilon_{ij} = \frac{1}{2} \sigma_{ij} \varepsilon_{ij} \qquad (6.3)$$

In the finite element method the potential energy is approximated as

$$\Pi = \underset{\sim}{u}^T \left[\int_{\Omega} \frac{1}{2} \underset{\sim}{B}^T \underset{\sim}{\underset{\sim}{D}} \underset{\sim}{B} d\Omega \right] \underset{\sim}{u} + W \qquad (6.4)$$

where $\underset{\sim}{\underset{\sim}{D}}$ is the constitutive matrix, $\underset{\sim}{B}$ is the strain-displacement matrix, W is the work performed by external loads, and $\underset{\sim}{u}$ is the vector of nodal displacements.

The solution of the problem is obtained using the principle of virtual displacements (or the minimum total potential energy):

$$\frac{\partial \Pi}{\partial \underset{\sim}{u}} = 0 \qquad (6.5)$$

Since the approximate potential energy is a function of the nodal displacements $\underset{\sim}{u}$ and the crack length a, we have

$$\frac{\partial \Pi}{\partial a} = \frac{\partial \Pi}{\partial a} + \frac{\partial \underset{\sim}{u}}{\partial a} \cdot \frac{\partial \Pi}{\partial \underset{\sim}{u}} \Big|_{a=\text{const}} \qquad (6.6)$$

where

$$\frac{\partial}{\partial a} \equiv \frac{\partial}{\partial a} \Big|_{\underset{\sim}{u}=\text{const}} \qquad (6.7)$$

Assuming that no body forces are present, no forces are applied to the surfaces of the crack, and that the fixed-grip end condition holds during the virtual crack extension, we obtain

$$\frac{\partial W}{\partial \dot{a}} = 0 \tag{6.8}$$

and

$$\frac{\partial \Pi}{\partial \dot{a}} = \frac{\partial U}{\partial \dot{a}} = G. \tag{6.9}$$

The fixed-grip end condition refers to the case where only specified displacements are applied to the boundary. It has been shown [105] that the value of the strain energy release rate remains unchanged if the fixed-grip end condition is replaced by a constant load on the boundary. The argument can be generalized to the case of arbitrary load-displacement hystory at the boundary by considering infinitesimal increments, as shown in Appendix 6. Using Equations (6.5), (6.8) and (6.9) in Equation (6.6), we obtain

$$\frac{\partial \Pi}{\partial a} = \frac{\partial \Pi}{\partial \dot{a}} = \frac{\partial}{\partial \dot{a}} \{\underset{\sim}{u}^T [\int_\Omega \frac{1}{2} \underset{\sim}{\underset{\sim}{B}}^T \underset{\sim}{\underset{\sim}{D}} \underset{\sim}{\underset{\sim}{B}} d\Omega] \underset{\sim}{u}\}$$

or

$$G = \frac{\partial}{\partial \dot{a}} \{\sum_e \underset{\sim}{u}^T [\int_{\Omega_e} \frac{1}{2} \underset{\sim}{\underset{\sim}{B}}^T \underset{\sim}{\underset{\sim}{D}} \underset{\sim}{\underset{\sim}{B}} d\Omega] \underset{\sim}{u}\} \tag{6.10}$$

where Ω^e is a typical finite element. The indicated integration is carried out over the master element [74]:

$$G = \frac{\partial}{\partial \dot{a}} \{\sum_e \underset{\sim}{u}^T [\int_{\Omega_e} \frac{1}{2} \underset{\sim}{\underset{\sim}{B}}^T \underset{\sim}{\underset{\sim}{D}} \underset{\sim}{\underset{\sim}{B}} |J| d\xi d\eta] \underset{\sim}{u}\} \tag{6.11}$$

Interchanging the order of integration and differentiation, which is possible because $\underset{\sim}{u}$ is kept constant during the differentiation, we obtain

$$G = \frac{1}{2} \sum_e \underset{\sim}{u}^T [\int_{\Omega_e} \frac{\partial}{\partial \dot{a}} (\underset{\sim}{\underset{\sim}{B}}^T \underset{\sim}{\underset{\sim}{D}} \underset{\sim}{\underset{\sim}{B}} |J| d\xi d\eta] \underset{\sim}{u} \tag{6.12}$$

The integrand in Equation (6.12) can be expanded as follows:

$$\frac{\partial}{\partial \dot{\underset{\sim}{a}}} [\underset{\sim}{B}^T \underset{\sim\sim}{D} \underset{\sim}{B} |J|] = \frac{\partial}{\partial \dot{\underset{\sim}{a}}} [\underset{\sim}{B}^T \underset{\sim\sim}{D} \underset{\sim}{B}] |J| + [\underset{\sim}{B}^T \underset{\sim\sim}{D} \underset{\sim}{B}] \frac{\partial |J|}{\partial \dot{\underset{\sim}{a}}} \tag{6.13}$$

where

$$\frac{\partial}{\partial \dot{\underset{\sim}{a}}} [\underset{\sim}{B}^T \underset{\sim\sim}{D} \underset{\sim}{B}] = [\frac{\partial \underset{\sim}{B}}{\partial \dot{\underset{\sim}{a}}}]^T \underset{\sim\sim}{D} \underset{\sim}{B} + \underset{\sim}{B}^T \underset{\sim}{D} [\frac{\partial \underset{\sim}{B}}{\partial \dot{\underset{\sim}{a}}}]. \tag{6.14}$$

The strain displacement matrix $\underset{\sim}{B}$ can be written in terms of the matrix of shape functions $\underset{\sim}{\Phi}$ as

$$\underset{\sim}{B} = \underset{\sim}{J}^{-1} \underset{\sim}{\Phi} \tag{6.15}$$

and therefore,

$$\frac{\partial \underset{\sim}{B}}{\partial \dot{\underset{\sim}{a}}} = \frac{\partial \underset{\sim}{J}^{-1}}{\partial \dot{\underset{\sim}{a}}} \underset{\sim}{\Phi} \tag{6.16}$$

Consider the identity

$$\underset{\sim}{I} = \underset{\sim}{J}^{-1} \underset{\sim}{J} \tag{6.17}$$

Differentiation with respect to a yields

$$0 = \frac{\partial \underset{\sim}{J}^{-1}}{\partial \dot{\underset{\sim}{a}}} \underset{\sim}{J} + \underset{\sim}{J}^{-1} \frac{\partial \underset{\sim}{J}}{\partial \dot{\underset{\sim}{a}}} \tag{6.18}$$

or

$$\frac{\partial \underset{\sim}{J}^{-1}}{\partial \dot{\underset{\sim}{a}}} = - \underset{\sim}{J}^{-1} \frac{\partial \underset{\sim}{J}}{\partial \dot{\underset{\sim}{a}}} \underset{\sim}{J}^{-1} \tag{6.19}$$

Substituting Equation (6.19) in Equation (6.16), we obtain

$$\frac{\partial \underset{\sim}{B}}{\partial \dot{\underset{\sim}{a}}} = - \underset{\sim}{J}^{-1} \frac{\partial \underset{\sim}{J}}{\partial \dot{\underset{\sim}{a}}} \underset{\sim}{J}^{-1} \underset{\sim}{\Phi} = - \underset{\sim}{J}^{-1} \frac{\partial \underset{\sim}{J}}{\partial \dot{\underset{\sim}{a}}} \underset{\sim}{B}. \tag{6.20}$$

Equation (6.15) takes the form

$$\frac{\partial}{\partial \dot{\underset{\sim}{a}}} [\underset{\sim}{B}^T \underset{\sim\sim}{D} \underset{\sim}{B}] = - [\underset{\sim}{J}^{-1} \frac{\partial \underset{\sim}{J}}{\partial \dot{\underset{\sim}{a}}} \underset{\sim}{B}]^T \underset{\sim\sim}{D} \underset{\sim}{B} - \underset{\sim}{B}^T \underset{\sim}{D} [\underset{\sim}{J}^{-1} \frac{\partial \underset{\sim}{J}}{\partial \dot{\underset{\sim}{a}}} \underset{\sim}{B}] \tag{6.21}$$

or

$$\frac{\partial}{\partial \dot{\underset{\sim}{a}}} [\underset{\sim}{B}^T \underset{\sim\sim}{D} \underset{\sim}{B} |J|] = [- \dot{\underset{\sim}{B}}^T \underset{\sim\sim}{D} \underset{\sim}{B} - \underset{\sim}{B}^T \underset{\sim\sim}{D} \dot{\underset{\sim}{B}}] |J| + \underset{\sim}{B}^T \underset{\sim\sim}{D} \underset{\sim}{B} \frac{\partial |J|}{\partial \dot{\underset{\sim}{a}}} \tag{6.22}$$

where

$$\dot{\underset{\sim}{B}} = [\underset{\sim}{J}^{-1} \frac{\partial \underset{\sim}{J}}{\partial \dot{a}} \underset{\sim}{B}] \tag{6.23}$$

Finally, substituting Equation (6.22) into Equation (6.11), we obtain the expression for the strain-energy release-rate,

$$G = \frac{1}{2} \sum_e \underset{\sim}{u}^T [\int_{\Omega_e} \{(- \dot{\underset{\sim}{B}}^T \underset{\sim\sim}{D} \underset{\sim}{B} - \underset{\sim}{B}^T \underset{\sim\sim}{D} \dot{\underset{\sim}{B}}) |J| + \underset{\sim}{B}^T \underset{\sim\sim}{D} \underset{\sim}{B} \frac{\partial |J|}{\partial \dot{a}}\} drds] \underset{\sim}{u} \tag{6.24}$$

where $\underset{\sim}{u}$ is the displacement vector, known from the finite element solution.

The derivatives of the Jacobian must be computed as (note that $\frac{\partial \underset{\sim}{J}}{\partial \dot{a}} = \frac{\partial \underset{\sim}{J}}{\partial a}$, since $\underset{\sim}{J}$ is independent of $\underset{\sim}{u}$),

$$\frac{\partial \underset{\sim}{J}}{\partial \dot{a}} = \begin{bmatrix} \sum_i \phi_{i,r} \frac{\partial x_i}{\partial \dot{a}} ; \sum_i \phi_{i,r} \frac{\partial y_i}{\partial \dot{a}} ; \sum_i \phi_{i,r} \frac{\partial z_i}{\partial \dot{a}} \\ \sum_i \phi_{i,s} \frac{\partial x_i}{\partial \dot{a}} ; \sum_i \phi_{i,s} \frac{\partial y_i}{\partial \dot{a}} ; \sum_i \phi_{i,s} \frac{\partial z_i}{\partial \dot{a}} \\ \sum_i \phi_{i,t} \frac{\partial x_i}{\partial \dot{a}} ; \sum_i \phi_{i,t} \frac{\partial y_i}{\partial \dot{a}} ; \sum_i \phi_{i,t} \frac{\partial z_i}{\partial \dot{a}} \end{bmatrix} \tag{6.25}$$

where (r,s,t) are the local coordinates of the isoparametric element, (x_i, y_i, z_i) are the global coordinates of the nodes of the element and the vector

$$\underset{\sim}{v} = \{\frac{\partial x_i}{\partial \dot{a}}, \frac{\partial y_i}{\partial \dot{a}}, \frac{\partial z_i}{\partial \dot{a}}\} \tag{6.26}$$

is the input vector that indicates the direction and shape of the virtual crack extension.

The derivatives of the determinant of the Jacobian must be computed as

$$\frac{\partial |\underset{\sim}{J}|}{\partial \underset{\cdot}{a}} = \frac{\partial}{\partial a} \det \begin{bmatrix} \sum_i \phi_{i,r} x_i & ; & \sum_i \phi_{i,r} y_i & ; & \sum_i \phi_{i,r} z_i \\ \sum_i \phi_{i,s} x_i & ; & \sum_i \phi_{i,s} y_i & ; & \sum_i \phi_{i,s}\ z_i \\ \sum_i \phi_{i,t} x_i & ; & \sum_i \phi_{i,t} y_i & ; & \sum_i \phi_{i,t} z_i \end{bmatrix} \tag{6.27}$$

It is worth noting that the summation in Equation (6.24) extends only over the elements connected to the crack because there is no deformation of the elements far away from the crack; that is,

$$\frac{\partial J}{\partial \underset{\cdot}{a}} = 0 \tag{6.28}$$

for elements not connected to the crack.

The evaluation of Equation (6.24) requires the displacements $\underset{\sim}{u}$ at the nodes of the (isoparametric) elements surrounding the crack. The elements used in the postprocessor can be coded independently of those used in the finite element program employed to obtain the displacements. At least in principle, they do not need to be of the same type. In the examples in this chapter, however, both the main finite element program and the postprocessor use isoparametric quarter-point elements.

6.3 Computational Aspects

In order to apply the method we must specify the direction of the virtual crack extension by means of a unit vector in the expected direction of growth. We give the direction of the VCE at least for each node on the crack front. However, for some meshes it is convenient to

use the mid-side nodes of the elements surrounding the crack front. Beyond that, any number of nodes can be used as long as they surround the crack front. The Jacobian derivative method uses the elements connected to these nodes to compute the strain energy release rate. Therefore the cost of the solution grows with the number of elements involved. But this cost is negligible compared to the cost of the finite element analysis of the complete structure. Usually the solution is insensitive to the number of elements involved in the postprocessing and only the crack tip elements need to be used.

All virtual crack extension methods rely on the displacement field obtained for the original crack shape. Therefore the virtual crack extension must be such that it preserves the shape of the crack. If the shape of the crack were to change, the nature of the singularity would change significantly and the solution for the original shape would be of no help in predicting the new situation. For two-dimensional problems, this means that the direction of the VCE is that of the crack itself. For three-dimensional problems two aspects need to be considered. First, the VCE must lie on the plane of the crack. This is a natural extension of the two-dimensional argument. It does not mean that the crack cannot grow out of its plane. It just means that we are unable to compute anything else with just one solution for the original shape. Second, the VCE must have the shape of the original crack. Once again, it does not seem right to pretend to change the shape of the crack when we only have the solution for one shape. However, deviations to this premise have been reported in the literature with some success. It is probable that no big errors are introduced violating the latter

requirement because the nature of the singularity supposedly does not change significantly as long as the crack remains in its original plane. The second requirement does not mean that the crack cannot grow with variable aspect ratio. Even more, we may be able to predict the direction of the growth based on the distribution of energy release rate along the crack front.

Since the Jacobian derivative method is a post-processor algorithm, we are tempted to use it with several probable shapes for the VCE. However, we found out that this is unnecessary. Just specifying a self similar VCE, we are able to compute the stress energy release rate distribution along the crack front of a curved crack. The Jacobian derivative method computes the contribution to the strain energy release-rate G(S) element by element. Computation of G(S) along the crack front is explained in the three-dimensional applications presented in the next section.

6.4 Applications

In order to demonstrate the applicability of the proposed technique, we present several numerical examples. Since it is computationally very expensive to use very refined meshes for three-dimensional problems, we use coarse meshes in all the examples. We use collapsed, quarter point elements around the crack tip [61,62,63] and quadratic isoparametric elements elsewhere.

6.4.1 Two-Dimensional Problems

We use a series of two-dimensional meshes with 17 quadratic elements and 62 nodes (Figure 6.1) to study three problems:

a) a plate with a single edge crack

b) a plate with a central crack and

c) a plate with symmetric edge cracks.

The three cases differ only in the boundary conditions. In all three cases, the load is uniform, applied as equivalent loads at the edge away from the crack. Symmetry along the crack line is exploited to model only one half of the specimen. For this example we assume that a plane stress condition holds. It must be noted that the value of the strain energy release rate depends linearly on the thickness of the model. The relationship between strain energy release rate and stress intensity factor holds when strain energy release rate is computed per unit thickness.

The three-dimensional mesh of Figure 6.2 is used to model the same two-dimensional problems. The three-dimensional mesh involves 147 nodes and provides almost exactly the same results as the two-dimensional models.

The present finite element solutions are compared with the solutions presented by Paris and Sih [105]. The results are tabulated in the form of correction factors to the stress intensity factor in an infinite medium. Therefore, the applicable stress intensity factor is

$$k = k_o * f(a/b)$$

Table 6.1 contains the results for a plate with a single edge crack. The plate has length 2L, width 2b = W and a crack of length a on one side. The finite element solution is compared with the solutions presented in [106]. The agreement is excellent even for a coarse mesh. The equation used to compute the stress intensity factor in an

infinite medium for this example is:

$$k_o = \sigma_o(a\pi)^{1/2}$$

Table 6.2 contains the results for a square plate with a crack at the center. The plate has length 2L, width 2b = 2W and a crack of length 2a. The present finite element solution is compared with the solutions of Paris and Sih [105] for L/W = ∞ and the finite element results of Hellen [72] for square plates. The agreement between the two finite element solutions is excellent even for a coarse mesh. The equation used to compute the stress intensity factor in an infinite medium for this example is the same as for the single edge crack.

Table 6.3 contains the results for a plate with a double edge crack. The plate has length 2L, width 2b = 2W and a crack of length a on each side. We impose symmetry conditions on the centerline that divides the plate between the two cracks, thus modelling 1/4 of the specimen. The finite element solution is compared with the solutions of Paris and Sih [105] for L/W = ∞. Discrepancies between the present results and those of Paris and Sih [105] required us to use a finer mesh. The refined model has 50 elements and 147 nodes. Therefore, we enhance not only the crack-tip-zone modelling but also the imposition of boundary conditions. However, the discrepancies still persist. The present results, however, compare reasonably well with the finite element results of Hellen [72], as shown in Table 6.3. The equation used to compute the stress intensity factor in an infinite medium for this example is:

$$k_o = \sigma(a\pi)^{1/2} \cdot \frac{2b}{a\pi} \tan\left(\frac{a\pi}{2b}\right)$$

6.4.2 Three-Dimensional Problems

Surface Crack in a Cylinder. Results are presented for a thick cylinder of internal radius R_i = 29.8 mm thickness t = 5 mm, length 2b = 200 mm, subjected to internal pressure P. A surface crack is located longitudinally on the outer surface. The shape of the crack is that of a segment of circle (see insert in Figure 6.4) with a = 2.3 mm, 1c = 13.6 mm. However, it approximates an elliptical crack for which other numerical studies exist [107]. Kaufmann et al. [108] presented experimental and numerical results for this particular crack shape.

A mesh with 275 elements and 4107 degrees of freedom is used to obtain the displacement field around the crack front. A layer of 22 collapsed, quarter-point elements [66] surround the crack front. Quadratic isoparametric elements model the rest of the specimen. Detail of the mesh around the crack front is shown in Figure 6.3. Four segments labeled S_1 to S_4 divide one half of the crack front. On each segment, four collapsed elements surround the crack front. The mesh becomes coarse rapidly toward the main portion of the cylinder.

The virtual crack extension direction is specified so as to produce a self similar growth of the crack. All the nodes of the elements surrounding the crack front are used in the VCE. These elements are those in the inner layer next to the crack front (see Figure 6.3). Therefore, for this example, the algorithm uses the two layers of elements surrounding the crack front to compute the strain energy release rate.

The Jacobian derivative method computes the contribution to the strain energy release rate element by element. Next, we add the

contributions to the strain energy release rate of all the elements that surround one sector (S_i) of the crack front at a time (see Figure 6.3). Then, we divide this value by the length of the crack front covered by the corresponding sector (S_i) to obtain the distribution of the strain energy release rate along the crack front.

In order to compare the results with others, we transform G(s) to K(s) by means of either a plane strain or plane stress assumption, whichever is appropriate:

$$\text{plane stress:} \quad K(s) = \sqrt{EG(s)}$$

$$\text{plane strain:} \quad K(s) = \sqrt{\frac{EG(s)}{1-\nu^2}}$$

The distribution of K(s) is shown in Figure 6.4 for the plane strain assumption, along with results from Raju and Newman [107] for a semielliptical crack with $t/R_i = 0.1$, $a/C = 0.4$, $a/t = 0.5$, and from Kaufman, et al. [108]. The results are normalized by the stress intensity factor K_o at $\phi = \pi/2$ for an elliptical crack embedded in an infinite body subjected to a uniform stress

$$K_o = \frac{2R_i^2 P}{R_o^2 - R_i^2}\sqrt{\frac{\pi a}{1 + 1.464\ (a/c)^{1.65}}}$$

Kaufman, et al. [108] computed the stress intensity factor using the plane strain assumption and the method of Reference [66]. Raju and Newman [107] used the 2D analytical solution to relate the stress intensity factor to stresses. Of course, all numerical solutions were truly three-dimensional. In our case, the distribution of G(s) is obtained directly from the three-dimensional analysis without any two-dimensional assumption. The solution by the present method closely

agrees with that presented in [108]. The discrepancy between our solution and that of [107] is due to the difference in the shapes of the cracks. While Raju and Newman [107] used a semi-elliptical crack, we used a circular-segment crack (see insert in Figure 6.4).

Side-Grooved Compact Test Specmens. It is well known that the compact test specimen shows small variation of the stress intensity factor along the crack front [109,110]. However, if the sides of the crack are grooved (see Figure 6.5) the stress intensity factor has an important variation through the thickness. Reference [111] presents numerical results and experimental evidence that the stress intensity factor grows considerably at the grooved side.

The geometry of the specimen is shown in Figure 6.5. Due to symmetry only a quarter of the specimen is modelled. A finite element mesh of 370 quadratic elements with 1985 nodes is uniformly refined toward the side of the specimen and toward the crack front. 3-D collapsed, quarter-point elements surround the crack front. Only elements surrounding the crack front are used in the postcomputation by the JDM. The plane-strain equations are used to transform the strain energy distribution along the crack front to a stress intensity factor distribution. The results are normalized with respect to the 2-D boundary collocation solution [112].

Through the thickness distributions of the stress intensity factor along the crack front for compact test specimens with and without grooved sides are shown in Figure 6.6 for a = 0.6 W, and B = 0.5 W. Solid lines represent the results of the present study (JDM) and symbol

markers are taken from Figure 6.4 of reference [111]. The maximum value for the smooth specimen differs by less than 0.2% from the value reported in reference [111] for a = 0.5 W. The agreement is excellent except perhaps for the 50% side-grooved specimen where differences in the finite element mesh and in the Poisson ratio may have more influence than in the other cases. Although the Poisson ratio was not reported in Reference [111], its effect on the stress intensity factor is small, at least for the two-dimensional problem [112]. In this study we used: $\nu = 0.33$ and $E = 10^7$. This example further demonstrates the applicability of the JDM to accurately evaluate the stress intensity factor distribution along the crack front of 3-D fractures. The Jacobian derivative method developed herein keeps all the advantages of the indirect methods, while adding new enhancements. Being an indirect method, it can be used with displacements obtained from a variety of techniques. In particular, even experimental techniques can be used. The method does not require costly mesh refinements, and it is not mesh sensitive. Unlike the VCEM, it does not require the specification of a small crack extension, which makes the JDM a more robust algorithm. Its applicability for three-dimensional curved cracks is demonstrated. The method will be applied to delaminations in composite materials along with a refined plate theory in the following chapter.

Appendix 6

Influence of the external work on the computation of the strain energy release rate.

The strain energy of the system can be written as:

$$U = \frac{1}{2} CP^2 \tag{A1}$$

where C is the compliance and P is the applied load. The external work for an infinitesimal reduction in the compliance of the system due to crack growth is:

$$dW = Pdu \tag{A2}$$

where u are the displacements at the point of application of the load. The energy available for crack propagation is

$$dE = dW - dU \tag{A3}$$

$$dE = Pdu - \frac{1}{2} d(CP^2) \tag{A4}$$

but

$$du = d(CP) = CdP + PdC \tag{A5}$$

therefore

$$dE = \frac{1}{2} P^2 dC \tag{A6}$$

In the general case where neither the load nor the displacements are held constant, the strain energy release rate is:

$$G = \frac{dE}{da} = \frac{1}{2} P^2 \frac{dC}{da} \tag{A7}$$

which shows no dependence on the derivatives of the applied load P or the displacements at the boundary u. Therefore, Equation (A7) is valid for the general case, even for the case of fixed-grip end conditions

(i.e., dW = 0). We conclude that the assumption of fixed-grip end conditions does not alter the value of the strain energy release rate. The fixed-grip end condition is automatically imposed in the Jacobian Derivative Method since only one solution for the displacement field u, for the initial configuration is used. This means that the displacements everywhere, and in particular at the boundary, are held fixed during the virtual crack extension used to compute the strain energy release rate (see Equation 6.7).

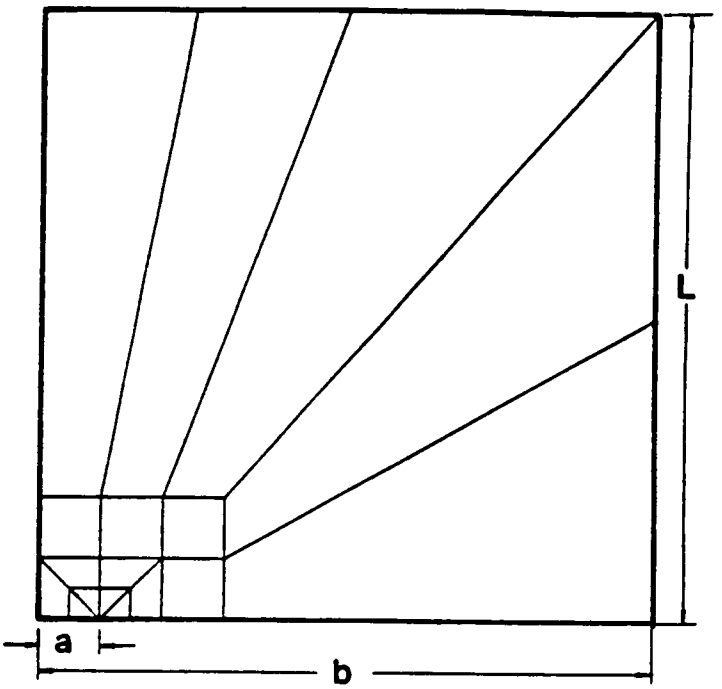

6.1 Two-dimensional finite element mesh for plates with various through-the-thickness cracks.

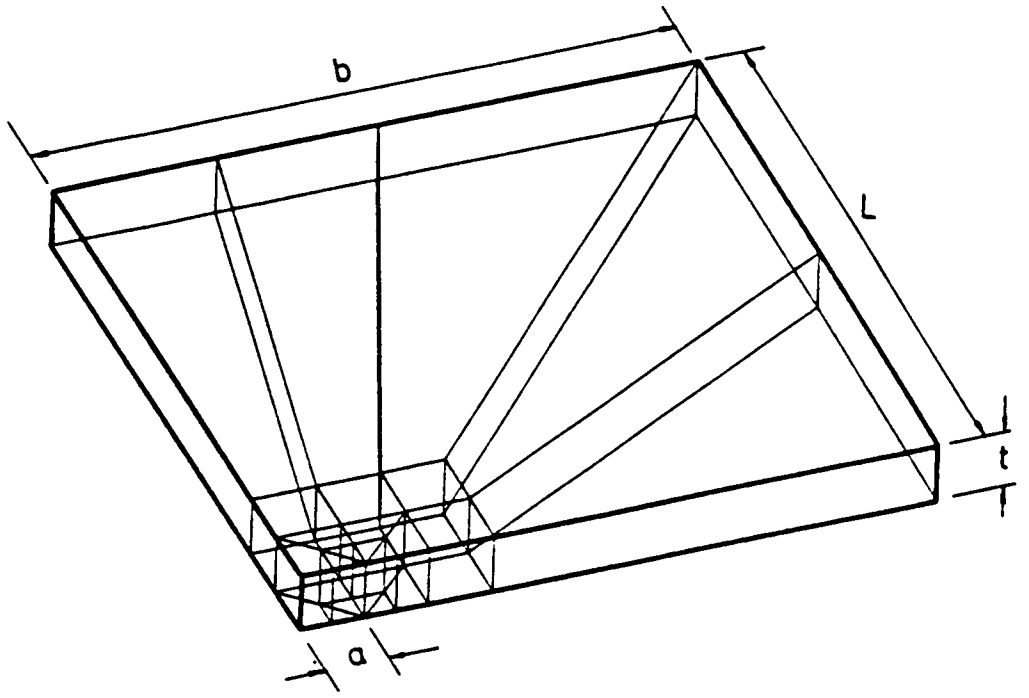

6.2 Three-dimensional finite element mesh for plates with various through-the-thickness cracks.

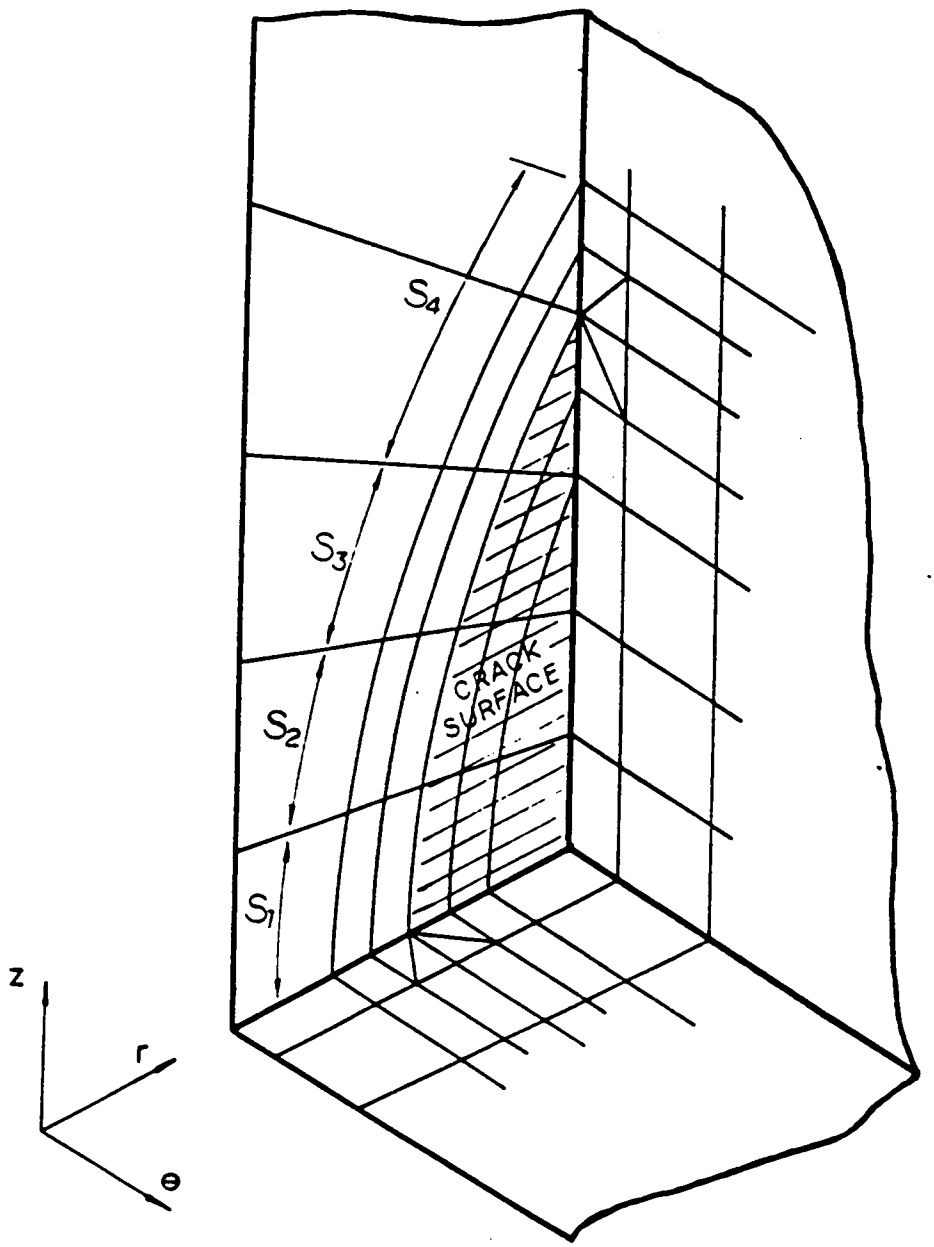

6.3 Detail of the cracked area of the cylinder with external crack. Only part of the mesh is shown. Hidden lines have been removed.

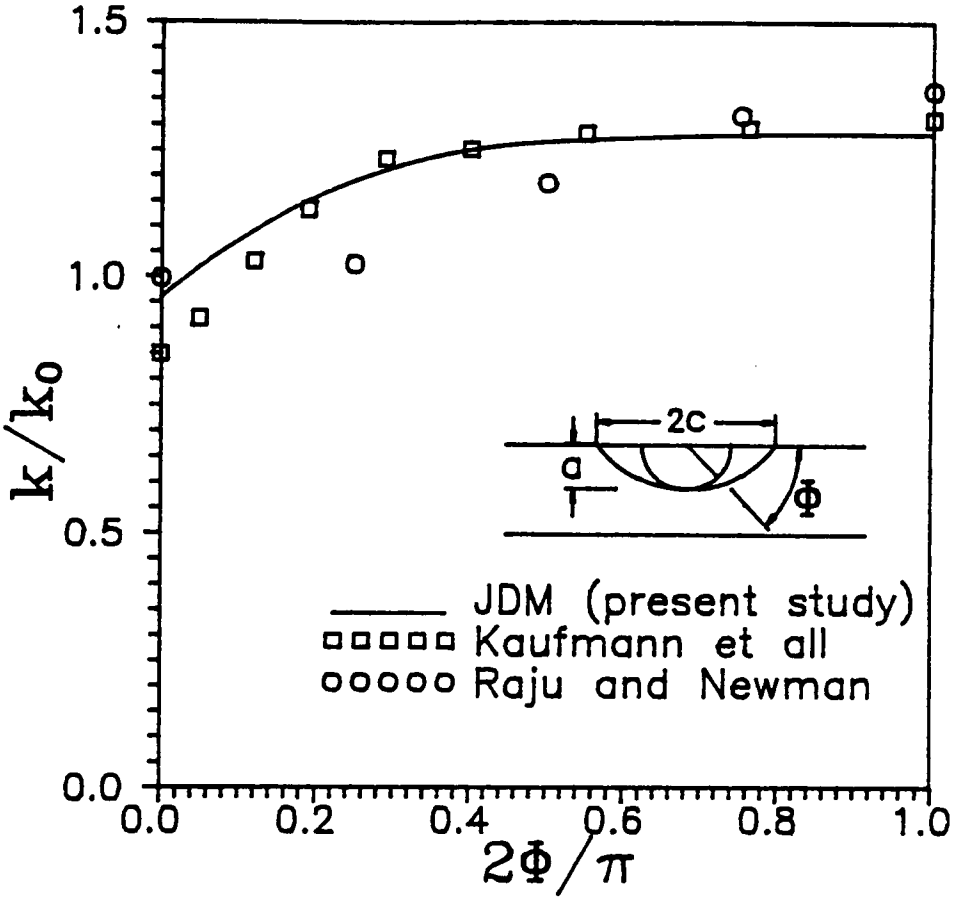

6.4 Stress intensity factor distributions along the crack front of an external surface crack on a cylinder under internal pressure.

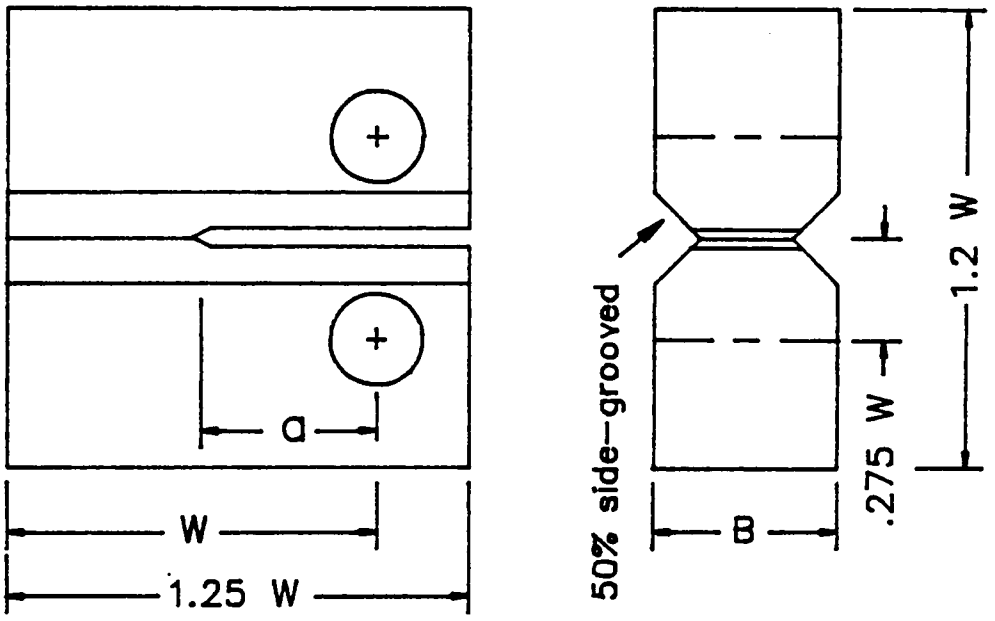

6.5 Side and front view of the 50% side-grooved compact-test specimen, B = 0.5 W, a = 0.6 W.

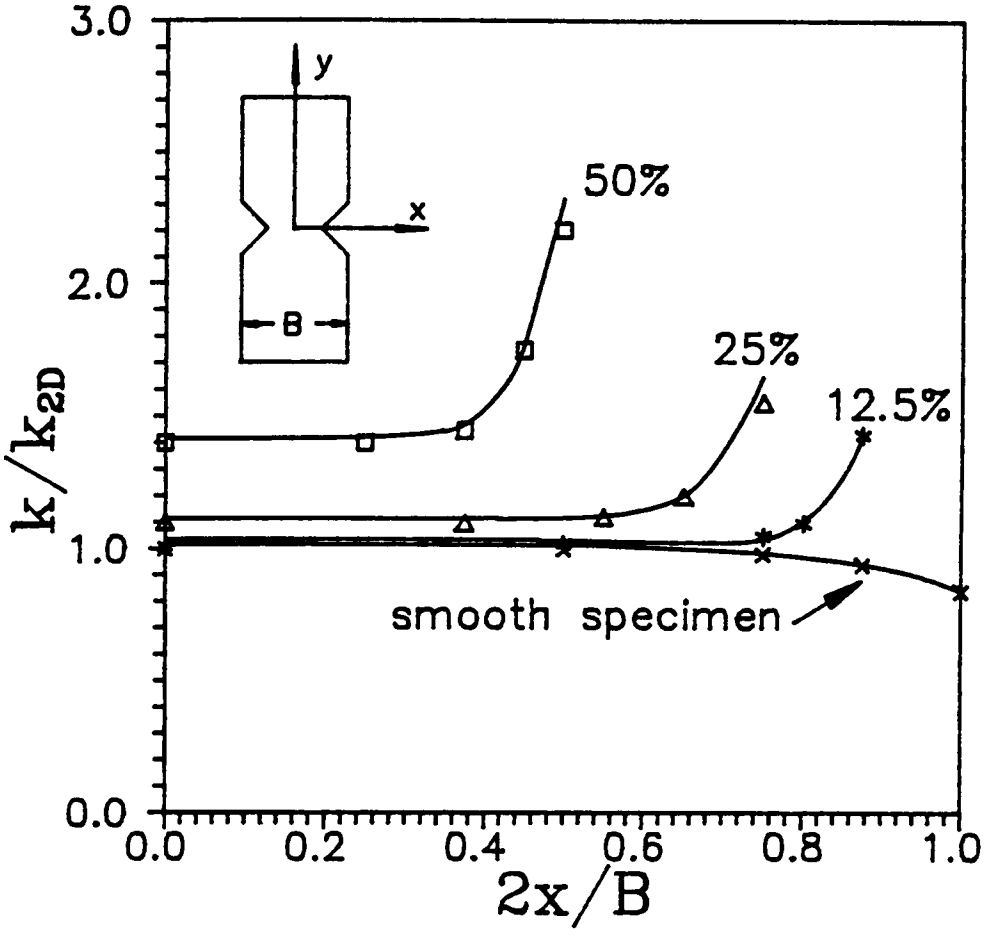

6.6 Through the thickness distribution of the stress intensity factor normalized with respect to the boundary collocation solution [22] for the smooth specimen X, 12.5% side-grooved *, 25% side-grooved Δ, and 50% side-grooved . Solid lines from JDM and symbol markers from Shih and deLorenzi.

Table 6.1. Values of f(a/b) for a plate with single edge crack.

a/b	JDM	GROSS	BOWIE
0.2	1.19	1.19	1.20
0.4	1.38	1.37	1.37
0.6	1.86	1.66	1.68
0.8	2.14	2.12	2.14
1.0	2.83	2.82	2.86

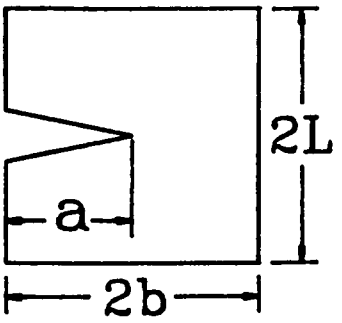

Table 6.2. Values of f(a/b) for a plate with central crack.

a/b	JDM L/W = 1	Hellen L/W = 1	Paris & Sih L/W = inf
0.1	1.02	1.02	1.00
0.2	1.06	1.05	1.03
0.3	1.13	1.12	1.06
0.4	1.23	1.21	1.13
0.5	1.34	1.33	1.27

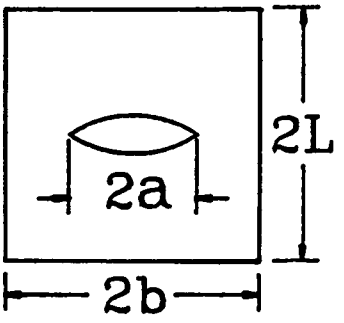

Table 6.3. Values of f(a/b) for a plate with double edge crack.

a/b	JDM 17 el.	JDM 50 el.	Hellen 32 el.	Paris & Sih L/W = inf
0.1	1.14		1.13	1.13
0.2	1.18		1.14	1.13
0.3	1.24		1.18	1.14
0.4	1.29		1.19	1.16
0.5	1.34		1.18	1.14

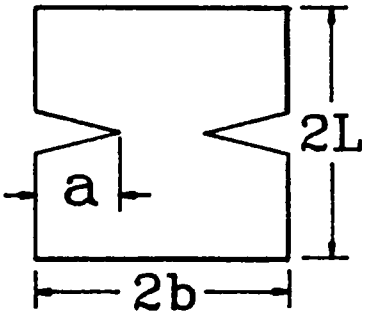

Chapter 7

A MODEL FOR THE STUDY OF DELAMINATIONS IN COMPOSITE PLATES

7.1 Introduction

Delamination buckling in laminated plates subjected to in-plane compressive loads is well recognized as a limiting factor on the performance of composite structures. While the accuracy of the analysis is of paramount importance to the correct evaluation of damage in composites, the cost of analysis precludes the use of three-dimensional models. This chapter deals with the formulation of a laminated plate theory that can handle multiple delaminations in composite plates.

The aspect ratio considerations limit the applicability of 3-D analysis to composite plates. A finite element model based on a plate theory does not have any through-thickness aspect ratio limitation because the thickness dimension is eliminated at the beginning. However, the hypothesis commonly used in conventional plate theories leads to a poor representation of stresses in cases of interest to us, namely, small thickness ratio (thickness over damage-size) problems and problems with dissimilar material layers (damaged and undamaged). These limitations are overcome by use of the Generalized Laminated Plate Theory with layer-wise smooth representation of displacements through the thickness. Geometric nonlinearity in the sense of von Karman will be included to capture the layer buckling.

The representation of displacements and stresses in the damaged area must be accurate. For the case of delaminations, an accurate solution is necessary for the application of a fracture criterion to

predict the onset of delamination growth. Among the fracture criteria, the energy criteria are the most accepted. The virtual crack extension method is applicable to delamination because the delamination is most likely to propagate in its own plane (the interface). An improved version of the virtual crack extension method (the Jacobian Derivative Method, Chapter 6) is utilized in the present study.

7.2 Formulation of the Theory

Analysis of delaminations in laminated composite plates requires an appropriate kinematical description of the plate to allow for separation (delamination buckling) and slipping (due to shear). This can be incorporated into the GLPT by proper modification of the expansion of the displacements through the thickness. The GLPT can model the kinematics of a layered plate, with provision for delaminations, using the following expansion of the displacements through the thickness of the plate:

$$u_1(x,y,z) = u(x,y) + \sum_{j=1}^{N} \phi^j(z)\, u^j(x,y) + \sum_{j=1}^{D} H^j(z)\, U^j(x,y)$$

$$u_2(x,y,z) = v(x,y) + \sum_{j=1}^{N} \phi^j(z)\, v^j(x,y) + \sum_{j=1}^{D} H^j(z) V^j(x,y)$$

$$u_3(x,y,z) = w(x,y) + \sum_{j=1}^{D} H^j(z)\, W^j(x,y) \qquad (7.1)$$

where the step functions H^j are computed in terms of the Heaviside step functions $\hat{H}$ as:

$$\begin{aligned} H^j(z) &= \hat{H}(z - z_j) = 1 \quad \text{for } z > z_j \\ H^j(z) &= \hat{H}(z - z_j) = 0 \quad \text{for } z < z_j \end{aligned} \qquad (7.2a)$$

In Equation (1) $\phi^j(z)$ are linear Lagrange interpolation functions, N is the number of layers used to model the laminate and D is the number of delaminations. The jump in the displacements at the j-th delaminated interface is given by U^j, V^j and W^j (see Figure 1). Using the step functions $H^j(z)$, we can model any number of delaminations through the thickness; the number of additional variables is equal to the number of delaminations considered. At delaminated interfaces, the displacements on adjacent layers remain independent, allowing for separation (buckling) and slipping. Since $H^j(z)$ is layer-wise constant, the transverse normal strain is $\varepsilon_{zz} = 0$. This restriction, based on a reasonable and usual assumption, allows us to reduce the complexity of the theory and the cost of its solutions. However, we can obtain $\varepsilon_{zz} \neq 0$ simply by augmenting the expansion through the thickness of the transverse displacement u_3.

A nonlinear analysis must be used for buckling of delaminated composites. Bifurcation analysis applicability is limited because of the bending-extension coupling of both the delaminated layers and the base laminate. Even laminates that are originally symmetric, once delaminated experience bending-extension coupling effects. Most likely the delamination(s) are unsymmetrically located and the resulting delaminated layers and base laminate become also unsymmetric. Therefore, in-plane compressive load produces lateral deflection and the primary equilibrium path is not trivial ($w \neq 0$) as was shown in Section 4.6.2.

Although nonlinear effects are important, rotations and displacements are not expected to be so large as to require a full

nonlinear analysis. Only the von Kármán nonlinearities in the kinematic equations need to be considered.

The linear strains of the theory are

$$\varepsilon_x = \frac{\partial u}{\partial x} + \sum_j^N \phi^j \frac{\partial u^j}{\partial x} + \underline{\sum_j^D H^j \frac{\partial U^j}{\partial x}} \tag{7.3a}$$

$$\varepsilon_y = \frac{\partial v}{\partial y} + \sum_j^N \phi^j \frac{\partial v^j}{\partial x} + \underline{\sum_j^D H^j \frac{\partial V^j}{\partial x}} \tag{7.3b}$$

$$\varepsilon_{xy} = \frac{1}{2}\left(\frac{\partial u}{\partial y} + \frac{\partial v}{\partial x}\right) + \frac{1}{2}\sum_j^N \phi^j\left(\frac{\partial u^j}{\partial y} + \frac{\partial v^j}{\partial x}\right) + \underline{\frac{1}{2}\sum^D H^i\left(\frac{\partial U^j}{\partial y} + \frac{\partial V^j}{\partial x}\right)} \tag{7.3c}$$

$$\varepsilon_z = 0 \text{ because } \frac{\partial H^j}{\partial z} = 0 \tag{7.3d}$$

$$\varepsilon_{xz} = \frac{1}{2}\left[\frac{\partial w}{\partial x} + \sum_j^N \frac{\partial \phi^j}{\partial z} u^j + \underline{\sum_j^D H^j \frac{\partial W^j}{\partial x}}\right] \tag{7.3e}$$

$$\varepsilon_{yz} = \frac{1}{2}\left[\frac{\partial w}{\partial y} + \sum_j^N \frac{\partial \phi^j}{\partial z} v^j + \underline{\sum_j^D H^j \frac{\partial W^j}{\partial y}}\right] \tag{7.3f}$$

where underlined terms are new terms that appear in the linear strains as a result of the introduction of the delamination variables U^j, V^j, W^j.

The nonlinear portion of the strains are:

$$\eta_x = \frac{1}{2}\left[\frac{\partial w}{\partial x} + \sum_j^D H^j \frac{\partial W^j}{\partial x}\right]^2 \tag{7.4a}$$

$$\eta_y = \frac{1}{2}\left[\frac{\partial w}{\partial y} + \sum_j^D H^j \frac{\partial W^j}{\partial y}\right]^2 \tag{7.4b}$$

$$\eta_{xy} = \frac{1}{2}\left[\frac{\partial w}{\partial x} + \sum_j^D H^j \frac{\partial W^j}{\partial x}\right]\left[\frac{\partial w}{\partial y} + \sum_j^D H^j \frac{\partial W^j}{\partial y}\right] \tag{7.4c}$$

$$\eta_{13} = \eta_{23} = \eta_{33} = 0 \tag{7.4d}$$

After expansion Equations (4) become

$$\eta_x = \frac{1}{2}\left(\frac{\partial w}{\partial x}\right)^2 + \underline{\frac{1}{2}\sum_{i}^{D}\sum_{j}^{D}\left(H^i H^j \frac{\partial W^i}{\partial x}\frac{\partial W^j}{\partial x}\right)} + \underline{\frac{\partial w}{\partial x}\sum_{i}^{D} H^i \frac{\partial W^i}{\partial x}} \tag{7.5a}$$

$$\eta_y = \frac{1}{2}\left(\frac{\partial w}{\partial y}\right)^2 + \underline{\frac{1}{2}\sum_{i}^{D}\sum_{j}^{D}\left(H^i H^j \frac{\partial W^i}{\partial y}\frac{\partial W^j}{\partial y}\right)} + \underline{\frac{\partial w}{\partial y}\sum_{i}^{D} H^i \frac{\partial W^i}{\partial y}} \tag{7.5b}$$

$$\eta_{xy} = \frac{1}{2}\frac{\partial w}{\partial x}\frac{\partial w}{\partial y} + \underline{\frac{1}{2}\sum_{i}^{D}\sum_{j}^{D}\left(H^i H^j \frac{\partial W^i}{\partial x}\frac{\partial W^j}{\partial y}\right)} + \underline{\frac{1}{2}\frac{\partial w}{\partial x}\sum_{j}^{D}\left(H^j \frac{\partial W^j}{\partial y}\right) + \frac{1}{2}\frac{\partial w}{\partial y}\sum_{i}^{D}\left(H^i \frac{\partial W^i}{\partial x}\right)}. \tag{7.5c}$$

$$\eta_{xz} = \eta_{yz} = \eta_z = 0, \tag{7.5d}$$

where the underlined terms are due to the delaminations. The remaining terms are the classical von Kármán nonlinear terms.

The virtual strain energy is given by

$$\delta U = \delta U_{CL} + \delta U_{CNL} + \delta U_{DL} + \delta U_{DNL} \tag{7.6a}$$

where

δU_{CL}: contribution of the classical linear terms

δU_{CNL}: contribution of the von Kármán classical nonlinear terms

δU_{DL}: contribution of the new linear terms [underlined in Equation (7.3)]

δU_{DNL}: contribution of the new nonlinear terms [underlined in Equation (7.5)] (7.6b)

The contribution of the classical linear terms is:

$$\delta U_{CL} = \int_V \{\sigma_x[\frac{\partial \delta u}{\partial x} + \sum_{j=1}^{N} \phi^j(z) \frac{\partial \delta u^j}{\partial x}]$$

$$+ \sigma_y [\frac{\partial \delta v}{\partial y} + \sum_{j=1}^{N} \phi^j(z) \frac{\partial \delta v^j}{\partial x}]$$

$$+ \sigma_{xy} [\frac{\partial \delta u}{\partial y} + \frac{\partial \delta v}{\partial x} + \sum_{j=1}^{N} \phi^j(z) (\frac{\partial \delta u^j}{\partial y} + \frac{\partial \delta v^j}{\partial x})]$$

$$+ \sigma_{xz} [\frac{\partial \delta w}{\partial x} + \sum_{j=1}^{N} \frac{\partial \phi^{j(z)}}{\partial z} u^j]$$

$$+ \sigma_{yz} [\frac{\partial \delta w}{\partial y} + \sum_{j=1}^{N} \frac{\partial \phi^j(z)}{\partial z} v^j]\} dV - \int_\Omega q \delta w dA \quad (7.7)$$

Integrating through the thickness and defining

$$(N_x, N_y, N_{xy}) = \int_{-\frac{h}{2}}^{\frac{h}{2}} (\sigma_x, \sigma_y, \sigma_{xy}) dz$$

$$(Q_x, Q_y) = \int_{-\frac{h}{2}}^{\frac{h}{2}} (\sigma_{xz}, \sigma_{yz}) dz$$

$$(N_x^j, N_y^j, N_{xy}^j) = \int_{-\frac{h}{2}}^{\frac{h}{2}} (\sigma_x, \sigma_y, \sigma_{xy}) \phi^j(z) dz$$

$$(Q_x^j, Q_y^j) = \int_{-\frac{h}{2}}^{\frac{h}{2}} (\sigma_{xz}, \sigma_{yz}) \frac{d\phi^j(z)}{dz} dz \quad (7.8)$$

we obtain

$$\delta U_{CL} = \int_{\Omega} \{N_x \frac{\partial \delta u}{\partial x} + \sum_{j=1}^{N} N_x^j \frac{\partial \delta u^j}{\partial z} +$$

$$+ N_y \frac{\partial \delta u}{\partial y} + \sum_{j=1}^{N} N_y^j \frac{\partial \delta v^j}{\partial x} + N_{xy}(\frac{\partial \delta u}{\partial y} + \frac{\partial \delta v}{\partial x})$$

$$+ \sum_{j=1}^{N} N_{xy}^j (\frac{\partial u^j}{\partial y} + \frac{\partial v^j}{\partial x}) + Q_x \frac{\partial \delta w}{\partial x} + \sum_{j=1}^{N} Q_x^j u^j$$

$$+ Q_y \frac{\partial \delta w}{\partial y} + \sum_{j=1}^{N} Q_y^j v^j - q\delta w\} dA. \qquad (7.9)$$

The contribution of the von Kármán nonlinear terms is:

$$\delta U_{CNL} = \int_{V} \{\sigma_x \frac{\partial w}{\partial x} \frac{\partial \delta w}{\partial x} + \sigma_y \frac{\partial w}{\partial y} \frac{\partial \delta w}{\partial y} + \sigma_{xy}(\frac{\partial w}{\partial x} \frac{\partial \delta w}{\partial y} + \frac{\partial \delta w}{\partial x} \frac{\partial w}{\partial y})\} dV$$

Integrating over the thickness and using the definitions (8) we obtain,

$$\delta U_{CNL} = \int_{\Omega} \{N_x \frac{\partial w}{\partial x} \frac{\partial \delta w}{\partial x} + N_y \frac{\partial w}{\partial y} \frac{\partial \delta w}{\partial y} + N_{xy} (\frac{\partial w}{\partial x} \frac{\partial \delta w}{\partial y} + \frac{\partial \delta w}{\partial x} \frac{\partial w}{\partial y})\} dA \qquad (7.10)$$

The contribution of the new linear terms is:

$$\delta U_{DL} = \int_{V} \{\sigma_x \sum_{i=1}^{D} H^i(z) \frac{\partial \delta U^i}{\partial x} + \sigma_y \sum_{i=1}^{D} H^i(z) \frac{\partial \delta V^i}{\partial y}$$

$$+ \sigma_{xy} \sum_{i=1}^{D} H^i(z) (\frac{\partial \delta U^i}{\partial y} + \frac{\partial \delta V^i}{\partial x})$$

$$+ \sigma_{xz} \sum_{i=1}^{D} H^i(z) \frac{\partial \delta W^i}{\partial x} + \sigma_{yz} \sum_{i=1}^{D} H^i(z) \frac{\partial \delta W^i}{\partial y}\} dv$$

Integrating through the thickness and introducing

$$(\hat{Q}_x^i, \hat{Q}_y^i) = \int_{-\frac{h}{2}}^{\frac{h}{2}} (\sigma_{xz}, \sigma_{yz}) H^i(z) dz \qquad (7.11)$$

$$(M_x^i, M_y^i, M_{xy}^i) = \int_{-\frac{h}{2}}^{\frac{h}{2}} (\sigma_x, \sigma_y, \sigma_{xy}) H^i(z) dz$$

we can write

$$\delta U_{DL} = \sum_{i=1}^{D} \Big[\int_S \{ \hat{Q}_x^i \frac{\partial \delta W^i}{\partial x} + \hat{Q}_y^i \frac{\partial \delta W^i}{\partial y} + M_x^i \frac{\partial \delta U^j}{\partial x} + M_y^i \frac{\partial \delta V^j}{\partial y}$$

$$+ M_{xy}^i \left(\frac{\partial \delta U^i}{\partial y} + \frac{\partial \delta V^i}{\partial x} \right) \} dx dy \qquad (7.12)$$

The contribution of the new nonlinear terms is:

$$\delta U_{DNL} = \int_S \int_{-\frac{h}{2}}^{\frac{h}{2}} \{ \sum_{i=1}^{D} \sum_{j=1}^{D} \Big[\sigma_x H^i(z) H^j(z) \frac{1}{2} \left(\frac{\partial W^i}{\partial x} \frac{\partial \delta W^j}{\partial x} + \frac{\partial W^i}{\partial x} \frac{\partial \delta W^j}{\partial x} \right)$$

$$+ \sigma_y H_i(z) H^j(z) \frac{1}{2} \left(\frac{\partial W^i}{\partial y} \frac{\partial \delta W^j}{\partial y} + \frac{\partial W^i}{\partial y} \frac{\partial \delta W^j}{\partial y} \right)$$

$$+ \sigma_{xy} H^i(z) H^j(z) \left(\frac{\partial W^i}{\partial y} \frac{\partial \delta W^j}{\partial x} + \frac{\partial W^i}{\partial x} \frac{\partial \delta W^j}{\partial y} \right) \Big]$$

$$+ \sigma_x \frac{\partial w}{\partial x} \sum_{i}^{D} H^i(z) \frac{\partial \delta W^i}{\partial x} + \sigma_y \frac{\partial w}{\partial y} \sum_{i}^{D} H^i(z) \frac{\partial \delta W^i}{\partial y}$$

$$+ \sigma_{xy} \frac{\partial w}{\partial x} \sum_{i}^{D} H^i(z) \frac{\partial \delta W^i}{\partial y} + \sigma_{xy} \frac{\partial w}{\partial y} \sum_{i}^{D} H^i(z) \frac{\partial \delta W^i}{\partial x}$$

$$+ \sigma_x \frac{\partial \delta w}{\partial x} \sum_{i}^{D} H^i(z) \frac{\partial W^i}{\partial x} + \sigma_y \frac{\partial \delta w}{\partial y} \sum_{i}^{D} H^i(z) \frac{\partial W^i}{\partial y}$$

$$+ \sigma_{xy} \frac{\partial \delta W}{\partial x} \sum_{i}^{D} H^i \frac{\partial W^i}{\partial y} + \sigma_{xy} \frac{\partial \delta w}{\partial y} \sum_{i}^{D} H^i(z) \frac{\partial W^i}{\partial x} \} dz dx dy.$$

Defining

$$(M_x^{ij}, M_y^{ij}, M_{xy}^{ij}) = = \int_{-\frac{h}{2}}^{\frac{h}{2}} (\sigma_x, \sigma_y, \sigma_{xy}) H^i(z) H^j(z) dz \qquad (7.13)$$

we can write

$$\delta U_{DNL} = \int_{\Omega} \{\sum_{i}^{D} [M_x^i (\frac{\partial w}{\partial x} \frac{\partial \delta W^i}{\partial x} + \frac{\partial \delta w}{\partial x} \frac{\partial W^i}{\partial x})$$

$$+ M_y^i (\frac{\partial w}{\partial y} \frac{\partial \delta W^i}{\partial y} + \frac{\partial \delta w}{\partial y} \frac{\partial W^i}{\partial y})$$

$$+ M_{xy}^i (\frac{\partial w}{\partial x} \frac{\partial \delta W^i}{\partial y} + \frac{\partial \delta w}{\partial x} \frac{\partial W^i}{\partial y}$$

$$+ \frac{\partial w}{\partial y} \frac{\partial \delta W^i}{\partial x} + \frac{\partial \delta w}{\partial y} \frac{\partial W^i}{\partial x})]$$

$$+ \sum_{i}^{D} \sum_{j}^{D} \frac{1}{2} M_x^{ij} (\frac{\partial W^i}{\partial x} \frac{\partial \delta W^j}{\partial x} + \frac{\partial \delta W^i}{\partial x} \frac{\partial W^j}{\partial x})$$

$$+ \frac{1}{2} M_y^{ij} (\frac{\partial W^i}{\partial y} \frac{\partial \delta W^j}{\partial y} + \frac{\partial \delta W^i}{\partial y} \frac{\partial W^j}{\partial y})$$

$$+ M_{xy}^{ij} (\frac{\partial W^i}{\partial y} \frac{\partial \delta W^j}{\partial x} + \frac{\partial W^j}{\partial x} \frac{\partial \delta W^i}{\partial y})\} d\Omega \qquad (7.14)$$

The boundary conditions are given below:

Geometric	Force
u	$N_x n_x + N_{xy} n_y$
v	$N_{xy} n_x + N_y n_y$
w	$Q_x n_x + Q_y n_y$
u^j	$N_x^j n_x + N_{xy}^i n_x$
v^j	$N_{xy}^j n_x + N_y^j n_y$
U^j	$M_x^j n_x + M_{xy}^j n_y$
V^j	$M_{xy}^j n_x + M_y^j n_y$
W^j	$\hat{Q}_{xz}^i n_x + \hat{Q}_{yz}^i n_y$. (7.15)

The lamina constitutive equations for the k-th lamina transformed to the structural coordinates x, y are:

$$\begin{Bmatrix} \sigma_x^k \\ \sigma_y^k \\ \sigma_{xy}^k \\ \sigma_{xz}^k \\ \sigma_{yz}^k \end{Bmatrix} = \begin{bmatrix} \overline{Q}_{11}^k & Q_{12} & \overline{Q}_{16}^k & 0 & 0 \\ \overline{Q}_{12}^k & Q_{22} & \overline{Q}_{26}^k & 0 & 0 \\ \overline{Q}_{16}^k & Q_{26} & \overline{Q}_{66}^k & 0 & 0 \\ 0 & 0 & 0 & \overline{Q}_{55}^k & \overline{Q}_{45}^k \\ 0 & 0 & 0 & \overline{Q}_{45}^k & \overline{Q}_{44}^k \end{bmatrix} \begin{Bmatrix} \varepsilon_x^k \\ \varepsilon_y^k \\ \gamma_{xy}^k \\ \gamma_{xz}^k \\ \gamma_{yz}^k \end{Bmatrix} \tag{7.16}$$

Substituting Equations (7.16) into the definitions of the stress resultants, we obtain the laminate constitutive equations,

$$\begin{Bmatrix} N_x \\ N_y \\ N_{xy} \end{Bmatrix} = \begin{bmatrix} A_{11} & A_{12} & A_{16} \\ & A_{22} & A_{26} \\ & & A_{66} \end{bmatrix} \begin{Bmatrix} \partial u/\partial x + 1/2\ (\partial w/\partial x)^2 \\ \partial v/\partial y + 1/2\ (\partial w/\partial y)^2 \\ \partial u/\partial y + \partial w/\partial x\ \partial w/\partial y \end{Bmatrix}$$

$$+ \sum_{j=1}^{N} \begin{bmatrix} B_{11}^j & B_{12}^j & B_{16}^j \\ & B_{22}^j & B_{26}^j \\ & & B_{66}^j \end{bmatrix} \begin{Bmatrix} \partial u^j/\partial x \\ \partial v^j/\partial y \\ \partial u^j/\partial y + \partial v^j/\partial x \end{Bmatrix}$$

$$+ \sum_{i=1}^{D} \begin{bmatrix} E_{11}^i & E_{12}^i & E_{16}^i \\ & E_{22}^i & E_{26}^i \\ & & E_{66}^i \end{bmatrix} \begin{Bmatrix} 2\partial w/\partial x\ \partial W^i/\partial x + \partial U^i/\partial x \\ 2\partial w/\partial y\ \partial W^i/\partial y + \partial V^i/\partial y \\ \partial w/\partial x\ \partial W^i/\partial y + \partial w/\partial y\ \partial W^i/\partial x + \partial U^i/\partial y + \partial V^i/\partial x \end{Bmatrix}$$

$$+ \sum_{i=1}^{D} \sum_{j=1}^{D} \begin{bmatrix} E_{11}^{ij} & E_{12}^{ij} & E_{16}^{ij} \\ & E_{22}^{ij} & E_{26}^{ij} \\ & & E_{66}^{ij} \end{bmatrix} \begin{Bmatrix} \partial W^i/\partial x\ \partial W^j/\partial x \\ \partial W^i/\partial y\ \partial W^j/\partial y \\ \partial W^i/\partial y\ \partial W^j/\partial x \end{Bmatrix} \tag{7.17}$$

$$\begin{Bmatrix} Q_x \\ Q_y \end{Bmatrix} = \begin{bmatrix} A_{55} & A_{45} \\ & Q_{44} \end{bmatrix} \begin{Bmatrix} \partial w/\partial x \\ \partial w/\partial y \end{Bmatrix} + \sum_{j=1}^{N} \begin{bmatrix} B_{55}^j & B_{45}^j \\ & B_{44}^j \end{bmatrix} \begin{Bmatrix} u^j \\ v^j \end{Bmatrix}$$

$$+ \sum_{i=1}^{m} \begin{bmatrix} E_{55}^i & E_{45}^i \\ & E_{44}^i \end{bmatrix} \begin{Bmatrix} \partial W^i/\partial x \\ \partial W^i/\partial y \end{Bmatrix} \qquad (7.18)$$

where

$$A_{pq} = \sum_{k=1}^{N} \int_{z_{k-1}}^{z_k} Q_{pq}^{(k)} dz; \quad (p,1 = 1,2,6,4,5)$$

$$B_{pq}^j = \sum_{k=1}^{N} \int_{z_{k-1}}^{z_k} Q_{pq}^k \phi^j dz; \quad (p,q = 1,2,6)$$

$$B_{pq}^j = \sum_{k=1}^{N} \int_{z_{k-1}}^{z_k} Q_{pq}^k \frac{d\phi^j}{dz} dz; \quad (p,q = 4,5)$$

$$D_{pq}^{ij} = \sum_{k=1}^{N} \int_{z_{k-1}}^{z_k} Q_{pq}^k \phi^j \phi^i dz; \quad (p,q = 1,2,6)$$

$$D_{pq}^{ij} = \sum_{k=1}^{N} \int_{z_{k-1}}^{z_k} Q_{pq}^k \frac{d\phi^j}{dz} \frac{d\phi^i}{dz} dz; \quad (p,q = 4,5)$$

$$E_{pq}^i = \sum_{k=1}^{N} \int_{z_{k-1}}^{z_k} Q_{pq}^k H^i(z) dz; \quad (p,q = 1,2,6,4,5) \qquad (7.19)$$

$$E_{pq}^{ij} = \sum_{k=1}^{n} \int_{z_{k-1}}^{z_k} Q_{pq}^k H^i(z) H^j(z) dz; \quad (p,q = 1,2,6)$$

Note that there are linear terms involving the delamination variables U, V, W. This linear effect suggests that delaminations may grow even prior to buckling and without peeling or σ_{zz} stress. The driving mechanisms are the modes II and III of fracture. Furthermore, we obtain,

$$\begin{Bmatrix} N_x^j \\ N_y^j \\ N_{xy}^j \end{Bmatrix} = \begin{bmatrix} B_{11}^j & B_{12}^j & B_{16}^j \\ & B_{22}^j & B_{26}^j \\ & & B_{66}^j \end{bmatrix} \begin{Bmatrix} \partial u/\partial x + 1/2\ (\partial w/\partial x)^2 \\ \partial y/\partial y + 1/2\ (\partial w/\partial y)^2 \\ \partial u/\partial y + \partial v/\partial x + \partial w/\partial x\ \partial w/\partial y \end{Bmatrix}$$

$$+ \sum_{i=1}^{N} \begin{bmatrix} D_{11}^{ij} & D_{12}^{ij} & D_{16}^{ij} \\ & D_{22}^{ij} & D_{26}^{ij} \\ & & D_{66}^{ij} \end{bmatrix} \begin{Bmatrix} \partial U^i/\partial x \\ \partial V^i/\partial y \\ \partial U^i/\partial y + \partial V^i/\partial x \end{Bmatrix}$$

$$+ \sum_{i}^{D} \begin{bmatrix} L_{11}^{ij} & L_{12}^{ij} & L_{16}^{ij} \\ & L_{22}^{ij} & L_{26}^{ij} \\ & & L_{66}^{ij} \end{bmatrix} \begin{Bmatrix} 2\partial w/\partial x\ \partial W^i/\partial x + \partial U^i/\partial x \\ 2\partial w/\partial y\ \partial W^i/\partial y + \partial V^i/\partial y \\ \partial w/\partial x\ \partial W^i/\partial y + \partial w/\partial y\ \partial W^i/\partial x + \partial U^i/\partial y + \partial V^i/\partial x \end{Bmatrix}$$

$$+ \sum_{r}^{D} \sum_{s}^{D} \begin{bmatrix} L_{11}^{rsj} & L_{12}^{rsj} & L_{16}^{rsj} \\ & L_{22}^{rsj} & L_{26}^{rsj} \\ & & L_{66}^{rsj} \end{bmatrix} \begin{Bmatrix} \partial W^r/\partial x\ \partial W^s/\partial x \\ \partial W^r/\partial Y\ \partial W^s/\partial y \\ \partial W^r/\partial y\ \partial W^s/\partial x \end{Bmatrix} \qquad (7.20)$$

where

$$L_{pq}^{ij} = \sum_{k=1}^{N} \int_{z_{k-1}}^{z_k} Q_{pq}^k H^i(z)\phi^j(z)dz;\ (p,q = 1,2,6)$$

$$L_{pq}^{rsj} = \sum_{k=1}^{N} \int_{z_{k-1}}^{z_k} Q_{pq}^k H^r(z)H^s(z)\phi^j(z)dz;\ (p,q = 1,2,6) \qquad (7.21)$$

and

$$\begin{Bmatrix} Q_x^j \\ Q_j^j \end{Bmatrix} = \begin{bmatrix} B_{55}^j & B_{45}^j \\ & B_{44}^j \end{bmatrix} \begin{Bmatrix} \partial w/\partial x \\ \partial w/\partial y \end{Bmatrix} + \sum_{i}^{N} \begin{bmatrix} D_{55}^{ji} & D_{45}^{ji} \\ & D_{44}^{ji} \end{bmatrix} \begin{Bmatrix} u^j \\ v^i \end{Bmatrix}$$

$$+ \sum_{i}^{D} \begin{bmatrix} L^{ij} & L_{45}^{ij} \\ & L_{44}^{ij} \end{bmatrix} \begin{Bmatrix} \partial W^i/\partial x \\ \partial W^i/\partial y \end{Bmatrix} \tag{7.22}$$

where

$$L_{pq}^{ij} = \sum_{k=1}^{N} \int_{z_{k-1}}^{z_k} Q_{pq}^{k} H^i(z) \frac{d\phi^j}{dz} dz; \quad (p,q = 4,5) \tag{7.23}$$

and

$$\begin{Bmatrix} \hat{Q}_{xz}^i \\ \hat{Q}_{yz}^i \end{Bmatrix} = \begin{bmatrix} E_{55}^i & E_{45}^i \\ & E_{44}^i \end{bmatrix} \begin{Bmatrix} \frac{\partial w}{\partial x} \\ \frac{\partial w}{\partial y} \end{Bmatrix} + \sum_{j}^{N} \begin{bmatrix} L_{55}^{ij} & L_{45}^{ij} \\ & L_{55}^{ij} \end{bmatrix} \begin{Bmatrix} u^j \\ v^j \end{Bmatrix}$$

$$+ \sum_{j=1}^{D} \begin{bmatrix} E_{55}^{ij} & E_{45}^{ij} \\ & E_{44}^{ij} \end{bmatrix} \begin{Bmatrix} \frac{\partial W^j}{\partial x} \\ \frac{\partial W^j}{\partial y} \end{Bmatrix}. \tag{7.24}$$

Once delaminations and nonlinear effects come into the picture, one new equation for each delamination is introduced. Along with the new equation, a new set of stress resultants is introduced [see Eqs. (7.11) and (7.13)]. These stress resultants lead to a new set of constitutive equations, as follows:

$$\begin{Bmatrix} M_x^i \\ M_y^i \\ M_{xy}^i \end{Bmatrix} = \begin{bmatrix} E_{11}^i & E_{12}^i & E_{16}^i \\ & E_{22}^i & E_{26}^i \\ & & E_{66}^i \end{bmatrix} \begin{Bmatrix} \partial u/\partial x + 1/2\ (\partial w/\partial x)^2 \\ \partial v/\partial y + 1/2\ (\partial w/\partial y)^2 \\ \partial u/\partial y + \partial v/\partial x + \partial w/\partial x\ \partial w/\partial y \end{Bmatrix}$$

$$+ \sum_{j=1}^{N} \begin{bmatrix} L_{11}^{ij} & L_{12}^{ij} & L_{16}^{ij} \\ & L_{22}^{ij} & L_{26}^{ij} \\ & & L_{66}^{ij} \end{bmatrix} \begin{Bmatrix} \partial u^j/\partial x \\ \partial v^j/\partial y \\ \partial u^j/\partial y + \partial v^j/\partial x \end{Bmatrix} \tag{7.25}$$

$$+\sum_{j=1}^{D}\begin{bmatrix} E_{11}^{ij} & E_{12}^{ij} & E_{16}^{ij} \\ & E_{22}^{ij} & E_{26}^{ij} \\ & & E_{66}^{ij} \end{bmatrix}\begin{Bmatrix} 2\partial w/\partial x\ \partial W^j/\partial x + \partial U^j/\partial x \\ 2\partial w/\partial y\ \partial W^j/\partial y + \partial V^j/\partial y \\ \partial w/\partial x\ \partial W^j/\partial y + \partial w/\partial y\ \partial W^j/\partial x + \partial U^j/\partial y + \partial V^j/\partial x \end{Bmatrix}$$

$$+\sum_{r}^{D}\sum_{s}^{D}\begin{bmatrix} E_{11}^{rsi} & E_{12}^{rsi} & E_{16}^{rsi} \\ & E_{22}^{rsi} & E_{26}^{rsi} \\ & & E_{66}^{rsi} \end{bmatrix}\begin{Bmatrix} \partial W^r/\partial x\ \partial W^s/\partial x \\ \partial W^r/\partial y\ \partial W^s/\partial y \\ \partial W^r/\partial x\ \partial W^s/\partial y \end{Bmatrix}$$

where

$$E_{pq}^{rsi} = \sum_{k=1}^{n}\int_{z_{k-1}}^{z_k} Q_{pq}^{k} H^r(z)H^s(z)H^i(z)dz;\ (p,q = 1,2,6) \qquad (7.26)$$

next,

$$\begin{Bmatrix} M_x^{ij} \\ M_y^{ij} \\ M_{xy}^{ij} \end{Bmatrix} = \begin{bmatrix} E_{11}^{ij} & E_{12}^{ij} & E_{16}^{ij} \\ & E_{22}^{ij} & E_{26}^{ij} \\ & & E_{66}^{ij} \end{bmatrix}\begin{Bmatrix} \partial u/\partial x + 1/2\ (\partial w/\partial x)^2 \\ \partial v/\partial y + 1/2\ (\partial w/\partial y)^2 \\ (\partial u/\partial y + \partial v/\partial x) + \partial w/\partial x\ \partial w/\partial y) \end{Bmatrix}$$

$$+\sum_{r=1}^{N}\begin{bmatrix} L_{11}^{ijr} & L_{12}^{ijr} & L_{16}^{ijr} \\ & L_{22}^{ijr} & L_{26}^{ijr} \\ & & L_{66}^{ijr} \end{bmatrix}\begin{Bmatrix} \partial u^r/\partial x \\ \partial v^r/\partial y \\ \partial u^r/\partial y + \partial v^r/\partial x \end{Bmatrix}$$

$$+\sum_{r}^{D}\begin{bmatrix} E_{11}^{ijr} & E_{12}^{ijr} & E_{16}^{ijr} \\ & E_{22}^{ijr} & E_{26}^{ijr} \\ & & E_{66}^{ijr} \end{bmatrix}\begin{Bmatrix} \partial w/\partial x\ \partial W^r/\partial x + \partial U^r/\partial x \\ \partial w/\partial y\ \partial W^r/\partial y + \partial V^r/\partial y \\ \partial w/\partial x\ \partial W^r/\partial y + \partial w/\partial y\ \partial W^r/\partial x + \partial U^j/j + \partial V^j/\partial x \end{Bmatrix}$$

$$+\sum_{r}^{D}\sum_{s}^{D}\begin{bmatrix} E_{11}^{ijrs} & E_{12}^{ijrs} & E_{16}^{ijrs} \\ & E_{22}^{ijrs} & E_{26}^{ijrs} \\ & & E_{66}^{ijrs} \end{bmatrix}\begin{Bmatrix} \partial W^r/\partial x\ \partial W^s/\partial s \\ \partial W^r/\partial y\ \partial W^s/\partial y \\ \partial W^r/\partial x\ \partial W^s/\partial y \end{Bmatrix} \qquad (7.27)$$

where,

$$E_{pq}^{ijrs} = \sum_{k=1}^{n} \int_{z_{k-1}}^{z_k} Q_{pq}^{k} H_j(Z) H^j(z) H^r(z) H^s(z) dz; \ (p,q = 1,2,6) \qquad (7.28)$$

When $\phi^j(z)$ are linear through each layer, the coefficients in the constitutive equations simplify to

$$E_{pg}^{i} = \sum_{k=i+1}^{N} Q_{pg}^{k} h^k$$

where i is the location of the delamination, i + 1 is the first layer above the delamination and N is the number of layers.

$$E_{pg}^{ij} = \sum_{k=j+1}^{N} Q_{pg}^{k} h^k \text{ for } j > i$$

$$E^{ijn} = \sum_{k=r+1}^{N} Q_{pg}^{k} h^k \text{ for } r > j \geq i$$

$$E^{yrs} = \sum_{k=s+1}^{N} Q_{pg}^{k} h^k \text{ for } s > r \geq j \geq i$$

If j indicates a layer number, we have

$$L_{pg}^{ij} \quad (p,1 = 1,2,6) = \begin{cases} Q^j \frac{h^j}{2} + Q^{j+1} \frac{h^{j+1}}{2} ; & j > i + 1 \\ Q^{j+1} \frac{h^{j+1}}{2} ; & j = i + 1 \\ 0 & \text{otherwise} \end{cases}$$

$$L_{pg}^{ij} \quad (p,g = 4,5) = \begin{cases} Q_{pg}^{j} h^j - Q_{pg}^{j+1} h^{j+1} ; & j > i + 1 \\ - Q_{pg}^{j+1} h^{j+1} ; & j = i + 1 \\ 0 & \text{otherwise} \end{cases}$$

and

$$L_{pg}^{rsj} = \begin{cases} Q^j \frac{h^j}{2} + Q^{j+1} \frac{h^{j+1}}{2} ; & j > r \geq s \\ Q^{j+1} \frac{h^{j+1}}{2} ; & j = r \geq s \\ 0 \qquad \text{otherwise} \end{cases}$$

This concludes the description of the laminate constitutive equations.

7.3 Fracture Mechanics Analysis

The deformation field obtained from GLPT is used to compute the strain energy release rate distribution along the boundary of the delamination. Delaminations usually exhibit planar growth, that is, the crack grows in its original plane. However, the shape of the crack may vary with time. For example, a crack shape initially elliptic usually grows with variable aspect ratio. Therefore, the crack growth is not self similar. However, a self similar virtual crack extension will be assumed in order to compute the distribution of the strain energy release rate G(s) along the boundary of the delamination.

The virtual crack extension method (Chapter 6) postulates that the strain energy release rate can be computed from the strain energy U and the representative crack length "a" as:

$$G(s) = dU/da \tag{7.29}$$

Actual implementations of the virtual crack extension method, however, approximate Equation (7.29) by a quotient DU/Da that in the limit as $D_a \to 0$, approximates the value of the strain energy release rate G. The Jacobian Derivative Method (JDM) (Chapter 6) computes Equation (7.29) exactly. The JDM does not involve an approximate derivative, so it does

not require that we choose the magnitude of the "virtual" crack extension Da.

The boundary of a delamination is specified as boundary conditions on the delamination variables U^j, V^j, and W^j, usually setting $V^j = V^j = W^j = 0$. A self similar virtual crack extension of the crack (delamination) is specified for the nodes on the boundary of the delamination, that is, the two components of the normal to the delamination boundary are given for each mode on the boundary. The JDM is then used at each configuration (or load step) to compute G(s) from the displacement field.

7.4 Finite-Element Formulation

The generalized displacements $(u,v,w,u^j,v^j, U^j, V^j, W^j)$ are expressed over each element as a linear combination of the two-dimensional interpolation functions ψ_i and the nodal values $(u_i,v_i,w_i, u_i^j,v_i^j, U^j, V^j, W^j)$ as follows:

$$(u,v,w,u^j,v^j, U^j,V^j,W^j) = \sum_{i=1}^{m} (u_i,v_i,w_i,u_i^j,v_i^j,U_i^j,V_i^j,W_i^j)\psi_i \qquad (7.30)$$

where m is the number of nodes per element. Using Equation (15), the linear components of the strains can be expressed in the form

$$\{e\} = [B]\{\Delta\}; \ \{e^j\} = [\overline{B}]\{\Delta^j\}; \ \{\overline{e}^j\} = [B]\{\overline{\Delta}^j\} \qquad (7.31a)$$

where

$$\{\Delta\}^T = \{u_1,v_1,w_1,\ldots,u_m,v_m,w_m\}$$

$$\{\Delta^j\}^T = \{u_1^j, v_1^j, \ldots, u_m^j, v_m^j\} \tag{7.31b}$$

$$\{\bar{\Delta}^j\}^T = \{U_1^j, V_1^j, W_1^j, \ldots, U_m^j, V_m^j, W_m^j\}$$

Similarly, the nonlinear component of the strains can be written in the form

$$\{\eta\} = [B_{NL}]\{\Delta\}; \quad \{\bar{\eta}^j\} = [B_{NL}]\{\bar{\Delta}^j\} + [\bar{B}_{NL}^j]\{\Delta\};$$

$$\{\bar{\eta}^{ij}\} = \frac{1}{2}[\bar{B}_{NL}^i]\{\bar{\Delta}^j\} + [\bar{B}_{NL}^j]\{\bar{\Delta}^i\} \tag{7.31c}$$

The matrices $[B]$, $[\bar{B}]$, $[B_{NL}]$ and $[\bar{B}_{NL}^j]$ are given in Appendix 7. Using Equation (7.31) in the virtual work statement (7.6a) we obtain the finite element model,

$$\begin{bmatrix} k^{11} & k_1^{12} & \ldots & k_N^{12} & k_1^{13} & \ldots & k_D^{13} \\ k_1^{21} & k_{11}^{22} & \ldots & k_{1N}^{22} & k_{11}^{23} & \ldots & k_{1D}^{23} \\ \vdots & \vdots & & \vdots & \vdots & & \vdots \\ k_N^{21} & k_{N1}^{22} & \ldots & k_{NN}^{22} & k_{N1}^{23} & \ldots & k_{ND}^{23} \\ k_1^{31} & k_{11}^{32} & \ldots & k_{1N}^{32} & k_{11}^{33} & \ldots & k_{1D}^{33} \\ \vdots & \vdots & & \vdots & \vdots & & \vdots \\ k_D^{31} & k_{D1}^{32} & \ldots & k_{DN}^{32} & k_{D1}^{33} & \ldots & k_{DD}^{33} \end{bmatrix} \begin{Bmatrix} \{\Delta\} \\ \{\Delta^1\} \\ \vdots \\ \{\Delta^N\} \\ \{\bar{\Delta}^1\} \\ \vdots \\ \{\bar{\Delta}^D\} \end{Bmatrix} = \begin{Bmatrix} \{q\} \\ \{q^1\} \\ \vdots \\ \{q^N\} \\ \{q^1\} \\ \vdots \\ \{q\} \end{Bmatrix} \tag{7.32}$$

where the submatrices $[k^{11}]$, $k_j^{12}]$, $[k_j^{21}]$, $[k_{ji}^{22}]$, $[k_{jr}^{23}]$, $[k_{rj}^{32}]$, $[k_{rs}^{33}]$ with $i,j = 1,\ldots,N$ and $r, s = 1, \ldots, D$ are given in Appendix 7.2. The load vectors $\{q\}$, $\{q^1\}\ldots\{q^1\}$ ... $\{q^N\}$, and $\{\bar{q}^1\},\ldots, \{\bar{q}^D\}$ are analogous to $\{\Delta\}$, $\{\Delta^1\}$, ... $\{\Delta^N\}$ and $\{\bar{\Delta}^1\}$, ... $\{\bar{\Delta}^D\}$ in Equation (7.31b). The

nonlinear algebraic system is solved by the Newton-Raphson algorithm. The components of the Jacobian matrix are given in Appendix 8.

The nonlinear equations are also linearized to formulate the eigenvalue problem associated with bifurcation (buckling) analysis,

$$([K_D] - \lambda[K_G])\cdot\underset{\sim}{\Phi} = \underset{\sim}{0} \tag{7.33}$$

where $[K_D]$ is the linear part of the direct stiffness matrix (7.32) and $[K_G]$ is the geometric stiffness matrix, obtained from the nonlinear part of Equation (7.32) by perturbation of the nonlinear equations around the equilibrium position.

7.5 Numerical Examples

First, two exmaples are presented in order to validate the proposed analysis. Closed form solutions can be developed for simple cases and they are used for comparison with the more general approach presented here.

7.5.1 Square Thin-Film Delamination

A square thin layer delaminated from an isotropic plate is peeled off by a concentrated load at its center. The base laminate is considered rigid with respect to the thin delaminated layer. An analytical solution for the linear deflection and strain energy release rate can be derived assuming the delaminated layer is clamped to the rigid base laminate [58]. Due to symmetry, one fourth of the square delamination is analyzed using a 2 x 2 and 5 x 5 mesh of 9-node delaminated elements. Either the clamped boundary condition is imposed on the boundary of the delamination or an additional band of elements with a closed delamination is placed around the delaminated area to

simulate the intact region. All different models produce consistent results for transverse deflections and average strain energy release rate. The finer mesh is necessary to obtain a smooth distribution of the strain energy release rate G along the boundary of a square delamination with side 2a, bending rigidity D under a concentrated load P, as shown in Figure 7.2. The linear solution for P = 10 compares well with the analytical solution. In Figure 7.3 we show the linear and nonlinear maximum delamination opening W and average strain energy release rate G_{av} as a function of the applied load P. It is evident that the membrane stresses that develop as a consequence of the geometric nonlinearity reduce considerably the magnitude of the average strain energy release rate. The Newton-Raphson method is used to compute the nonlinear solution.

7.5.2 Thin-Film Cylindrical Buckling

Using the cylindrical bending assumptions and classical plate theory, a closed form solution can be developed for the postbuckling of a through-the-width thin delamination [113]. In this example we consider an isotropic thin layer delaminated from a thick plate in its entire width. Due to symmetry, only one half of the length of the plate strip is modelled with a nonuniform mesh of 7 plate elements. The cylindrical bending assumption is satisfied by restraining all degrees of freedom in the y-direction. The base laminate is considered much more rigid than the thin delaminated layer so that it will not buckle nor deflect during the postbuckling of the delaminated layer. First, an eigenvalue (buckling) analysis is performed to obtain the buckling load

and corresponding mode shape. Then a Newton-Raphson solution for the postbuckling configuration is sought. Excellent agreement is found in the jump discontinuity displacements U and W across the delamination. The values of delamination opening W and strain energy release rate G are shown in Figures 7.4 and 7.5 as a function of the applied load, where ε_{cr} is the critical strain at which buckling occurs for a delamination length 2a. The comparisons with analytical solutions presented in this section demonstrate the capabilities for modelling delaminated composite plates and buckling with the proposed theory. An efficient plate bending element has been developed and validated by comparison to existing solutions for delaminated plates. The present approach has computational advantages over full 3-D elasticity analysis. Its generality can be exploited in the analysis of real composite structures, with complexities that exceed the capabilities of 2-D analysis or approximate analytical solutions. The present approach can be used either to assess the structural consequences of existing damage or to perform parametric studies to optimize the damage tolerance of composite structures. Application to more complex situations is presented in the following sections.

7.5.3 Axisymmetric Circular Delamination

The axisymmetric buckling of a circular, isotropic, thin-film delamination can be reduced to a one-dimensional nonlinear ordinary differential equation problem [49] by using the Classical Plate Theory (CPT). One quarter of a square plate of total width 2b with a circular delamination of radius a is modelled in this work using GLPT elements

capable of representing discontinuities of the displacements at the interfaces between layers. The symmetry boundary conditions used are:

$$u(0,y) = u^i(0,y) = U^j(0,y) = 0$$

$$v(x,0) = v^i(x,0) = V^j(x,0) = 0$$

with i = 1,...,N and j = 1,...,D; where N is the number of layers and D is the number of delaminations through the thickness; in this example D = 1. The boundary of the delamination is specified by setting to zero the jump discontinuity conditions V^j, V^j and W^j on the boundary of the delamination and wherever the plate is not delaminated. The boundary of the plate is subjected to the following clamped boundary conditions, that produce a state of axisymmetric stress on the circular delamination:

$$u^i(b,y) = U^j(b,y) = 0 \; ; \; N_x(b,y) = -\hat{N}$$

$$v^i(x,b) = V^j(x,b) = 0 \; ; \; N_y(x,b) = -\hat{N}$$

where $\hat{N}$ is a uniformly distributed compressive force per unit length. The same material properties are used for the delaminated layer of thickness t and for the substrate of thickness (h - t). To simulate the thin-film assumptions, a ratio h/t = 100 is used. First an eigenvalue (buckling) analysis is performed to obtain the buckling load and corresponding mode shape. Then a Newton-Raphson solution for the postbuckling is sought. The Jacobian Derivative Method, Chapter 6, is used at each converged equlibrium solution to compute the distribution of the strain energy release rate G(s) along the boundary of the

delamination. For this example, G(s) is a constant. Its value, depicted in Figure 7.6 as a function of the applied load, is in excellent agreement with the approximate, analytical solution [49].

7.5.4 Circular Delamination Under Undirectional Load

In this example we analyze a circular delamination, centrally located in a square plate of total width 2c and subjected to a uniformly distributed inplane load N_x. The example is set up to allow comparisons to be made with numerical results obtained by using a full three-dimensional finite element program [57]. Contrary to the last example, this problem does not admit an axisymmetric solution. Therefore, the distribution G(s) is variable along the boundary of the delamination, as shown in Figures 7.9 and 7.10. A quasi-isotropic laminate [±45/0/90] of total thickness h = 4 mm with a circular delamination of diameter 2a located at 0.4 mm deep is considered. The material properties are those of AS4/PEEK: $E_1 = 13.4 \times 10^{10}$ Pa, $E_2 = 1.02 \times 10^{10}$ Pa, $G_{12} = 0.552 \times 10^{10}$ Pa, $G_{23} = 0.343 \times 10^{10}$ Pa, $\nu_{12} = 0.3$. As is well known, the quasi-isotropic laminate exhibits equivalent isotropic behavior when loaded in its plane. The bending behavior, however, depends on the orientation. To avoid complications in the interpretation of the results introduced by the non-isotropic bending behavior, an equivalent isotropic material is used in Reference [57], where the equivalent stiffness components of the 3-D elasticity matrix are found from:

$$\bar{C}_{ij} = \frac{1}{8} \sum_{k=1}^{N} (C_{ij})^k$$

Due to the transverse incompressibility used in this work, it is more

convenient and customary to work with the reduced stiffness. Equivalent material properties can be found directly from the A-matrix of the quasi-isotropic laminate as follows: first, compute the equivalent reduced stiffness coefficients

$$Q_{ij} = A_{ij}/h$$

where h is the total thickness of the plate and A_{ij} are the components of the A-matrix obtained according to the Equation 2.11b. Next, the equivalent material properties can be found as:

$$E_{11} = Q_{11} - Q_{22}$$

$$E_{22} = Q_{22}(1 - \frac{Q_{22}}{Q_{11}})$$

$$G_{12} = Q_{33}$$

$$G_{23} = Q_{55}$$

$$\nu_{12} = \frac{Q_{11}E_{11} - E_{11}^2}{Q_{11}E_{22}}$$

An eigenvalue analysis reveals that the delaminated portion of the plate buckles at N_x = 286,816 N/m for a = 15 mm and at N_x = 73,666 N/m for a = 30 mm. In Figure 7.7 we plot the maximum transverse opening of the delamination as a function of the applied inplane strain ε_x. The differences observed with the results of Reference [57] are due to the fact that in the latter an artificially zero transverse deflection is imposed on the base laminate to reduce the computational cost of the three-dimensional finite element solution. The differences are more important for a = 30 mm, as indicated by the dashed line in Figure 7.7 that represents the transverse deflection w of the midplane of the

plate. The square symbols indicate the total opening (or gap) of the delamination, while the solid line is the opening reported in Reference [57] with w = 0. The differences on total opening W and transverse deflection w have an impact on the distribution of the strain energy release rate, as can be appreciated in Figure 7.9. Both solutions (3-D elements [57] and the present 2-D elements) coincide for the small delamination of radius a = 15 mm in Figure 7.8. For the larger radius a = 30 mm, the assumption w = 0 is no longer valid and discrepancies can be observed in Figure 7.9, although the maximum values of G coincide and the shapes of the distributions of G are quite similar. Mesh refinement, with at least two elements close to the delamination boundary, has to be used. This is not because of the computation of the strain energy release rate G(s), but due to the fact that deflections and slope change abruptly in a narrow region close to the delamination boundary, similarly to the phenomena described in Reference [114]. In Figure 7.8 and 7.9 we plot the distribution of the strain energy release rate G(s) along one-quarter of the boundary of the delamination denoted by s, where s = 0 corresponds to (x = a, y = 0) and s = $a\pi/2$ to (x = 0, y = a), for two different delamination radii a = 15 mm and a = 30 mm, respectively. Negative values of G(s) indicate that energy should be provided to advance the delamination in that direction. Obviously the delamination will not spontaneously grow in that direction. Negative values are usually obtained as a result of delaminated surfaces that come in contact, thus eliminating the contribution of Mode I of fracture although not of Modes II and III. The present analysis does not include contact constraints and therefore layers may overlap. As noted in

Reference [57] G(s) in the region without overlap is not significantly affected by imposing contact constraints on the small overlap area.

7.5.5 Unidirectional Delaminated Graphite-Epoxy Plate

A circular delamination of radius a = 5 in in a square plate of side 2c = 12 in made of unidirectional Graphite-Epoxy is considered next. The thickness of the plate is h = 0.5 in and the delamination is located at a distance t = 0.005 in from the surface. An eigenvalue (buckling) analysis is used to obtain the magnitude of the inplane load under which the thin delaminated layer buckles. Due to the anisotropy of the material used in this example, it is interesting to study the effect of different combinations of loads N_x and N_y, characterized by the load ratio

$$r = \frac{N_x - N_y}{N_x + N_y}$$

In Figure 7.10 we plot the magnitude of the buckling load as a function of the load ratio r, with $-1 < r < 1$. The distribution of the strain energy release rate G(s) along the boundary $s = a\phi$ with $0 < \phi < \pi/2$ is plotted in Figures 7.11 to 7.15 for different values of the load ratio r with $-1 < r < 1$, and several values of the applied inplane load, in multiples λ of the buckling load N_{cr}. Figure 7.11 for r = 1, (i.e., $N_x = N$ and $N_y = 0$) clearly indicates that the delamination is likely to propagate in a the direction approximately perpendicular to the load direction. In Figure 7.12, r = 0.5 indicates that $N_y = 1/2\ N_x$. The introduction of some load in the direction perpendicular to the fibers causes the maximum value of G to align closer to the x-axis. That

effect remains for all the other load ratios considered in Figures 7.13 to 7.15. The fact that both the magnitude and the shape of the distribution G(s) changes as the load ratio changes motivates Figure 7.16. It can be seen that of all the combinations of loads, all being five times the corresponding critical load, r = 0.5 produces a quite small amplitude of G(s) along the entire boundary of the delamination. This fact suggests that the propagation (or arrest) of delaminations is greatly influenced by the anitostropy of the material and the predominant loads.

Appendix 7

Strain-Displacement Matrices in the Finite Element Formulation

The strains appearing in Equation (7.3) are

$$\{e\} = \begin{Bmatrix} \frac{\partial u}{\partial x} \\ \frac{\partial v}{\partial y} \\ \frac{\partial u}{\partial y} + \frac{\partial v}{\partial x} \\ \frac{\partial w}{\partial x} \\ \frac{\partial w}{\partial y} \end{Bmatrix}, \quad \{e^j\} = \begin{Bmatrix} \frac{\partial u^j}{\partial x} \\ \frac{\partial v^j}{\partial y} \\ \frac{\partial u^j}{\partial y} + \frac{\partial v^j}{\partial x} \\ u^j \\ v^j \end{Bmatrix}; \quad \{\eta\} = \begin{Bmatrix} \frac{1}{2}\left(\frac{\partial w}{\partial x}\right)^2 \\ \frac{1}{2}\left(\frac{\partial w}{\partial y}\right)^2 \\ \frac{\partial w}{\partial x}\frac{\partial w}{\partial y} \\ 0 \\ 0 \end{Bmatrix}$$

$$\{\bar{e}^i\} = \begin{Bmatrix} \frac{\partial U^i}{\partial x} \\ \frac{\partial V^i}{\partial x} \\ \frac{\partial U^i}{\partial y} + \frac{\partial V^i}{\partial x} \\ \frac{\partial W^i}{\partial x} \\ \frac{\partial W^i}{\partial y} \end{Bmatrix}; \quad \{\bar{\eta}^i\} = \begin{Bmatrix} \frac{\partial w}{\partial x}\frac{\partial W^i}{\partial x} \\ \frac{\partial w}{\partial y}\frac{\partial W^i}{\partial y} \\ \frac{\partial w}{\partial x}\frac{\partial W^i}{\partial y} + \frac{\partial w}{\partial y}\frac{\partial W^i}{\partial x} \\ 0 \\ 0 \end{Bmatrix}$$

$$\{\bar{\eta}^{ij}\} = \frac{1}{2}\begin{Bmatrix} \dfrac{\partial W^i}{\partial x}\dfrac{\partial W^j}{\partial x} \\ \dfrac{\partial W^i}{\partial y}\dfrac{\partial W^j}{\partial y} \\ \dfrac{\partial W^i}{\partial x}\dfrac{\partial W^j}{\partial y} + \dfrac{\partial W^i}{\partial y}\dfrac{\partial W^j}{\partial x} \\ 0 \\ 0 \end{Bmatrix}$$

The matrices $[B]$, $[\bar{B}]$ and $[B_{NL}]$ appearing in the strain-displacement relations (7.31) are

$$[B]_{(5x3m)} = \begin{bmatrix} \dfrac{\partial \psi_i}{\partial x} & 0 & 0 \\ 0 & \dfrac{\partial \psi_i}{\partial y} & 0 \\ \dfrac{\partial \psi_i}{\partial y} & \dfrac{\partial \psi_i}{\partial x} & 0 \\ 0 & 0 & \dfrac{\partial \psi_i}{\partial x} \\ 0 & 0 & \dfrac{\partial \psi_i}{\partial y} \end{bmatrix} \qquad [\bar{B}]_{(5x2m)} = \begin{bmatrix} \dfrac{\partial \psi_i}{\partial x} & 0 \\ 0 & \dfrac{\partial \psi_i}{\partial y} \\ \dfrac{\partial \psi_i}{\partial y} & \dfrac{\partial \psi_i}{\partial x} \\ \psi_i & 0 \\ 0 & \psi_i \end{bmatrix}$$

$$[B_{NL}]_{(5x3m)} = \frac{1}{2}\begin{bmatrix} 0 & 0 & \frac{\partial w}{\partial x}\frac{\partial \psi_i}{\partial x} \\ 0 & 0 & \frac{\partial w}{\partial y}\frac{\partial \psi_i}{\partial y} \\ 0 & 0 & \frac{\partial w}{\partial x}\frac{\partial \psi_i}{\partial y} + \frac{\partial w}{\partial y}\frac{\partial \psi_i}{\partial x} \\ 0 & 0 & 0 \\ 0 & 0 & 0 \end{bmatrix}$$

$$[\bar{B}^j_{NL}] = \begin{bmatrix} 0 & 0 & \frac{1}{2}\frac{\partial W^j}{\partial x}\frac{\partial \psi_i}{\partial x} \\ 0 & 0 & \frac{1}{2}\frac{\partial W^j}{\partial y}\frac{\partial \psi_i}{\partial y} \\ 0 & 0 & \frac{1}{2}\left(\frac{\partial W^j}{\partial x}\frac{\partial \psi_i}{\partial y} + \frac{\partial W^j}{\partial y}\frac{\partial \psi_i}{\partial x}\right) \\ 0 & 0 & 0 \\ 0 & 0 & 0 \end{bmatrix}$$

with (i = 1,...,m).

Appendix 8

Stiffness Matrices in the Finite Element Formulation

$$[k^{11}] = [B]^T[A][B] + [B]^T[A][B_{NL}] + 2[B_{NL}]^T[A][B] + 2[B_{NL}]^T[A][B_{NL}]$$

$$+ \sum_j^D ([B]^T[E^j][\bar{B}^j_{NL}] + 2[B_{NL}]^T[E^j][\bar{B}^j_{NL}] + 2[\bar{B}^j_{NL}][E^j][B]$$

$$+ 2[\bar{B}^j_{NL}][E^j][B_{NL}]) + 2\sum_j^D \sum_r^D [\bar{B}^j_{NL}]^T[E^{jr}][\bar{B}^r_{NL}].$$

$$[k^{12}_j] = [B]^T[B^j][\bar{B}] + 2[B_{NL}]^T[B^j][\bar{B}] + 2\sum_r^D [\bar{B}^r_{NL}]^T[L^{rj}][\bar{B}]$$

$$[k^{21}_j] = [\bar{B}]^T[B^j][B] + [\bar{B}]^T[B^j][B_{NL}] + \sum_r^D [\bar{B}^T[L^{rj}][\bar{B}^r_{NL}]$$

$$[k^{22}_{jr}] = [\bar{B}]^T[D^{jr}][\bar{B}].$$

$$[K^3_j] = [B]^T[E^j][B] + [B]^T[E^j][B_{NL}] + \sum_r^D ([B]^T[E^{rj}][\bar{B}^r_{NL}])$$

$$+ 2[B_{NL}]^T[E^j][B] + 2[B_{NL}]^T[E^j][B_{NL}] + \sum_i^D (2[B_{NL}]^T[E^{ij}][\bar{B}^i_{NL}])$$

$$+ 2\sum_r^D ([\bar{B}^r_{NL}]^T[E^{jr}][B] + [\bar{B}^r_{NL}]^T[E^{jr}][B_{NL}]) + 2\sum_r^D \sum_s^D ([\bar{B}^r]^T[E^{jrs}][\bar{B}^S_{NL}])$$

$$[k^{23}_{ji}] = [\bar{B}]^T[L^{ij}][B] + [\bar{B}]^T[L^{ij}][B_{NL}] + \sum_r^D [\bar{B}]^T[L^{rij}][\bar{B}^r].$$

$$[k^{32}_{ij}] = [B]^T[L^{ij}][\bar{B}] + 2[B_{NL}]^T[L^{ij}][\bar{B}] + 2\sum_r^D [\bar{B}^r]^T[L^{irj}][\bar{B}].$$

$$[k^{31}_j] = [B]^T[E^j][B] + [B]^T[E^j][B_{NL}] + \sum_r^D ([B]^T[E^{jr}][\bar{B}^r_{NL}])$$

$$+ 2[B_{NL}]^T[E^j][B] + 2[B_{NL}]^T[E^j][B_{NL}] + 2\sum_r^D ([B_{NL}]^T[E^{jr}][\bar{B}^r_{NL}])$$

$$+ 2\sum_r^D [\bar{B}^r_{NL}]^T[E^{rj}][B] + [\bar{B}^r_{NL}]^T[E^{rj}][B_{NL}]) + 2\sum_r^D\sum_s^D ([\bar{B}^r_{NL}]^T[E^{rjs}][\bar{B}^s_{NL}])$$

Jacobian Matrix:

$$[J] = \begin{bmatrix} \frac{\partial\{R^o\}}{\partial\{\Delta\}} & \frac{\partial\{R^o\}}{\partial\{\Delta'\}} & \cdots & \frac{\partial\{R^o\}}{\partial\{\Delta^N\}} & \frac{\partial\{R^o\}}{\partial\{\bar{\Delta}^1\}} & \cdots & \frac{\partial\{R^o\}}{\partial\{\bar{\Delta}^D\}} \\ \frac{\partial\{R^1\}}{\partial\{\Delta\}} & \frac{\partial\{R^1\}}{\partial\{\Delta^1\}} & \cdots & \frac{\partial\{R^1\}}{\partial\{\Delta^N\}} & \frac{\partial\{R^1\}}{\partial\{\bar{\Delta}^1\}} & \cdots & \frac{\partial\{R^1\}}{\partial\{\bar{\Delta}^D\}} \\ \vdots & \vdots & & \vdots & \vdots & & \\ \frac{\partial\{R^N\}}{\partial\{\Delta\}} & \frac{\partial\{R^N\}}{\partial\{\Delta^1\}} & \cdots & \frac{\partial\{R^N\}}{\partial\{\Delta^N\}} & \frac{\partial\{R^N\}}{\partial\{\bar{\Delta}^1\}} & \cdots & \frac{\partial\{R^N\}}{\partial\{\bar{\Delta}^D\}} \\ \frac{\partial\{\bar{R}^1\}}{\partial\{\Delta\}} & \frac{\partial\{\bar{R}^1\}}{\partial\{\Delta^1\}} & \cdots & \frac{\partial\{R\ \}}{\partial\{\Delta^N\}} & \frac{\partial\{\bar{R}^1\}}{\partial\{\bar{\Delta}^1\}} & \cdots & \frac{\partial\{\bar{R}^1\}}{\partial\{\bar{\Delta}^D\}} \\ \vdots & \vdots & & \vdots & \vdots & & \vdots \\ \frac{\partial\{\bar{R}^D\}}{\partial\{\Delta\}} & \frac{\partial\{\bar{R}^D\}}{\partial\{\Delta^1\}} & \cdots & \frac{\partial\{R\ \}}{\partial\{\Delta^N\}} & \frac{\partial\{\bar{R}^D\}}{\partial\{\bar{\Delta}^1\}} & \cdots & \frac{\partial\{\bar{R}^D\}}{\partial\{\bar{\Delta}^D\}} \end{bmatrix}$$

where

$$\{R^o\} = [k^{11}]\{\Delta\} + \sum_j^N [k^{12}_j]\{\Delta^j\} + \sum_j^D [k^{13}_j]\{\bar{\Delta}^j\}$$

$$\{R^j\} = [k^{21}_j]\{\Delta\} + \sum_r^N [k^{22}_{jr}]\{\Delta^r\} + \sum_r^D [k^{23}_{jr}]\{\bar{\Delta}^r\}$$

$$\{\bar{R}^j\} = [k^{31}_j]\{\Delta\} + \sum_r^N [k^{32}_{jr}]\{\Delta^r\} + \sum_r^D [k^{33}_{jr}]\{\bar{\Delta}^r\}$$

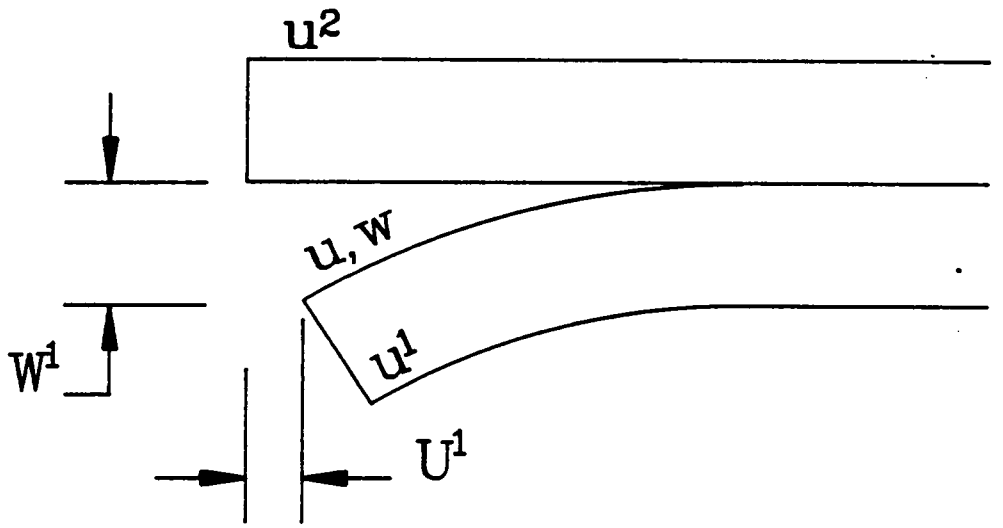

7.1 Kinematical description for delaminated plates.

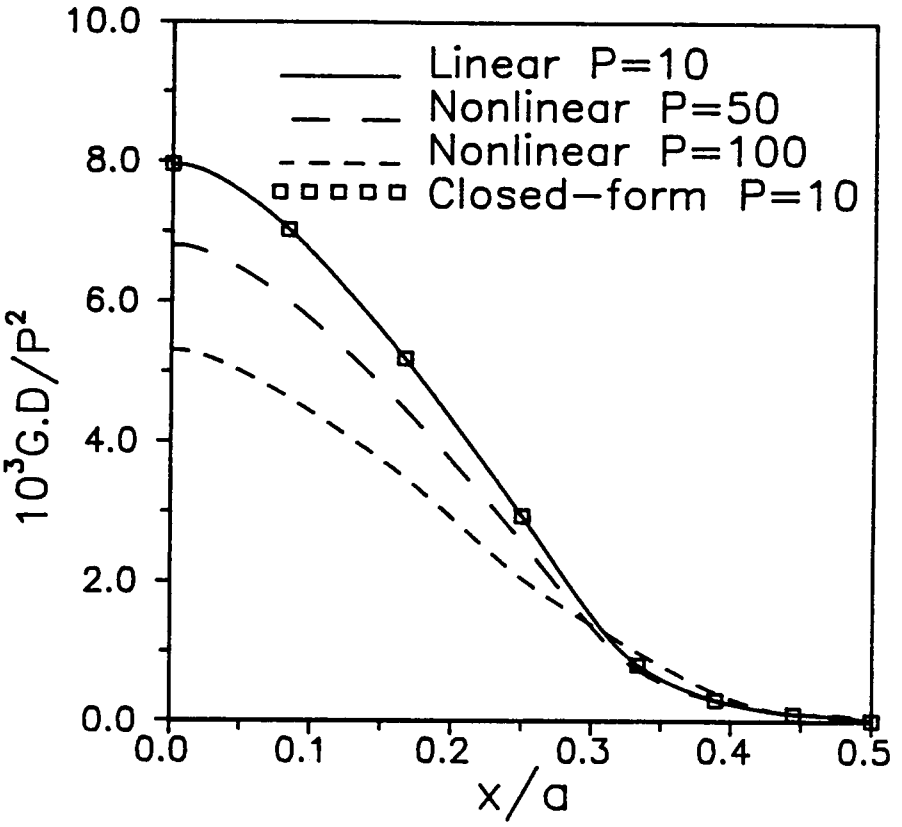

7.2 Distribution of the strain energy release rate G along the boundary of a square delamination of side 2a peeled off by a aconcentrated load P.

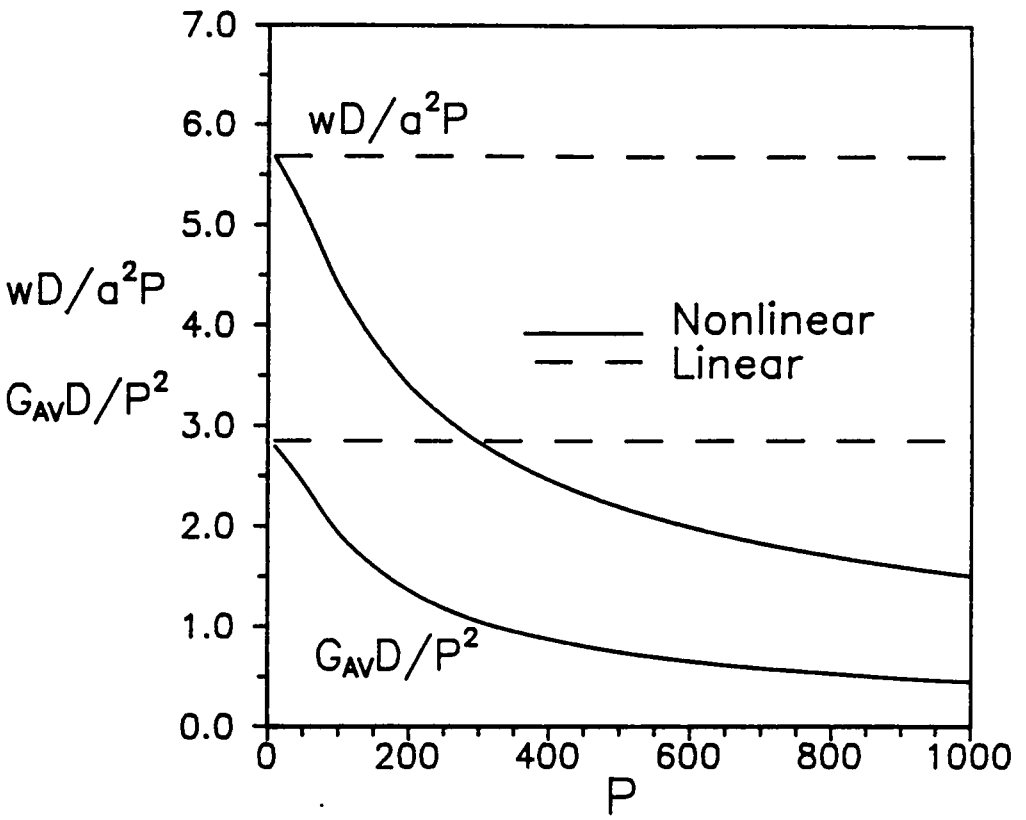

7.3 Maximum delamination opening W and average strain energy release rate G_{AV} from the nonlinear analysis of a square delamination.

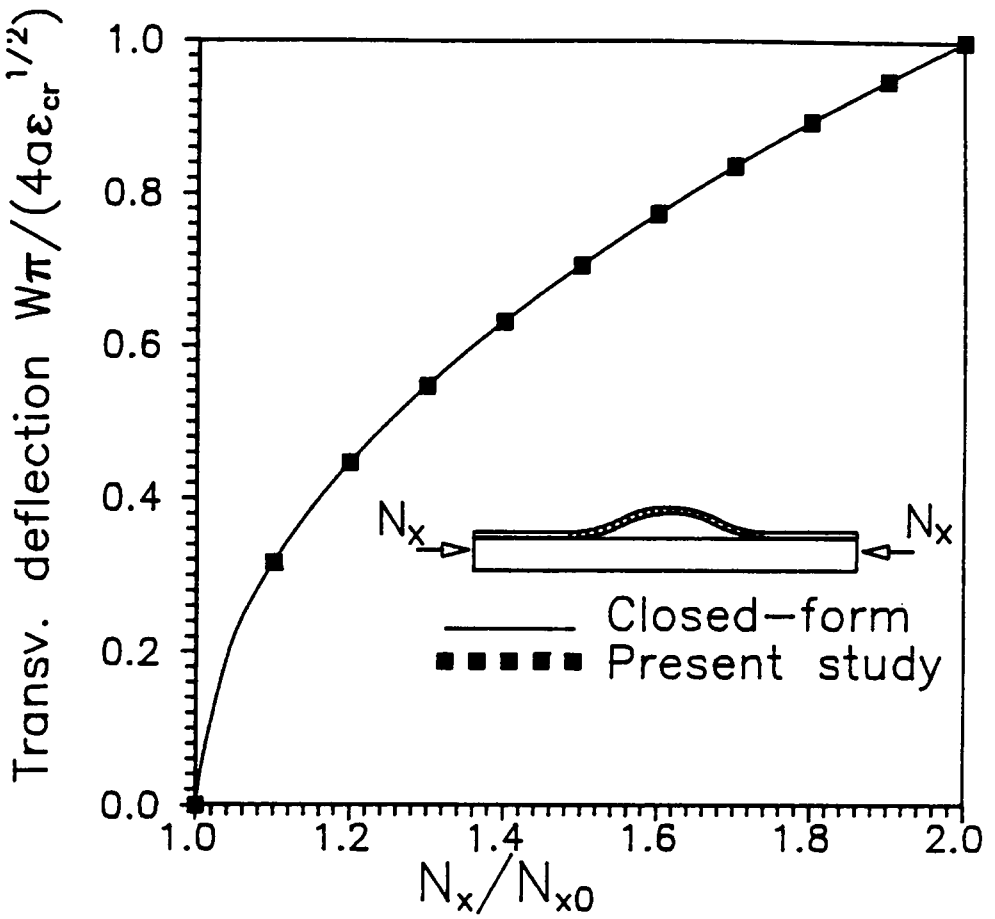

7.4 Maximum delamination opening W for a thin film buckled delamination.

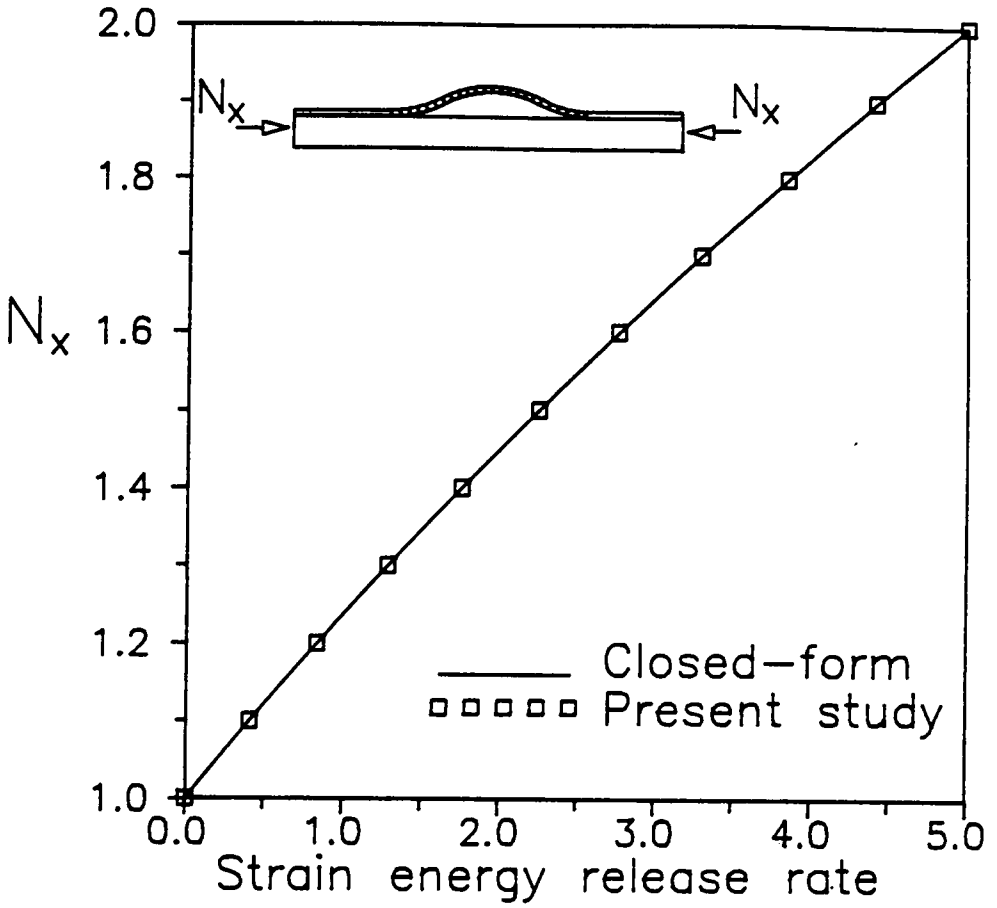

7.5 Strain energy release rate G for a thin film buckled delamination.

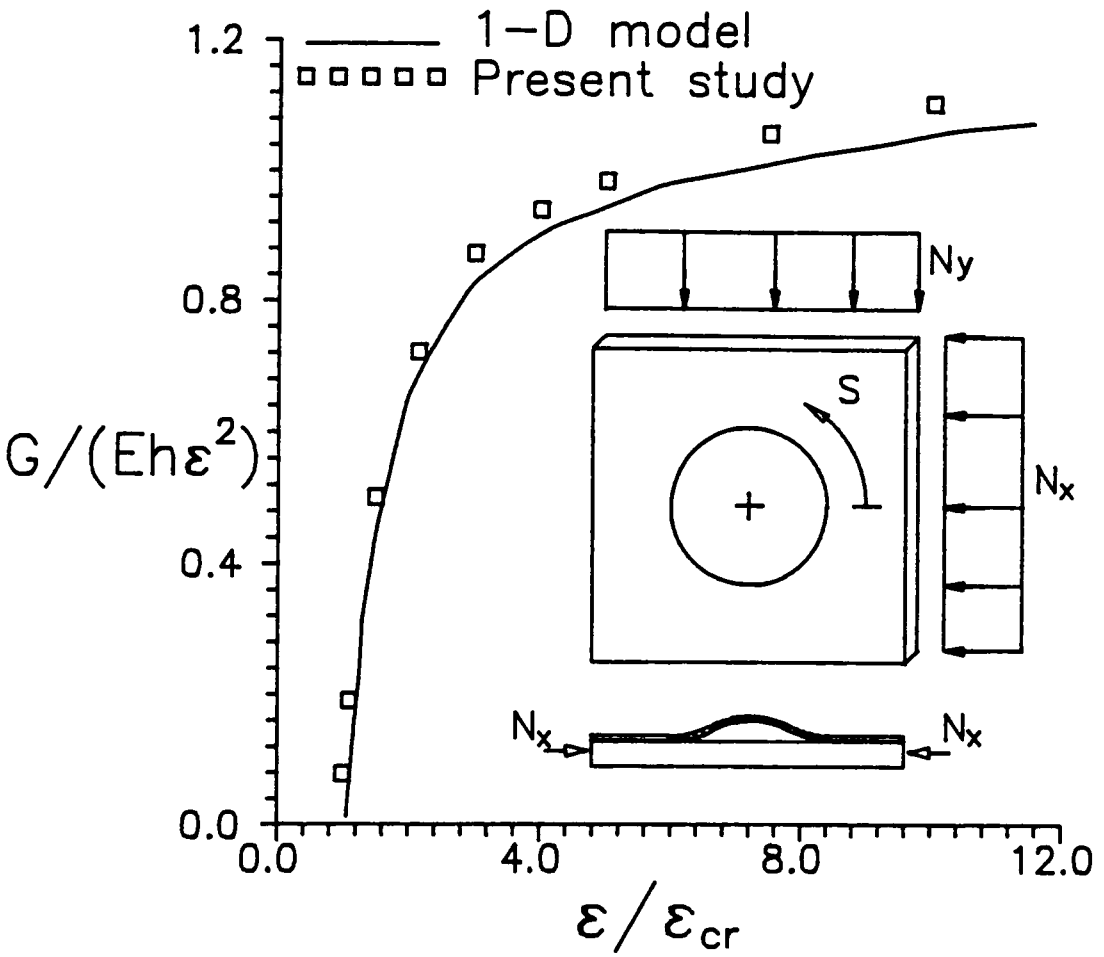

7.6 Strain energy release rate for a buckled thin-film axisymmetric delamination as a function of the inplane load.

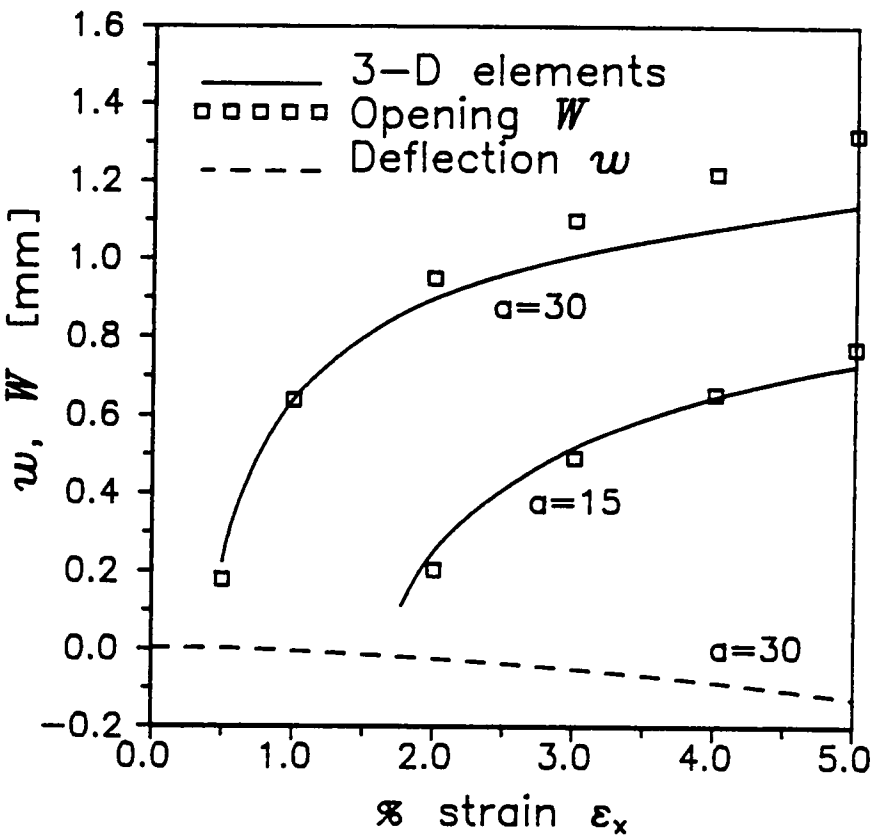

7.7 Maximum transverse opening W of a circular delamination of diameter 2a in a square plate subjected to inplane load N_x as a function of the inplane uniform strain ε_x.

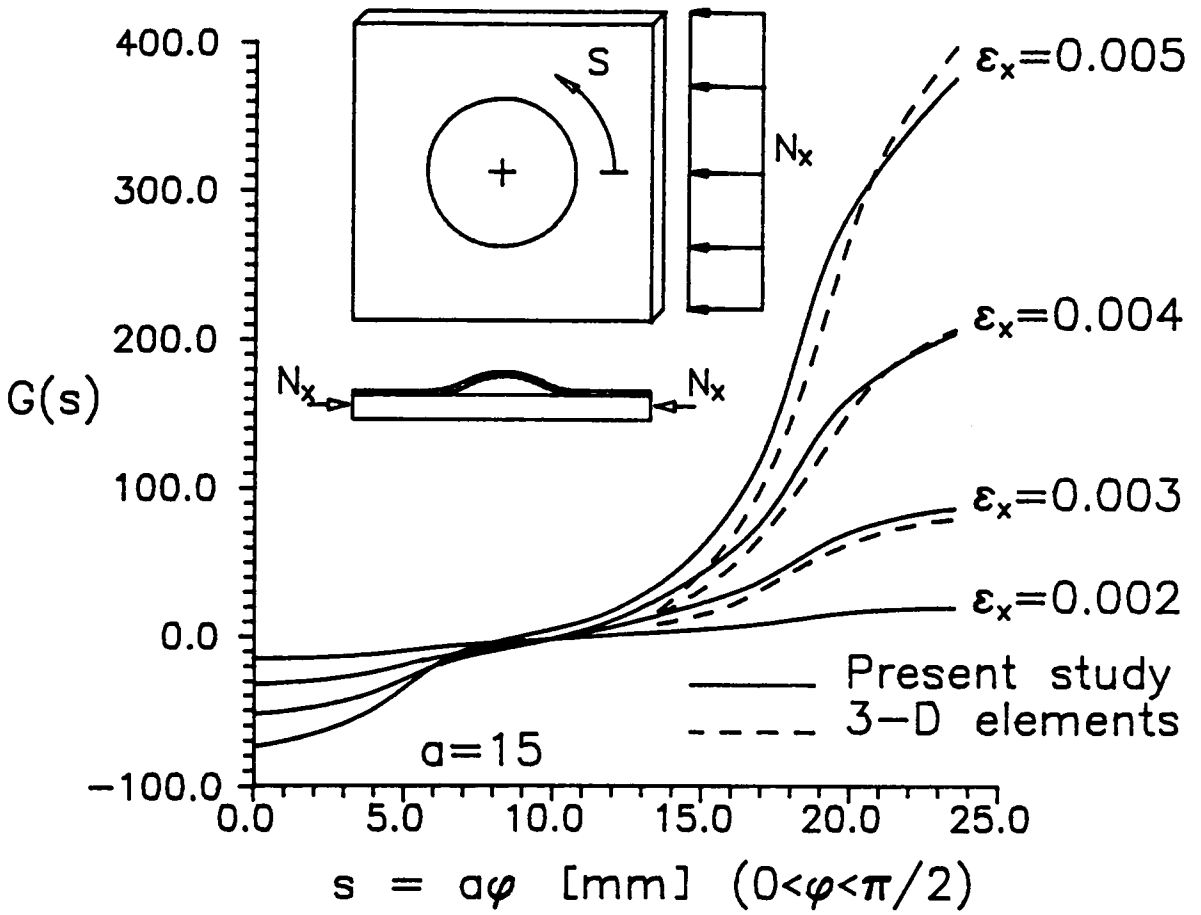

7.8 Distribution of the strain energy release rate G(s) along the boundary of a circular delamination of diameter for several values of the applied inplane uniform strain ε_x.

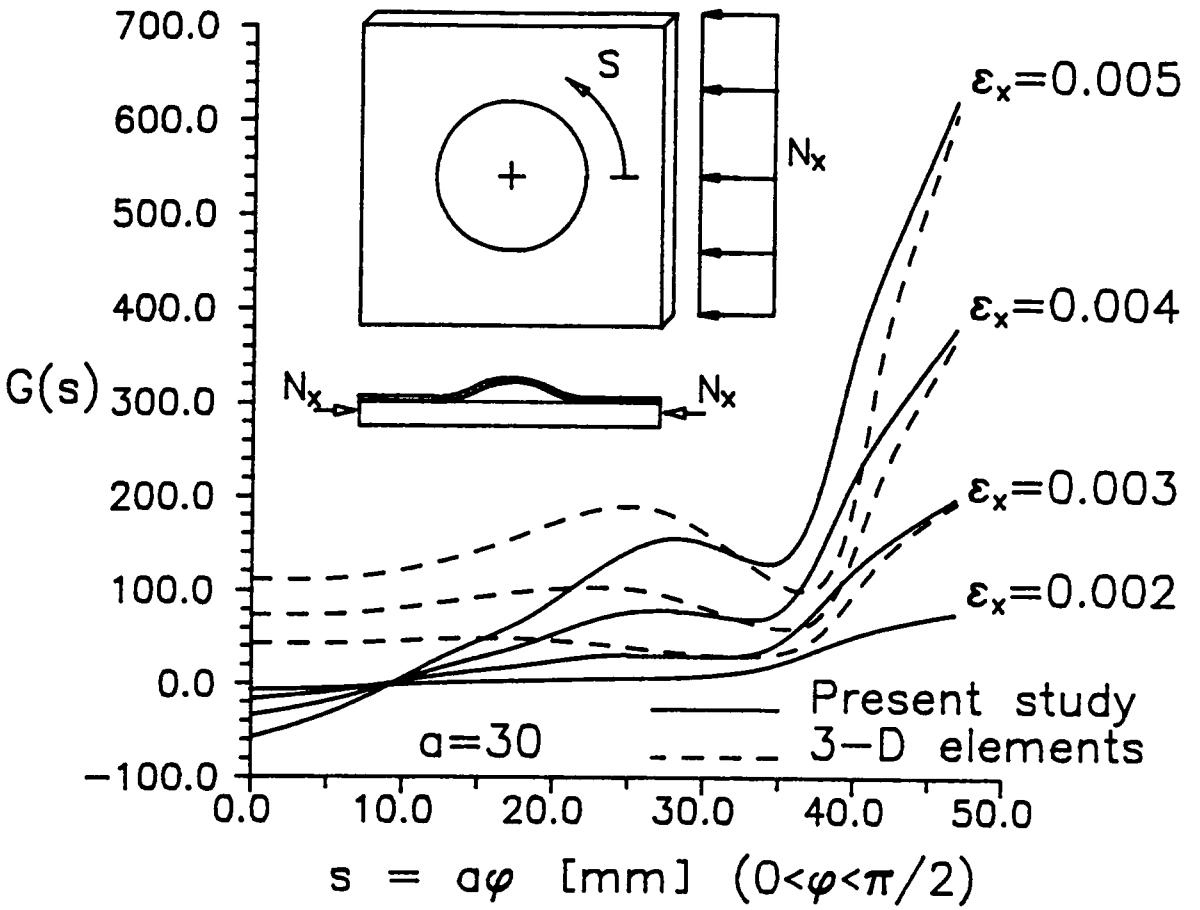

7.9 Distribution of the strin energy release rate G(s) along the boundary of a circular delamination of diameter 2a = 60 mm for several values of the applied inplane uniform strain ε_x.

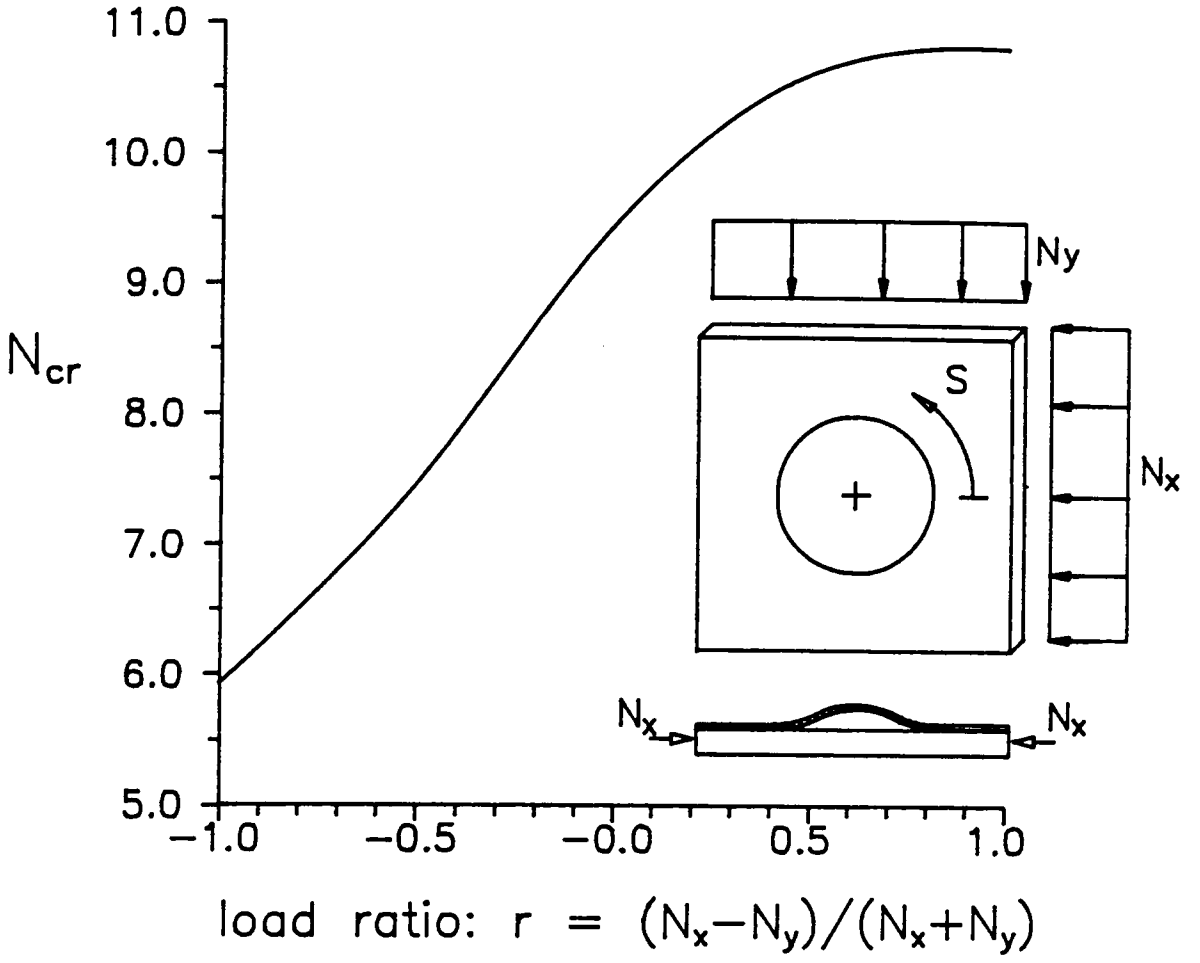

7.10 Buckling load as a function of the ratio between the magnitude of the loads applied along two perpendicular directions N_x and N_y for a circular delamination of radius a = 5 in, in a square plate of side 2c = 12 in, made of unidirectional Gr - Ep oriented along the x-axis.

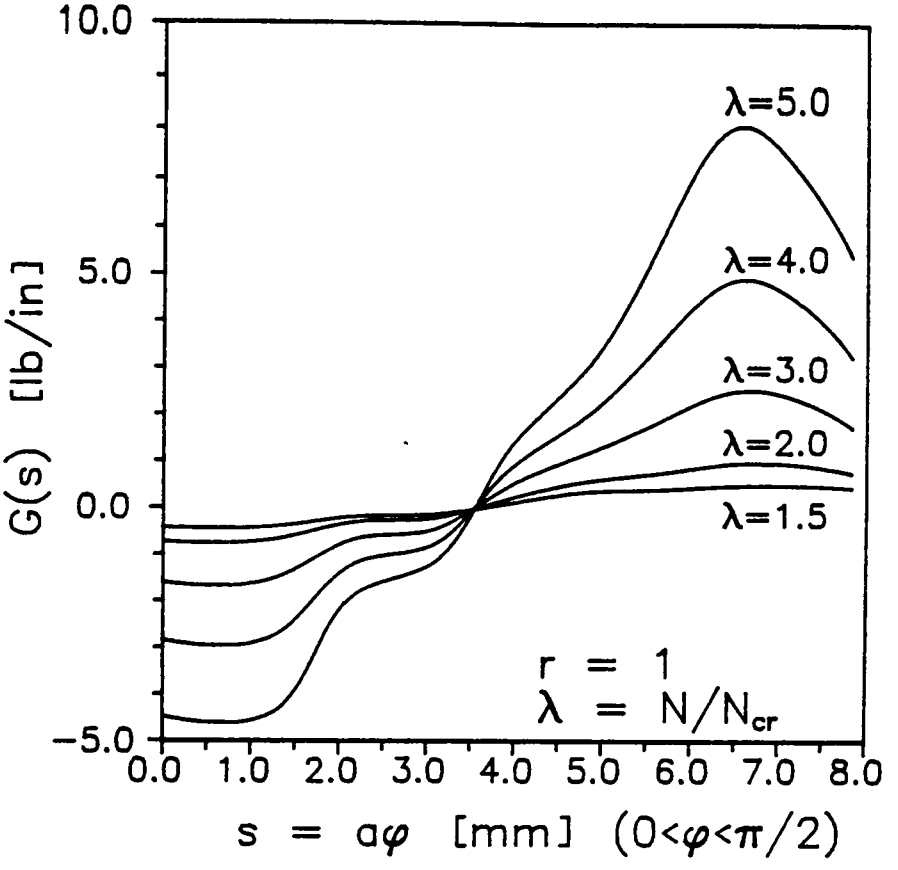

7.11 Distribution of the strain energy release rate G(s) along the boundary s of a circular delamination of radius a = 5 in for r = 1 (c.f. Caption 7.10) for several values of the applied load N.

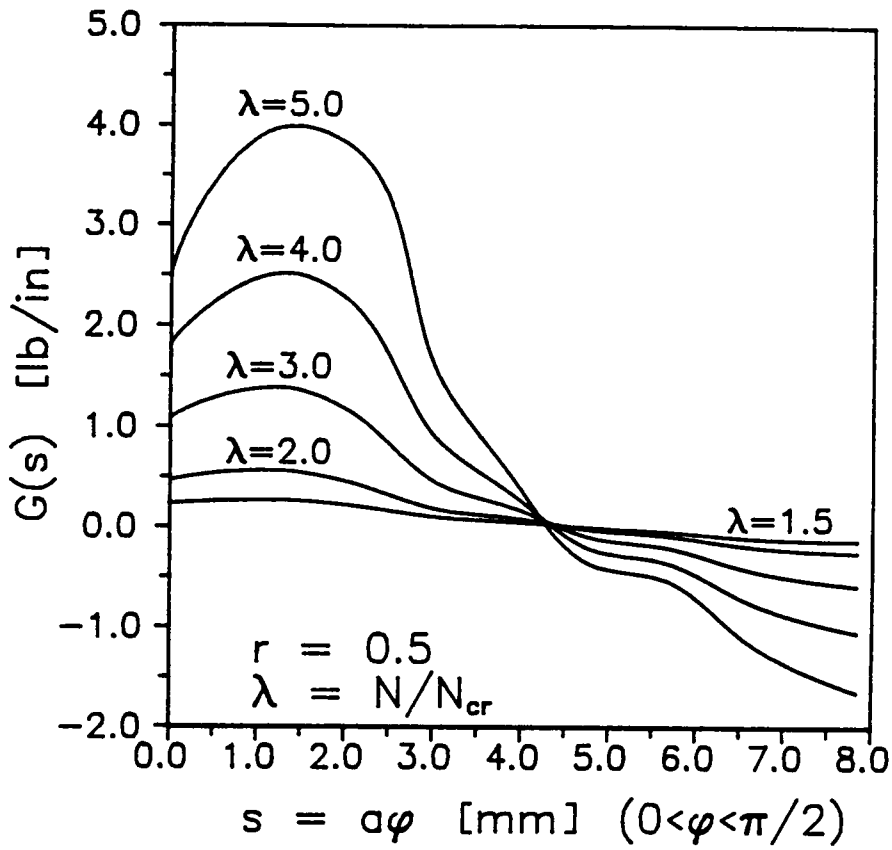

7.12 Distribution of the strain energy release rate G(s) along the boundary s of a circular delamination of radius a = 5 in for r = 0.5 (c.f. Caption 7.10) for several values of the applied load N.

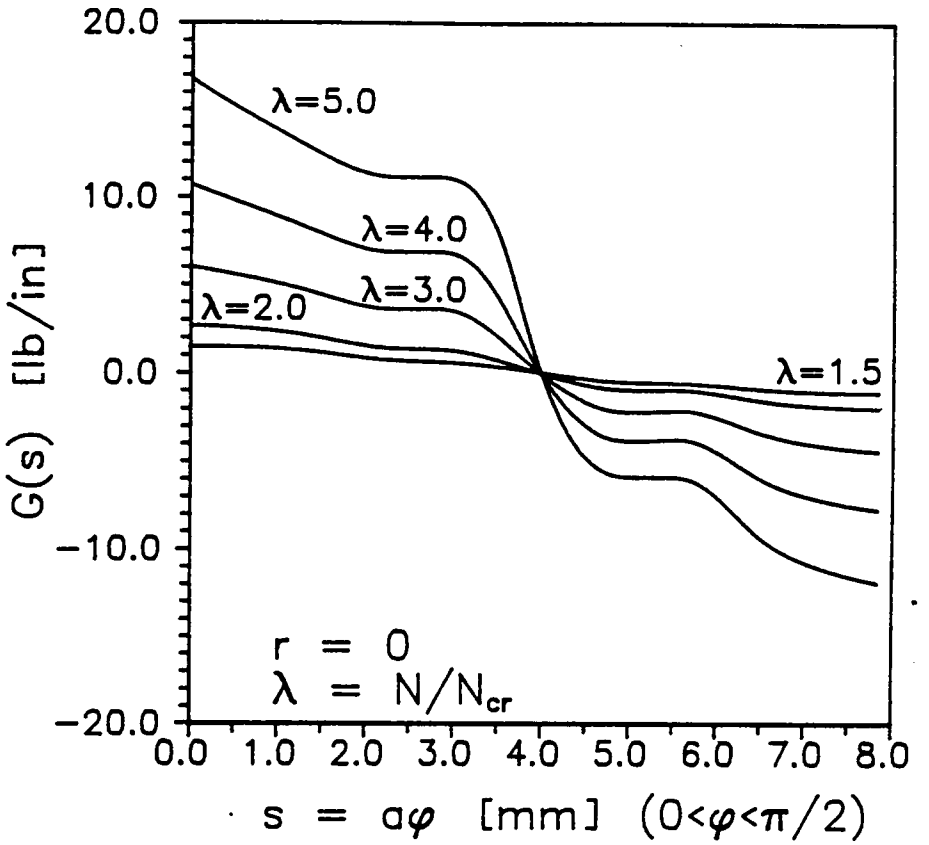

7.13 Distribution of the strain energy release rate G(s) along the boundary s of a circular delamination of radius a = 5 in for r = 0 (c.f. Caption 7.10) for several values of the applied load N.

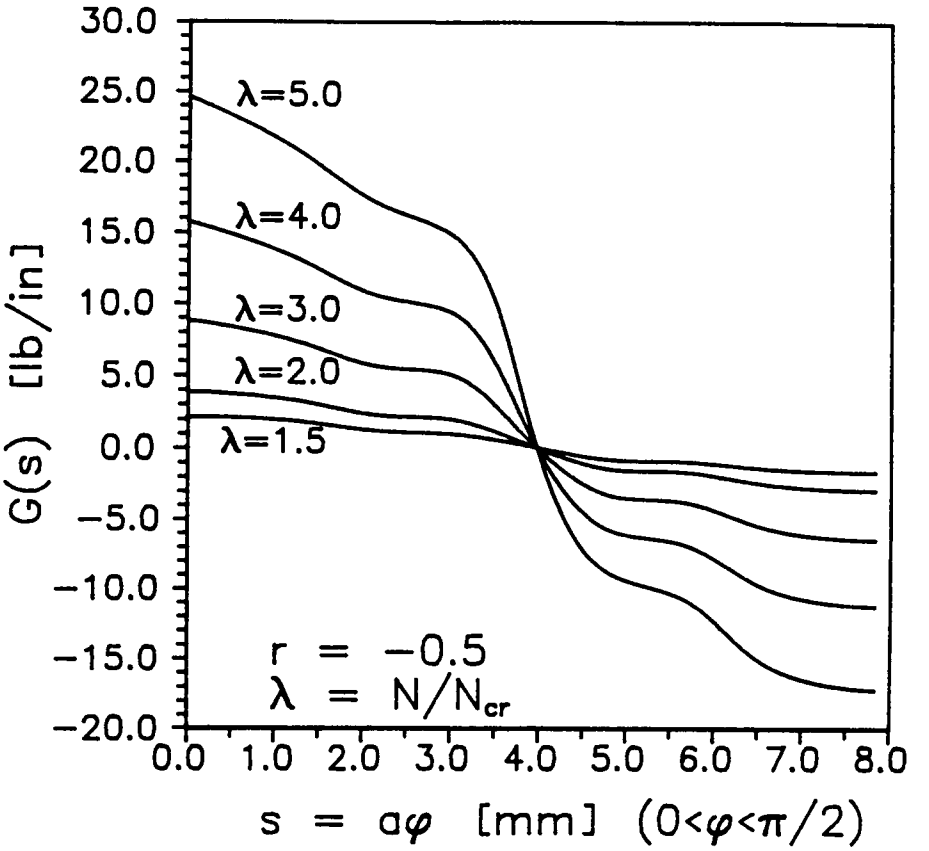

7.14 Distribution of the strain energy release rate G(s) along the boundary s of a circular delamination of radius a = 5 in for r = -0.5 (c.f. Caption 7.10) for several values of the applied load N.

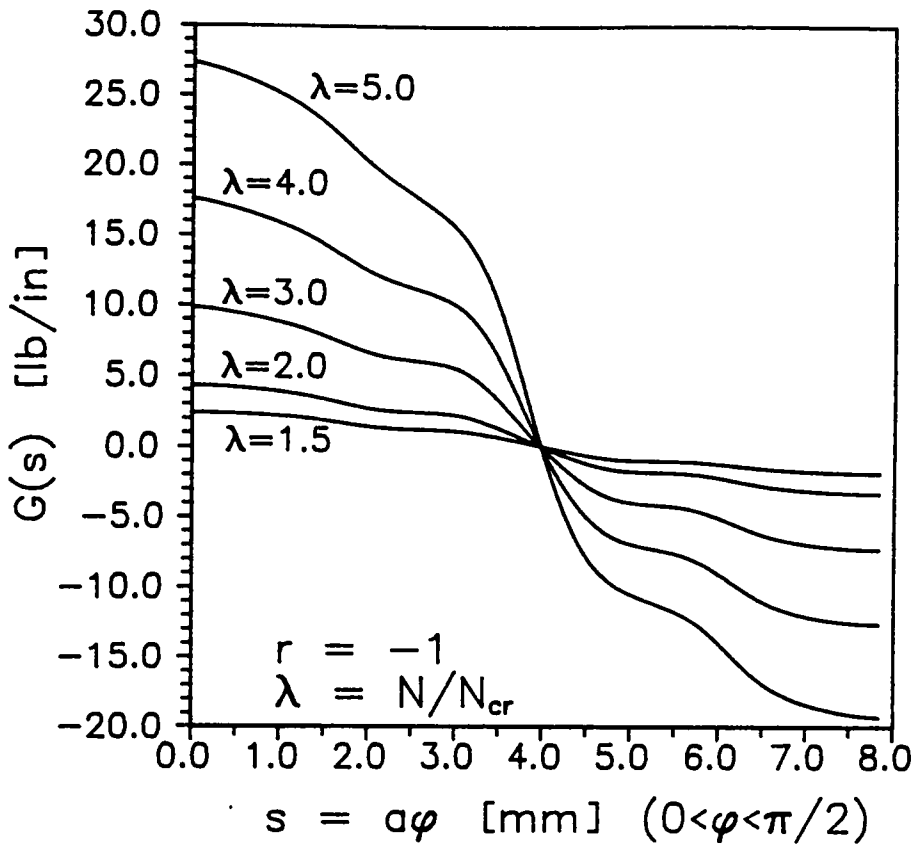

7.15 Distribution of the strain energy release rate G(s) along the boundary s of a circular delamination of radius a = 5 in for r = -1 (c.f. Caption 7.10) for several values of the applied load N.

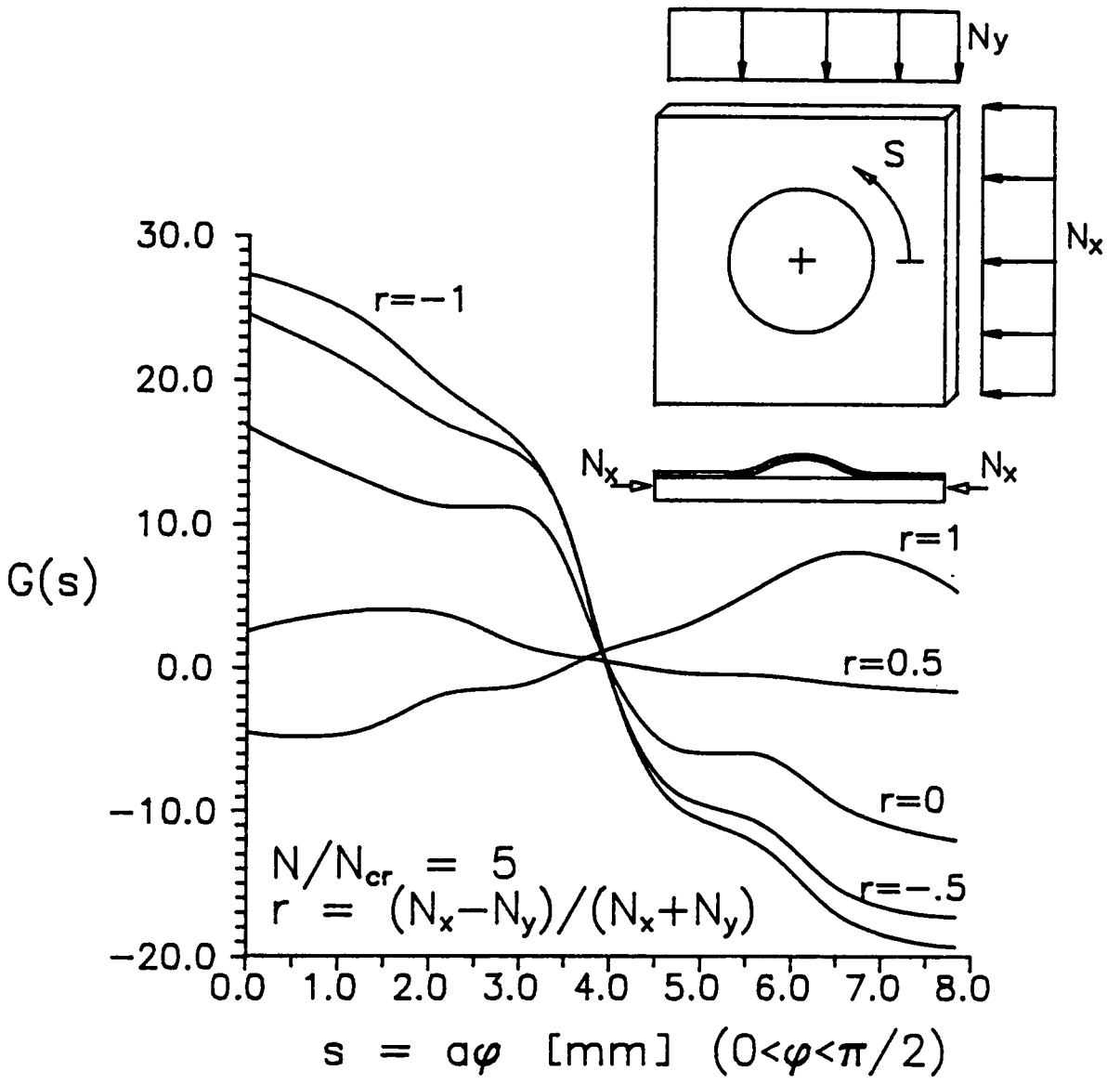

7.16 Distribution of the strain energy release rate G(s) along the boundary of a circular delamination of radius a = 5 in (c.f. Caption 7.10) for several values of the load ratio -1 < r < 1 to show the influence of the load distribution on the likelihood of delamination propagation.

Chapter 8

SUMMARY AND CONCLUSIONS

8.1 Discussion of the Results

The Generalized Laminate Plate Theory (GLPT) provides an adequate framework for the analysis of laminated plates and shells. Particularly, the layer-wise linear approximation of the displacements through the thickness and the use of Heaviside Step functions to model delaminations prove to be the most cost effective approach for an accurate analysis of local effects in laminated composite plates and shells. Numerous comparisons with existing theories have been presented for the global behavior of laminated plates in order to validate the formulation developed herein and to highlight the effects of shear deformation, particularly for hybrid composites. However, it must be noted that the computational cost of the proposed analysis makes it not attractive for prediction of global behavior when compared with conventional theories. For the prediction of local effects (i.e., delaminations, interlaminar stresses, etc.), the theory and formulation presented in this study shows its potentiality as a cost effective alternative to three-dimensional elasticity analysis. The theory and formulation can also be used in a global-local analysis scheme wherein the local regions are modelled using the GLPT and global regions are modelled using less refined theories, say the first-order laminate theory.

The Generalized Laminate Plate Theory has been validated in this study by a comprehensive set of closed form solutions and comparing the

obtained results to 3-D elasticity solutions and to other plate theories as well (see Chapter 2). The analytical solutions developed are used as a benchmark for the finite element solutions in Chapter 3. A number of examples are presented to illustrate the accuracy stress distributions predicted by the GLPT.

The linear theory presented in Chapter 2 is extended to geometrically nonlinear analysis in Chapter 4. The finite element method is used to obtain solutions to a variety of cases, including buckling and postbuckling of laminated plates. The buckling problem is formulated and its application to laminated composites is discussed. New results related to the effect of bending extension coupling and symmetry boundary conditions are presented.

A general nonlinear theory of laminated cylindrical shells is developed in Chapter 5 along the same lines as the Generalized Laminate Plate Theory. The theory incorporates geometric nonlinearity and transverse compressibility. Closed form solutions are developed for the linear case.

A formulation and associated algorithm for the computation of the strain energy release rate is developed in Chapter 6. The Jacobian derivative method (JDM) uses the isoparametric mapping of the domain to compute the derivative of the strain energy with respect to the crack length in the context of the finite element method. Although the JDM has applicability to any fracture mechanics problem, it is used primarily to evaluate the distribution of strain energy release rate along the boundary of delaminations between layers of laminated composite plates.

A model for the study of delaminations in composite plates is developed in Chapter 7. The theory includes the same displacement distribution in the individual layers as the Generalized Laminate Plate Theory of Chapter 2 but additionally is capable of representing displacement discontinuity conditions at interfaces between layers. The new model, along with the JDM, produces accurate predictions of strain energy release rates at the boundary of delaminations of arbitrary shape in general laminated composite plates. The theory is able to present multiple delaminations through the thickness of the plate.

8.2 Related Future Work

It is expected that the excellent prediction of stress distributions attainable with this type of analysis be used along with meaningful failure theories to predict failure initiation and propagation in composite laminates. Due to the computational cost associated with this model, it should be used primarily for local effects, i.e., delaminations, detailed stress analysis, impact, etc. Transition elements must be developed to join regions modelled by Generalized Laminate Plate Theory to regions modeled by less expensive theories in global-local analysisi procedures. Also, the Generalized Laminate Plate Theory can be used as a postprocessor to enrich the stress prediction of the First-Order Shear Deformation Theory.

REFERENCES

1. Reddy, J. N., "A Generalization of Two-Dimensional Theories of Laminated Plates," Commun. Applied Numer. Methods, Vol. 3, pp.113-180, 1987.

2. Baset, A. B., "On the Extension and Flexure of Cylindrical and Spherical Thin Elastic Shells," Phil. Trans. Royal Soc., Ser. A, Vol. 181, No. 6, pp. 433-480, 1890.

3. Boussinesq, J., "Etude Nouvelle Sur l'Equilibre et le Mouvement des Corps Solides Elastique Dont Certain Dimensions Sont Trespetites par Rapport a d'autre, J. Math., Paris ser. 2, Vol. 16, p. 125, 1871; and J. Math., Paris Ser. 3, Vol. 5, p. 329, 1879.

4. Hildebrand, F. B., Reissner, E., and Thomas, G. B., "Notes on the Foundation of the Theory of Small Displacements of Orthotropic Shells," NACA, Technical Note 1833, 1975.

5. Hencky, H., "Uber die Berrucksichtigung der Schubverzerrung in Ebenen Platten," Ing. Arch., Vol. 16, pp. 72, 1947.

6. Mindlin, R. D., "Influence of Rotary Inertia and Shear on Flexural Motions of Isotropic, Elastic Plates," J. Appl. Mech., Vol. 18, p. 31, 1951.

7. Yang, P. C., Norris, C. H., and Stavsky, Y., "Elastic Wave Propagation in Heterogeneous Plates," Int. J. Solids Structures, Vol. 2, pp. 665-684, 1966.

8. Uflyand, Y. S., "The Propagation of Waves in the Transverse Vibrations of Bars and Plates," Prikl. Mat. Mekh., Vol. 18, p. 31, 1951.

9. Reissner, E., "The Effect of the Shear Deformation on the Bending of Elastic Plates," J. Appl. Mech., Vol. 12, pp. 69-77, 1945.

10. Reissner, E. and Stavsky, Y., "Bending and Stretching of Certain Types of Heterogeneous Aeolotropic Elastic Plates," J. Appl. Mech., Vol. 28, p. 402, 1961.

11. Stavsky, Y., "Bending and Stretching of Laminated Aeolotropic Plates," Proc. ASCE, J. Eng. Mech. Div., EM6, Vol. 87, p. 31, 1961.

12. Lekhnitskii, S. G., "Anisotropic Plates, English Translation," MIR Publishers, 1981, (First Ed. in Russian 1950).

13. Pagano, N. J., "Analysis of the Flexure Test of Bidirectional Composites," J. Comp. Mat., Vol. 1, pp. 336-343, 1968.

14. Stavsky, Y., "On the Theory of Heterogeneous Anisotropic Plates," Doctor's Thesis MIT, 1959; and AFTDR WADD-TR-60-746, 1960.

15. Ambartsumyan, S. A., Theory of Anisotropic Plates, Technomic, 1969.

16. Whitney, J. M., "The Effect of Transverse Shear Deformation on the Bending of Laminated Plates," J. Comp. Mat., Vol. 3, pp. 534-547.

17. Reddy, J. N., Energy and Variational Methods in Applied Mechanics, Wiley Interscience, New York, 1984.

18. Reddy, J. N., "A Review of the Literature on Finite Element Modeling of Laminated Composite Plates," Shock Vib. Dig., Vol. 17, No. 4, pp. 3-8, 1985.

19. Whitney, J. M., and Pagano, N. J., "Shear Deformation in Heterogeneous Anisotropic Plates," J. Appl. Mech., Vol. 37, pp. 1031-1036, 1970.

20. Whitney, J. M., "Stress Analysis of Thick Laminated Composite and Sandwich Plates," J. Comp. Mat., Vol. 6, pp. 426-440, 1972.

21. Whitney, J. M., and Sun, C. T., "A Higher Order Theory for Extensional Motion of Laminated Composites," J. Sound and Vibr., Vol. 30, pp. 85-97, 1973.

22. Nelson, R. B., and Lorch, D. R., "A Refind Theory of Laminated Orthotropic Plates," J. Appl. Mech., Vol. 41, pp. 171-183, 1974.

23. Lo, K. H., Christensen, R. M., and Wu, E. M., "A High-Order Theory of Plate Deformation-Part 2: Laminated Plates," J. Appl. Mech., Vol. 44, pp.669-676, 1977.

24. Reddy, J. N., "A Simple Higher-Order Theory for Laminated Composite Plates," J. Appl. Mech., Vol. 51, pp. 745-752, 1984.

25. Yu, Y. Y., "A New Theory of Elastic Sandwich Plates-One Dimensional Case," J. Appl. Mech., Vol. 26, pp. 415-421, 1959.

26. Durocher, L. L., and Solecki, R., "Steady-State Vibrations and Bending of Tranversely Isotropic Three-Layer Plates," Developments in Mechanics, Vol. 8, Proc. 14th Midwestern Mech. Conf., pp. 103-124, 1975.

27. Mau, S. T., "A Refined Laminated Plate Theory," J. Appl. Mech., Vol. 40, pp. 606-607, 1973.

28. Srinivas, S., "Refined Analysis of Composite Laminates," J. Sound and Vibr., Vol. 30, pp. 495-507, 1973.

29. Sun, C. T., Whitney, J. N., "On Theories for the Dynamic Response of Laminated Plates," AIAA Paper No. 72-398, 1972.

30. Seide, P., "An Improved Approximate Theory for the Bending of Laminated Plates," Mechanics Today, Vol. 5, pp.451-466, 1980.

31. Librescu, L., "Improved Linear Theory of Elastic Anisotropic Multilayered Shells, Part I," Mekhanika Polimerov, No. 6, pp. 1038-1050, 1975.

32. Librescu, L., "Improved Linear Theory of Elastic Anisotropic Multilayered Shells, Part II," Mekhanika Polimerov, No. 1., pp. 100-109, 1976.

33. Librescu, L., "Non-Linear Theory of Elastic Anisotropic Multilayered Shells," Advanced Problems in Applied Mechanics (Ed. L. I. Sedov) Moskow pp. 453-466, 1974.

34. Pryor, C. W., Jr., and Barker, R. M., "A Finite Element Analysis Including Transverse Shear Effects for Applications to Laminated Plates," AIAA J., Vol. 9, pp. 912-917, 1971.

35. Reissner, E., "On a Certain Variational Principle and a Proposed Application," Int. J. Num. Meth. Engng., Vol. 20, pp. 1366-1368, 1984.

36. Murakami, H., "Laminated Composite Plate Theory with Improved In-Plane Responses," J. Appl. Mech., Vol. 53, pp. 661-666, 1986.

37. Toledano, A., and Murakami, H., "A Composite Plate Theory for Arbitrary Laminate Configurations," J. Appl. MEch., Vol. 54, pp. 181-189, 1987.

38. Chaudhuri, R. A., "An Equilibrium Method for the Prediction of Transverse Shear Stresses in a Thick Laminated Plate," Comp. and Str., Vol. 23, pp. 139-146, 1986.

39. Obreimoff, J. W., "The Splitting Strength of Mica," Proc. Roy. Soc., A127, p. 290, 1980.

40. Inoue, I., and Kobatake, Y., "Mechanics of Adhesive Joints, Part IV: Peeling Test," Applied Scientific Research (A), Vol. 8, p. 321, 1959.

41. Chai, Herzi. "The Growth of Impact Damage in Compressively Loaded Laminates." Thesis California Institute of Technology, 1982.

42. Simitses, G. J., Sallam, S. and Yin, W. L., "Effect of Delamination of Axially Loaded Homogeneous Laminated Plates," AIAA Journal, Vol. 23, p. 1437-1440, 1985.

43. Kachanov, L. M., "Separation Failure of Composite Materials," Polymer Mechanics, Vol. 12, pp. 812-815, 1976.

44. Ashizawa, M., "Fast Interlaminar Fracture of a Compressively Loaded Composite Containing a Defect, Fifth DOD-NASA Conference on Fibrous Composites in Structural Design, New Orleans, LA, 1981.

45. Sallam, S. and Simitses, G. J., "Delamination Buckling and Growth of Flat, Cross-Ply Laminates," Composites and Structures, Vol. 4, pp. 361-381, 1985.

46. Kapania, R. K. and Wolfe, D. R., "Delamination Buckling and Growth in Axially Loaded Beam-Plates," AIAA Paper 87-0878-CP, SDM Conference, Monterrey, CA, 1987.

47. Webster, J. D., "Flaw Criticality of Circular Disbond Defects in Compressive Laminates," CCMS Report 81-03, 1981.

48. Bottega, W. J. and Maewal, A., "Delamination Buckling and Growth in Laminates," Journal of Applied Mechanics, Vol. 50, pp. 184-189, 1983.

49. Yin, W-L., "Axisymmetric Buckling and Growth of a Circular Delamination in a Compressed Laminate," Int. J. Solids and Structures, Vol. 21, pp. 503-514, 1985.

50. Fei, Z. and Yin, W-L, "Axisymmetric Buckling and Grow of a Circular Delamination in a Compressed Laminate," Int. J. Solids and Structures, Vol. 21, pp. 503-514, 1985.

51. Wolfe, D. R., "Delaminationo Buckling, Postbuckling, and Growth in Axially Loaded Beam-Plates," M.S. Thesis, Aerospace and Ocean Engineering, Full Version, 1988.

52. Kapania, R. K. and Wolfe, D. R., "Buckling of Axially Loaded Beam-Plate with Multiple Delaminations," J. Pressure Vessel Technology, Vol. 11, pp. 151-158, 1989.

53. Chai, H., Babcock, C. D., and Knauss, W. G., "One Dimensional Modelling of Failure in Laminated Plates by Delamination Buckling," Int. J. Solids and Structures, Vol. 17, pp. 1069-1083, 1981.

54. Shivakumar, K. N. and Whitcomb, J. D., "Buckling of a Sublaminate in a Quasi-isotropic Composite Laminate," J. Composite Materials, Vol. 19, 1985.

55. Chai, H. and Babcock, C. D., "Two-dimensional Modelling of Compressive Failure in Delaminated Laminates," J. Composite Materials, Vol. 19, pp. 67-98, 1985.

56. Whitcomb, J. D., "Finite Element Analysis of Instability Related Delamination Growth," Jour. Comp. Mat., Vol. 15, pp. 113-180, 1981.

57. Whitcomb, J. D., "Instability-related Delamination Growth of Embedded and Edge Delaminations," NASA TM 100655, 1988.

58. Whitcomb, J. D. and Shivakumar, K. N., "Strain-energy Release-rate Analysis of a Laminate with a Postbuckled Delamination," NASA TM 89091, 1987.

59. Wilt, T. E., Murthy P. L. N., and Chamis, C. C., "Fracture Toughness Computational Simulation of General Delaminations in Fiber Composites," AIAA Paper 88-2261, pp. 391-401, 1988.

60. Yin, W-L, Sallam, S. N., and Simitses, G. J., "Ultimate Axial Load Capacity of a Delaminated Beam-plate," AIAA Journal, Vol. 24, pp. 123-128, 1986.

61. Henshell, R. D. and Shaw, K. G., "Crack Tip Elements are Unnecessary," Int. Jour. Num. Meth. Eng., Vol. 9, pp. 495-507, 1975.

62. Barsoum, R. S., "Application of Quadratic Isoparametric Finite Elements in Linear Elastic Fracture Mechanics," Int. Jour. of Fracture, Vol. 10, pp. 603-605, 1975.

63. Barsoum, R. S., "Triangular Quarter Point Elements as Elastic and Perfectly-plastic Crack Tip Elements," Int. Jour. Num. Meth. Eng., Vol. 11, pp. 85-98, 1977.

64. Raju, I. S. and Newman, J. C., Jr., "Methods for Analysis of Cracks in Three-dimensional Solids," NASA TM 86266, 1984.

65. Tong, P., Pian, T. H. H., and Lasry, S. J., "A Hybrid-element Approach to Crack Problems in Plane Elasticity," Int. Jour. Num. Meth. Eng., Vol. 7, pp. 297-308, 1973.

66. Chan, S. K., Tuba, I. S., and Wilson, W. K., "On the Finite Element Method in Linear Fracture Mechanics," Eng. Fract. Mech., Vol. 2, pp. 1-17, 1970.

67. Raju, I. S. and Newman, J.C., "Three-dimensional Finite-element Analysis of Finite-thickness Fracture Specimens," NASA TN D-8414, 1977.

68. Raju, I. S. and Newman, J. C., "Stress-Intensity Factors for a Wide Range of Semi-elliptical Surface Cracks in Finite-thickness Plates," Eng. Fract. Mech., Vol. 11, pp. 817-829, 1979.

69. Rice, J. R., "A Path Independent Integral and the Approximate Analysis of Strain Concentrations by Notches and Cracks," J. of App. Mech., Vol. 35, pp. 379-386, 1968.

70. Rybicki, E. F. and Kanninen, M. F., "A Finite Element Calculation of Stress Intensity Factors by a Modified Crack Closure Integral," Eng. Fract. Mech., Vol. 9, pp. 931-938, 1977.

71. Ramamurthy, T. S., Krishnamurthy, K., and Badari, Naryana K., "Modified Crack Closure Integral with Quarter Points Elements," Mech. Res. Comm., Vol. 13, No. 4, pp. 179-186, 1986.

72. Hellen, T. K., "On the Method of Virtual Crack Extensions," Int. Jour. Num. Meth. Eng.., Vol. 9, pp. 187-207, 1975.

73. Parks, D. M., "A Stiffness Derivative Finite Element Technique for Determination of Elastic Crack Tip Stress Intensity Factors," Int. Jour. of Fracture, Vol. 10, pp. 487-502, 1974.

74. Reddy, J. N., An Introduction to the Finite Element Method, McGraw Hill, New York, 1984.

75. Reddy, J. N., "Mechanics of Laminated Composite Structures, Theory and Analysis," Lecture Notes, Virginia Polytechnic Institute and State University, 1988.

76. Pagano, N. J., "Exact Solutions for Composite Laminates in Cylindrical Bending," J. Composite Materials, Vol. 3, p. 398-411, 1969.

77. Pagano, N. J., "Exact Solutions for Rectangular Bidirectional Composites and Sandwich Plates," J. of Composite Materials, Vol. 4, pp. 20-35, 1970.

78. Goldbery, J. L. and Schwartz, A. J., Systems of Ordinary Differential Equations, An Introduction, Harper and Row Publishers, 1972.

79. Srinivas, S. and Rao, A. K., "Bending, Vibration and Buckling of Simply Supported Thick Orthotropic Rectangular Plates and Laminates," Int. J. Solids Struct., Vol. 6, pp. 1463-1481, 1970.

80. Reddy, J. N., "A Note on Symmetry Considerations in the Transient Response of Unsymmetrically Laminated Anisotropic Plates," Int. Jour. Num. Meth. Eng., Vol. 20, 175-198, 1984.

81. Chaudhuri, R. A., "An Approximate Semi-Analytical Method for Prediction of Interlaminar Shear Stress in an Arbitrary Laminated Thick Plate," Computers and Structures, Vol. 25, No. 4, pp. 627-636, 1987.

82. Noor, A. K., "Free Vibraitons of Multilayered Composite Plates," AIAA Journal, Vol. 11, pp. 1038-1039, 1975.

83. Way, S., "Uniformly Loaded, Clamped, Rectangular Plates with Large Deflection," Proc. 5th Int. Cong. Appl. Mech., John Wiley, New York, pp. 123-138. 1938.

84. Brush, D. and Almroth, B., Buckling of Bar, Plates and Shells, McGraw Hill, 1975.

85. Dupuis, G. A., Pfaffinger, D. D., and Marcal, P. V., "Effective use of Incremental Stiffness Matrices in Non-linear Geometric Analysis," IUTAM Symp. on High Speed Computing of Elastic Structures, Liege, Aug. 1970.

86. Gallagher, R. H. and Maw, S. T., "A Method of Limit Point Calculation in Finite Element Structural Analysis," NASA CR 12115, Sept. 1972.

87. Jones, R. M., Mechanics of Composite Materials, Scripta Book Co., Washington, DC, 1975.

88. Love, A. E. H., "On the Small Free Vibrations and Deformations of the Elastic Shells," Phil. Trans. Roy, Soc., (London), Ser. A, Vol. 17, pp. 491-546, 1988.

89. Naghdi, P. M., "A Survey of Recent Progress in the Theory of Elastic Shells," Appl. Mech. Reviews, Vol. 9, No. 9, pp. 365-368, 1956.

90. Bert, C. W., "Analysis of Shells," Analysis and Performance of Composites, L. J. Broutman (ed.), Wiley, New York, pp. 207-258, 1980.

91. Dong. S. B., "Free Vibrations of Laminated Orthotropic Cylindrical Shells," J. Acoust. Soc. Am., Vol. 44, No. 6, pp. 1628-1635, 1968.

92. Bert, C. W. Baker, J. L., and Egle, D. M., "Free V ibrations of Multilayer Anisotropic Cylindrical Shells," J. Comp. Mat., Vol. 3, pp. 480-499, 1969.

93. Stavsky, Y. and Loewy, R., "On Vibrations of Heterogeneous Orthotropic Cylindrical Shells," J. Sound and Vib., Vol. 15(2), pp. 235-256, 1971.

94. Koiter, W. T., "A Consistent First Approximation in the General Theory of Thin Elastic Shells," Proceedings of the Symposium on The Theory of Thin Elastic Shells, Delft, 24-28 August, 1959.

95. Hildebrand, F. B., Reissner, E., and Thomas, G. B., "Note on the Foundations of the Theory of Small Displacements of Orthotropic Shell," National Advisory Comm. Aero. Tech. Notes, No. 1833, 1949.

96. Luré, A. I., Statics of Thin Elastic Shells, Gostekhizdat, Moskva, 1947 (in Russian).

97. Reissner, E., "Stress-Strain Relations in the Theory of Thin Elastic Shells," J. Math. Phys., Vol. 31, pp. 109-119, 1952.

98. Srinivas, S., "Analysis of Laminated, Composite Circular Cylindrical Shells with General Boundary Conditions," NASA TR R-412, 1974.

99. Donnell, L. H., "Stability of Thin-Walled Turbes Under Torsion," NACA Report 479, 1933.

100. Bathe, K. J. and Sussman, T. D., "An Algorithm for the Construction of Optimal Finite Element Meshes in Linear Elasticity," Computer Methods for Nonlinear Solids and Structural Mechanics, AMD-54, pp. 15-36, 1983.

101. Haber, R. B. and Koh, H. M., "Explicit Expressions for Energy Release Rates Using Virtual Crack Extensions," Int. Jour. Num. Meth. Eng., Vol. 21, pp. 301-315, 1985.

102. DeLorenzi, H. G., "Energy Release Rate Calculations by the Finite Element Method," Eng. Fract. Mech., Vol. 21, No. 1, pp. 129-143, 1985.

103. Lin, S. C. and Abel, J. F., "Variational Approach for a New Direct-Integration Form of the Virtual Crack Extension Method," Int. Jour. Fracture, Vol. 38, pp. 217-235, 1988.

104. Coulomb, J. L., "A Methodology for the Determination of Global Electromagnetical Quantities from a Finite Element Analysis and its Application to the Evaluation of Magnetic Forces, Torques and Stiffness," IEEE Transactions on Magnetics, Vol. MAG-19, No., 6, 1983.

105. Gordon, J. G., Fracture Mechanics of Polymers, Halsted Press, New York, 1984.

106. Paris, P. C. and Sih, G., "Fracture Toughness Testing and Its Applications," ASTM Special Technical Publication, No. 381, pp. 30-81, 1965.

107. Raju, I. S. and Newman, J. C., "Stress-Intensity Factors for Internal and External Surface Cracks in Cylindrical Vessels," J. Press. Vessel Tech. Trans., ASME, Vol. 104, pp. 293-298, 1982.

108. Kaufmann, G. H., Lopergolo, A. M., Idelsohn, S. R. and Barbero, E. J., "Evaluation of Finite Element Calculations in a Part-Circular Crack by Coherent Optics Techniques," Experimental Mechanics, pp. 154-157, June 1987.

109. Raju, I. S. and Newman, Jr., J. C., "Methods for Analysis of Cracks in Three-Dimensional Solids," NASA Technical Memorandum 86266, July 1984.

110. Tseng, A. A., "A Comparison of Finite Element Solutions for the Compact Specimen," Int. Jour. of Fracture, Vol. 17, pp. 125-129, 1981.

111. Shih, C. F. and deLorenzi, H. G., "Elastic Compliances and Stress-Intensity Factors for Side-Grooved Compact Specimens," Int. Jour. of Fracture, Vol. 13, pp. 544-548, 1977.

112. Newman, J. C., Jr., "Stress Analysis of the Compact Specimen Including the Effects of Pin Loadings," Fracture Analysis, ASTM STP, Vol. 560, pp. 105-121, 1973.

113. Wan-Lee, Yin, "The Effects ofLaminated Structure on Delamination Buckling and Growth," J. Comp. Mat., Vol. 22, pp. 502-517, 1988.

114. Bodner, S. R.,"The Post-buckling Behavior of a Clamped Circular Plate," Quart. Appl. Math., Vol. 12, pp. 397-401, 1954.

The vita has been removed from the scanned document